ERASMUS MUNDUS MSC PROGRAMME

COASTAL AND MARINE ENGINEERING AND MANAGEMENT
COMEM

Analysis of Spectra, Wave Grouping and Long Wave Phenomena of Real Measured Wind Waves in Coastal Waters

UNIVERSITAT POLITÈCNICA DE CATALUNYA

June 2011

Mauricio Alberto Wesson Vizcaino

4053664

The Erasmus Mundus MSc Coastal and Marine Engineering and Management is an integrated programme organized by five European partner institutions, coordinated by Delft University of Technology (TU Delft).
The joint study programme of 120 ECTS credits (two years full-time) has been obtained at three of the five CoMEM partner institutions:

Norges Teknisk- Naturvitenskapelige Universitet (NTNU) Trondheim, Norway
Technische Universiteit (TU) Delft, The Netherlands
City University London, Great Britain
Universitat Politècnica de Catalunya (UPC), Barcelona, Spain
University of Southampton, Southampton, Great Britain

The first year consists of the first and second semesters of 30 ECTS each, spent at NTNU, Trondheim and Delft University of Technology respectively.
The second year allows for specialization in three subjects and during the third semester courses are taken with a focus on advanced topics in the selected area of specialization:
Engineering
Management
Environment
In the fourth and final semester an MSc project and thesis have to be completed.
The two year CoMEM programme leads to three officially recognized MSc diploma certificates. These will be issued by the three universities which have been attended by the student. The transcripts issued with the MSc Diploma Certificate of each university include grades/marks for each subject. A complete overview of subjects and ECTS credits is included in the Diploma Supplement, as received from the CoMEM coordinating university, Delft University of Technology (TU Delft).

Information regarding the CoMEM programme can be obtained from the programme coordinator and director

Prof. Dr. Ir. Marcel J.F. Stive
Delft University of Technology
Faculty of Civil Engineering and geosciences
P.O. Box 5048
2600 GA Delft
The Netherlands

Thesis Directors:

Dr. Cesar Mosso A.
Laboratori d'Enginyeria Maritima, LIM/UPC
Lecturer

Prof. Agustín Sánchez-Arcilla
Laboratori d'Enginyeria Marítima, LIM/UPC
Director

ETS Enginyers de Camins, Canals i Ports
Universitat Politècnica de Catalunya

Preface

A thesis/dissertation in partial fulfillment of the requirements of the degree of Msc in Civil Engineering Coastal and Marine Engineering and Management (CoMEM).

Universitat Politècnica de Catalunya

16th June 2011

Summary and keywords

Wave Spectra, Wave Groups, Bound Long Waves, Hilbert Huang Spectra, Surf Beats, Wave Measurements, Infragravity Waves.

Real coastal waves measured at 4 different locations in the world were analyzed in detail. Long travelled swell measured in the Pacific coast of Costa Rica, wind swell from the Atlantic coast of Costa Rica, short period wind waves from the Ebro Delta in Mediterranean coast of Spain, and waves measured during the passing of Hurricane Wilma near Cancun, Mexico were analyzed. A total of 5795 wave records from the sites above were analyzed.

A statistical stability analysis of the wave data was done. The measured wave height distribution was compared with the Raleigh distribution. The corresponding significant wave height and period distribution based on the zero down crossing method was obtained for all the records. The joint individual wave height-period distribution was obtained and the characteristic statistic wave heights and periods were obtained. The time variation of these parameters, including the skewness and kurtosis of the time series were obtained to determine the statistical stability of the data.

A detailed spectral analysis using the Fourier transform was done on all the records. The whole record for each location was represented as time variant frequency energy spectrogram. The highest measured record's spectra for each site were examined in detail. The peakedness, band width, grouping, regularity spectral parameters, and the six principal moments of all the wave records were obtained. The spectra were then compared to the JONSWAP spectrum. Special attention was taken into the non-linear components present in the spectra.

Temporal and energetic wave grouping parameters were analyzed using the run length theory. Low frequency modulation was examined against grouping observation. The capability of the variance spectra based on the Fourier transform to describe the measured wave grouping was analyzed and confirmed through the spectral grouping parameter Ka.

The long waves present in the records were analyzed using a low pass filter. Spectral analysis was carried out on the filtered time series. The results between the different sites were compared and Longuet-Higgins set down equation under wave groups was calibrated and validated to predict the long wave spectral significant wave height, given the wave spectral significant height, the peak spectral period and the water depth outside the breaker zone.

A spectral analysis using the Hilbert Huang method was done to the most energetic measured events of each record. A detail comparison was done between the result of the Fourier transform variance spectral analysis and the Hilbert Huang method. The limitations of the Fourier based spectra and the new Hilbert Huang transform spectra were examined in detail.

Acknowledgements

First of all I have to thanks my companion during the past years who happens also to be a student in the CoMEM program, Cinthya Gomez. My family in particular my father which has been responsible for collecting the field wave data within Costa Rica since my absence deserves a special acknowledgment. None of this work would have been possible without his patience and his support carrying out the required wave measurements, and dealing with all the problems and issues of offshore field work within the Costa Rican work framework would have made this work impossible.

Xavi Jimenez and the CIEM staff at UPC are acknowledged for providing the laboratory and field wave data to carry out the present work. The CoMEM coordinators at each of the attended Universities, Professor Øivind Asgeir from NTNU, Professor Marcel Stive from TU Delft and Professor Augustin Sanchez Arcilla from UPC are acknowledged for their support thru out the whole program.

The Costa Rican Institute of Marinas and Piers, CIMAT, is greatly thanked for providing the wave measurement data along the Pacific coast for this work. Recope is also thanked for allowing the use of the measured wave data along the Atlantic coast of Costa Rica for the present work. Rodolfo Silva is also thanked for providing the measured wave data off Puerto Morales in Cancun for the present work, and a special acknowledgement is also done to the UPC for providing the measured wave data at the Ebro Delta.

All the friendship and companion from CoMEM program classmates is highly rewarded, they have helped in the development of the final thesis work with their support. All the CoMEM staff is also acknowledge for their support, in particular Hege Hernes from NTNU, Mariette van Tilburg and Madelon Burgmeijerfrom TUDelft and Genoveva Comas from UPC have all been supporting throughout the whole program.

All the professors and lecturers involved in the CoMEM program, the knowledge they have transmitted has permitted the work done.

Finally and most important my UPC thesis directors, Cesar Mosso which has had the patience to carefully read and advice all my work and the profound review done by Professor Augustin Sanchez Arcilla has permitted the work to transcend and provide further insight into the realm of waves in Coastal Waters.

Table of Contents

List of Figures

List of tables

1.0 Introduction

Waves are the most important phenomenon that affects coastal and marine structures. Before the half of the 20th century the wave records were obtained through visual observations. The most important parameter determined was the "significant wave height" based on the visually observed sea state. In 1944 Munk proposed a procedure for the observation and interpretation of recorded wave data. Nowadays there is widespread use of different instruments that use the wind wave variance spectrum based on the fast Fourier transform as a standard description.

It is well documented that waves in the ocean travel in groups. The grouping of ocean waves appears stronger in narrow banded variance spectrum conditions, as swell records, hence the importance of analyzing long travelled swell which presents such characteristics. It is also documented that wave grouping affect the stability of some marine structures, particularly floating structures[1]. Wave grouping is also associated with the modulation of cross shore wave generated currents, hence with beach morphology[2]. Wave groups have also been associated with a series of coastal engineering problems, among them we can mention surf beat and surf zone hydrodynamics, harbor resonance[3] and, oscillations of vessels among others.

Even though the importance of these phenomena seems clear, wave grouping or its effects are not always incorporated into design methods. The main reasons is because with the variance spectra, obtained through the Fourier transform, (energy spectra), it is difficult to directly account for wave grouping or the associated bound long waves. In order to account for wave groups a variety of theories and parameters are used to characterize the wave groups. According to Medina and Hudspeth the main existing analysis methods of wave groups are, the correlation function by Rye (1982), Markov chains developed by Kimura (1980), envelop methods SIWEH or $H^2(t)$ by Funke and Mansard (1979), the Run Length theory by Goda (1970) and the three axes by Hudspeth and Medina (1988). The Hilbert transform has previously been used to analyze deep water wave modulation[4], and wave grouping as well, more recently Veltcheva (2002) has analyzed wave and group transformations using the new Hilbert Huang Transform Method.

Munk and Tucker independently discovered and recorded in the late 1940's small amplitude waves with periods between 25 and 100 seconds, they were defined by Munk as "surf beat". Long wave action responsible for harbor agitation problems is a coupled problem with wave grouping. Bowers (1979), analyzed harbor resonance due to set down under wave groups. When wave groups travel they produce a set down which is called the bound long wave, creating a trough where the highest waves of the group travel and a crest in the lower waves. This bound long wave can be freed either by wave breaking, when it encounters steep changes in bathymetry or by wave diffraction[5]. Once the bound long wave is free it travels at its own celerity and attains the characteristics of very

[1] Medina J.R., Hudspeth R.T. "A Review of the analyses of ocean wave groups"Coastal Engineering, 14 (1990) 515-542
[2] Haller H.C., Dalrymple R.A. "Looking for Wave Groups in the Surf Zone", Coastal Dynamics '95
[3] Bowers, E.C. "Wave gouping and harbor design", Coastal Engineering, June 1988, 237-258
[4] Melville W.K. "Wave Modulation and Breakdown", Journal of Fluid Mechanics (1983), **128**:489-506

long wave with very high reflection coefficients and low dissipation. It is documented that the surge natural oscillation period for large ships is close to the long wave period which increases the ship's motion interrupting harbor operations, and in some cases breaking mooring lines. The natural period of harbors is also in the order of the of the long wave period, this can lead to resonance within the harbor, undesired movement of ships, and stopping of harbor operations, with large economic implications and accidents. Small craft harbors also suffer from agitation and this problem has been previously analyzed for marinas in the Pacific Coast of Costa Rica[5]. In order to accurate model and design new harbors the characteristics of the long waves, and wave groups, have to be determined accurately. The associated long wave height and period are then the important design characteristics which need to be considered and accurately analyzed.

The generation of the long wave due to the wave groups is a non-linear process known as wave-wave interaction. This wave-wave interaction is hardly included in steady state spectral models. In order to study the resonance phenomena, Boussinesq type models, which can handle wave-wave interaction, are used. However, the grouping information of the incoming wave trains must be incorporated within the open offshore boundary, either in its low frequency energy or in the occurrence probability of run lengths.

Currently there are debates whether the wind wave variance spectrum, based on the Fourier Transform, is enough to characterize the temporal physical behavior of the wave energy.[6] Among the basic assumptions that a given realization requires in order to correctly apply a Fourier transformation is that it should be a stochastic, stationary, linear process[7]. For a given time history a Fourier transformation represents the signal in a finite number of time invariant harmonic components. In our case, the recorded time history of water surface elevation, important features of the wave record, like the wave groups and bound long waves, are difficult to analyzed and characterize with this method. The energy beating that the wave groups produce through its time history have to be represented in a time averaged energy spectrum obtained through the Fourier transform. There have been methods proposed to analyze the wave groups, among them the Smooth Instantaneous Wave History, SIWEH, proposed by Funke and Mansaard (1980), or the run length theory by Goda (1983). More recently Huang (1998), proposed a new methodology, the Hilbert Huang Transform, HHT, which provides detailed energy, frequency, temporal representation of the wave record. The purpose of this work is to analyze the spectra, the wave grouping and long wave characteristics of the wind wave spectrum using the Fourier transform and Run Length theory and compare its results with the Hilbert Huang transform.

The work has been carried out using several wave measurement sets in different sites around the world of very wave conditions in coastal waters. The first wave data set has been obtained in an exposed site off the Pacific coast of Costa Rica. These wave measurements have been carried for the government of Costa Rica in order to provide a calibration for an operational wave forecasting system. The wave measurements have been carried out intermittently since 2008 until present; however they are only activated when there are "storm" conditions

[5] Cox, J.C. and Wesson M.V., "Manipulating Harbor Geometries to Defeat Long Wave Agitation Problems" ASCE Ports 2007.
[6] Liu, Paul C, "Is the wind wave frequency spectrum outdated", Ocean Engineering 27 (2000) 577–588
[7] Titchmarsh, E.C., 1948 "Introduction to the theory of Fourier Integrals" Oxford University Press, Oxford, UK

forecasted. Recently the wave measurements have been carried out continuously. In the present study two sets of representative long swell measurements will be analyzed. The first campaign consists of approximately one month of wave measurements carried out from August to October 2010, and the second campaign was of *continuous* measured data from the 12th and ended the 19th of November 2010. The continuous wave record has been divided into time series of 1024 seconds of duration.

The second data set consists of 10 days of wave measurements from Ebro Delta located in the Catalan Coast. These wave measurements were carried out from the 1st to the 10th of November 1996 as part of the Ebro Delta 96 campaign. The third data set consisted of 1 month of wave measurements on the Atlantic coast of Costa Rica carried out in December 2010. All of the above wave measurements were carried out using a submersible pressure sensor.

The last data set that was analyzed consisted of 9 days of wave measurements off Cancun in Mexico, during October 1995 when hurricane Wilma struck the coast. The measurement location was in the eye's path of the storm. In this case the measurements were carried out using an acoustic AWAC profiler.

2.0 Orientation

2.1 Problem Definition

Wave grouping, the tendency of waves to appear in groups, and long wave phenomenon are considered to be very important in coastal engineering and ocean engineering. Several studies relate coastal engineering problems with these two phenomena. Medina and Hudspeth (1990) did a review of the analyses of ocean wave groups. In their review they summarized the coastal phenomena and engineering problems related to wave grouping. Some of the coastal, port and ocean engineering problems that have been associated with these phenomena are:

- ***Harbor resonance*** studied by; Tucker, 1950; Bowers, 1977; Rye, 1982; and Bruun, 1985.
- ***Damage and capsizing of ships*** studied by; Ewing, 1973; and Goda, 1976.
- ***Forces on mooring lines and Oscillation and Position of Vessels*** studied by; Hsu and Blenkarn, 1970; Johnson, et al 1978; Kimura, 1980; Rye, 1982; Sand, 1982; Bruun, 1985; Mase and Iwagaki, 1986; Bowers, 1988.
- ***Design of Marine Structures***; Burchart, 1979; Sand, 1982; Longuet-Higgins, 1984;
- ***Run-up Overtopping;*** Johnson, 1978; Kimura, 1980; Rye, 1982; Bruun, 1985; Mase and Iwagaki, 1986.
- ***Surf beat, Set up and Set down, and Surf-zone dynamics***; Munk, 1946; Tucker, 1950; Bowers, 1977; Rye, 1982; Sand, 1982; Mase and Iwagaki, 1986; Battjes, 1988; and Bowers, 1988.
- ***Design wave uncertainties***, Medina and Hudspeth 1987.
- ***Rubble mound stability,*** Johnson, 1978; Rye, 1982; Burchart, 1979; Bruun, 1985; Mase and Iwagaki, 1986; Van der Meer and Pilarcysk, 1984.

Burchart (1979) showed that wave groups produced a jump in wave height which affects wave run-up and run-down, furthermore the stability of dolos armour layers were also affected by wave steepness and wave period[8]. It is clear that wave grouping and bound long wave phenomena are of sum importance in coastal and ocean engineering problems.

The importance of wave grouping and long wave phenomenon is clear from the previous list. For the harbor resonance problem it is well documented that the excitation period of large vessels is of several minutes, far from wind wave periods. This excitation occurs from long period water fluctuations outside the harbor related to the wave groups[9]. In order to accurately model, and design a harbor against resonance the external excitation, the main boundary condition of any model, should be well documented and understood. Hence the study of these phenomena with the new available tool, the Hilbert Huang Transform may be part of the solution to this problem.

[8] Burcharth, H.F., 1979. "The effect of wave grouping on on-shore structures". Coastal Eng.,2: 189--199.
[9] Bowers E. C. "Harbor resonance due to set-down beneath wave groups", . Fluid Mech. (1977), vol. 79, part 1, pp. 71-92

Spectral models, based on the Fourier transform, have limited capacity to model these phenomena due to the fact that a wave spectra obtained through a Fourier transform losses all information related to wave phasing, hence the variation of wave energy in a time history due to phenomena as wave groups might be lost. Fourier spectra cannot handle nonlinear waves; hence bound long waves are not accurately represented.

There are several methodologies to analyze a time dependant signal. Wavelet type analysis has been incorporated to take into account the variation in time history of the energy; however the most commonly used the Morlet wavelet analysis uses Fourier transform and is unable to analyze nonlinear waves[10].More recently Huang 1998, proposed a new method, the Hilbert Huang Transform.

The Hilbert transform is based on an empirical decomposition of the main modes within the time history, empirical mode decomposition. The individual characteristic oscillations are obtained through the decomposition of the time history signal; this process is defined in the method as empirical mode decomposition, which is obtained assuming that the signal is composed of different intrinsic mode functions, where each intrinsic mode function represents an embedded characteristic oscillations. Moments and marginals are easily defined with the Hilbert Spectrum H(w,t), and they can provide information like amplitude modulation and range of instantaneous frequencies.

The application of the Hilbert Huang Transform, (Huang N. 1998), is a recent development and it can provide further understanding of grouping and long wave phenomena in non-linear non stationary seas. The measured long travelled swell can contain important wave grouping and non-linear effects[11] the Hilbert Huang transform should provide an in depth insight into this phenomena.

The understanding and comprehension of the wave grouping and long wave nonlinear complex phenomena using the new developed Hilbert Huang transform method can provide a new view of the non stationary non linear spectral characteristics of these phenomena. The wave modulation done through grouping and its associated long wave phenomena is responsible for a large variety of coastal engineering problems, from harbor agitation to sediment transport, and the insight that the new HHT method provides on these phenomena is crucial to provide a new view of wave spectrum and development of new analysis tools.

[10] Veltcheva A. B. “Wave and Group Transformation by a Hilbert Spectrum” Coastal Engineering Journal, Vol. 44, No. 4 (2002) 283-300

[11] Goda Y. “Analysis of Wave Grouping and Spectra of Long-travelled Swell” 1983, Port and Harbor Research Institute Japan.

2.2 Objectives

The general purpose of this work is to analyze the spectra, wave grouping and long wave phenomenon of different measured wave conditions.

Specifically:

- Analyze the statistics of the wave measurements
- Describe the swell source and storm characteristics of the different measurements.
- Obtain the Spectra and spectral characteristics of the wave measurements using the fast Fourier transform.
- Analyze the wave grouping phenomena suing the run length theory and compare it with the obtained spectral characteristics.
- Analyze the bound long wave characteristics of the record with the Fourier transform using a low pass filter on the data.
- Obtain the Hilbert Spectrum, through the Hilbert Huang transform method and compare the results with the variance spectrum obtained using the fast Fourier transform
- Determine spectral characteristics that accurately describe the wave grouping.
- Determine the long wave energy present in the different sea states and obtain a equation to include this energy based on sea state parameters.

2.3 Scope of the Work

The present work is based on the study of several wave measurements available from 4 completely different locations. The first data sets analyzed consisted of three wave measurement campaigns off the Pacific coast of Costa Rica, the first campaign consists of approximately one month of wave measurements carried out from August to October 2010, the second campaign was of *continuous* measured data started the 12th and ended the 19th, of November, the third campaign was of *continuous* measurements carried out from the 24th of November to the 3rd of December all in 2010.

The second data set consists of 10 days of wave measurements from Ebro Delta located in the Catalan Coast. These wave measurements were carried out from the 1st to the 10th of November 1996 as part of the Ebro 96 campaign.

The third data set consisted of 1 month of *continuous* wave measurements on the Atlantic coast of Costa Rica carried out in December 2010. All of the above measurements were carried out using a submersible pressure sensor.

The last data set that was analyzed consisted of 1 month of wave measurements off Cancun in Mexico, during October 1995 when hurricane Wilma struck the coast.

First the source of the measured storms will be determined using the global Wavewatch III model's hindcast from NOAA for the long travelled swell measurements off the coast of the Pacific Coast of Costa Rica. The wave measurements will be compared qualitatively with the hindcasts from the model for the long travelled swell.

A detailed analysis of the wave measurements will be done to the whole record identifying energetic wave events and calm conditions. For the whole record a statistical stability analysis of the wave data will be done comparing the wave height measured distribution to the Raleigh distribution. The corresponding significant wave height and period distribution will be obtained. The joint individual wave height-period distribution will be obtained and the characteristic statistic wave heights and periods will be obtained. The time variation of these parameters, including the skewness of the time histories will be used to determine the statistical stability of the data.

A detailed spectral analysis using the Fourier transform will be done on all the records. The whole record for each location will be represented as time variant frequency energy spectrogram. The five highest measured record's spectra will be plotted and examined in detail. The peakedness, band width, grouping, regularity parameters, and six principal moments of all the wave record obtained. The spectra will be compared to JONSWAP spectrum. Special attention will be taken into the non-linear components present in the spectra. The skewness and wave asymmetry will be calculated. Further details are given in the methodology.

Temporal and energetic wave grouping parameters will be analyzed using the run length theory. Low frequency modulation will be examined against grouping observation.

The long waves will be analyzed using a low pass filter. The results will be compared with the results from the Hilbert spectra and the Fourier Spectra.

A spectral analysis using the Hilbert Huang method will be done for the most energetic measured events of each record. The detail comparison will be done between the result of the Fourier transform variance spectral analysis and the Hilbert Huang method. Instantaneous time windows will used to compare the marginal frequency Hilbert spectrum with the Fourier Spectrum.

The following will not be included in the present study:

- Validation or Calibration of the hindcast information will not be done.
- Wave modeling to the measuring sites will not be done.
- Wavelet Analysis.
- Non-linear Fourier Transforms.
- Spectral or Boussinesq or other wave propagation models will not used to analyze the information or harbor resonance.
- Directional Analysis.

2.4 Methodology

The methodology used to analyze the wave information is divided in 5 main steps which are explained below. Each proposed step is contained in the work, in main or subchapters. Figure 1 represents a generalized flow chart for the analysis of the wave records. Given the different types of the wave record analyzed, long travelled swell or shorter period storm conditions, the flow chart has been generalized. The parameters presented to describe the methodology used are only briefly introduced. Their complete physical and mathematical description is presented in the Technology State of the Art Chapter.

The analysis of the wave data was done using WESS, Wave Ensemble Analysis Software, developed by Mauricio Wesson during the present thesis work based on WAFO, Wave Analysis for Fatigue and Oceanography developed by Lund University of Mathematics and the Norwegian University for Science and Technology. WAFO is a toolbox of Matlab® routines for statistical analysis and simulation of random waves and random loads. WESS uses several commands of WAFO to analyze large wave data sets. WESS is composed of 5 modules; Basic Statistics based on the zero down crossing of each time series, Spectral Analysis using the fast Fourier Transform, Wave Grouping Analysis based on the correlation coefficient between successive waves and the Run Length Theory, Long Wave Spectral Analysis using a low pass filter and module to obtain the Hilbert Huang spectrum, including its marginal. The results for each module are presented in figures with all the necessary information within them. The theoretical details of each module are presented in chapter 2.5, State of the Art of the Spectral, Wave Grouping and Long Wave Analysis. The Hilbert Huang Transform is also incorporated in the software as is a new non linear methodology to obtain wave surface elevation from pressure measurements within WESS.

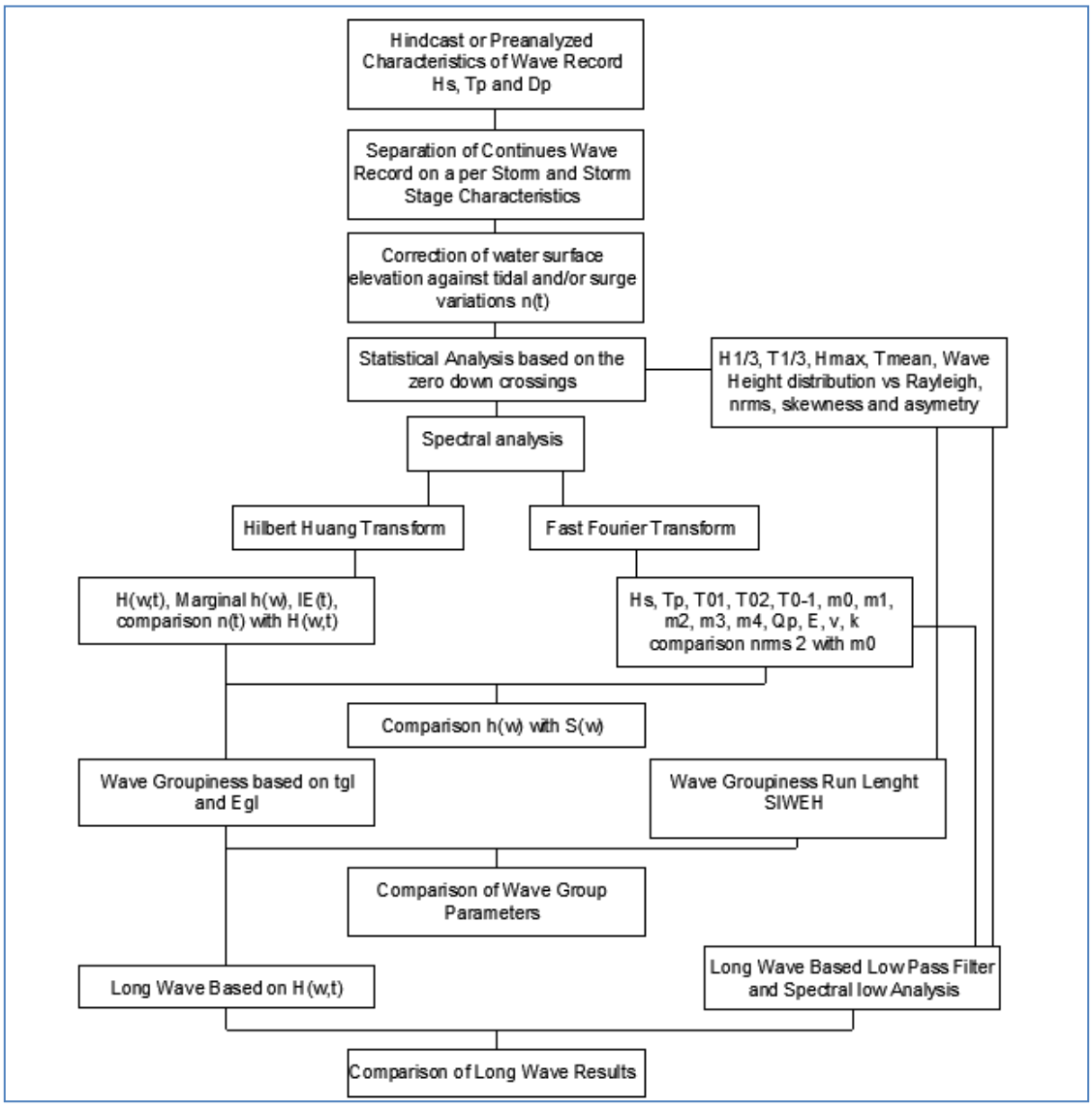

Figure 1: Flow Chart of Methodology Used

2.4.1 Statistical Analysis of the records based on the zero down-crossing method

Using the zero-down crossing, the statistical wave height values H_{max}, $H_{1/10}$, $H_{1/3}$, H_{rms} and the correspondingly wave periods $T_{1/3}$, $T_{1/10}$ and T_{mean},(definitions of these parameters in chapter 2, section 2.5.1) temporal variation will be obtained for all the time series available in the wave record. All of these parameters are defined by the International Association of Hydraulic Research permanent congress.

The marginal distribution of individual wave heights will be calculated and checked against the theoretical Rayleigh distribution for wave heights. The temporal variation of the ratios between the characteristic wave

heights will be used to determine the temporal changes in the fit of the Rayleigh distribution for all the wave records. For the wave periods the marginal distribution will obtained and the correlation between the measured characteristics periods will be obtained. Then the joint individual wave height and wave period will be obtained for the record, identifying the periods of the individual highest waves.

The ratio of the highest measured wave to the significant wave height obtained with the zero down crossing will also be examined in detail. The data will be checked against spurious wave information.

The skewness and asymmetry of the time series will be analyzed.

2.4.2 Calculation and Analysis of Fast Fourier Transform Spectra

A spectral analysis based on the fast Fourier transform will be carried out on all the times series for each wave record analyzed. This information will be used to develop a spectrogram which depicts the temporal energy variation of the whole record through the wave measurements. This information will be used to obtain the different storm events, and the general characteristics of these storms, including the temporal variation of the peak period, the frequency distribution of the energy within the storms, and the presence of low frequency energy. The spectrogram will provide the finger print of the different sea states analyzed in the present work.

The temporal variation of the spectral significant wave height, obtained from the first moment will be obtained and compared against previously calculated wave heights obtained using the zero-down crossing method. The temporal variation of the spectral periods T_{m02}, and T_{m0-1} will also be obtained and compared with the periods obtained with the zero down crossing method. The ratio between the spectral significant and significant wave height will be examined for the different wave records. The ratios between the spectral and statistical periods will also be examined.

A detail analysis will be done on the five highest spectra of the most energetic wave conditions of each wave record. The spectral moments, and peak frequencies will be obtained. The highest wave spectrums will be compared with the JONSWAP spectrum, determining the fit to this parametric representation and the peakdness enhancement parameter during these energetic conditions. Even though TMA spectra is a more accurate representation of the depth limited wave conditions, and Ochi Hubble spectra is more accurate to represent bimodal wave conditions the JONSWAP spectra was used given its extensive application in coastal engineering and for comparison purposes of previous research done with it.

The temporal variation of the spectral characteristics will be examined for the whole record. The temporal variation of the peakdness parameter, the spectral bandwidth, the spectral broadness, the spectral groupiness and the narrowness parameter will be obtained. The temporal variation of these parameters will be compared with the obtained spectrogram to determine if they actually depict the observed spectral changes. The

parameters that actually can depict these changes of the spectral shapes will be used to determine their ability to predict real wave groupiness and infra gravity wave content.

2.4.3 Analysis of Wave Groups

The wave grouping characteristics of all the time series of the different wave records will be analyzed. First the correlation coefficient between successive waves, for a lag number of waves from 1 to 4 will be obtained for the whole record, with its standard deviation. Then the temporal variation of the correlation coefficient between two successive wave heights will be obtained. The temporal variation of this parameter will be first compared qualitatively with the spectral parameters to determine if any of them can be correlated with this parameter.

Then the occurrence and exceedance probability for run length of waves above two threshold values will be obtained from the wave records. These run lengths will based upon the zero down crossing method for the definition of the individual waves. The threshold value that will be used will be the mean wave height and the statistical significant wave height. The occurrence and exceedance probability will be compared with Kimura's (1980) theory and this will be done for all the time series in the wave available wave records.

The mean run lengths for run of waves above the two previously defined wave threshold values will be obtained for each wave record. The temporal variation of these parameters will then be obtained and compared with the correlation coefficient between two successive wave heights and the previously obtained spectral parameters. A detail description of the group length theory can be found in section 2.5.3.

2.4.4 Long Wave Analysis

All the time series from the different wave records will be analyzed for the presence of infra gravity wave energy within them. A low pass filter will be used to analyze the presence of long waves in the separated records. The spectra of the low frequency waves will be obtained using the Fast Fourier transform. The long wave spectra will also be obtained from the short wave Fourier coefficients through the transfer function proposed by Hansen, 1978 and procedure developed by Sand 1982. The result will be compared to determine the amount of free long wave energy present in the records by defining the long wave spectral height based on the zeroth moment of the long wave spectra. The peak frequency of the long wave spectra will also be used to determine the peak period associated with the obtained long wave. The resolution, or degrees of freedom, used to calculate the spectra will be varied to prevent infinite periods.

The long wave spectra will also be studied using the wave grouping information. The long wave characteristics will be compared with the mean run lengths[12].

The obtained long wave characteristics will be compared with intrinsic mode functions of the record, obtaining the respective spectra of representative parts of the record to evaluate the Hilbert Huang transform ability to detect the long waves in the record.

2.4.5 Calculation and Analysis of Hilbert Huang Transform Spectra

The Hilbert Huang Transform is a relatively new methodology to obtain the energy, frequency and time distribution of a signal.

For the most energetic wave conditions, obtained with the fast Fourier Transform, the intrinsic mode functions will be obtained based on the empirical mode decomposition method. Secondly the Hilbert transform will be applied. The amplitude, phase and instantaneous frequency are then calculated. The original data expressed as the real part of the complex expansion considered a generalized form of the Fourier expansion, designated as Hilbert energy spectrum $H(\omega,t)$.

The calculated Hilbert spectrum is then plotted with its respective time series using the instantaneous energy. These plots are then examined for non-stationary behavior in the time series.

The marginal spectrum, integrating over the time period, is then calculated and compared with the corresponding previously calculated spectra using the fast Fourier Transform.

[12] Sand S.E. "Wave Grouping Described by Bound Long Waves".

2.5 State of the Art of the Spectral, Wave Grouping and Long Wave Analysis

This chapter provides a brief theoretical explanation of all the parameters and methods used for the analysis of the wave records, from the basic statics of the mean wave height to the spectral analysis are introduced.

2.5.1 Statistical Analysis of a Wave Record based on zero-down crossing

The analysis of wave characteristics based on water surface elevations are referred in literature as short term statistics. In short wave statistics the wave height and wave period are considered stochastic variables. The basis of this analysis is the zero crossings of the surface water elevation to a mean water level. The definition of a wave in a record is down by counting either two consecutive down crossings or up crossings. Figure 2 shows a typical water surface elevation record with three waves defined by the zero-down crossing method marked with arrows. The basic information contained are the differences in elevation from the lowest amplitude to the highest amplitude before another zero down crossing, this defines the wave heights, Hi and the time between successive zero down crossings defines the period of each wave Ti. It is clear that the number of waves on a record will depend on the recorded time and the corresponding periods of each wave. It is recommended to have at least one hundred waves in a record.

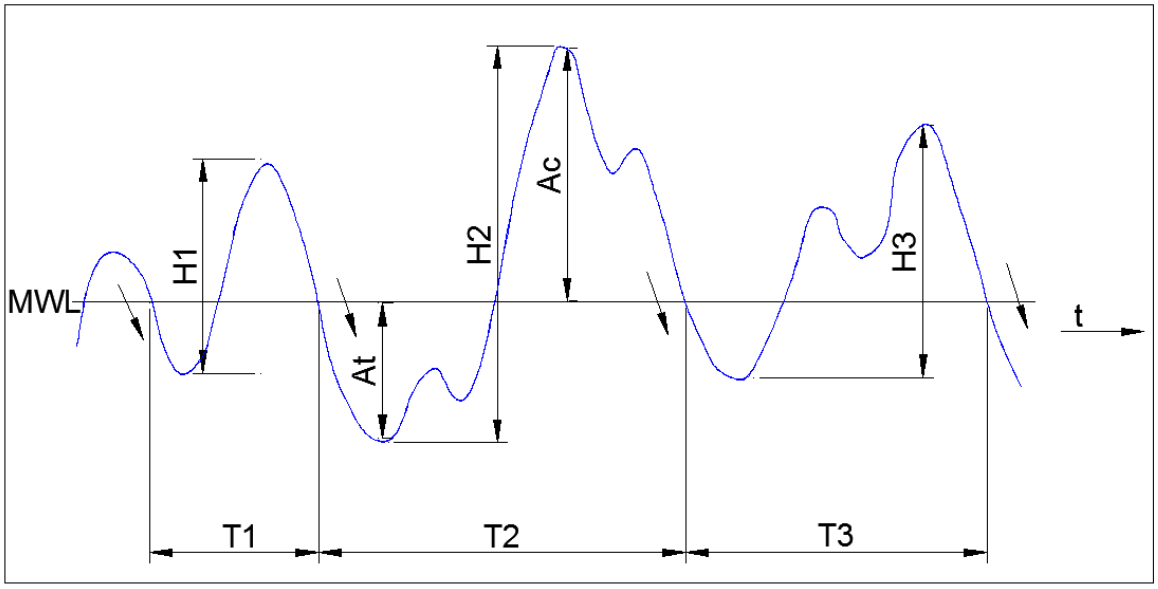

Figure 2: Zero down crossing method to define the wave heights and periods.

A series of statistics are derived from such a record on the wave heights and the wave period. The most used ones are defined below:

Highest Wave: Correspond to the wave with the highest height H_{max} in the record. Its height and period are reported as the highest wave, in our case H2 from figure 2.

Highest one-tenth wave: The total numbers of waves, Hi with Ti, are ordered from the highest wave height to lowest. The average of the first tenth of the waves is reported as $H_{1/10}$ and $T_{1/10}$.

Significant Wave Height: From the same descending ordered waves, using their wave height, the average of the highest one third is obtained and is defined as significant wave height $H_{1/3}$, and significant wave period $T_{1/3}$. This wave height and period is usually reported as the sea condition.

Mean Wave: This represents the mean of the measured wave heights and the wave periods respectively, and it is represented as H_{mean}($\bar{H}$) and Tz.

Root Mean Square wave height: This wave height has been argued to represents more accurately the energy in the wave field. It is represented as H_{rms}, and it is defined by equation 1.

$$Hrms = \sqrt[2]{\frac{1}{N}\sum_{i=1}^{N} H^2}$$

Eq. (1)

The previously defined values are obtained for each measured time series of the ensemble of measured waves, the obtained results of these characteristic wave values. The obtained results of such an analysis using the developed software are shown in figure 3.

The surface water elevation follows a Gaussian distribution and it is well documented that the wave heights in sufficiently long record follow a probabilistic distribution. This distribution is known as the Rayleigh distribution after Lord Rayleigh used it to describe sounds emitted from an infinite number of sources in the 19th century. Longuet–Higgins proposed to use this distribution for describing individual wave heights and it is given in equation 2.

$$p(h) = \frac{2H}{H_{rms}^2} e^{-\left(\frac{h}{Hrms}\right)^2}$$

Eq. (2)

The Rayleigh cumulative distribution is given in equation 3. A comparison between the measured and theoretical Rayleigh distribution is shown in figure 4 and the cumulative distribution is shown in figure 5.

$$P(H < h) = F(h) = 1 - e^{-\left(\frac{h}{Hrms}\right)^2}$$

Eq. (3)

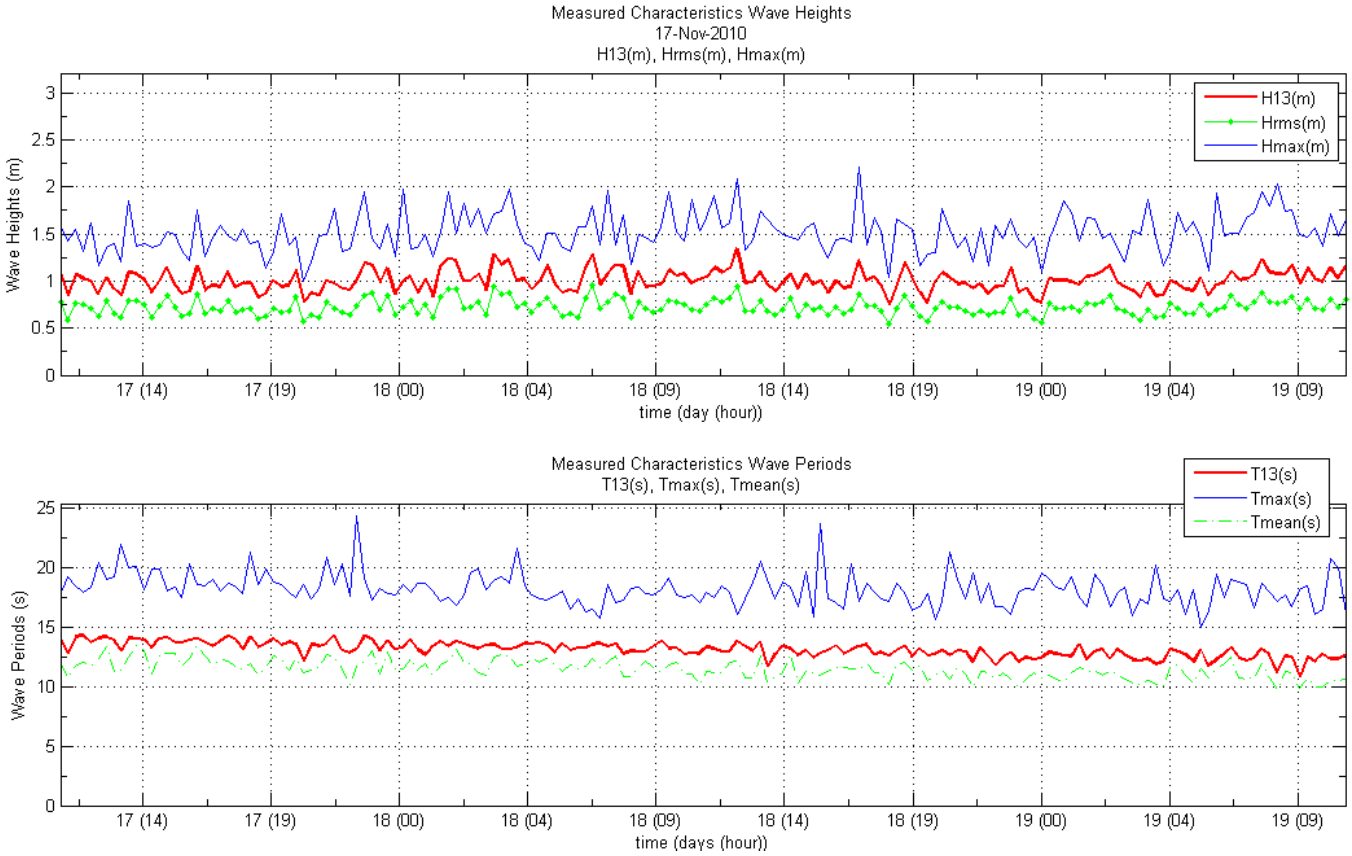

Figure 3: Wave Statistic Characteristics Obtained with WES.

Using the Rayleigh distribution the theoretical relation between the representative wave heights defined above, assuming the same number of waves in the record, can be obtained. These relations are defined in equation 4.

$$H_{1/3} = 1.60\overline{H}\,, \quad H_{1/10} = 2.03\overline{H}$$

Eq. (4)

The maximum wave height cannot be theoretically defined unless the number of waves in the record is given. Computations show that the highest expected wave out of record composed of N waves can be found by the following expression:

$$E[H_{max}] \approx Hs\left(\sqrt{\left(\frac{\ln N}{2}\right)} + \frac{0.57}{\sqrt{8\ln N}}\right)$$

Eq. (5)

Goda (1983), compared wave records that exhibit a small departure to the Rayleigh distribution, this departure is relative to the frequency spectrum of the record. This same departure was observed in the analyzed data.

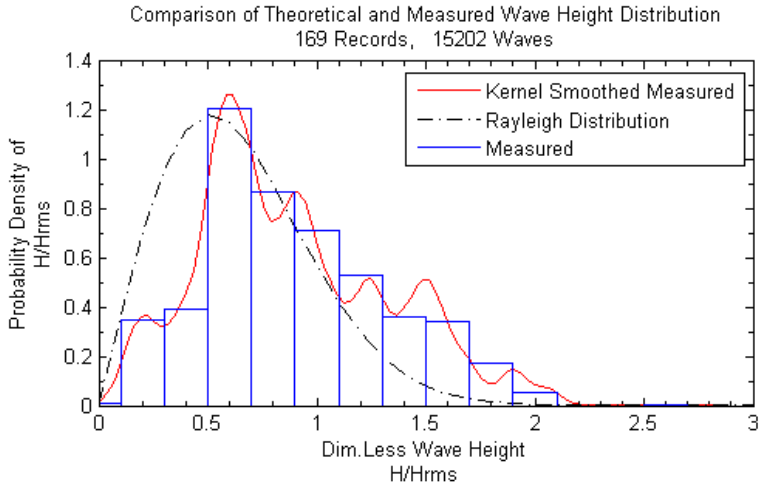

Figure 4: Rayleigh wave height distribution compared with measured wave height distribution obtained with WES

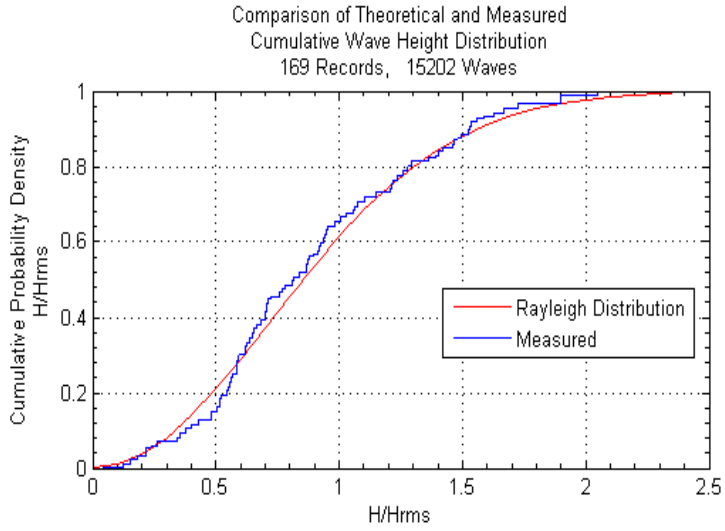

Figure 5: Rayleigh cumulative wave height distribution compared to measured distribution obtained with WES

The joint distribution of individual wave heights and periods is usually reported. This distribution helps in determining at which wave periods the highest waves occur. A dimensionless joint individual wave height period distribution is shown in figure 6 for a bimodal distributed sea state.

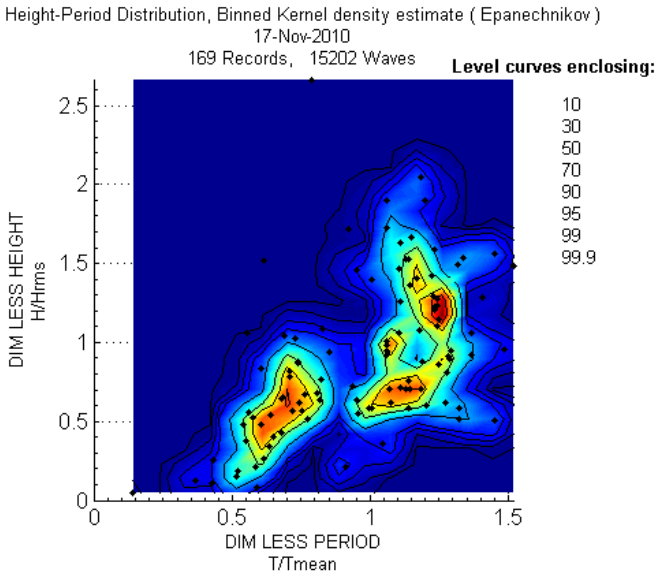

Figure 6: Joint Individual Wave Height-Period Distribution obtained with WES

2.5.2 Spectral Analysis

2.5.2.1 Spectral analysis based on the Fourier transform

The Fourier Transform

Given the fact that ocean waves appear as random phenomena, with different elevations and periods in a given wave field it makes it very hard to only characterize the "sea state" by the statistical definitions presented in previous chapter. In order to provide a more accurate description the ***linear wave theory,*** is used to model the sea as composed of a finite sum of random *linear waves* as depicted in equation 6 for the one dimensional case in a given location.

$$\eta(t) = \sum_{n=1}^{N} a_n \cos(\omega_n t + \phi_n)$$

Eq. (6)

Where **a** is the amplitude, ω is the angular frequency and ϕ is the phase defined as in *linear wave theory* as a random variable in between 0 and 2π. For convenience equation 6 can also be expressed as a time series X(t). Equations 6 and 7 are the same and represent a Fourier expansion.

$$X(t) = \sum_{n=1}^{N} a_n e^{(i\omega_n t + \phi_n)}$$

Eq. (7)

The spectrum of a wave record is obtained through the decomposition of the irregular water surface elevation signal into a series of sinusoidal components each with its associated frequency and elevation. After the decomposition of the original signal each component will have an associated unique frequency and amplitude. This analysis is very powerful since it shows in a condensed way the amount of energy present in the original signal per existing frequency (period) in the wave record. This analysis is one of the most important and of common use in coastal engineering and ocean engineering as in many other scientific fields. The spectrum S(ω) can be defined from equation 8, however to give a clearer picture equation 8 represents it as the summation of the amplitude squared over a range of angular frequency and its units are typical meters squared times second, m^2*s. The spectrum represents the amount of energy present in a given sea state per frequency bin.

$$S(\omega)d\omega = \sum_{\omega}^{\omega+d\omega} \frac{1}{2} a_n^2$$

Eq. (8)

The decomposition of the realizations of a stationary process, a time series, into a series of sinusoidal components can only be done if the time series dies out in time, given that the variance of time histories of measured waves is constant and they do not die out, the decomposition can only be done using the autocovariance function of the process, given that this function, the autocovariance, approaches to zero as time increases[11].

The variance spectrum of a stationary process X(t) with autocovariance $C_X(\tau)$ with the properties described above is then defined by the Fourier transform in equation 9.

$$S_X(\omega) = \frac{1}{\sqrt{2\pi}} \int_{-\infty}^{\infty} C_X(\tau) e^{-i\omega\tau}\, d\tau$$

Eq. (9)

G.H. Hardy showed in 1933 that the autocovariance $C_X(\tau)$ and the variance spectrum $S_X(\omega)$define the Fourier transform[13] with equation 10.

$$C_X(\tau) = \frac{1}{\sqrt{2\pi}} \int_{-\infty}^{\infty} S_X(\omega) e^{i\omega\tau}\, d\omega$$

Eq. (10)

[13] G.H. Hardy, "A Theorem Concerning Fourier Transforms". J. London Math. Soc . 8 (1933) 227–231

Equations 9 and 10 are known as the Wiener-Khintchine relations after their originators.

The factor $\frac{1}{\sqrt{2\pi}}$ is often only shown in the variance spectrum $S_X(\omega)$ as $\frac{1}{2\pi}$, which does not make a difference in the calculation however when calculating the variance spectra one should be clear where this factor is.

Different literature defines the quantity $S_X(\omega)$ with different names, energy spectrum, spectral density, power spectrum, etc… The name given here, the variance spectrum has been chosen after Naess 2007 recommendation since the variance is defined as autocovariance evaluated at τ=0:

$$\sigma_X^2 = C_X(0) = \int_{-\infty}^{\infty} S_X(\omega) d\omega$$

Eq. (11)

It is then clear, from equation 8, that the spectrum represents variance of the amplitudes in the wave record per frequency range.

For the present engineering analysis of data the one sided variance spectrum, defined as $S_X^+(\omega) = 2S_X(\omega), \ \omega \geq 0$, in the frequency domain f in Hertz as $S_X^+(f) = 2\pi S_X^+(\omega)$ will be used.

The spectrum of a measured time series is obtained by carrying out a harmonic analysis of the water surface profile $\eta(t)$, and finding the Fourier coefficients of a finite Fourier series defined in equation 11, A_n and B_n shown in equations 13 and 14.

$$\eta(t_k) = \frac{Ao}{2} + \sum_{n=1}^{\frac{N}{2}-1} \left(A_n cos\frac{2\pi n}{N} t_k + B_n sin\frac{2\pi n}{N} t_k\right) + \frac{A_{N/2}}{2} cos\pi t_k$$

Eq. (12)

$$A_n = \frac{2}{N} \sum_{t_k}^{N} \eta(t_k) cos\frac{2\pi n}{N} t_k$$

Eq. (13)

$$B_n = \frac{2}{N} \sum_{t_k}^{N} \eta(t_k) sin\frac{2\pi n}{N} t_k$$

Eq. (14)

This process is done by the software routine provided by WAFO, dat2spec, using a Parzen window as smoothing function. A variance spectrum with its associated time series is shown in figure 7.

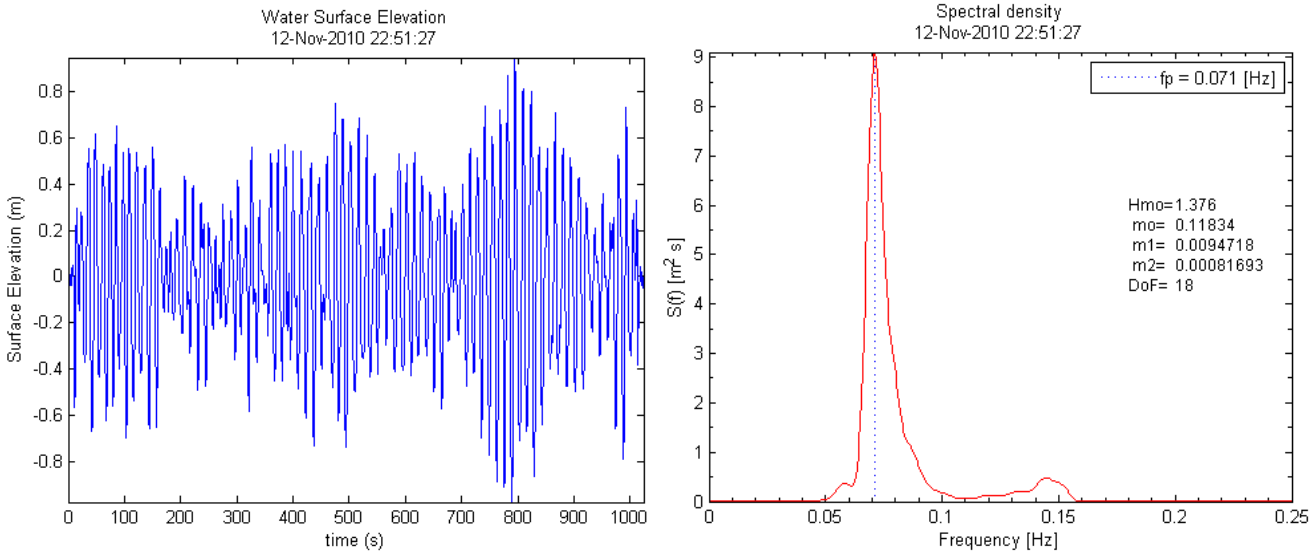

Figure 7: Variance spectrum for a given time series

Spectral Values derived from the Variance Spectra

One of the main advantages that the spectral analysis, done with the fast Fourier transform, has over other existing methodologies is that descriptive quantities of the "sea state" can be directly obtained from the variance spectra. The spectral shape is very important in engineering applications, wave group formation is more pronounced in narrow sharply peaked spectrum, when the spectrum is used for calculating response spectra given transfer functions the shape of the spectra may under estimate the forces of oscillating structures tuned to peak frequency conditions[14].

The Spectral Moments are some of these quantities. The spectral moments are defined by equation 15, for k=-2,-1,0,1,2,3, and 4.

$$m_k = \int_{f=0}^{\infty} f^k S(f) df$$

Eq. (15)

Since the spectral moment m_0 represents the variance of the water surface elevation, $\sigma = \sqrt{m_0}$, given the definition of the spectrum, equation 8, it can be related to the significant wave height as:

$$H_s = H_{mo} = 4\sqrt{m_0}$$

Eq. (16)

[14] Rye, Henrick "The Stability of some currently used wave parameters" Coastal Engineering, 1(1977) 17-30.

The mean wave period, T_z in angular frequency or T_{mo2} in Hertz is also obtained from the spectral moments as:

$$T_{m02} = \sqrt{\frac{m_0}{m_2}} \quad , \bar{T_z} = 2\pi\sqrt{\frac{m_0}{m_2}}$$

Eq. (17)

Furthermore the peak spectral period, Tp, is defined as the inverse of the frequency where the highest energy is found. When a spectra is obtained from real waves it is common to obtain several spectral peaks. These peaks can be related to different sea state conditions occurring at the same time, e.g. short wind waves and swell at the same time, hence two peaks are obtained. In the present work the highest energy peak is reported with the lowest and highest frequency peak found.

More recently, in the design of coastal structures, given the importance of the lower frequency energy has in the shallow water, the period Tm0-1 has been defined as in equation 18, with the argument that it is better descriptor than the mean or peak spectral period[15].

$$T_{m0,-1} = \sqrt{\frac{m_0}{m_{-1}}}$$

Eq. (18)

The parameters mention above, the first moment wave height H_{mo}, the peak spectral period Tp, the mean wave period T_{m02}, and the energetic period T_{m0-1} in combination with the maximum wave height are typically used to characterize the spectral characteristics of the ensemble of wave time series measurements, such a representation is given in figure 8 from the developed software WESS.

Given the fact that the spectra does contain much more information of the "sea state", several parameters have been defined to characterize the "type" of spectra hence the type of sea state, as spectral width parameters ε, ν and the spectral peakedness Q_p . These parameters are given by equations 19, 20 and 21 respectively. These parameters can be used to compare the statistical theories of sea waves with the analyzed data[16]. These parameters are also useful as a descriptive tool of other wave phenomena as grouping or bound long presence in the field.

Since the Rayleigh distribution is intended to be applied to narrow-banded spectra Cartwright and Longuet-Higginns introduced the index of spectral bandwidth ε shown in equation 18. The closer ε to 0 the narrower the spectra, while it can be considered white noise if it is equal to 1.

[15] Verhagen, VanVledder, EslamiArab, "A PRACTICAL METHOD FOR DESIGN OF COASTAL STRUCTURES IN SHALLOW WATER" Delft Technical University, 2008.
[16] Goda, Yoshimi, "Random Seas and Design in Maritime Structures", 2000.

$$\varepsilon = \sqrt{1 - \frac{\overline{T_p^2}}{\overline{T_z^2}}} \qquad \varepsilon = \sqrt{1 - \frac{m_2^2}{m_0 m_4}}$$

Eq. (19)

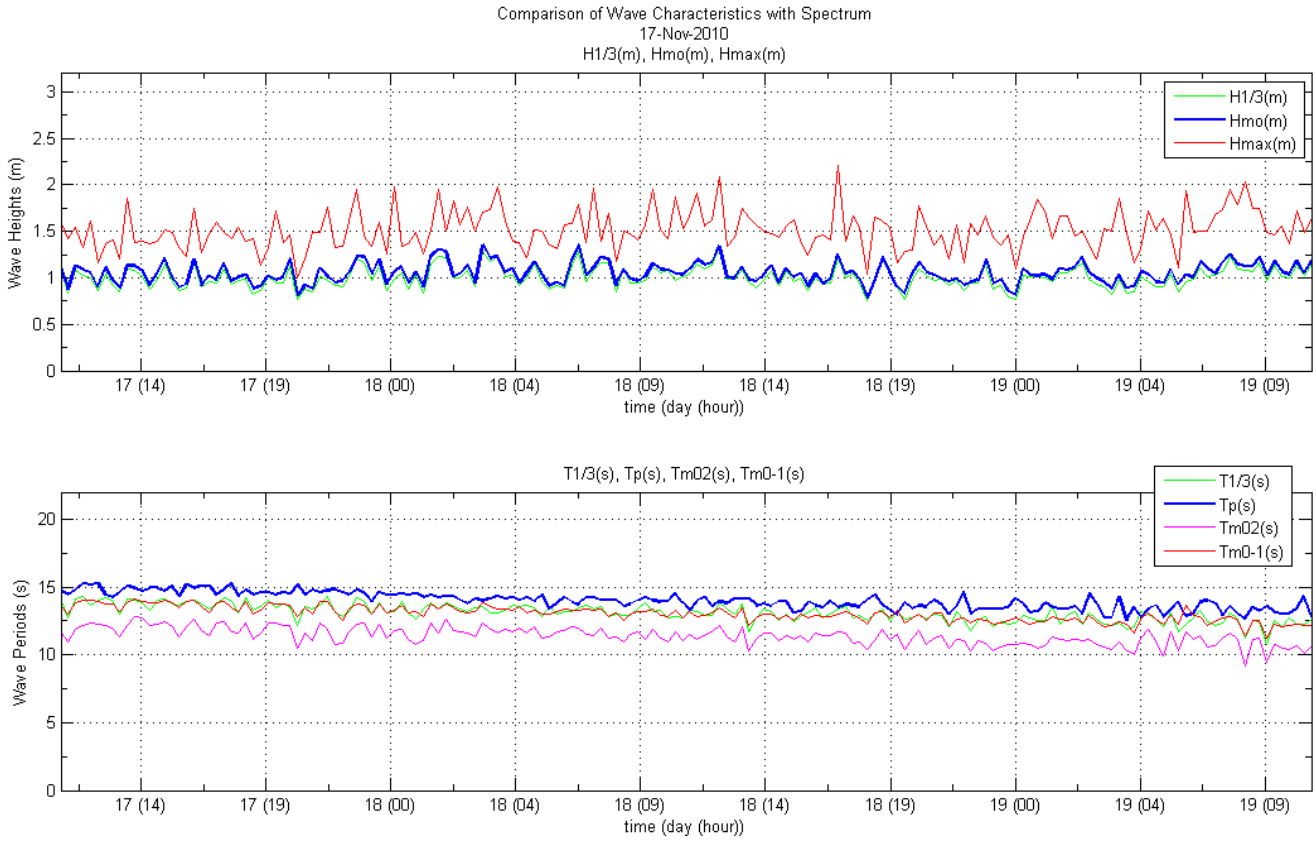

Figure 8: Spectral Characteristics obtained from WES

Longuet-Higgins also introduced the parameter ν to characterize the narrowness of the spectral bandwidth defined in equation 19.

$$\nu = \sqrt{\frac{m_0 m_2}{m_1^2} - 1}$$

Eq. (20)

Goda 1970 proposed the parameter Qp, shown in equation 21, to describe the "peakedness" of the spectral peak. Qp takes values of 5 to 8 for long travelled swell and 2 to 3 for wind waves. This parameter can be related to the groupiness of the wave conditions measured. The spectral peakdness parameter, Qp, takes the value of 1 for

white noise, the value of 2 for the Person-Moskowitz spectra, the value of 3.13 for a JONSWAP spectrum with γ equal to 3 and 5.57 for a JONSWAP spectra with γ equal to 10.

$$Q_p = \frac{2}{m_0^2}\int_0^\infty fS^2(f)df$$

Eq. (21)

According to Rye (1981) Qp is the only parameter which is not dependant on the high-frequency cut-off choice, and it distinguishes very well the peak sharpness. Rye recommends applying Q_p rather than ε, or ν when characterizing a spectrum[17]. He showed that these other parameters including T_{mo1} and T_{mo2} are unstable to the cut off frequency used to evaluate them. The cut off frequency refers to the highest frequency used in the calculations, which in the case of waves measured with a pressure sensor are going to be related to the depth of the pressure sensor.

Rice (1944) had proposed the parameter alpha, a, which is coupled to the narrowness of the spectrum[18].

$$\alpha = \frac{\frac{1}{2\pi}\sqrt{\frac{m_2}{m_0}}}{\frac{1}{2\pi}\sqrt{\frac{m_4}{m_2}}}$$

Eq. (22)

Alpha is equal to the expected number of mean level up crossings per time unit divided by number of local maxima per time unit, alpha is the number of maxima per wave, the smaller alpha the more irregular is the sea state, if high frequency components are present, alpha is small and the sea state is "rippled"[19].

The wave groupiness has also been related to the spectrum. Ka, κ, attempts to measure to what extent high local extremes come in groups. It is related to the envelope behavior[20].

$$\kappa = \frac{1}{m_0}\left|\int S(\omega)e^{i\omega T_{m02}}d\omega\right|$$

Eq. (23)

[17] Rye, Henrik, "The stability of some currently used wave parameters", Coastal Engineering, 1 (1977) 17-30
[18] Cartwright & Longuet-Higgins: The statistical distribution of the maximum of a random function (Proc Royal Soc of London, Ser A) vol 237, pp 212-232, 1956
[19] Professor Georg Lindgren, email personal communication, Lund University of Mathematics, Sweden 2010.
[20] Tucker, M.J.: Recommended standard for wave data sampling and near-real time processing. Ocean Engineering, vol 20, pp 459-474, 1993

Mathematically κ is equal to the ratio |r(Tm02)|/r(0), k is the correlation between two values in the wave process, taken at a time Tz apart. If Ka is near one it means that a very high peak has a tendency to be followed by a very low value after a time lag Tz, (usually r(Tz)<0, in the North Sea), and another high value after another time lag Tz. The low value may be a local minimum and the high value a local maximum, they do not be to be exactly local minima or maxima[21].

The above parameters are calculated for the time series wave ensemble by WESS using the function spec2char of WAFO. An example output of such calculation is shown in figure 9.

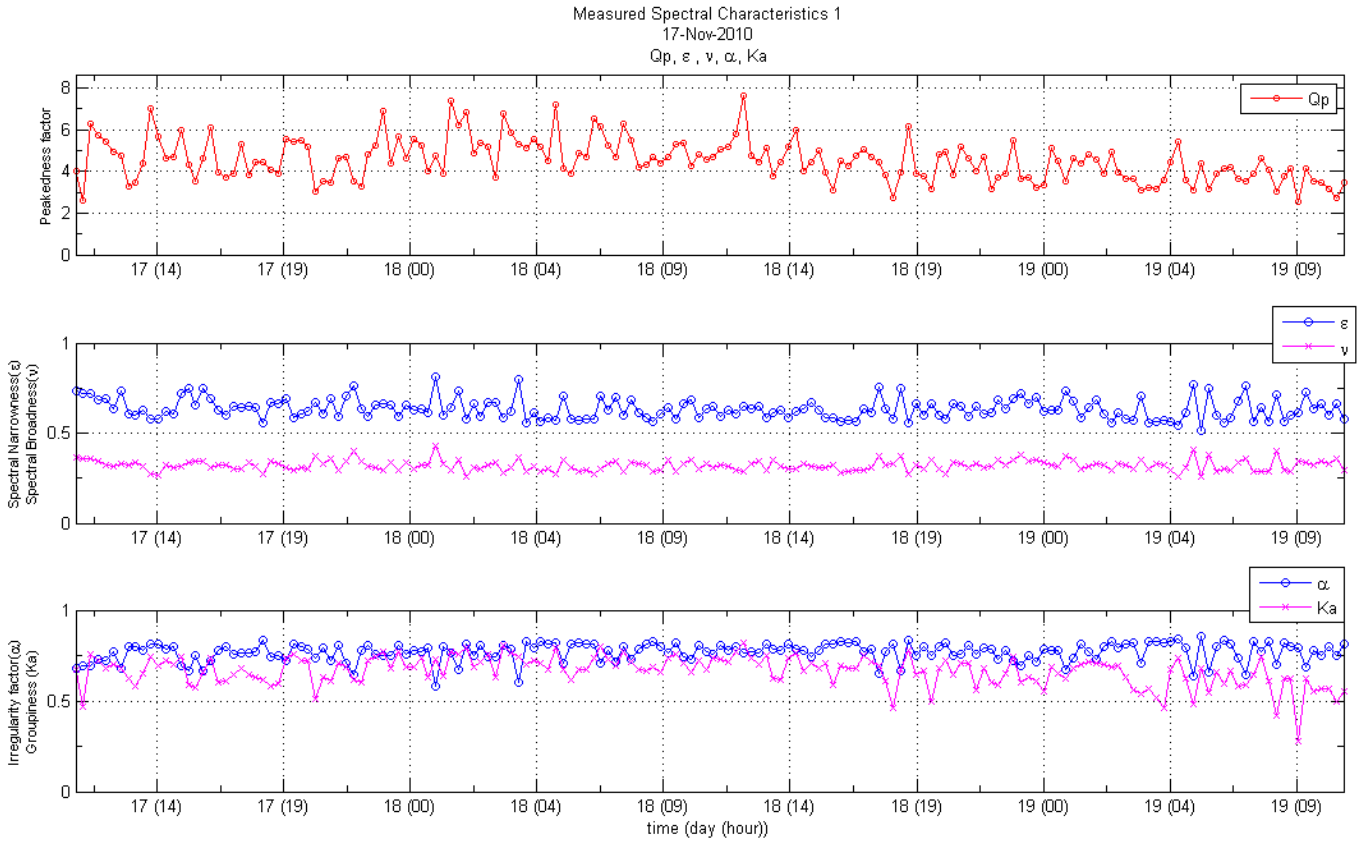

Figure 9: Temporal Spectral Derived Parameters obtained from WES

Even though with the above spectral parameters description, a true representation of the energy distribution during the whole measurement period, the ensemble of spectra, gives a better picture of content of wave energy per frequency varying in time. Snodgrass, Groves, Hasselmann, Miller, Munk and Powers, used such representations to study the propagation of swell across the pacific[22]. During their study in 1966 they analyzed

[21] Igor Rychlik, Mike Lin, Georg Lindgren, " Markov based correlations of damage cycles in Gaussian and non-Gaussian loads". Probabilistic Engineering Mechanics, vol 10, pp 103-115, 1995.

[22] F. E. SNODGRASS, G. W. GROVES,, K. F. HASSELMANN, G. R. MILLER, W. H. MUNK AND W. H. POWERS, "Propagation of Ocean Swell across the Pacific", Philosophical Transactions of the Royal Society of London. Series A, Mathematical and

wave measurements in New Zeeland, Samoa, Palmyra, Hawaii and Alaska. Using the spectral time variation of measured events they recognized that waves lose their energy primarily in the generation zone, were as during their travel across the pacific the attenuation was lower, they also observed a background spectra in the whole Pacific.

The temporal spectral variation is obtained with the developed software WESS using the dat2spec function of WAFO, figures 10 and 11 show the output obtained.

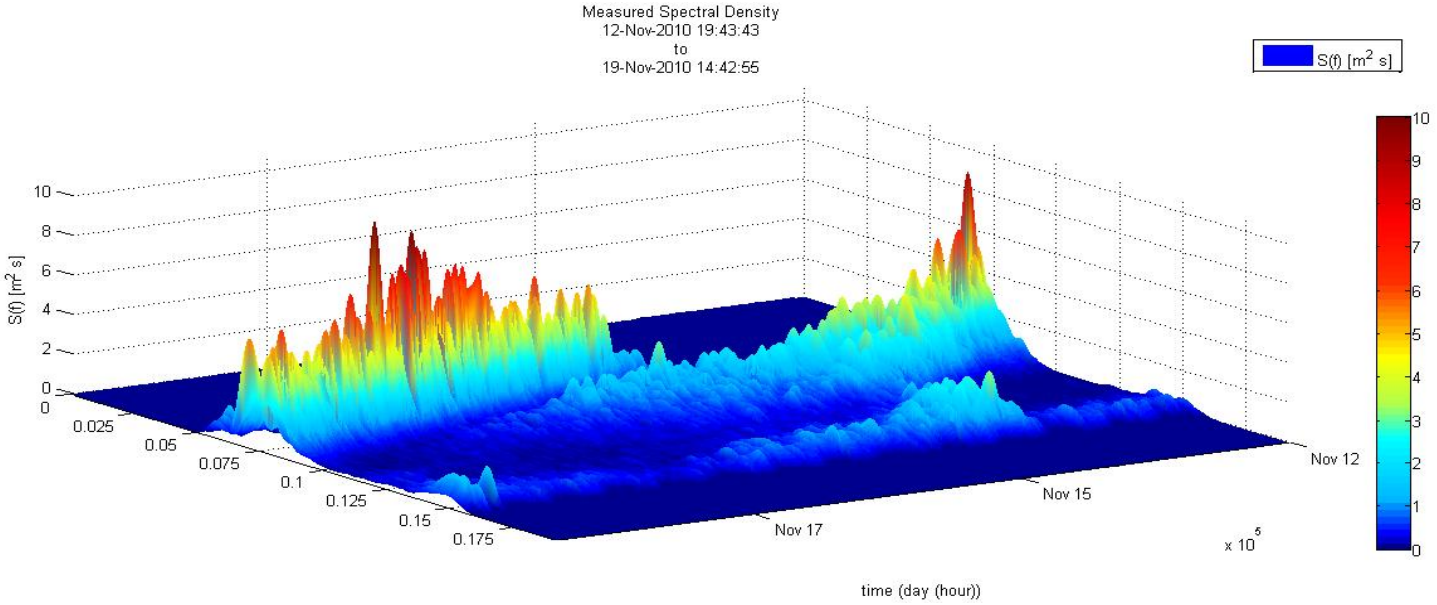

Figure 10: 3D Temporal spectrogram (spectral energy-frequency-time) variation obtained with WESS

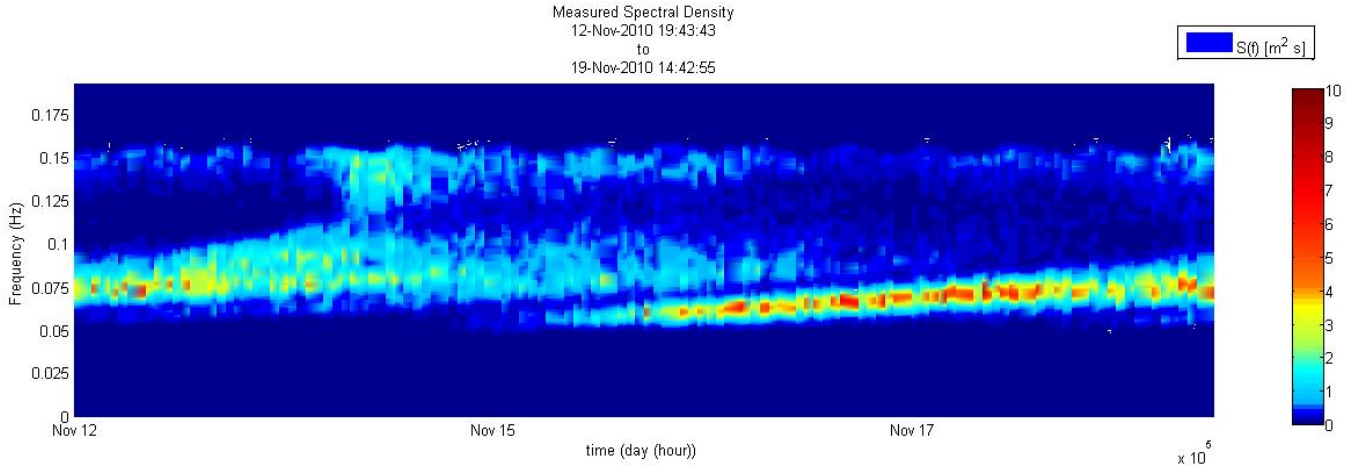

Figure 11: Temporal Spectral Variation obtained from WES

Wave Spectral Formulations

Another of the main advantages of the spectral analysis of a wave record is the fact that previously different "sea states" have been analyzed and fitted to functions that relate the function, defined as "spectral shape", to basic parameters as it might be wind speed, significant wave height and peak spectral period, or to storm development stage, meaning wave conditions within the generation zone, fully developed seas or swell conditions. This parametric representation of a given sea state are currently used to carry out physical and numerical modeling, in some cases without in depth thought of their physical meaning and background.

Many different types of spectral functions have been proposed and are available in the literature. One of the most commonly used and oldest is the Pierson-Moskowitz spectrum. Even though the original proposed spectrum was based on wind parameters[23], the Pierson-Moskowitz spectrum has been modified in order to be a function of the significant wave height and peak spectral frequency, the commonly used form of this spectrum is given by equation 24.

$$S(f) = \frac{5}{16 f^5} H_{mo}^2 f_p^4 e^{-\frac{5 f_p^4}{4 f^4}}$$

Eq. (24)

The Joint North Sea Wave Program spectrum was later proposed based on the Pierson-Moskowitz spectrum by Hasselman 1973, after analyzing series of data collected in the North Sea. The spectrum proposed incorporates an enhancement factor γ for wave-wave interaction over long distances and further development of the spectrum[24]. The JONSWAP spectrum is given in equation 25 and it is shown compared to the Pierson-Moskowitz spectrum in figure 3.

$$S(f) = S_{PM}(f)\gamma^{e^{\left[\frac{-(f-f_p)^2}{(2\sigma^2 f_p^2)}\right]}}$$

Eq. (25)

Where S_{PM} refers to the Pierson-Moskowitz spectrum, γ is enhancement parameter, σ=0.09 for f>fp. In the present work the JONSWAP will be used as a comparison tool with the spectra obtained from the analyzed measurements given its wide application in coastal engineering and for comparison purposes with previous research.

[23] Pierson, Willard J., Jr. and Moskowitz, Lionel A. Proposed Spectral Form for Fully Developed Wind Seas Based on the Similarity Theory of S. A. Kitaigorodskii, *Journal of Geophysical Research*, Vol. **69,** p.5181-5190, 1964

[24] Hasselmann, Measurements of wind-wave growth and swell decay during the joint North Sea wave project (JONSWAP)., 1973.

The enhancement parameter was found to have values up to 7 when the JONSWAP spectra was developed, however this spectra have been used to fit long travelled swell data, with a good fit of the data Goda (1981), and a γ enhancement parameter of 9 and higher was reported. Given the fact that this parameter has been previously used to characterize measured waves of long travelled swell, the JONSWAP spectrum will be used in the present work.

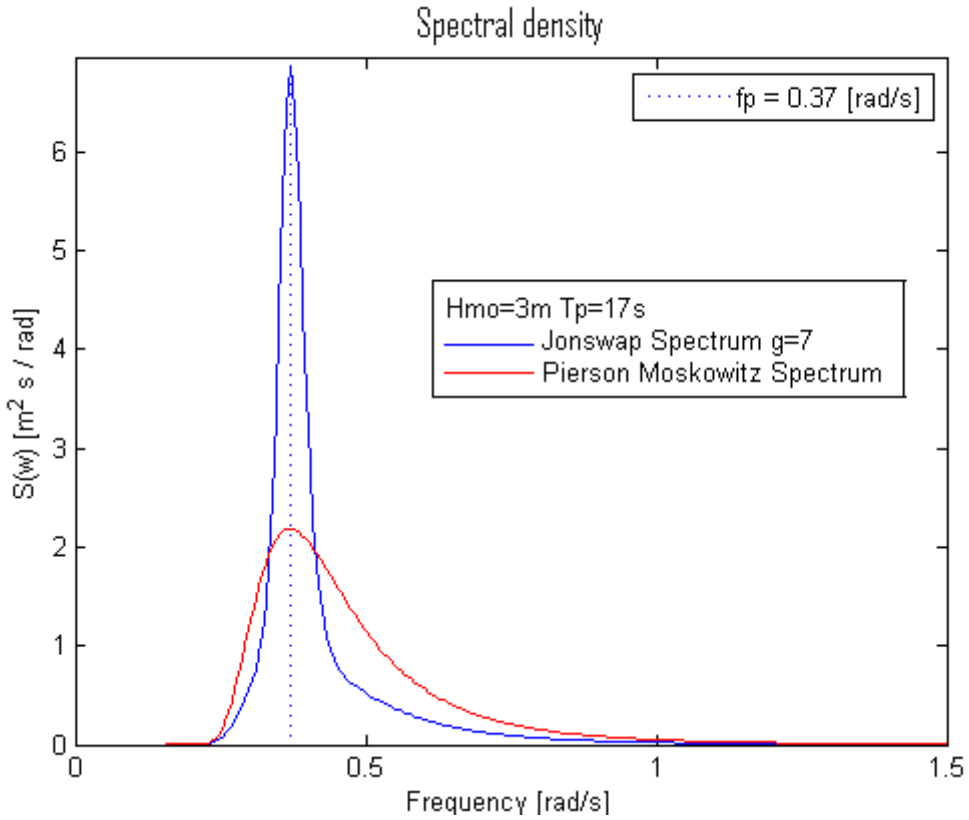

Figure 12: Typical JONSWAP AND Pierson Moskowitz Spectrum

Rye (1977) found a relationship between the enhancement parameter γ and the spectral peakdness parameter Qp, he summarized the relationship as:

γ = 1.00 3.30 7.00

Qp =2.00 3.15 4.65

In the present study the correlation between these two parameters has been examined.

The Pierson Moskowitz spectrum corresponds to a JONSWAP spectrum when the enhancement factor γ is equal to 1. Both spectrums can be correlated by means of this enhancement factor as shown in figure 13. Where Spm max refers to the peak spectral energy of the Pierson Moskowitz spectrum, and Smax the real spectral energy

peak. This relation was used to obtain the equivalent γ enhancement parameter for the real measured spectrum. First the significant wave height and peak period were obtained for the measured spectrum, then the equivalent Pierson Moskowitz spectra was calculated, then the ration between the peak energy of the measured spectra and the calculated Pierson Moskowitz spectra was used to determine the equivalent γ. This was done to all the measurements using the developed software WES and WAFO wich was modified to accept γ values higher than 7, and example out of such a adjustment for swell waves is shown in figure 14.

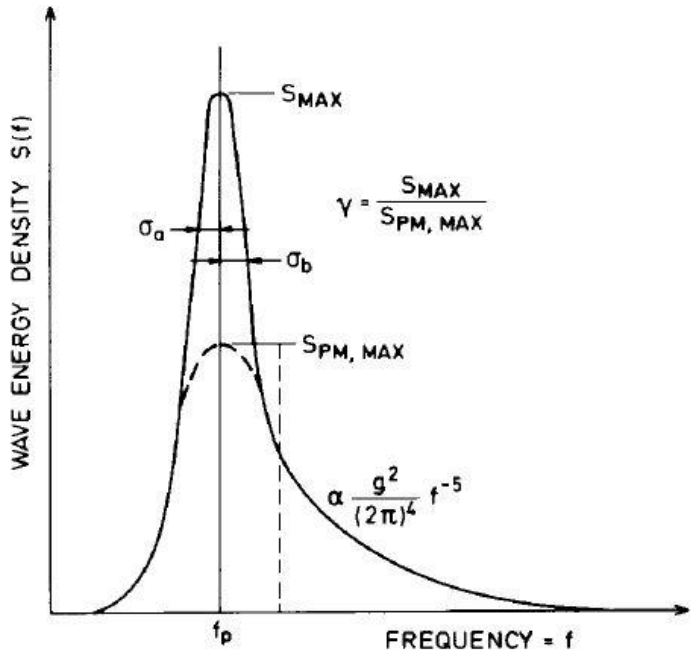

Figure 13: Typical JONSWAP Spectrum Rye (1977)

Apart from the Pierson Moskowitz and the JONSWAP spectra many other synthetic spectral functions have proposed. Including double peaked spectra as the Torsethaugen spectrum, TMA spectrum that corresponds to a JONSWAP spectrum modified for limited depth conditions and the six parameter bimodal Ochi and Hubble spectrum. These other spectral functions were not used in present work due to time limitations, nevertheless future research and fit of measured data to these different spectra is highly recommended.

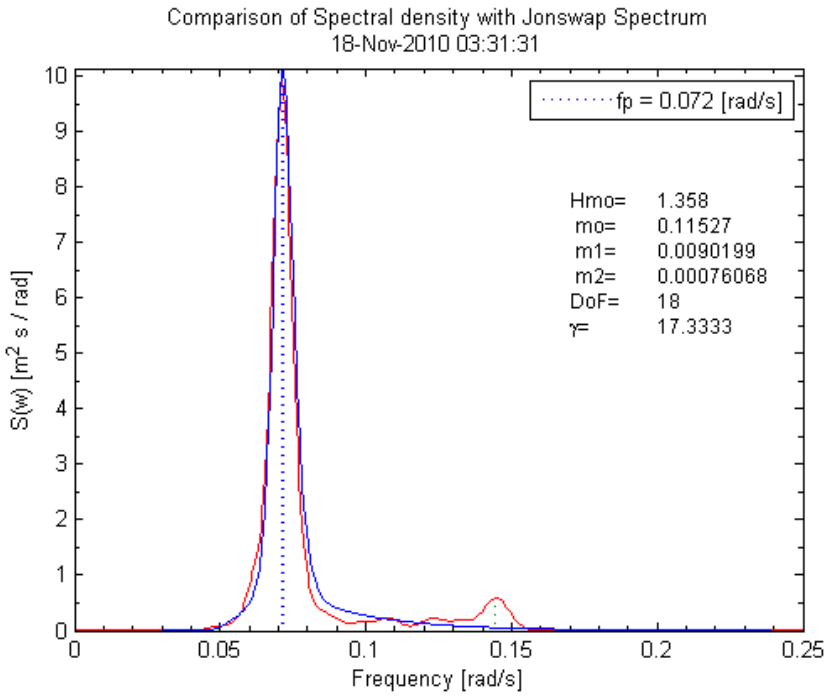

Figure 14: Fit of Measured Spectrum to a JONSWAP Spectrum.

Spectral Resolution, Spectral Shape and Accuracy

The previously defined spectral parameters and spectral functions are all dependant on calculations done to obtain the spectrum. The spectral shape obtained in the calculations will vary considerably depending on the degree of resolution used when carrying out the calculations. Typically when calculating spectra from measurements smoothing functions are also applied, these smoothing functions affect the degree of resolution, which is inversely proportional to the degree of freedom. The variation of the degrees of freedom will modify the spectrum shape, including the number of peaks found in the spectra. The different shapes affect significantly the spectral parameters obtained from the spectra since they are dependent on the energy distribution of the given spectra[25].

The number of degrees of freedom from a spectrum depends on the N number of points in the record, Δt, the measuring interval and M, the number of lags by:

$$DF = \frac{2N - \frac{M}{2}}{M}$$

Eq.(26)

[25] Chakrabarti S. and Cooley R. "The stability of some currently used wave parameters – a discussion", Coastal Engineering, 1(1977) 359-365

The frequency resolution is then defined as:

$$\Delta f = \frac{1}{2M(\Delta t)}$$

Eq.(27)

Chakrabarti and Cooley (1977) found that the spectral parameters and average periods show large variations with different values of frequency cut off and degrees of freedom used when calculating the spectra. They recommended that any statistical parameters obtained from wave energy density distribution should appear with their associated degrees of freedom and cut off frequency used.

In the present study a Parzen window was used as a smoothing function over the covariance calculated spectrum. The associated degrees of freedom were calculated for each spectral estimate and reported. The cut off frequency was estimated by the WAFO function dat2spec. No low frequency cutoff was used.

The effect of using different degrees of freedom when calculating the spectrum is showed in figures 15. It can be seen that the amount of energy is distributed very different when the degrees of freedom are changed. This value is very important depending on our target frequency range of interest, when the frequency resolution is lower, larger Δt, lower frequency phenomena can be analyzed. We need from 4 to 0.5 Hz to analyze gravity waves (Periods from 1 to 30 second), while we need 5 to 10 minutes to analyze tides (Periods from 3 to 24 hours).

Figures 15 show the calculated spectra for a given sea state varying the degrees of freedom in the calculation. The smoothest spectra, upper left corner, was calculated with 75 degrees of freedom, while the sharpest one, lower right corner, was calculated using 3 degrees of freedom. The effect on the first moment is low, however the effect of the used degrees of freedom for the calculation increases with the higher order moments. The second moment shown in the figures varies from 0.00459 to 0.00338 for 75 and 3 degrees of freedom. The spectral parameters that depend on the higher order moments will be more susceptible to the degrees of freedom used in the spectral calculation. For the analyzed case given the observed variation in the second moment due to the variation in the degrees of freedom the mean spectral period would vary in the extreme case between 13.73 and 11.78 seconds. The peak frequency also varies greatly with the used spectral resolution; this has large implications on the JONSWAP peak enhancement parameter used, the obtained Qp and it clearly shows why this value should always be indicated when analyzing real measured data.

For the present study the degrees of freedom used varied between 9 and 18 for the gravity wind waves, for the long wave analysis the degrees of freedom varied between 3 and 6, nevertheless the length of the wave records affected significantly the results.

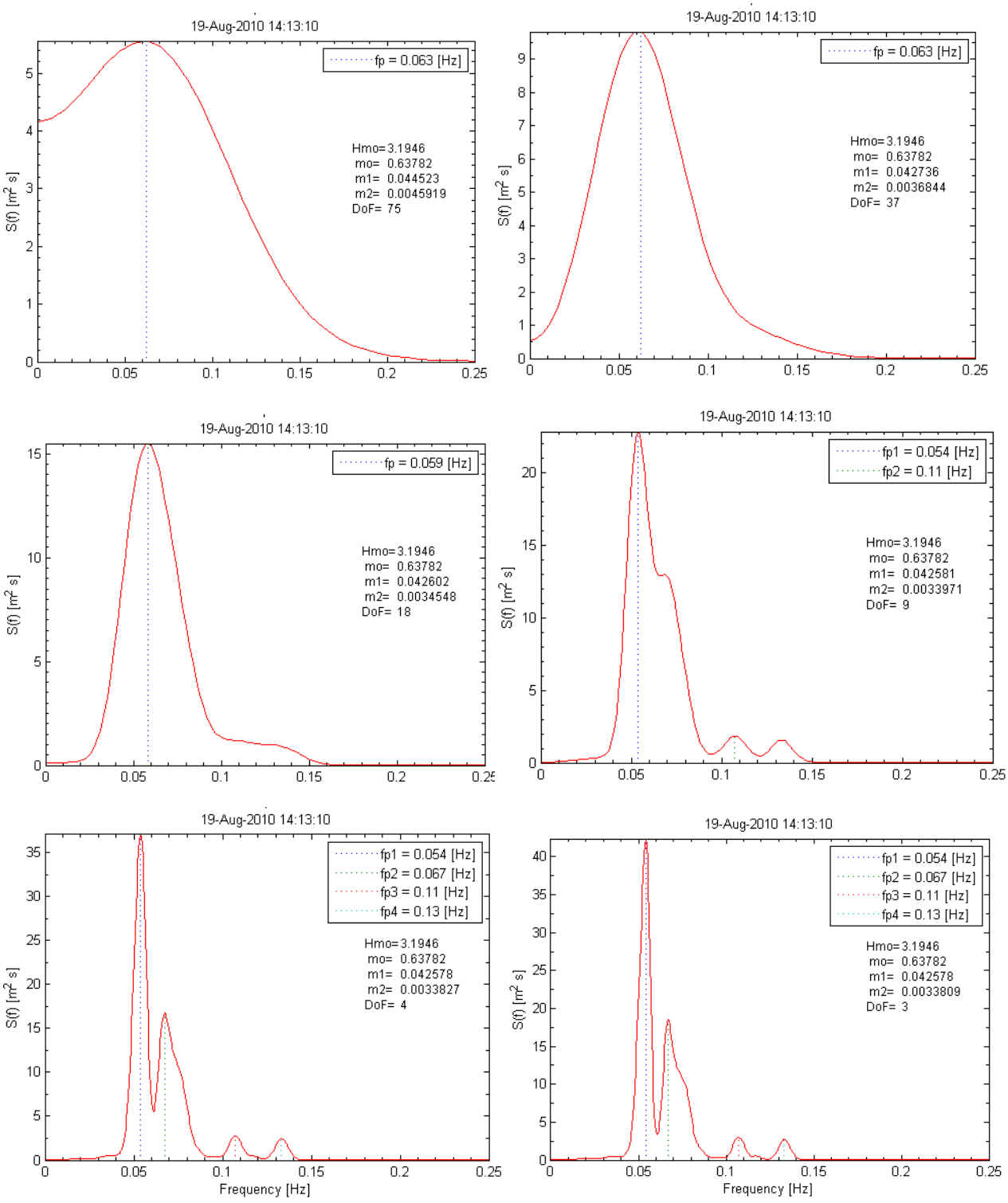

Figures 15: Effect of the degrees of Freedom on Spectral Calculation.

Limitations of the Fourier Transform Variance Spectra

Even though the different proposed functions to represent the variance spectra of ocean waves are very practical; they have important limitations that should be considered. When the spectra is obtained using the Fourier Transform from non-linear or a non-stationary waves the Fourier transform requires additional harmonic components to simulate the data.

The sea surface profile presents asymmetry with respect to mean water level, the grouping phenomena challenges the stationary requirement of the Fourier transform, furthermore in shallow water waves present a steep front and mild back part[26].Since high storm waves, shallow water waves, and swells present non-linearity or appear in groups the spectra obtained with the Fourier transform induces spurious harmonic components to appear. This can lead to a misleading energy-frequency distribution. The spurious harmonic components include the bound long wave representation within the spectra, which is not an accurate representation of the frequency energy distribution. Goda (1983) reported the appearance of these spurious harmonics in the spectra due to the nonlinear conditions of the analyzed long travelled swell in the Pacific coast of Costa Rica. Spurious harmonic components obtained in the spectral analysis, sub-harmonics and super-harmonics appeared with secondary peak frequencies of 0.008 and 0.11 Hz (125 and 9 seconds) respectively. Goda recommended ignoring these secondary frequencies.

The application of the Fourier transform is then limited to the area where the linear theory is applicable. Mehaute (1969) reviewed the validity of various wave theories, his results are presented in figure 16. The bound long wave phenomenon is not included in the linear theory.

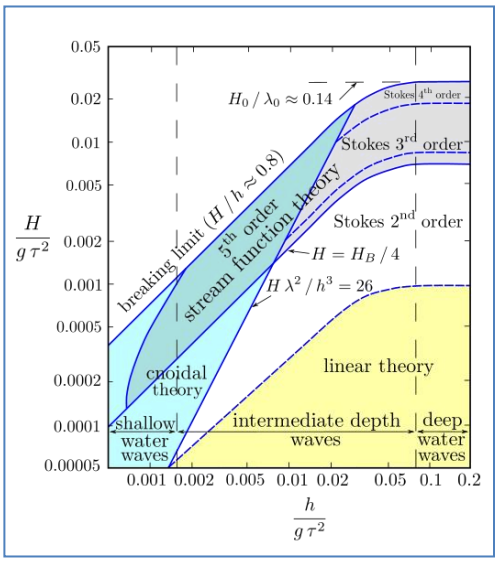

Figure 16: Validity of Wave Theories Mehaute (1969). http://en.wikipedia.org/wiki/Cnoidal_wave

[26] Bosboom J., Stive M.J.F, "Coastal Dynamics" Lecture Notes CT4305, Delft Technical University, 2010.

Furthermore long travelled swell can present large asymmetries as shown in figure 17, which are hard to model with the linear theory, or harmonic solutions.

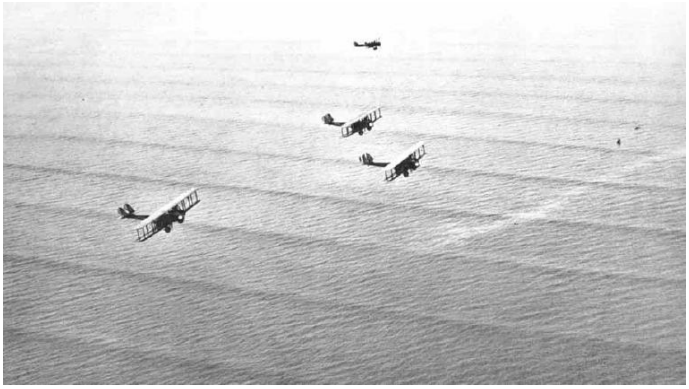

Figure 17: Swell waves near Panama 1933. http://en.wikipedia.org/wiki/Cnoidal_wave

It is clear then that the spectral analysis based on the Fourier transform, which uses the linear wave theory has very important limitations. Nevertheless this tool has proven to be effective during the last 50 years in the development of our understanding of the ocean waves processes, but given the imminent limitations, consideration of methods to incorporate the non-linear and non stationary reality of ocean waves should be investigated and considered to further improve our understanding of the real physical phenomena.

2.5.2.2 Spectral analysis based on the Hilbert Huang transform

Given the clear limitations that the Fourier transform has, other methods have been proposed. One characteristic of these methods is that they include the time variable in order to account for non-stationary phenomenon in the signal. The Morlet wavelet method is one of them, however it is also based on the Fourier transform, with all its inherent limitations. This method will not be discussed further. The Hilbert transform, introduced by David Hilbert in 1905, has previously been used in the analysis of signals that are not stationary since it provides frequency-energy time description of the signal. The application of the Hilbert transform had been highly limited due to the fact that its analysis is restricted to cases where no "riding waves" within the signal exist. Filter methods have been proposed in order to avoid this problem, however removing the riding waves will highly limit the analysis since part of the existing physical phenomena is being eliminated. If this riding waves are not treated somehow the Hilbert transforms produces negative "instantaneous frequencies" which nave no physical meaning at all. The Hilbert transform Y(t), of a realization X(t) is defined as:

$$Y(t) = \frac{1}{\pi} P \int_{-\infty}^{\infty} \frac{X(t')}{t - t'} dt'$$

Eq. (28)

Where P is the Cauchy principal value. The Hilbert transform is the convolution of the X(t) with 1/t. With the Hilbert transform X(t) and Y(t) form a complex conjugate pair, defining Z(t) as:

$$Z(t) = X(t) + iY(t) = a(t)e^{i\theta(t)}$$

Eq. (29)

In equation 29 a(t) is the amplitude and θ(t) is the phase angle at a given time t, defined by equation 30.

$$a(t) = \sqrt{X^2(t) + Y^2(t)} \quad , \quad \theta(t) = \arctan \frac{Y(t)}{X(t)}$$

Eq. (30)

Using equation 31, the instantaneous frequency is defined as:

$$\omega = \frac{d\theta(t)}{dt}$$

Eq. (31)

The concept of instantaneous frequency is highly controversial[27]. The fact that, in the Fourier analysis, the frequency is defined from the sine or cosine function that is present through out the whole duration of the realization X(t) with a constant amplitude has lead to the definition of the frequency as the oscillation of one full wavelength. Hence in the Fourier spectra, the energy reflected per frequency bin denotes its presence through out the whole duration of the signal. As Huang (1998) points this does not make sense for non-stationary data.

Even with stationary data, if we consider non-linear asymmetric waves where the fronts are steep and the back is larger and milder, two frequencies would exist within one wave, a faster frontal part and a slower back part. These two frequencies cannot be obtained through the traditional Fourier transform. The instantaneous frequency, defined in equation 26, can represent this frequency shift.

The Empirical Decomposition Method

Huang (1998) proposed a new method to analyze the time series, without filtering information out, to obtain a well behaved Hilbert transform. This method is called the empirical mode decomposition EMD. The empirical mode decomposition method extracts the "intrinsic mode functions" of the time series which guaranties a well behaved Hilbert transform. The name Hilbert Huang transform was designated by NASA to the combination of the Empirical Decomposition Method and the Hilbert Spectral Analysis. The main concept of the Empirical Decomposition method is identifying the riding waves by finding the trend that represents the mean local average.

An intrinsic mode function must satisfy two conditions in order to guaranty a well behaved Hilbert transform. (1) The number of extrema and of zero crossings must be equal or differ at most by one in the whole data, and (2) the mean value of the envelopes of the local maxima and the envelope of the local minima must be zero. In this way within an intrinsic mode function the instantaneous frequency will not shift due wave asymmetries. According to Huang (1998) the intrinsic mode function represents the oscillation mode imbedded in the data.

The empirical mode decomposition method is a sifting process with which we can extract the intrinsic mode functions embedded within the time series. The sifting process serves to eliminate riding waves and to make the data more symmetric. Huang proposed to use the time lapse between successive extrema as the definition of the time scale of the intrinsic oscillation mode. Once these extrema points have been identified an upper envelope is defined by connecting the maxima points with a cubic spline. The same process is repeated with the minima points producing a lower envelope.

Schlurmann proposes to incorporate additional interior points such as, interior inflection points, interior extrinsic curvature extrema points and interior characteristic points derived by the minimum value theorem. Furthermore he recommends the incorporation of additional boundary data points following the slope between previous maxima and minima and distanced at the same interval between previous maxima or minima respectively. These

[27] Huang, N. "The empirical mode decomposition and the Hilbert spectrum for nonlinear and non-stationary time series analysis". The Royal Society London, 1998.

recommendations improve substantially the spline fitting and eliminate large swings of the envelope splines near the ends[28].

Once the upper and lower envelopes of the data have been obtained their mean value $\bar{m}_1$ is obtained. The first component of the data is the defined as:

$$X(t) - \bar{m}_1 = h_1$$

Eq. (32)

The newly obtained data h_1 is then inspected to determine if it satisfies the two previously defined conditions of an intrinsic mode function. If the data does not meet the conditions of an intrinsic mode function then the sifting process is repeated using h_1 as the data, and obtaining the cubic spline upper and lower envelopes for h_1 and defining a second component as shown in equation 33.

$$h_1 - \bar{m}_{11} = h_{11}$$

Eq. (33)

The process is repeated until the obtained difference h_{1k} meets the conditions of an intrinsic mode function. This defines the first intrinsic mode of the data.

$$h_{1(k-1)} - \bar{m}_{1k} = h_{1k} \qquad \text{Eq. (34)}$$

Here h_{1k} is the first intrinsic mode c_1, which contains the lowest frequencies of the signal.

Huang introduced a stopping criterion for the sifting process to end in order guarantee that the intrinsic mode functions retain physical sense of amplitude and frequency modulations. He proposed limiting the standard deviation from two consecutive sifting results between 0.2 and 0.3. The standard deviation is defined by equation 35.

$$SD = \sum_{t=0}^{T} \left[\frac{\left| (h_{1(k-1)}(t) - h_{1k}(t) \right|^2}{h_{1(k-1)}^2(t)} \right]$$

Eq. (35)

The process is then repeated obtaining the remaining intrinsic mode functions of the system as:

$$X(t) - c_1 = r_1$$

Eq. (36)

[28] Schlurmann T., Datig M., "Performance and limitations of the Hilbert-Huang transformation (HHT) with an application to irregular water waves". Ocean Engineering nro 31, 2004.

In equation 36 r_1 is the residue after the extraction of the first intrinsic mode of the function, which contains information of the longer periods within the data. This residue is then treated as the new data and the sifting process is repeated until the residue r_n is sufficiently small to predetermined value or when it becomes a monotonic function in which no intrinsic mode function can be extracted.

The obtained intrinsic mode functions are then unique and specific for particular time series; they are obtained from the local characteristics of the signal. After the empirical decomposition process we can represent the original data by equation 37.

$$X(t) = \sum_{j=1}^{n} c_j + r_n$$

Eq. (37)

The obtained intrinsic mode functions are then checked for orthogonality. Huang proposes the following index of orthogonality.

$$IO = \sum_{t=0}^{T} \left(\sum_{j-1}^{n+1} \sum_{k=1}^{n+1} \frac{C_j(t) C_k(t)}{X^2(t)} \right)$$

Eq. (38)

To exemplify the process figure 18 presents a time history X(t) of a wave surface elevation record. The wave measurements correspond to 2048 continuous samples at 1 Hz, which corresponds to approximately 38 minutes. Several wave groups are visible in the record, the wave conditions were calm. The data was decomposed through the empirical decomposition method. Figure 19 shows the obtained intrinsic mode functions after applying the empirical mode decomposition. A total of 10 intrinsic mode functions were found. The reduction in the associated frequency to each intrinsic mode function is visible.

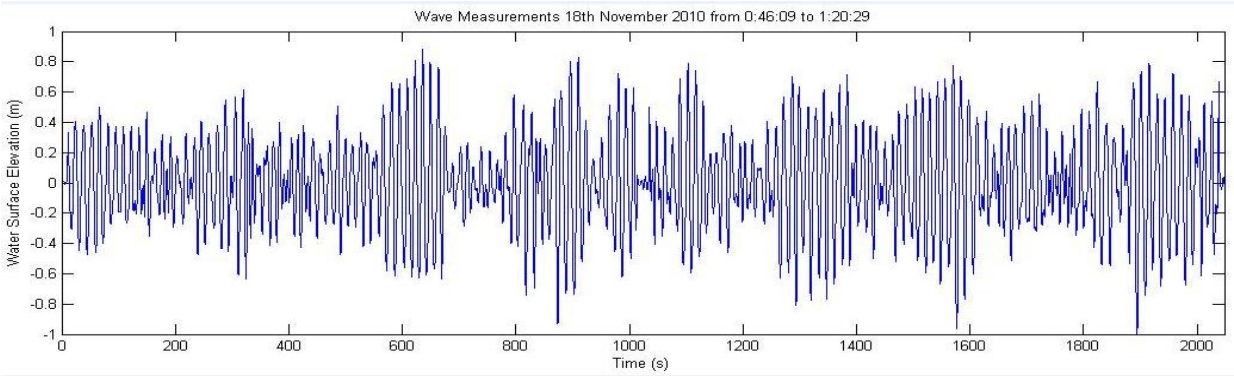

Figure 18: Water surface elevation record Pacific Coast of Costa Rica

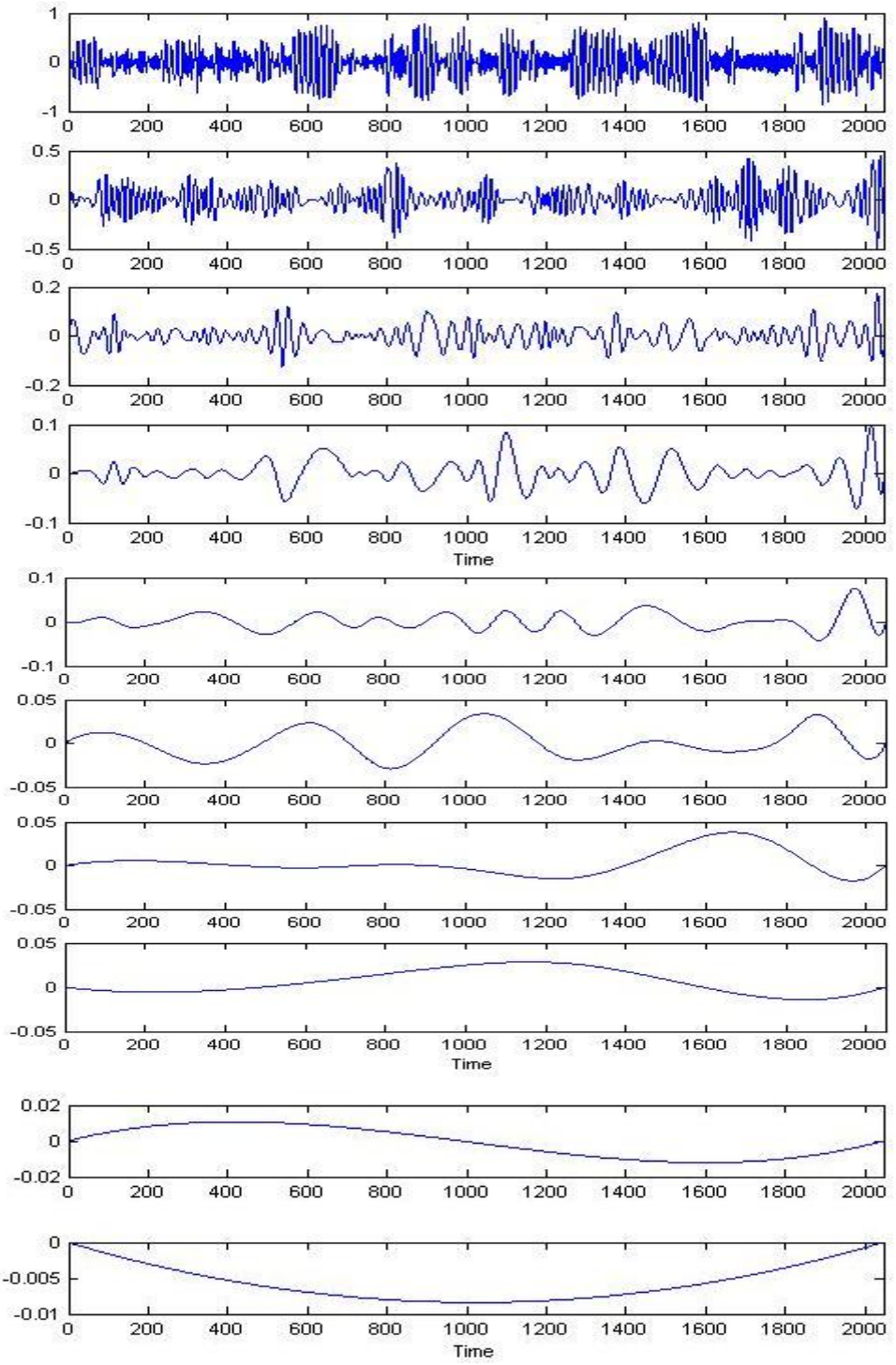

Figure 19: Intrinsic Mode Functions of measured wave conditions

According to several authors the Hilbert Huang transform provides an unprecedented detailed representation of the energy, frequency, time of a given time series[29]. The method assumes that a signal consists of several different intrinsic mode functions (IMF), each of them represents a embedded oscillation, which are found with the empirical mode decomposition (EMD). Veltecheva (2002) found physical meaning of the intrinsic mode functions with the wave groups and wave transformation in the surf zone.

The Hilbert Spectrum

Once the intrinsic mode functions have been obtained through the empirical decomposition method, the Hilbert transform is applied to each one of them. The data is then expressed from equations 30, 31 and 32 as:

$$X(t) = \sum_{n=1}^{N} a_n(t) e^{i \int \omega_n(t) dt}$$

Eq. (39)

Comparing equation 39 with equation 7, we can see that the intrinsic mode function represents a generalized Fourier expansion, with the ability to represent non stationary data. Also in the intrinsic mode functions the amplitude can vary for a given a frequency.

Using equation 39 we can represent the amplitude, frequency variation in time, this distribution is denominated the Hilbert Spectrum, H(ω,t). If we use the amplitude squared we obtain the same units of the Fourier based variance spectra, with the difference that the frequency is now a function of time. Figure 20 shows the time dependant Hilbert spectrum obtained for each of the previously obtained intrinsic mode functions.

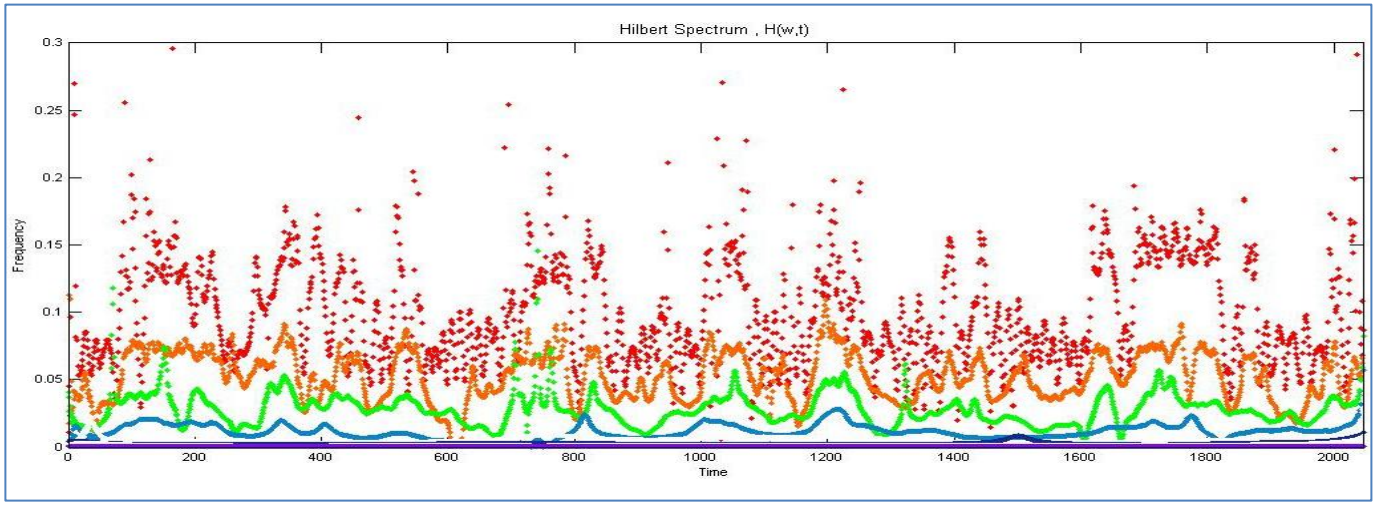

Figure 20: Hilbert Spectrum, H(ω,t)

[29] Veltecheva A. D. "Wave and Group Transformation by the Hilbert Spectrum", Coastal Engineering Journal 2002

The spectrum is only representing the time-frequency variation of each intrinsic mode. If we want to include the energy we need to generate a three dimensional graph in which the z coordinate represents the squared surface elevation of the corresponding intrinsic mode function figure 21.

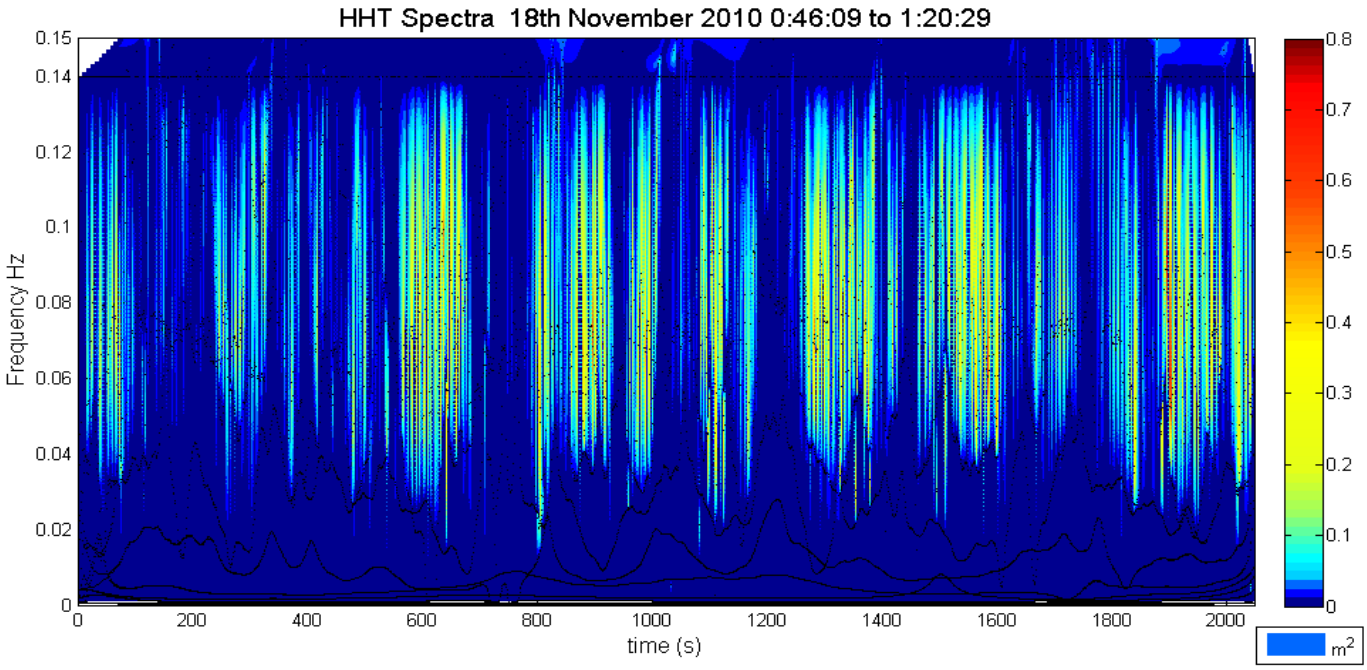

Figure 21: Hilbert Spectrum Obtained with WES

Spectral Values derived from the Hilbert Spectrum

It is also possible to obtain the marginal if we integrate the Hilbert spectrum over time as:

$$h(\omega) = \int_0^T H(\omega, t)dt$$

Eq. (40)

The marginal Hilbert spectrum represents the contribution to each amplitude, or energy, per frequency during the whole duration of the measurements time span. Huang (1996) pointed out the meaning of the Hilbert marginal spectrum and the Fourier spectra are different, since in the Fourier case the amplitude, (energy), is assumed to have remained constant through out the whole time span with a given frequency, while in the Hilbert case it means that during the whole time span there is higher likelihood of the existence of a given energy at a certain frequency that is represented in the spectrum.

The marginal spectrum, h(ω) of the previously obtained Hilbert spectrum (figure 21) is shown in figure 22. The spectrum obtained using the Fourier Transform is also shown. This was obtained via Welch's method, with a Hamming window of 64, which divides the time series into 32 exact windows.

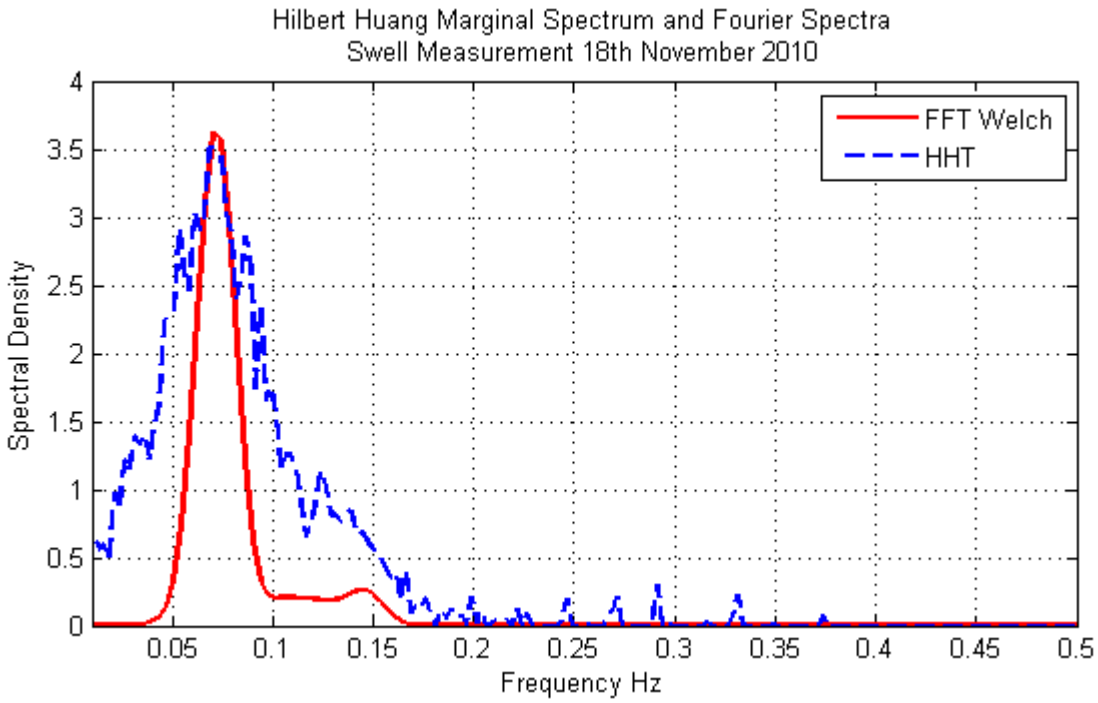

Figure 22: Hilbert Huang Marginal Spectrum obtained using WES

The amount of energy in the lower frequencies that is obtained using the Hilbert Huang Transform is higher than the one obtained using the fast Fourier transform, as was reported by Hwang P., Huang N.,[30]2003. The different distribution of wave energy has an impact in the design of ocean and coastal structures. The currently used spectrum based on the Fourier transform may underestimate the impact of the low frequency energy present in the system.

The instantaneous energy can also be obtained from the Hilbert spectrum and it is represented as:

$$IE(t) = \int_0^{\infty} H^2(\omega, t) d\omega$$

Eq. (41)

Since the Hilbert spectrum can represent non-stationary data, Huang(1998) proposes to examine the degree of stationarity of the data through Degree of stationarity.

[30] Hwang P., Huang N. "A note on analyzing nonlinear nonstationary ocean wave data", Applied Ocean Research 25 (2003).

$$DS(\omega) = \frac{1}{T}\int_0^T \left(1 - \frac{T * H(\omega,t)}{h(\omega)}\right)^2 dt$$

Eq. (42)

For a stationary and linear process the Hilbert spectrum, H(ω,t), would consist of horizontal contour lines where the energy is present at a given frequency, no frequency variation in time. In this case the degree of stationarity would be 0.

Spectral moments and variables can also be obtained for the Hilbert spectrum or the Hilbert marginal spectrum as in the Fourier based variance spectrum. However their physical interpretation still has to be researched within the coastal engineering community.

2.5.3 Wave Grouping Phenomenon

It is well known that waves in the ocean appear in groups. They are the consequence of different waves travelling amongst each other. Under the Fourier view a set of cosine functions each with its own amplitude and frequency and direction. In deepwater where the wave groups travel at half the speed of the waves the, wave groups appear and disappear randomly, however at shallow water, where the wave group velocity is closer to the individual wave velocity the wave groups create a temporal distribution of the wave energy. In shallow waters wave grouping defies the “random seas” concept since real ocean waves appearing in groups may not be completely randomly distributed.

There have been many different parameters proposed to describe the wave groups. They are based on wave statistics, Markov chains, wave signal envelope and more recently from the Hilbert Spectra. The methods included are based on the “linear seas” which was validated by Goda (1983), using wave measurements from the Port of Caldera in the Pacific Coast of Costa Rica. The Hilbert Huang transform provides new insight to the non-linear interaction of wave groups, and has already been used as a tool to analyze wave groups (Veltcheva 2002).

The different linear wave analysis methods propose different parameters for the characterization of the wave groups. Hudspeth and Medina (1990) reviewed the existing linear analyses methodologies and parameters of ocean wave groups. They showed that the Smooth Instantaneous Wave Energy History, SIWEAH, introduced by Funke and Mansard, 1979 and the groupiness factor is not an appropriate parameter to characterize run lengths, which will not be included in this work.

Hudspeth and Medina (1990) also showed that in order to evaluate wave groupiness only one of the five more commonly used parameters is needed since the parameters are interrelated. In their work the spectral peakdness parameter Qp, defined by equation 19, was a good parameter to describe wave grouping. Goda used the parameter Qp, and correlation between two successive waves with the run length theory to describe the wave

grouping of long travelled swell. Qp has been previously introduced, and it has been shown its dependence on the degrees of freedom of the analyzed spectrum.

The correlation coefficient between two successive wave heights has been shown to describe accurately, Goda (1983) the wave grouping phenomena. The correlation coefficient between two successive wave heights, γ_{HH} is given by:

$$\gamma_{HH}(k) = \frac{1}{\sigma_H^2}\frac{1}{N_0 - n}\sum_{k=1}^{N_0-n}(H_k - \bar{H})(H_{k+n} - \bar{H})$$

Eq.(43)

Where σ_H denotes the standard deviation, N_0 the number of zero down crossing waves, and $\bar{H}$ the mean wave height in the record and k is the lag in number of waves. Figure 23 shows the calculated correlation coefficient for one record.

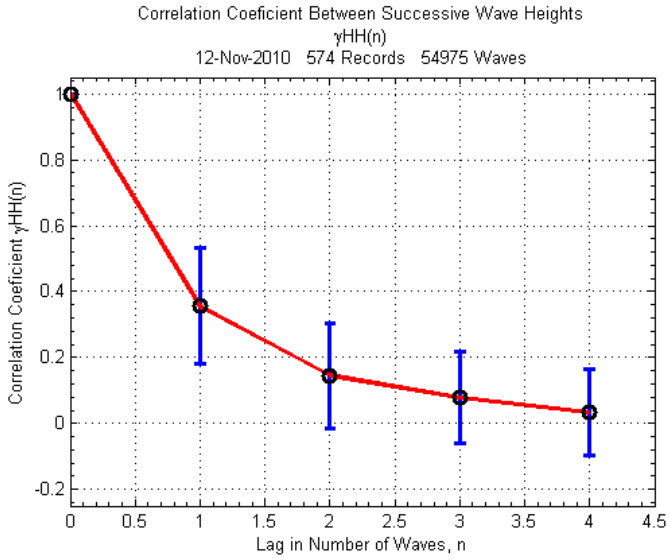

Figure 23: Correlation coefficient between successive waves

Run Length for Mutually Correlated Wave Heights

Goda(1970) gave the probability of a length of a run of high waves, L_{ht}, as the number of consecutive wave heights higher than a specified threshold, h_t. This threshold level is typically either the mean wave height, H_{mean} or the significant wave height $H_{1/3}$. Using this concept Goda showed that the assumption of linear superposition for random seas is not compatible with the assumption that the wave heights are uncorrelated. Figure 24 shows a numerical generated surface water profile with three wave groups with the definition of run length. If we set the threshold value at 0.5 meters we find that a run starts approximately at 160 seconds, with 8 waves above our

threshold value. The length run is found after obtaining the individual wave heights from the zero down crossing method.

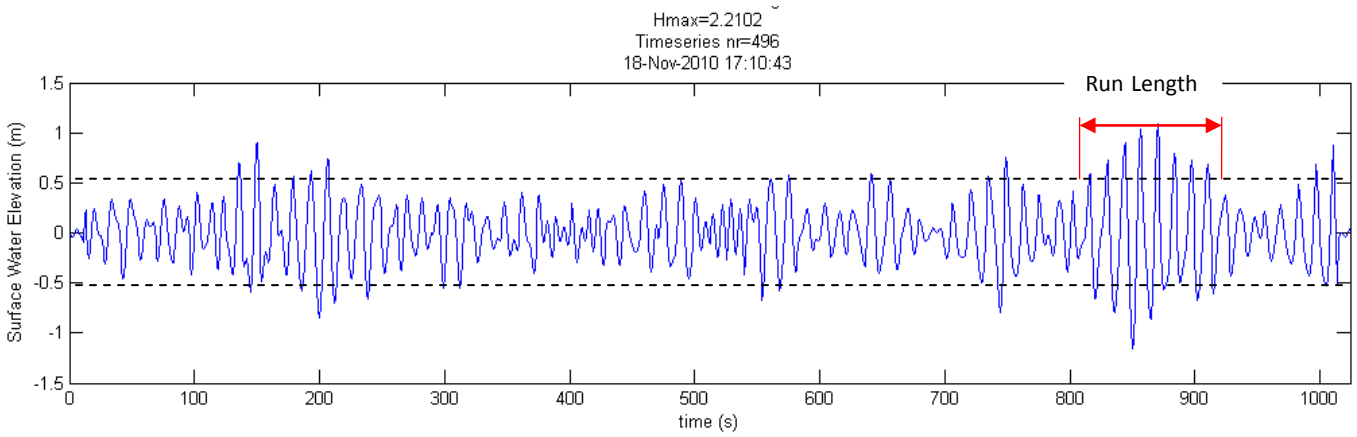

Figure 24: Run Length Concept

The run length is obtained from a given record by counting the number of groups and the number of waves in each group in which the individual wave heights exceed a certain threshold value. In the present work the run length was calculated for all the wave records available, and was presented as the probability occurrence of a group with a given number of waves for $H>H_{mean}$ and $H>H_{1/3}$.

The calculated value was compared with the values obtained from the theory of a run length introduced by Goda (1970). The theory starts by defining the probability that a wave height exceeds a threshold value is p_0, and the non-exceedance is q_0 where $p_0+q_0=1$. The probability that a run of a length j will occur in the ensemble of runs of several lengths is given by,

$$P_1(j) = p_0^{j-1} q_0$$

Eq.(44)

The mean and standard deviation of the run length is $j_1=1/q_0$ and $\sigma(j_1) = \sqrt{p_0/q_0}$. Kimura (1980) presented a theory for the run length for the case of mutually correlated wave heights. This theory will be used to corroborate the calculated run lengths from the wave records.

Kimura's theory defines the joint probability density function for two successive wave heights, H_1 and H_2, with a given a marginal probability function approximately by the Rayleigh distribution q(H) is given by equation 45:

$$p(H_1, H_2) = \frac{4H_1H_2}{(1-4\rho^2)H_{rms}^4} e^{\left[-\frac{1}{1-4\rho^2}\frac{H_1^2+H_2^2}{H_{rms}^2}\right]} I_0\left[\frac{4H_1H_2\rho}{(1-4\rho^2)H_{rms}^2}\right]$$

Eq.(45)

Where I_0 is the Bessel function of the zero[th] order moment, H_{rms} is the mean root square value of the times series and ρ is a correlation parameter which is related to the correlation coefficient of successive waves by,

$$\gamma_{HH}(1) = \frac{E(2\rho) - (1 - 4\rho^2)\frac{K(2\rho)}{2} - \frac{\pi}{4}}{1 - \frac{\pi}{4}}$$

Eq.(46)

E and K are the complete elliptical integrals of the first and second kinds. The joint probability density function of two successive wave heights is shown in figure 25, where q (H_1) is given by the Rayleigh distribution shown in figure 26.

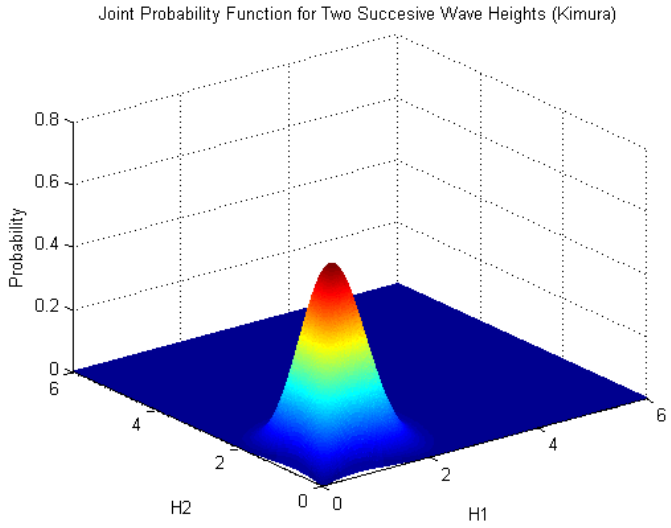

Figure 25: Joint probability density function of two successive wave heights p(H_1,H_2)

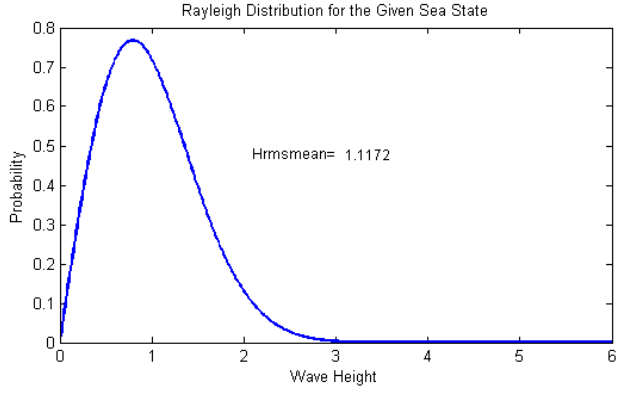

Figure 26: Rayleigh probability density function q(H_1)

The probability that neither H_1 nor H_2 exceeds a threshold wave height H* is given by p_{11} and of simultaneous exceedance p_{22},

$$p_{11} = \frac{\iint_0^{H*} p(H_1,H_2) dH_1 dH_2}{\int_0^{H*} q(H_1) dH_1}$$

$$p_{22} = \frac{\iint_{H*}^{\infty} p(H_1,H_2) dH_1 dH_2}{\int_{H*}^{\infty} q(H_1) dH_1}$$

Eq.(47)

Then the probability of the run with a given length j is given by,

$$P_1(j) = p_{22}^{j-1}(1 - p_{22})$$

Eq.(48)

The mean length of the runs is then obtained by,

$$\overline{J_1} = \frac{1}{(1 - p_{22})}$$

Eq.(49)

In order to apply the run length theory developed by Kimura to field data, the correlation parameter ρ is solved numerically in equation 46, since 2ρ can have a value higher than 1 only the real part of the complete elliptical integrals of the first kind should be used, given the obtained correlation coefficient between successive wave heights of equation 43. The procedure was incorporated into the Wave Ensemble Statistics Software, WESS. Figure 27 shows the theoretical and measured run length obtained for representative period.

The run length is a Markov chain type analysis which is independent of spectral estimates; hence it is considered a true measure of the occurrence and length of wave groups.

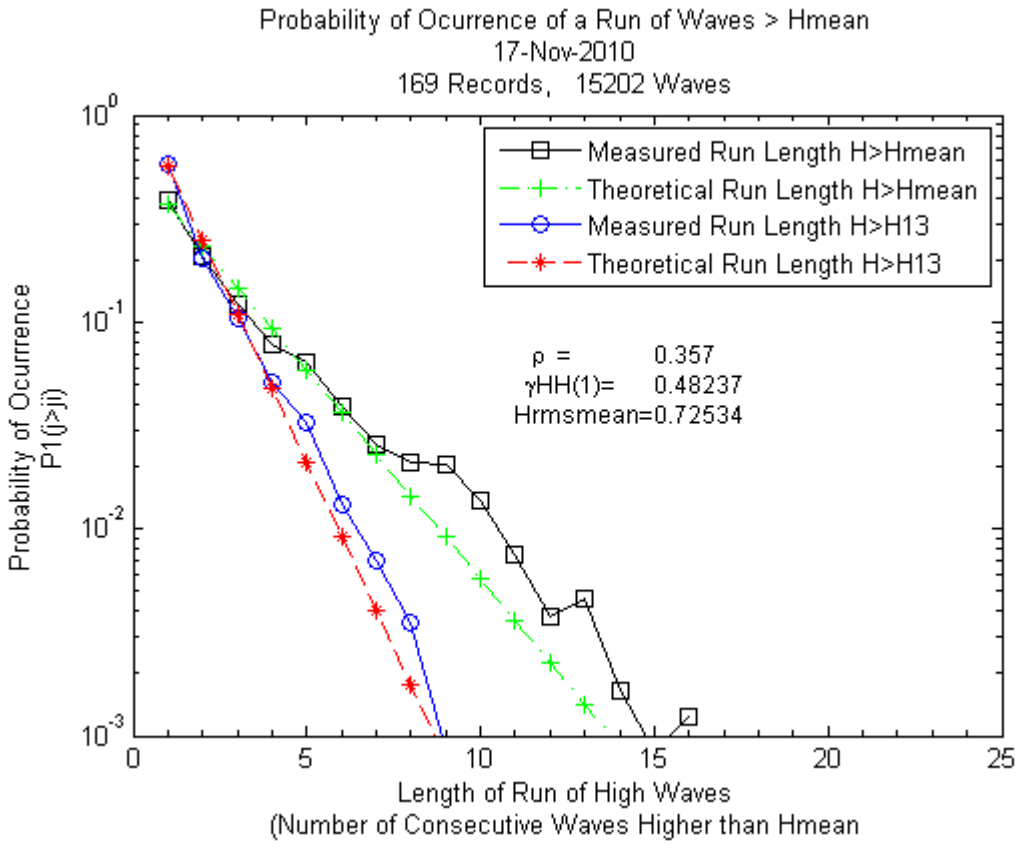

Figure 27: Occurrence probability of a run of waves with length j.

The developed software, WESS, also estimates the temporal variation of the mean run length and the correlation coefficient between two successive waves, shown in figure 28.

Goda found that the spectral peakdness parameter, Q_p, (see equation 21) describes the statistics of the expected run lengths. However, Goda points out that the spectral peakdness parameter is sensitive to spectral resolution. He found that the larger the spectral peakdness the larger the length runs of high waves. The correlation between these parameters is analyzed in detail.

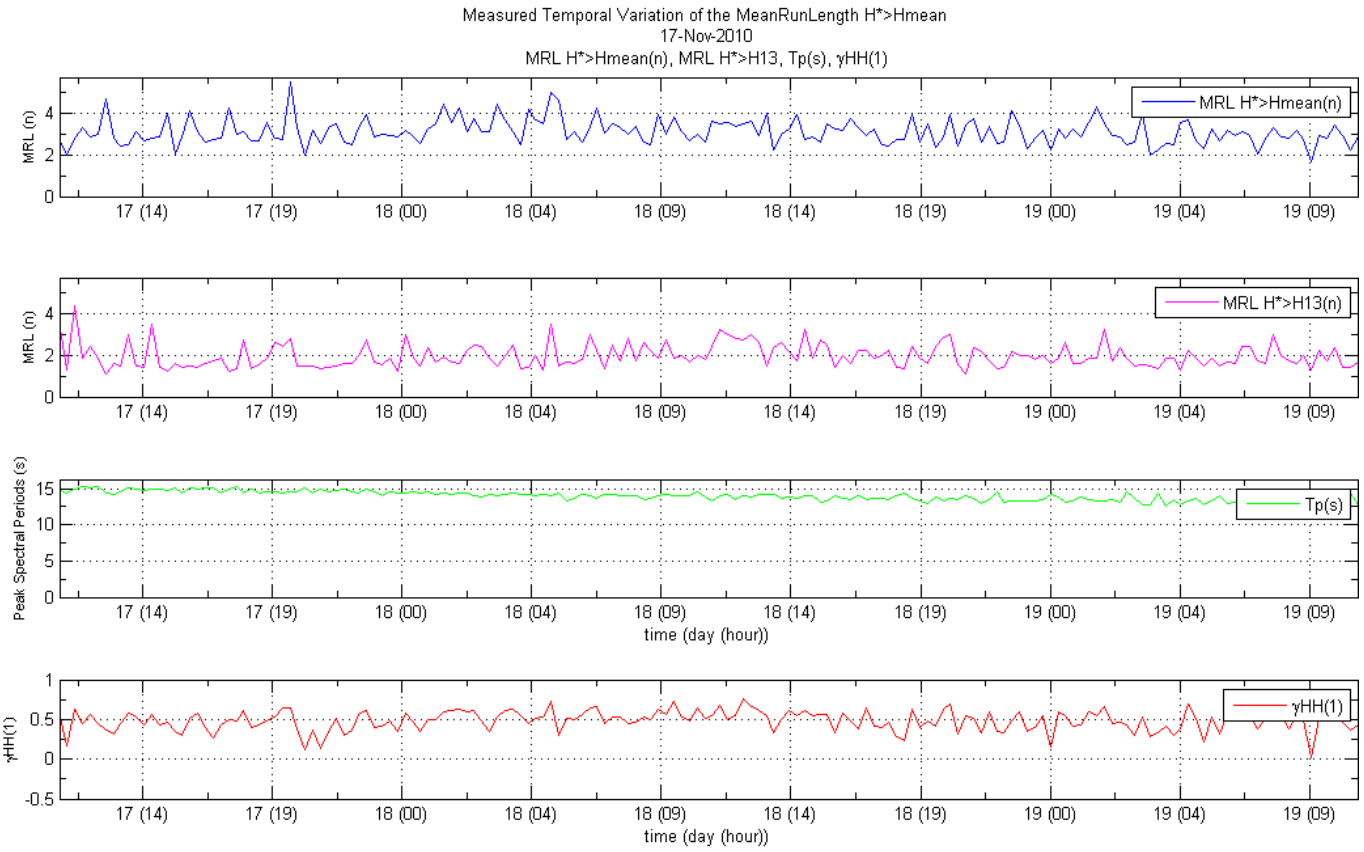

Figure 28: Temporal Variation of the mean run length and the correlation coefficient between two successive waves.

Time Group length and Group energy from the Hilbert Huang Transform

Veltcheva, (2002) proposed using the instantaneous energy derived from the Hilbert Spectrum, equation 50, as means to determine the boundary of the individual wave groups. The wave groups in the Hilbert spectrum H(w,t), appear as energy packets, the beginning and the end of the wave groups appear as a increase in the local frequency and decrease in the energy. Veltcheva proposed using a threshold energy level of the highest one third of the instantaneous energy, IE(t). The individual wave groups are then characterized by a time group length, tgr, and a group energy Egr.

The time group length is determine as two successive crossings of the threshold energy level. The wave groups determined in this way should correspond to the run of high waves as determined by Goda (1970). The group is obtained as the integration of the instantaneous energy IE(t) over the determined group length.

$$Egr = \int_0^{tgr} IE(t)dt$$

Eq. (50)

Veltcheva used the mean value of time group length and group energy obtained for comparison purposes. The possibility to use this recommendation will be examined in detail, according to Goda 1983 the wave grouping phenomenon in a record of 100 waves has a wide range of variation.

2.5.4 Long Wave Phenomenon

Munk and Tucker independently discovered and recorded in the late 1940's small amplitude waves with periods between 25 and 100 seconds, they were defined by Munk as "surf beat". Munk (1949) and Tucker (1950) found a linear correspondence between the "surf beat" and wind waves, later Tucker found a correlation between the long wave troughs and wind wave group crests.

The name given to the long waves mainly depends on their period; gravity waves were defined after Kinsmann 1965 for waves with periods between 1 and 30 seconds. Infragravity waves were defined as waves with periods between 30 seconds and 5 minutes, though gravity is still the primary restoring force, long-period waves were defined from 5 minutes to 24 hours, hence including tides. In the present work our primary focus is to analyze the infra gravity waves, product of gravity wave interactions with wave periods from 30 seconds up to several minutes. These waves will be named infra gravity or long waves in the present work irrespectively.

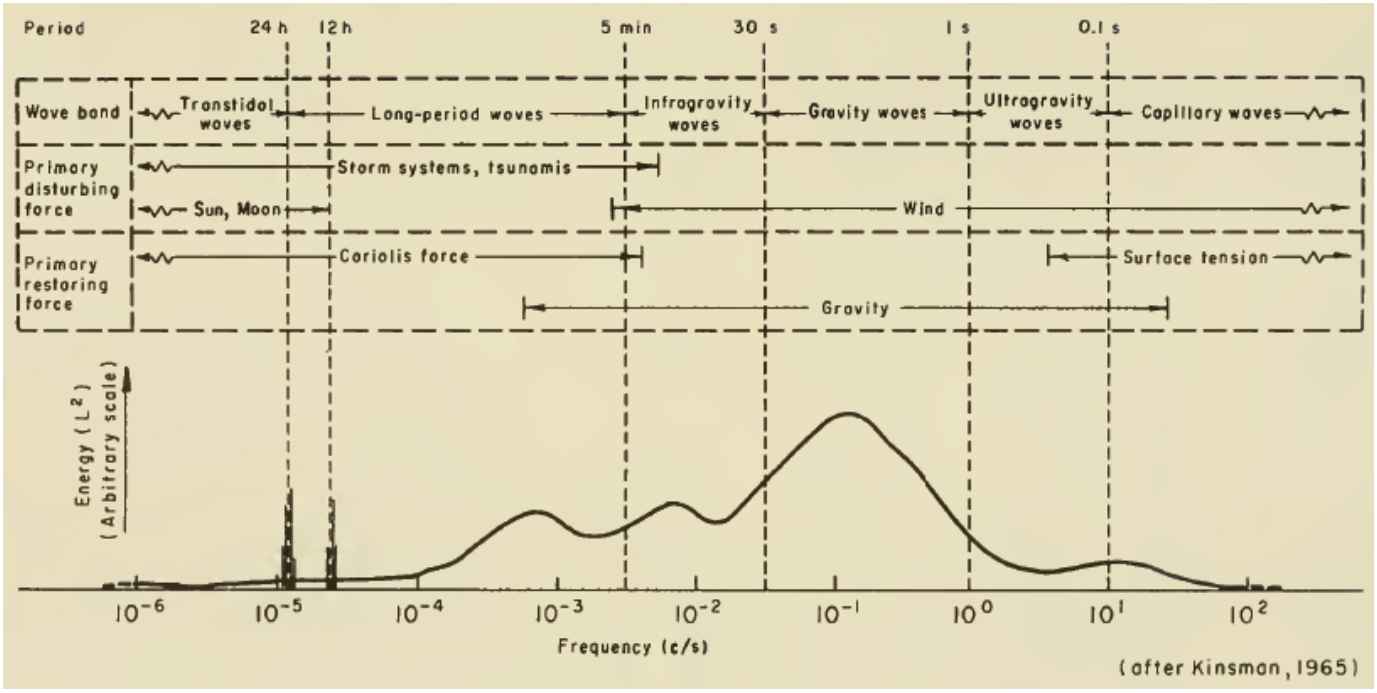

Figure 29: Approximate distribution of ocean surface wave energy after Kinsman 1965 (Shore Protection Manual 1984)

Longuet-Higgins & Stewart (1964) described the local set-down under a group of waves produced by the group. The effect was explained from the increased water particle velocities under the higher waves of the wave group, as indicated by the Bernoulli equation this should produce a local water pressure reduction. Given that the pressure will be lower under the group of higher waves than the spaces of smaller waves in between the groups a local set down beneath the higher waves a consequently local setup under the smaller waves will occur. This water surface disturbance induces a wavelike flow and so the bound long wave is formed.

Given the fact that in deepwater the group wave velocity is half of the wave velocity the bound long wave will continuously appear and disappear. In shallow water where the wave velocity is closer to the group velocity a more persistent pattern should appear allowing for larger set-down and set-up to occur. For waves in shallow water Longuet-Higgins derived the set-down beneath a group of waves with height H:

$$H_{Long} = \frac{3gH^2}{4\omega^2 d^2}$$

Eq. (51)

In equation 51 ω is the angular frequency and d is the water depth. It is clear that the longer the wave period, which means lower angular frequency, the higher the expected long wave height disturbance. A visible effect of the "bound long wave" is surf beat which is created after the long wave has been "freed" from the wave group after the waves break[31]. Furthermore, Bowers (1977), showed theoretically and physically that the natural modes of resonance of a harbor can be excited by the set down beneath wave groups, the bound long wave.

Sand S.E., 1982 described wave grouping using the bounded long waves. He points out that long waves are a consequence of the radiation stress. He also points out that long waves are of second order according to the derivations of Bowers (1977) and Dean and Sharma (1981) based on the Laplace equation. Their wave number and frequency are characterized by the differences k_n-k_m and f_n-f_m, the long waves receive contributions of frequency pairs n,m of the linear (short) wave components. Figure 30 shows a numerical long wave.

[31] E.C. Bowers. "Harbor resonance due to set down beneath wave groups". Hydraulics Research Station, Wallingford, Oxfordshire, 1977.

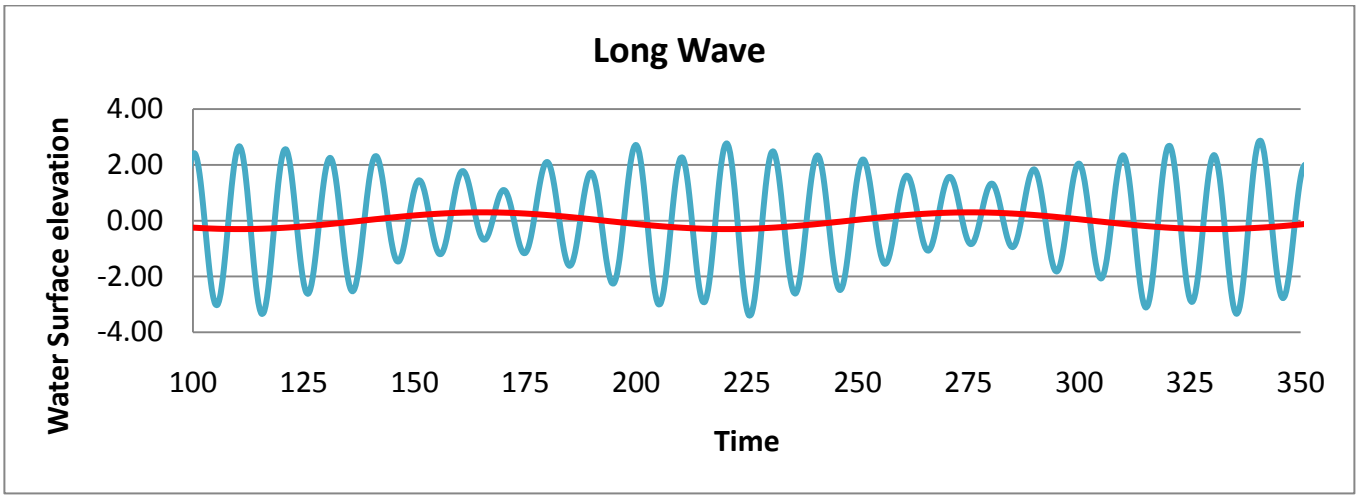

Figure 30: Long Wave

These long waves as have been mentioned travel at the wave group speed and their wave length is determined by the group length; hence they do not follow the dispersion equation. They are the result of secondary interaction between wave components. Hence they are non-linear. As it has been shown previously the Fourier spectral analysis is very limited in representing these non-linear components. It is considered not accurate to represent the long wave energy using the fast Fourier transform within the gravity waves.

Goda (1983) used the theory of secondary wave interaction in shallow water given by Tick (1963), and corrected by Hamada (1965) to analyze the secondary wave interaction between spectral components of measured long travelled swell. The theory was developed for long crested waves without directional spreading, which makes it appropriate for the long crested swell. The secondary spectrum is obtained using the following equations:

$$S^{(2)}(f_1) = \int_{-\infty}^{\infty} K(\omega, \omega_1) S^{(1)}(f_1 - f) S^{(1)}(f) df$$

Eq. (52)

Where $K(\omega,\omega_1)$ is given by:

$$K(\omega,\omega_1) = \frac{1}{4}\left(\frac{gkk'}{\omega(\omega_1-\omega)} + \frac{\omega(\omega_1-\omega)}{g} - \frac{\omega_1^2}{g} + \frac{\omega_1^2\left(\frac{g(\omega_1-\omega)k^2 + g\omega k'^2}{\omega(\omega_1-\omega)\omega_1} + \frac{2gkk'}{\omega(g(\omega_1-\omega)} + \frac{\omega(\omega_1-\omega)-\omega_1^2}{g}\right)}{g|k+k'|\tanh|k+k'|h - \omega_1^2} \right)^2$$

Eq. (53)

Where h is the water depth and the angular frequencies ω and ω_1 and wave numbers are related by the dispersion equations:

$$\omega^2 = gk\tanh kh, \qquad (\omega_1 - \omega)^2 = gk'\tanh k'h$$

Eq. (54)

Goda compared the linear and non-linear components his results are shown in figure 31. It can be seen that the super-harmonic features are completely explained by the secondary nonlinear components. However, according to his results there is much more energy in the lower frequencies than what the linear Fourier spectrum shows, particularly it can be seen that for 0.01 Hz, (100 seconds) the order of magnitude expected for the bound long wave, there is 5 times more energy obtained with the second order spectrum.

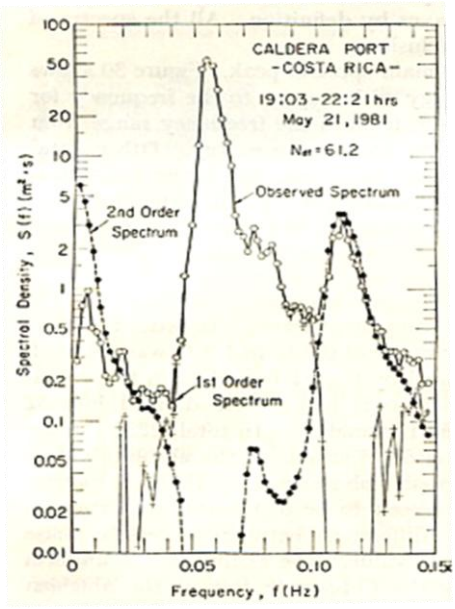

Figure 31: Linear and Non-Linear Spectral Components Observed by Goda 1983.

The observed differences indicate more low frequency energy than obtained using the Fourier Transform. Goda indicates that a higher order interaction theory would be necessary to explain this excess of the low frequency components. This result shows the inadequacy of using the Fourier spectrum to describe the long waves within the gravity waves.

Several attempts have been made to measure the long wave energy using low pass filters, Sand (1982). The low pass filter eliminates waves that have a frequency higher than a certain threshold cutoff frequency. This allows for a more accurate representation of the energy of long waves through the Fourier transform. In the present work a low pass filter, the Butter filter, was implemented. Two different cut off frequencies were implemented, the first according to the maximum measured zero down crossing period, and the second one was set at the

mean run length. These cuts off frequencies for the low pass filter vary from time series to time series, hence is an adaptive filter. The secondary low frequency peak and energy, Hmo, was then obtained using the Fourier transform on the filtered signals. This procedure was implemented within the developed software, WESS. The obtained filtered long wave is shown in figure 32.

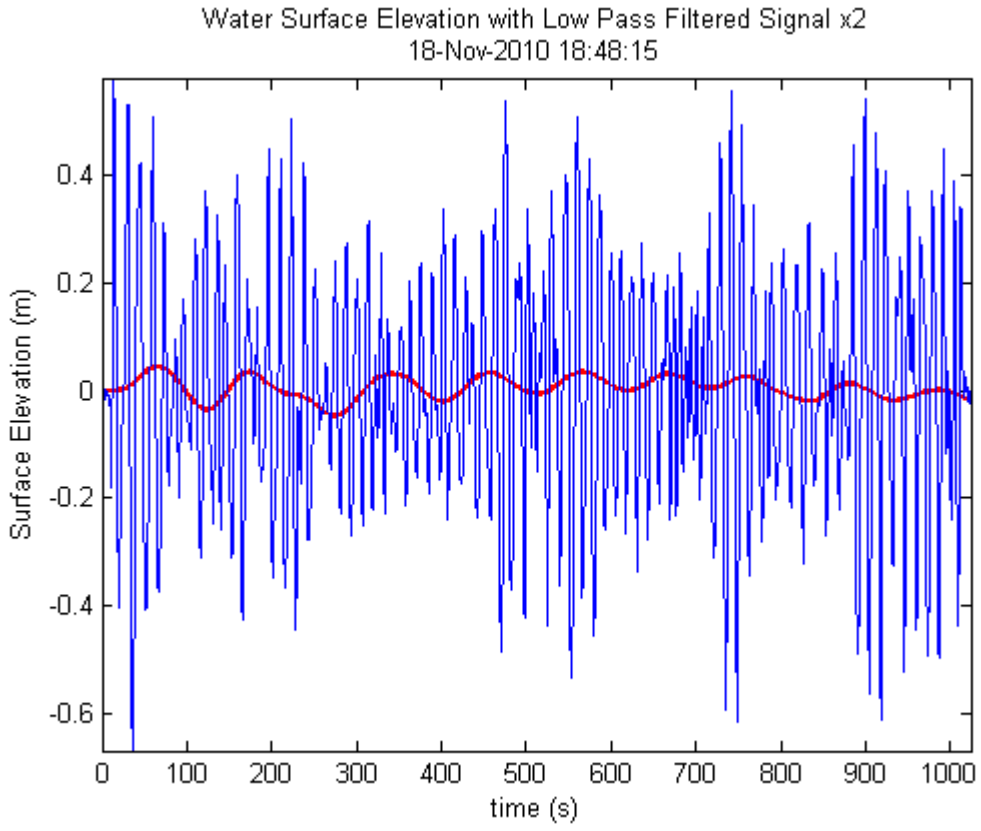

Figure 32: Filtered long wave from original signal

The obtained signal was obtained for all the time series of the ensemble, and later a spectral analysis using the Fourier transform was carried out using the developed software WESS. The result obtained spectra allows for the calculation of the peak periods and energy content of the long wave. Figure 33 shows one of the long wave spectra. For the calculation of the long wave spectra the degrees of freedom used had to be lowered for resolution purposes. The number of long waves present in a given time series depend on the length of the wave record. For a 1024 second long record, four long waves of 256 seconds, or two waves of 512 seconds, or one wave of 1024 seconds could be present, from equations 26 and 27 it is clear that to target this waves we need to increase the increase the number of lags. Given the low number of long waves, continuous wave records of at least three hours are required for an accurate statistics, however this long continuous records are hardly available. Further research is required using long continuous wave records.

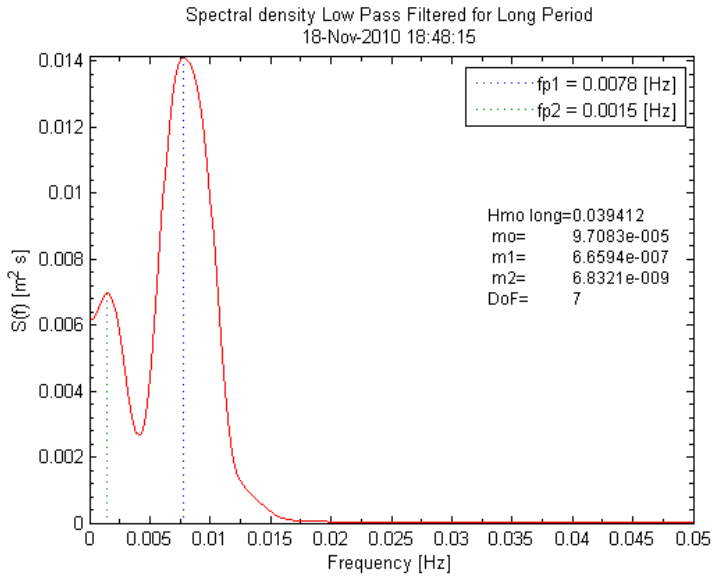

Figure 33: Long Wave Spectra

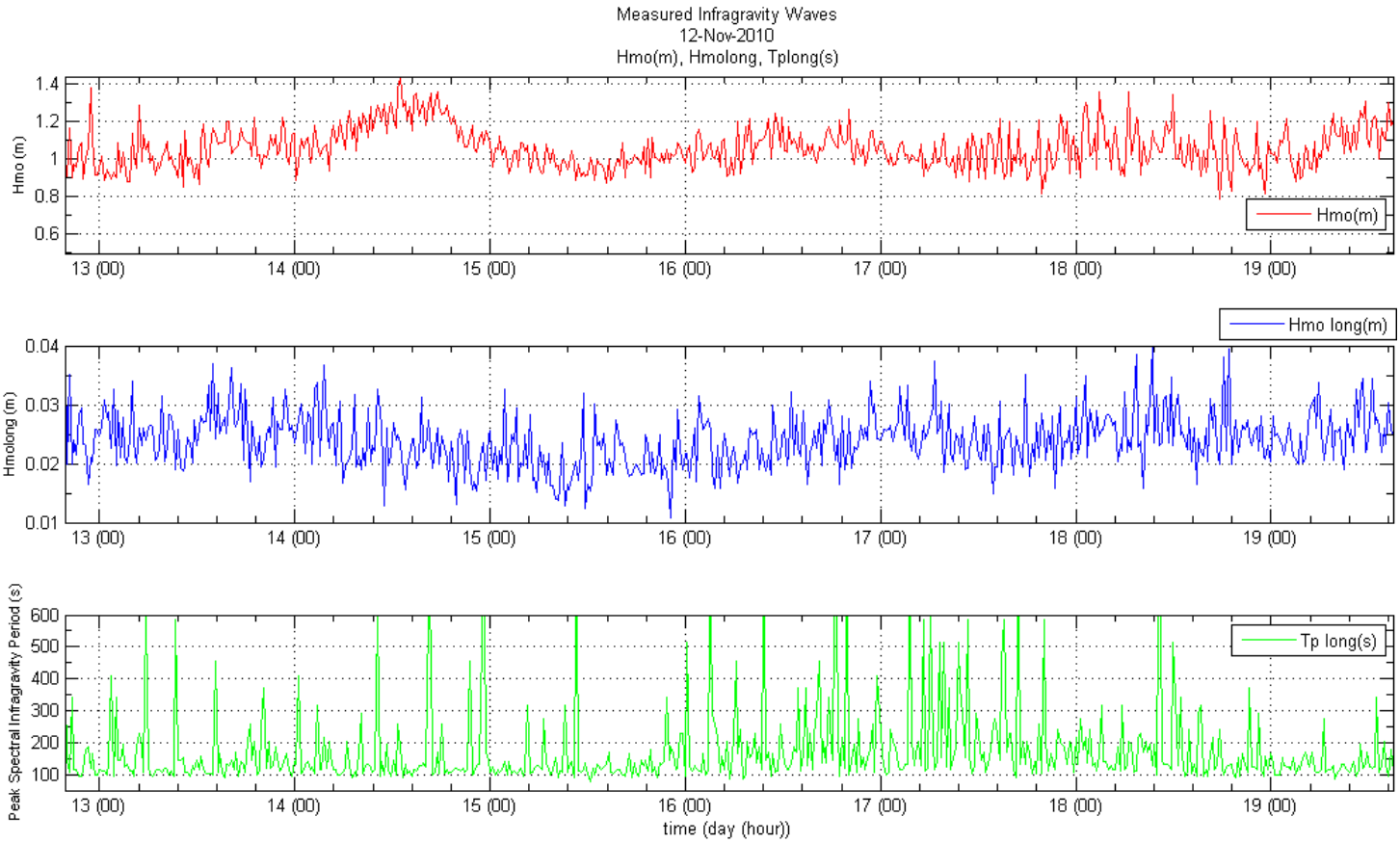

Figure 34: Long Wave Temporal Variation

Hwang and Huang (2003) compared the spectrum of wind generated waves using the Hilbert Huang marginal spectrum, and the Fourier based spectrum. They obtained a considerably higher spectral density for the low frequency portion than the linear Fourier based spectra, but at the peak and higher frequencies less energy is present in the Hilbert Huang marginal spectrum. The reason for this result is attributed to the different interpretations of wave nonlinearity between both methods. As mentioned before Fourier based spectral methods decomposes nonlinear waves into its base frequency and higher harmonics and some spectral energy is then transferred from their lower frequency sub-harmonics to higher harmonics. Fourier then will tend to overestimate the spectral level for frequencies higher than the spectral peak. On the other hand the Hilbert Huang spectrum interprets wave nonlinearities in terms of frequency modulation and the nonlinear energy remains bounded to its corresponding frequency because of the instantaneous frequency definition. It would be then expected to find a better description of the bound long wave phenomena by means of the Hilbert Huang Transform. However no such study has been found as reference.

2.5.5 Wave Measurements Using a Submersible Pressure Sensor

Wave measurements carried out by subsurface pressure sensors have been employed extensively because of their practicality since 1947. The pressure variation of the water column can be related to several physical phenomena of different time scales, tides, surge, setup, and waves. When working with waves a transfer function has been widely used to transform the measured pressure variations into wave oscillations. There are limitations when using a subsurface pressure sensor when measuring wind waves. We need that the depth at where the sensor is located is affected by the waves; this depth is exponentially frequency dependant, the shorter frequencies reach the deepest while the higher frequencies die out faster. The second limitation is related with the transfer function used to obtain the wave energy from the pressure readings, a spectral analysis using the Fourier transform through the fft algorithm of the data is required to obtain adequate results of the wave energy spectrum, to obtain the wave surface information, we need to use inverse fft to obtain the time series. This procedure can filter out non-linear process such as the bound long wave information.

Bishop and Donelan (1986) found that using the spectral analysis provided reliable estimates of the surface wave heights, they concluded that a well designed pressure transducer system using spectral analysis of the data and a transfer function based on the linear wave theory will give estimates of wave heights of +/-5%. Wave by wave analysis is strongly not recommended and should be avoided since one zero crossing wave can contain energy within other frequencies than the zero crossing frequency[32].

The spectral method assumes that the pressure under a wave can be expressed as,

[32] CRAIG T. BISHOP and MARK A. DONELAN, “Measuring Waves with Pressure Transducers”, Coastal Engineering, 11 (1987) 309-328.

The total measured pressure variation can be expressed as (Lamb, 1932):

$$P = -\rho g z + \rho \frac{\partial \phi}{\partial t} - \frac{1}{2}\rho(u^2 + w^2) + p_{atm} + \rho\gamma(t)$$

Eq. (55)

Where P is the total pressured (measured), ρ the density of the liquid, g the gravitational acceleration, z the submergence depth, u and w the horizontal and vertical wave orbital velocity, $p_{atm\ the}$ atmospheric pressure, γ(t) a function of time and ϕ the velocity potential.

Given that the kinetic energy term and γ(t) are of second order a first order expression is obtained,

$$\frac{p'}{\rho} = \frac{\partial \phi}{\partial t}$$

Eq. (56)

From linear wave theory the velocity potential is given by,

$$\frac{\partial \phi}{\partial t} = \frac{\eta \omega^2}{k} \frac{\cosh k(d+z)}{\sinh kd}$$

Eq. (57)

Relating the first order expression for subsurface pressure head to the surface wave height as H:

$$H = \frac{p'}{\rho g} \frac{\cosh kd}{\cosh k(d+z)}$$

Eq. (58)

In this expression sometimes a correction factor N is introduced in the right hand side. In this expression the wavenumber, k=2π/L, with L the wave length, is given by the wave dispersion equation, ω^2=gktanh(kh), with ω the angular frequency, ω=2π/T. Since the wave length is unknown in a discrete series of pressure points, a spectral solution is applied, using Ncoshkd/coshk(d+z) as the transfer function,

$$S_s(f) = \left[\frac{N(f)\cosh(kd)}{\cosh k(d+z)}\right] S_p(f)$$

Eq. (59)

Where Ss is the water surface elevation spectrum and Sp is the pressure spectrum, here N(f) is a water depth, frequency dependant correction factor. Once the wave elevation spectrum has been obtained we would need to apply the inverse Fourier transform on it to obtain the time series using,

$$\eta(t) = \sum_{i=0}^{n} \frac{A_i}{Kp(\omega_i)} \cos(\omega_i t - \epsilon_i)$$

Eq. (60)

Where A is the amplitude, ω the angular frequency and ε the phase angle.

During these two phases we lose non-linear information, as is the bound long wave. Wang (1986) proposed a method based on the curvature, trying to define an instantaneous angular frequency, assuming a sinusoidal water profile to reconstruct the time series.

A new method is proposed in this thesis obtain the water surface time series from the measured subsurface water pressure. The new method is described below; validation of this new method is currently being carried out. Some previously defined equations are repeated here for convenience. To the best of our knowledge no similar method has been previously proposed for the transformation of pressure record to free water surface wave record.

NEW METHOD TO RECOVER THE WATER SRUFACE TIME SERIES FROM SUBSURFACE PRESSURE MEASUREMENTS

A- Pressure Variation Signal

We obtain the pressure variation, after removing tide, information of the discrete signal of N points as:

$$p' = P - \frac{1}{N}\sum_{k=1}^{N} P_k$$

Eq. (61)

p´ shows the measured pressure fluctuations.

B- This signal is then decomposed using Huang´s empirical decomposition method.

Huang's empirical decomposition method is used to decompose the signal into its intrinsic mode functions h_k as is described in chapter 2.5.2.2.

$$h_{1(k-1)} - \bar{m}_{1k} = h_{1k}$$

C- The Hilbert transform is applied to each Intrinsic Mode Function and the instantaneous frequency is obtained

The Hilbert transform is used to obtain the instantaneous frequency for each k IMF as:

$$y_k(t) = \frac{1}{\pi} P \int_{-\infty}^{\infty} \frac{x_k(t')}{t - t'} dt'$$

For each k intrinsic mode function x(t) and y(t) form a complex conjugate function such that:

$$z_k(t) = x_k(t) + iy_k(t) = a_k(t)e^{i\theta_k(t)}$$

The instantaneous frequency is then defined as:

$$\omega(t) = \frac{d\theta(t)}{dt}$$

Hence we have a frequency per intrinsic mode function in the time domain which can also be represented as the Hilbert Huang spectrum. Figure 35 shows the calculated Hilbert Huang Spectrum for a given time series analyzed with the instantaneous frequency and energy content of the obtained intrinsic mode functions.

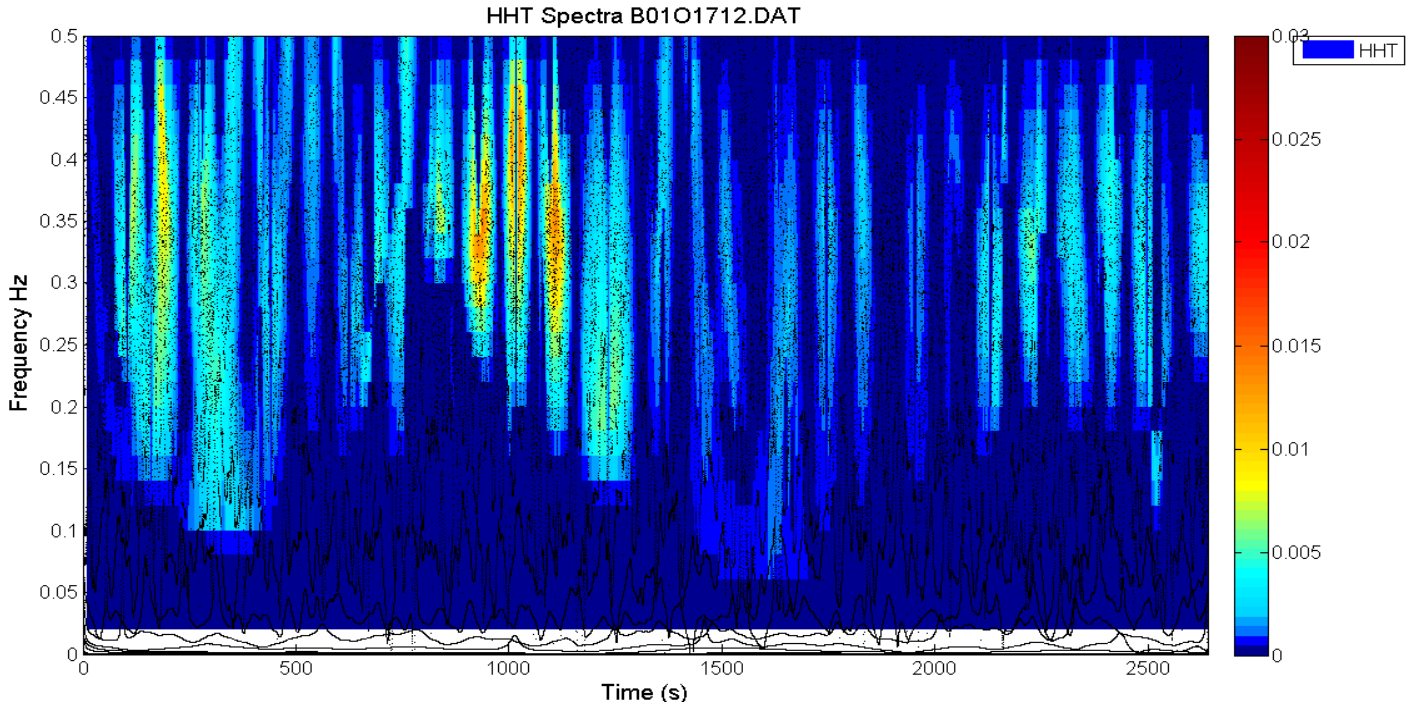

Figure 35: Hilbert Huang Spectrum to be applied to transfer function

D- Transfer Function

Assuming that the dispersion relation is applicable to the decomposed pressure signal we solve it for each intrinsic mode function and instantaneous frequency to obtain the instantaneous wave number K, using:

$$\omega(t)^2 = gk(t)tanh(k(t)d)$$

Eq. (62)

With the instantaneous wave number we use the common transfer function, applied to each k intrinsic mode function, to obtain the equivalent water surface elevation for each intrinsic mode function:

$$\eta_k(t) = \frac{p'_k(t)}{\rho g}\frac{coshk_k(t)d}{coshk_k(t)(d+z)}$$

Eq. (63)

Cutoff frequencies are used as the minimum frequency will be given by the inverse of the total sample period, and the maximum frequency will be given by the dynamic pressure and the dispersion relation obtaining the maximum wave number, k by,

$$k = \frac{1}{h}cosh^{-1}\left(\frac{\rho g a}{p}\right)$$

Eq. (64)

Where ρ is the water density, g the acceleration of gravity, a the minimum target amplitude, and p the minimum measurable pressure from the equipment used depending on its accuracy and precision (Given by the manufacturer).

E- Wave Surface Elevation Reconstruction

Using the property of the intrinsic mode functions, that the original pressure signal can be reconstructed by adding the pressure intrinsic mode functions, we reconstruct the water surface elevation adding the N wave surface intrinsic mode functions.

$$\eta(t) = \sum_{k=1}^{N} \eta_k(t)$$

Eq. (64)

The wave surface elevation time series has been obtained.

A comparison between the spectral and new method for a given time series is shown below these procedure was incorporated into the developed software WES, carrying out the new procedure for every pressure time series.

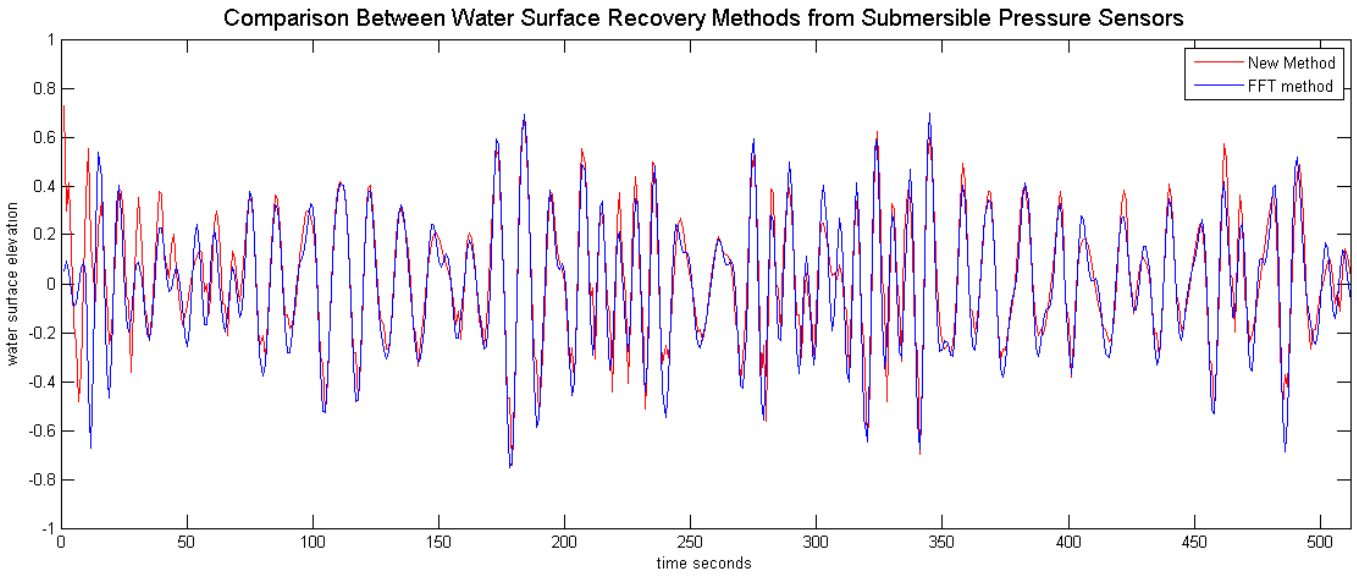

Figure 36: Water surface elevation recovery comparison between fft method and new method

The method validation was carried out comparing the results obtained from analyzing time series of water surface elevation obtained by submersible pressure gauges by both methods. Differences were obtained in the spectra, more energy in the lower frequencies were obtained with the new method, while the amount of energy content in the higher frequencies was lower. Figures 37 and 38 show the obtained spectrogram of long travelled swell using the FFT and new method based on the HHT.

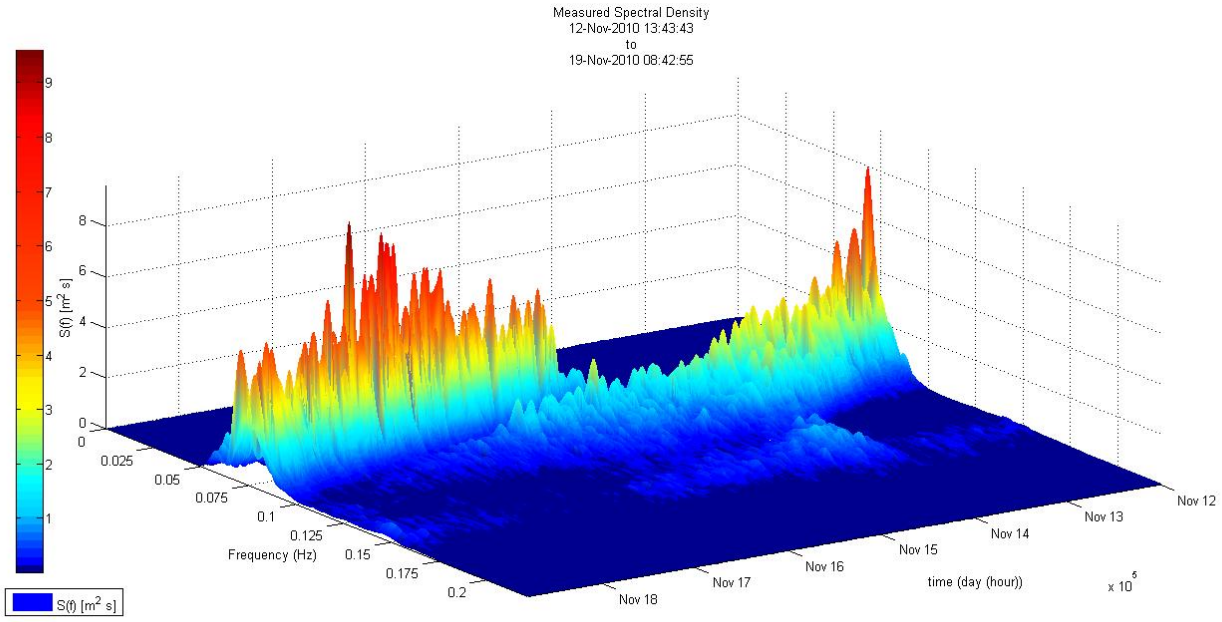

Figure 37: Spectrogram for long travelled swell obtained using new proposed method for water surface reconstruction from pressure readings

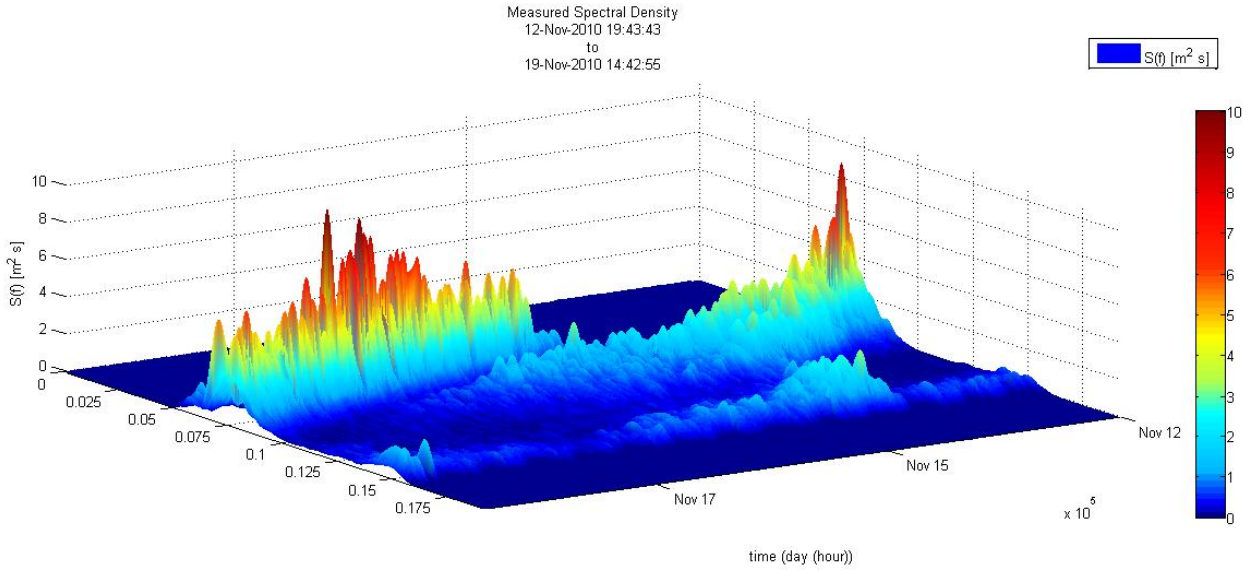

Figure 38: Spectrogram for long travelled swell obtained using traditional FFT method from pressure readings.

Validation of the new proposed method using wave flume measurements

In order to assess the accuracy and precision of the new proposed method, to obtain the free water surface elevation through pressure reading, simultaneous wave measurements, using pressure and resistance wave gauges were analyzed. Large scale experiments were conducted at CIEM wave flume of the maritime engineering laboratory LIM of the Universidad Polytechnic de Barcelona, Spain. During these experiments the water surface profile was monitored at several simultaneous locations using submersible pressure sensors and conductivity surface gauges. The measurements included irregular and regular wave conditions with wave heights varying from 0.25 to 0.491 meters and periods ranging from 2.5 to 4 seconds. The pressure readings were analyzed using the new proposed method and compared to the exact solution given by the water surface reading obtained by the conductance (resistance) surface gauges.

Flume and Experiment Setup

The wave flume at CIEM is one of the largest in the world; it is 100 meters long, 3 meters wide and 5 meters deep, hence experiments are close to full scale conditions. The wave generation system is a hydraulic based wedge wave generator. The generated waves can be regular or irregular, allowing for user defined spectra or parametric spectra including solitary waves. A PC-based active absorption system has been designed allowing for long tests without problems of spurious flume induced reflections.

Figure 39: CIEM Wave flume

The equipment used during the experiments included two resistance-type twin wire wave height gauges and 6 submersible pressure sensors. Two of the pressure sensors PS02 and PS05 were directly below the resistance gauges WG03 and WG04; hence the readings from these two sensors were compared with water surface elevation measured by the resistance gauges. The two wave measurement locations along the channel were located at water depths of 1.8 and 1.9 meters, the pressure sensors were located at a water depth of 0.5 meters, a cross section of the equipment setup is shown in figure 40.

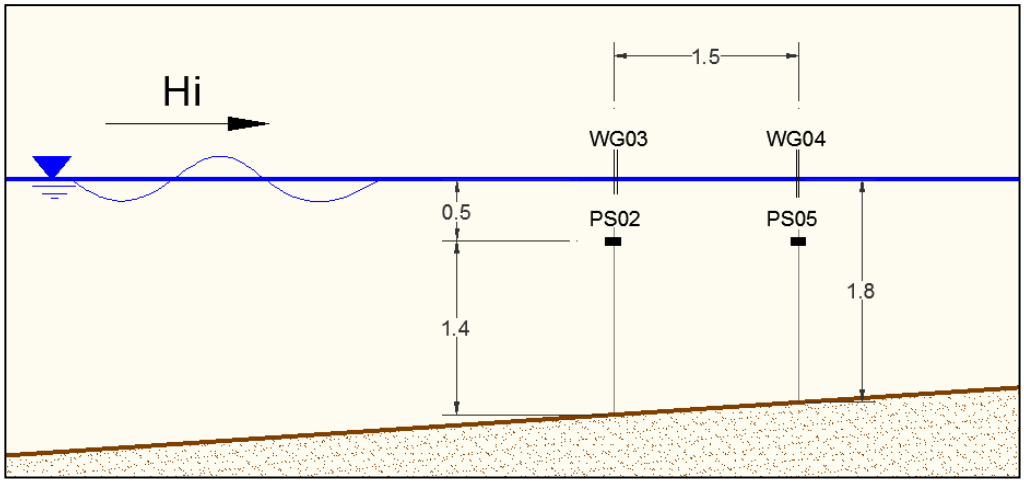

Figure 40: Equipment setup at CIEM

The obtained and analyzed data are the result of a research investigation done at CIEM over a rigid bottom. The specific project of the data used was Dynamics of Beaches, sponsored by *Human Capital and Mobility Programme (Scientific and Technical Cooperation Networks)* from the Commission of European Communities, from Directorate General XII-Science, Research and Development. (1194-1998) Contract NºCHRX-CT93-0392.

Equipment Used

The resistivity or conductance sensors used are composed physically by a support element with two parallel wires with a small separation which are aligned perpendicularly to the wave direction. These wires are the extremes of an electric circuit that closes in contact with water. In this way when circulating a high frequency electric AC current it is possible to measure the conductance (inverse of resistance) between both wires. This conductance is proportional to the length of the underwater part of the wires and its conductivity. Given the water conductance, which is obtained through a calibration procedure and it is constant through the tests, the registered changes in conductance equivalent to changes in the free water surface.

The conductance sensors provide a good linear response, with a precision of up to 0.1mm. However they need constant calibration, and they can induce a capillary error around the piercing of the water surface. This capillary error is very small given of the dimensions of CIEM flume. The calibration procedure used is a static one, in which

the gauge is introduced at small known increments in the water and a regression is obtained. At CIEM the lowest regression coefficient accepted R^2>0.999.

During the tests STS submersible pressure sensors were used. These pressure sensors have a measurement range of 0 to 400 mbar and a precision of +-0.4 cm. The pressure readings are obtained through the deformation of a sensor element, typically quartz, done by the fluid action. Through an electronic circuit this information is transformed to an electrical signal proportional to the measured pressure. The static and dynamic pressures are measured. These pressure gauges can also be used to obtain the wave forces generated on a structure, and internal pressures on porous media.

Temporal series were obtained from all the gauges at a simultaneous sampling frequency of 8Hz.

The tests

Four tests were analyzed for the two wave gauges locations, three with irregular wave conditions and one with regular waves. In all the tests the water level was maintained constant, with 3 meters of water depth at the wedge location and a sloping bottom, with wave gauges WG03 and PC02 at 1.9 meters water depth and WG04 and PC05 at 1.8 meters of water depth. The irregular waves were obtained through the parametric JONSWAP spectra with γ=3.3. The wave characteristics of each test are shown in table 1.

Table 1: Laboratory Input Test Wave Conditions

Irregular Waves	Hs (m)	Tp (s)
A	0.353	4.0
B	0.370	3.0
C	0.390	2.5
Regular Waves	H (m)	T (s)
I	0.491	3.5

Results

The measured water surface profile with the conductance gauges and the calculated water surface profile from the pressure readings were compared in two ways. First, the obtained time series were compared qualitatively, plotting both time series for all the tests, and secondly the spectrum was compared. The obtained result for the irregular waves case A at locations WG03-PC02 is shown in figure 41. In general a good agreement is found, however the water surface profile calculated from the pressure sensor, using the new procedure based on the HHT, presents high frequency noise not registered with the conductance gauge. This noise was present in all the time series obtained through the new method. Lowering the high frequency cut off frequency in the new method reduced the measured noise; however the wave peaks were then slightly under estimated. Second order Stokes

dynamic pressure expression was then used to convert the frequency dependent intrinsic mode functions to water surface intrinsic mode functions, however the results did not change.

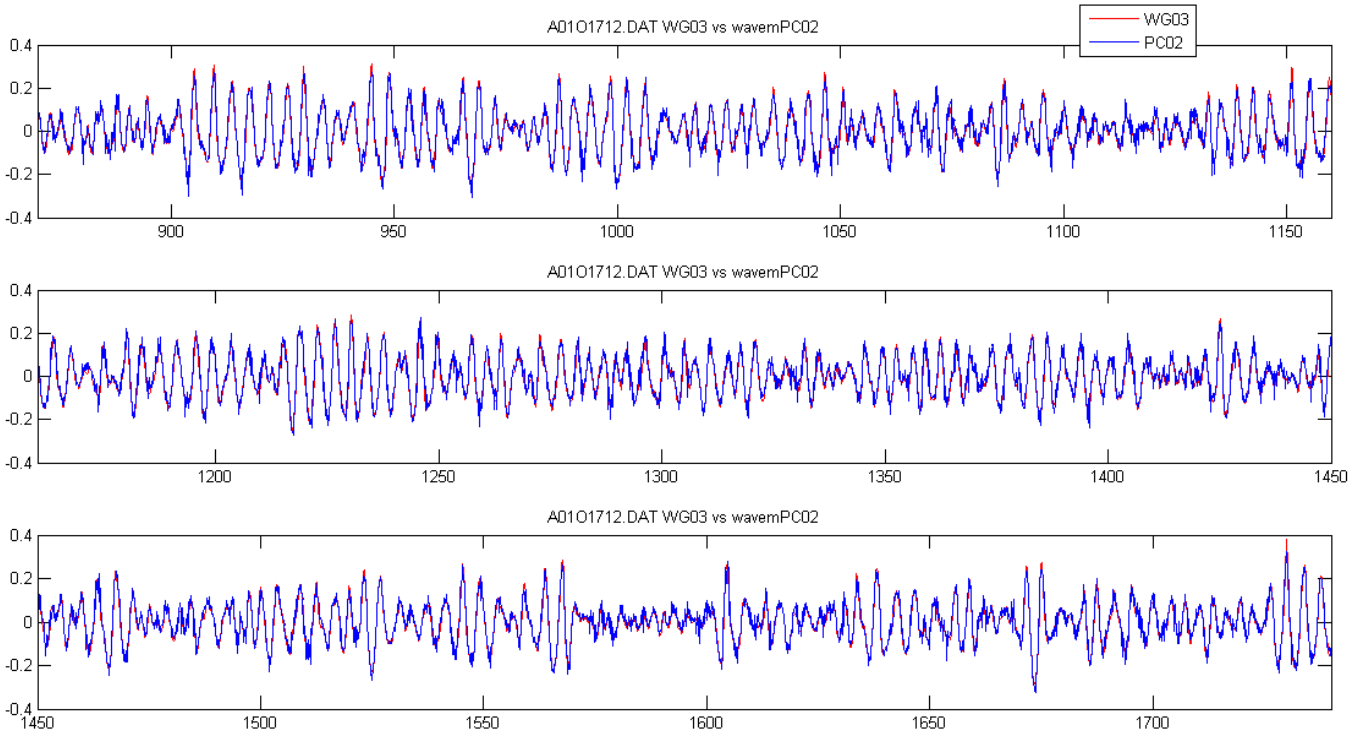

Figure 41: Time series comparison for PC02 and WG03

Then the regular wave condition, case I, was investigated. The comparison results between the measured water surface with the conductance gauge and the calculated one using the new proposed method for the regular wave condition is shown in figure 42. Again high frequency noise at the crest and the trough of the wave was found. This noise was also dependent on the cutoff high frequency selected. Given the fact that the sampling was done at 8Hz, the variation of the instantaneous frequency obtained through Hilbert spectrum could produce very high instantaneous frequencies if the pressure signal is not smooth and continuous, any pressure jump could lead to very high frequencies, that when Kp, the dynamic pressure transfer function, is applied it increases the errors and large high frequency variations can appear in the calculated signal.

The high frequency noise error was found to be due to small noise or abrupt changes in the pressure signal, which have a high instantaneous frequency, which are then amplified given the nature of the transfer function used. It is estimated that if other type of transfer function is used, for example dependant on lower frequency response, for example a ships surge motions, the error amplification wouldn't occur.

Figure 43 shows the measured pressure fluctuations and the calculated water surface profile using the new method based on HHT. The amplification of small fluctuations in the pressure signal is seen in the calculated water surface profile.

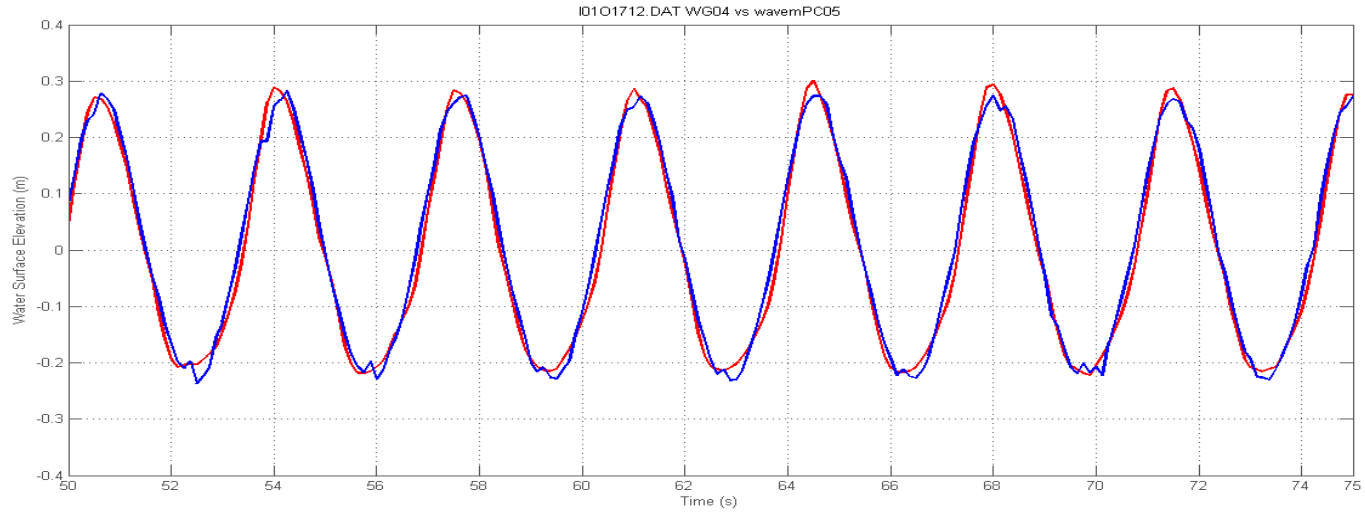

Figure 42: Water surface time series comparison for WG04 and processed PC05

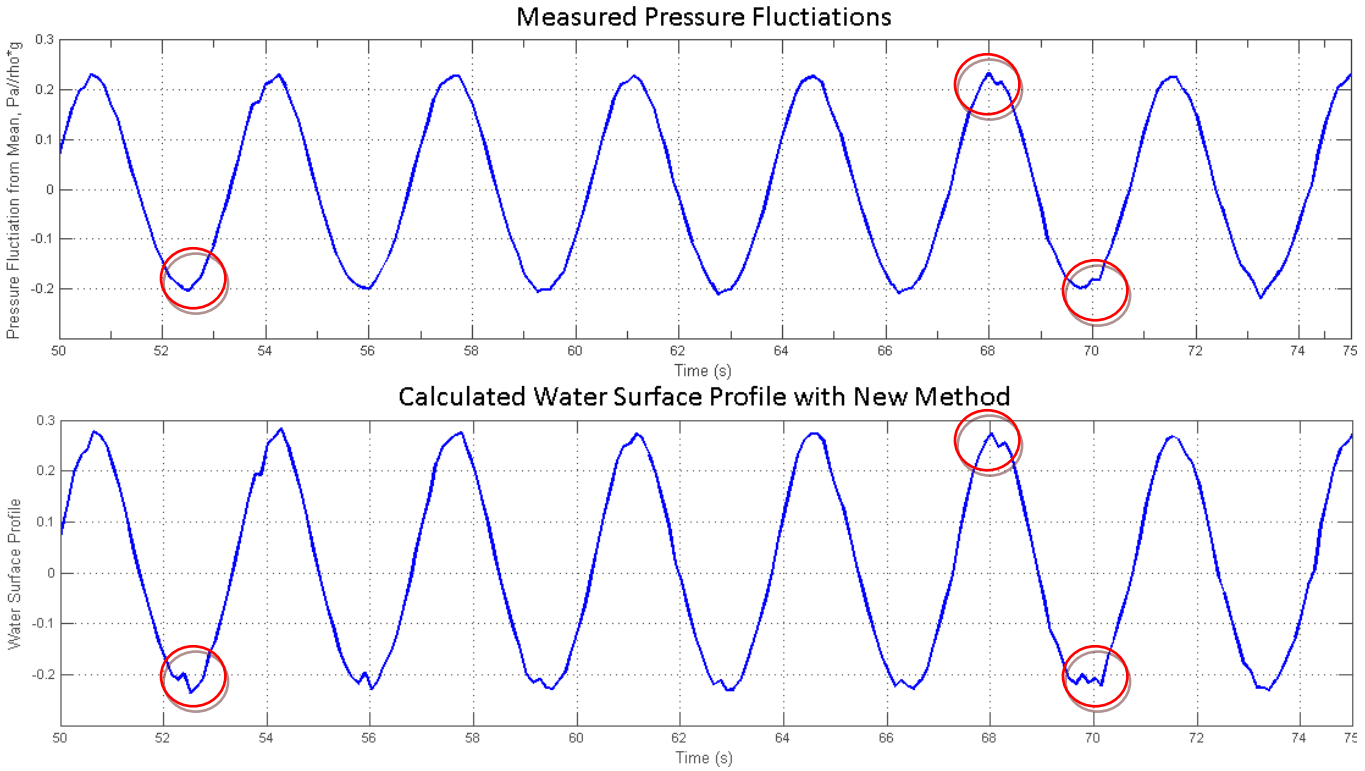

Figure 43: Pressure and Calculated Water Surface Profile for PC05 regular waves

The effect of these errors, induced by the pressure signal and the transfer function, were analyzed comparing the FFT spectra obtained through the capacitance gauges and the reconstructed water surface elevation through the

new method. The significant wave height, spectral peaks, and first and second moments were compared. Figures 44 to 51 shows the obtained spectra for cases A, B, C and I at for gauges WG03-PC02 and WG04-PC05 respectively.

In general good agreement is obtained in the calculated significant wave height, and spectral peaks, however there are differences in the first and second moments. The difference in spectral energy per frequency was then investigated.

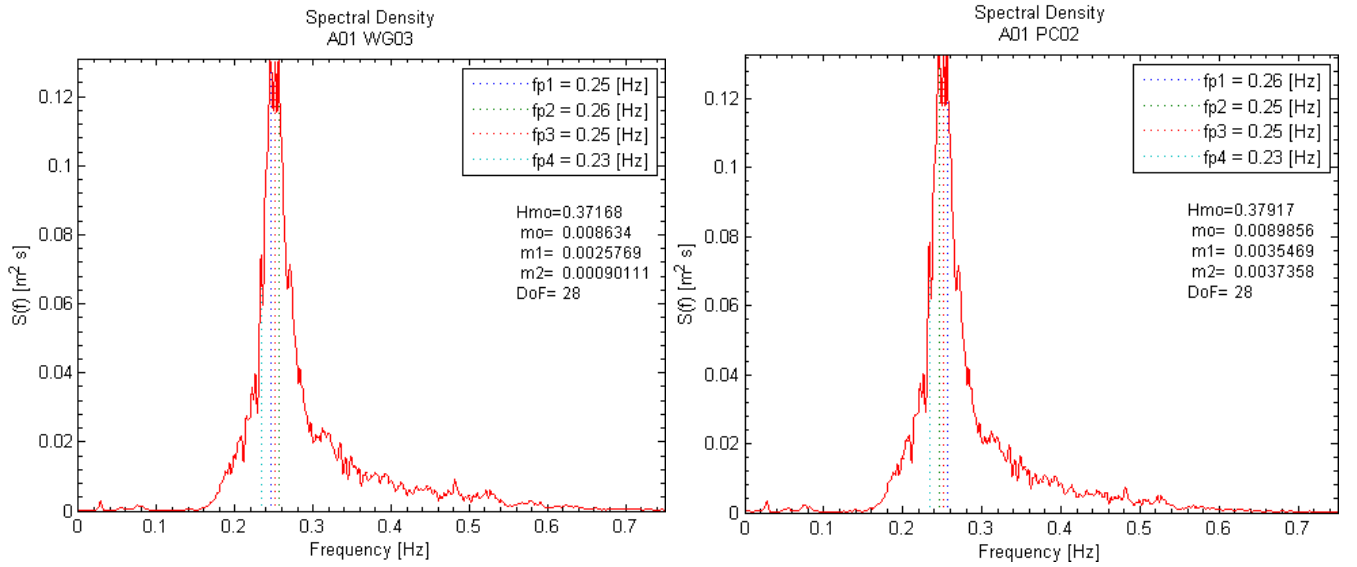

Figure 44: Spectra for WG03 and PC02 Case A

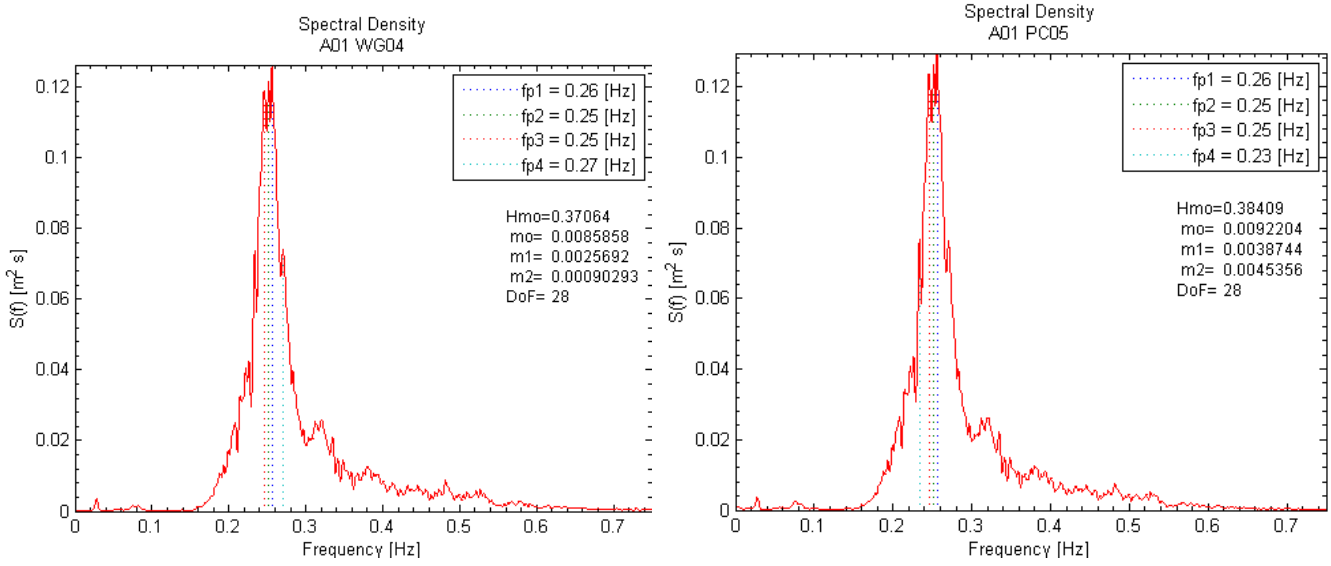

Figure 45: Spectra for WG04 and PC05 Case A

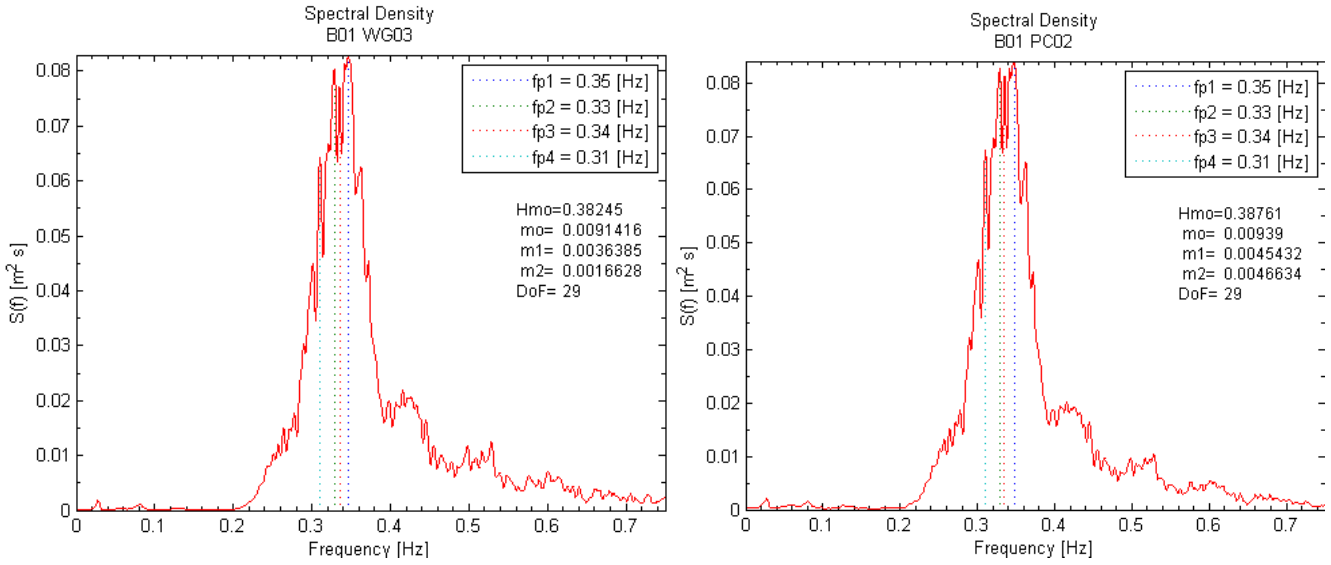

Figure 46: Spectra for WG03 and PC02 Case B

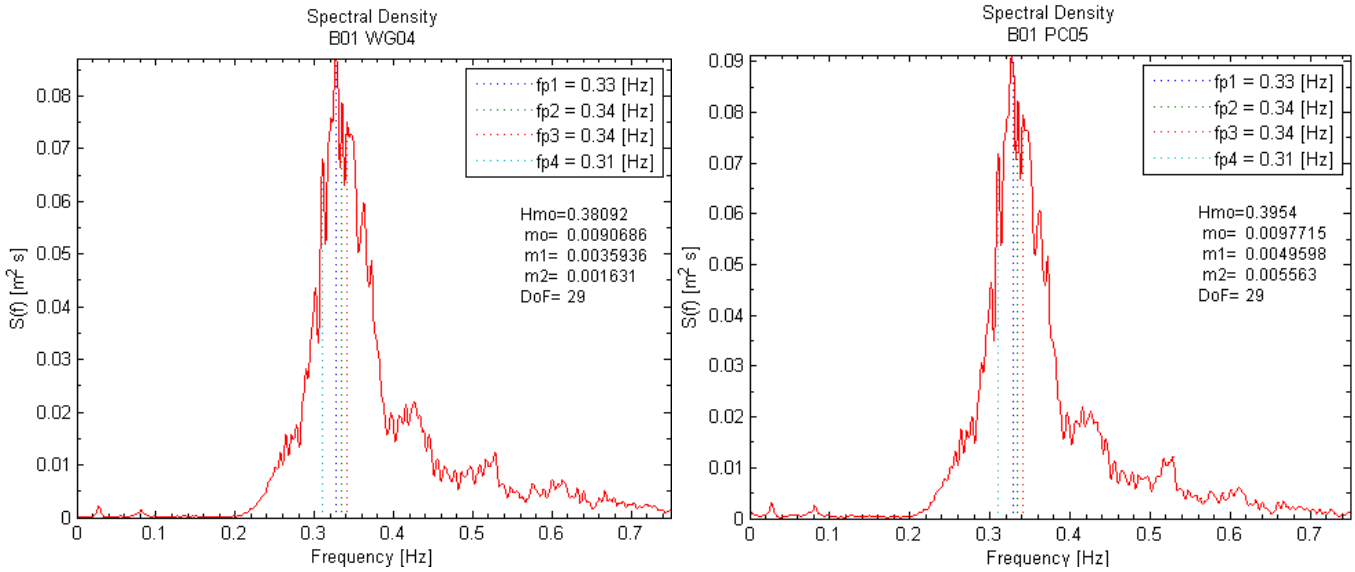

Figure 47: Spectra for WG04 and PC05 Case B

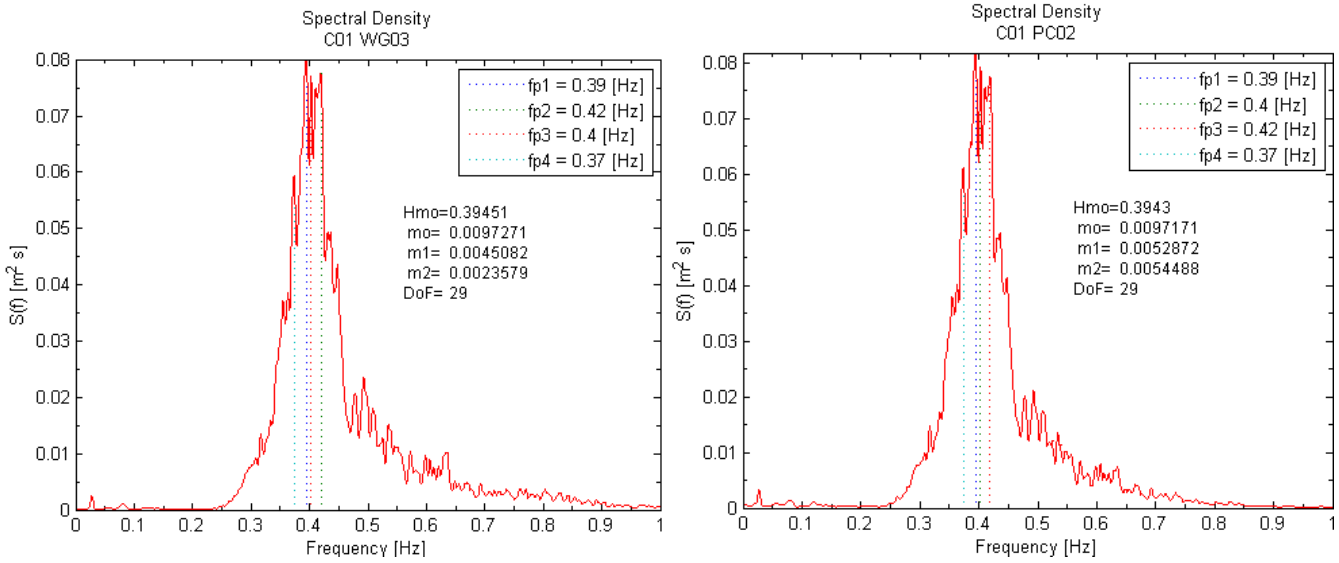

Figure 48: Spectra for WG03 and PC02 Case C

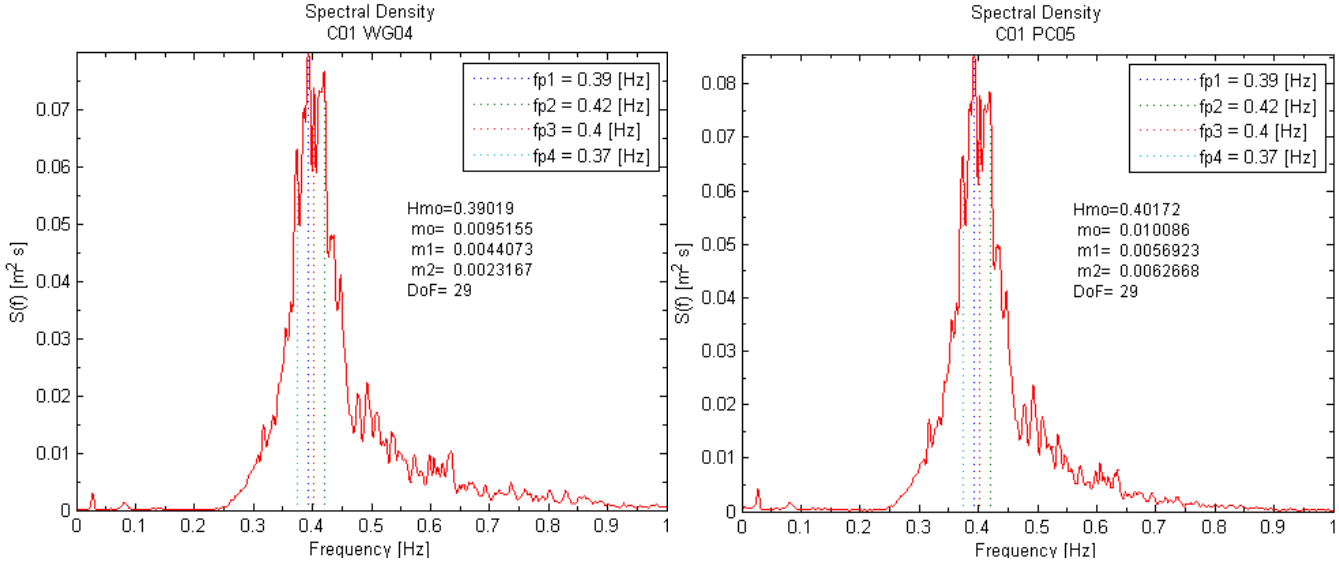

Figure 49: Spectra for WG04 and PC05 Case C

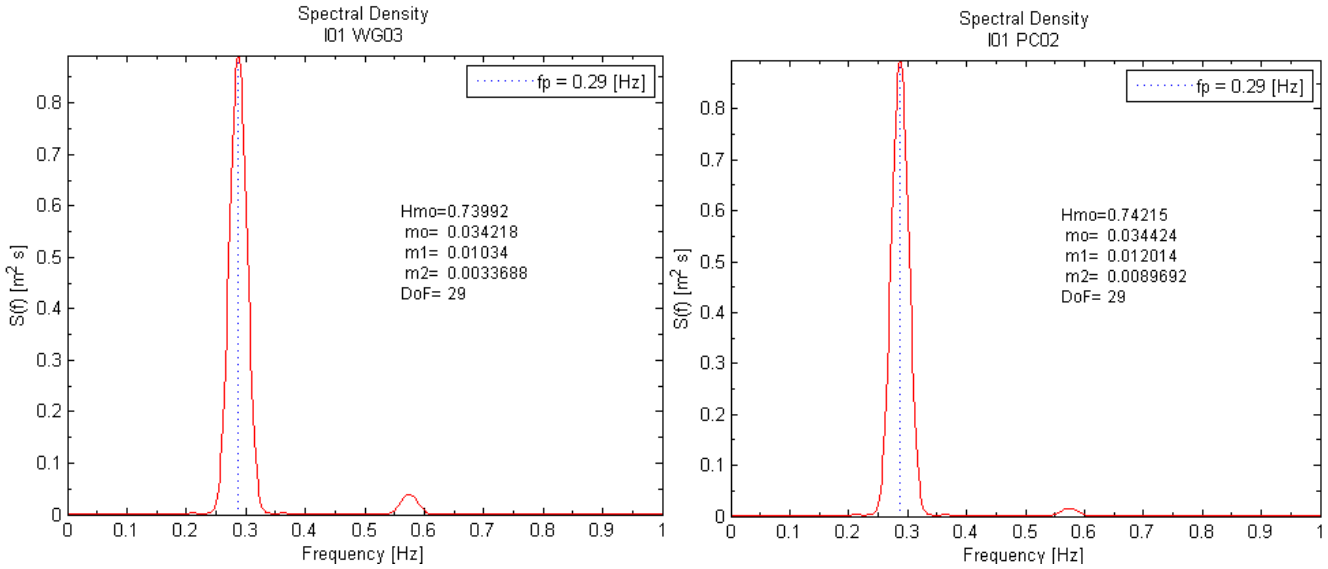

Figure 50: Spectra for WG03 and PC02 Case I

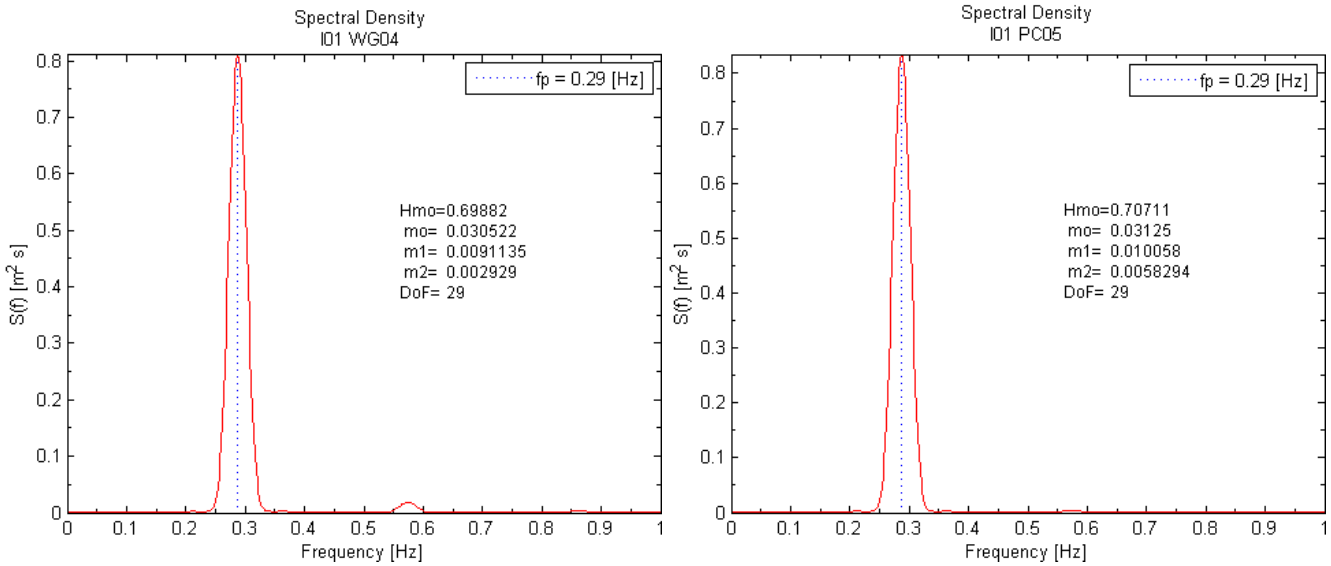

Figure 51: Spectra for WG04 and PC05 Case I

The obtained percentage error for the significant wave height and the peak spectral moments was obtained. The results are shown in table 2. The percentage error for the significant wave heights varied between 0.25% for case C WG03-PC02 and 3.67% for case B WG04-PC05. The percentage error for location WG04-PC05 is noticeable larger than for location WG03-PC02 in all cases. With regards to the peak spectral periods, the only error found was for the first case, however given the large set of data and the number of degrees used when calculating the spectra, 29, the high spectral resolution caused that at least 4 different spectral peaks were obtained for the

irregular wave cases. The 4 spectral peaks were the same in all cases; however in case A the order was changed. The error in spectral peak frequency is therefore practically zero.

Table 2: Percentage Error for the Significant Wave Height and Peak Frequency between the exact measurements and the calculated values with the new method.

	Hs (m)			fp (s)		
Irregular Waves	WG	PC	%Err	WG	PC	%Err
A WG03-PC02	0.372	0.379	1.88%	0.25	0.26	4.00%
A WG04-PC05	0.371	0.384	3.50%	0.26	0.26	0.00%
B WG03-PC02	0.382	0.388	1.57%	0.35	0.35	0.00%
B WG04-PC05	0.381	0.395	3.67%	0.33	0.33	0.00%
C WG03-PC02	0.395	0.394	0.25%	0.39	0.39	0.00%
C WG04-PC05	0.39	0.401	2.82%	0.39	0.39	0.00%
Regular Waves						
I WG03-PC02	0.74	0.742	0.27%	0.29	0.29	0.00%
I WG04-PC05	0.699	0.7047	0.82%	0.29	0.29	0.00%
	Mean		1.85%	Mean		0.50%

When comparing the spectral estimates in detail it was noticed that in general the higher frequencies were underestimated by the new method, and the lower frequencies were over estimated. This effect is responsible for the differences observed in the estimated first and second spectral moments. The inverse effect is obtained when calculating the free water surface through the spectral method, and many authors (Bishop and Donelan, Cavaleri, Grace) have reported these difference. For the spectral method based on the Fourier transform a frequency dependant N factor has been introduced. Figure 52 shows the N factor found from previous works.

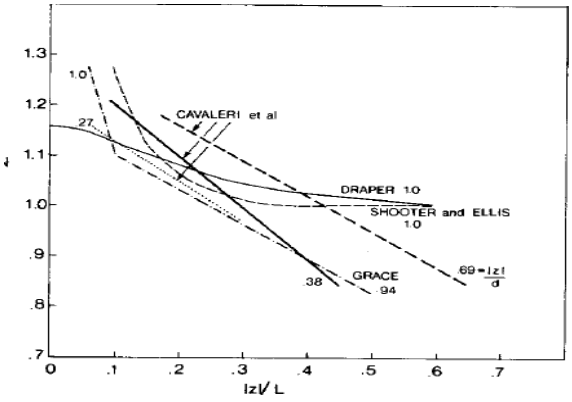

Figure 52: N correction factor for Spectral Method by previous researchers. (from Bishop Donelan 1987)

The frequency dependant N factor was then obtained for the analyzed data. First N was obtained as a function of the relative depth |z|/L. In our case |z| is always 0.50 meters, and the wave length was obtained for all the frequencies of the spectra at water depths of 1.8 and 1.9. The obtained correction factor N=Sw/Swp (wave spectral density divided wave spectral density obtained from the pressure record for each frequency bin), in figure 53, shows how the method is over estimating low frequencies and higher frequencies are under estimated.

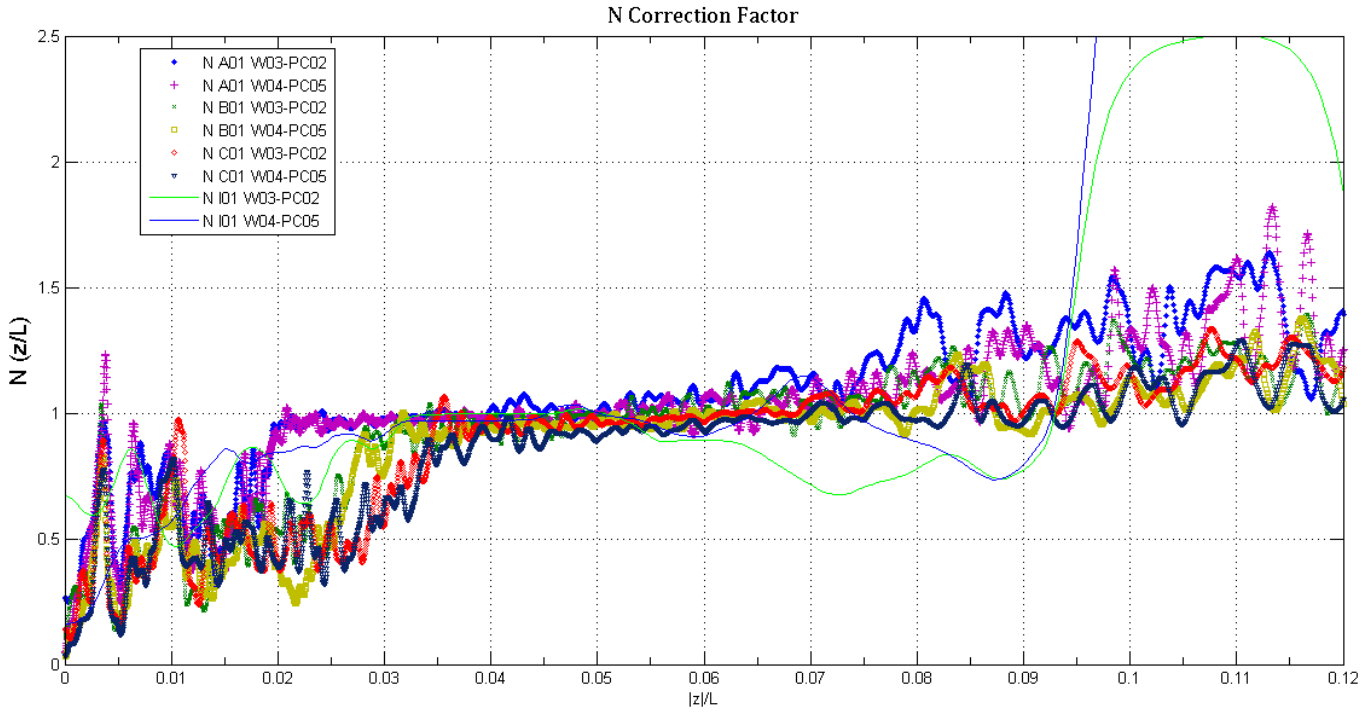

Figure 53: N correction factor as a function of relative depth |z|/L for the new proposed method.

For the analyzed spectra the water depth where the pressure sensor was located was relatively low, 0.5 meters. In all cases the spectral peak lies between relative depths of 0.02 and 0.083. The lowest relative depth was obtained for the case A where the input period was 4 seconds, for this case the zone were N is close to one also shifts towards the lower relative depths. Given this shift in stable results, and the fact that the significant wave height and periods were accurately obtained it is considered that the relative depth is not a good predictor for the N value. However a clear frequency dependant error is observed.

The obtained error in spectral energy content per frequency was then plotted against a normalized spectral frequency, fi/fp, where fi are the spectral frequencies and fp is the peak spectral frequency. Figure 54 shows the obtained relation of the correction factor N against the normalized spectral frequency. A stable zone, between 0.8fp and 1.2fp is visible. This stable zone explains why in all the obtained spectra there is a good agreement in the significant wave height and peak spectral periods, but a poor agreement in the first and second moment.

There seems to be a rotation in the spectra around its peak frequency, where frequencies lower than 0.8fp are overestimated and frequencies higher than 1.2*fp are underestimated.

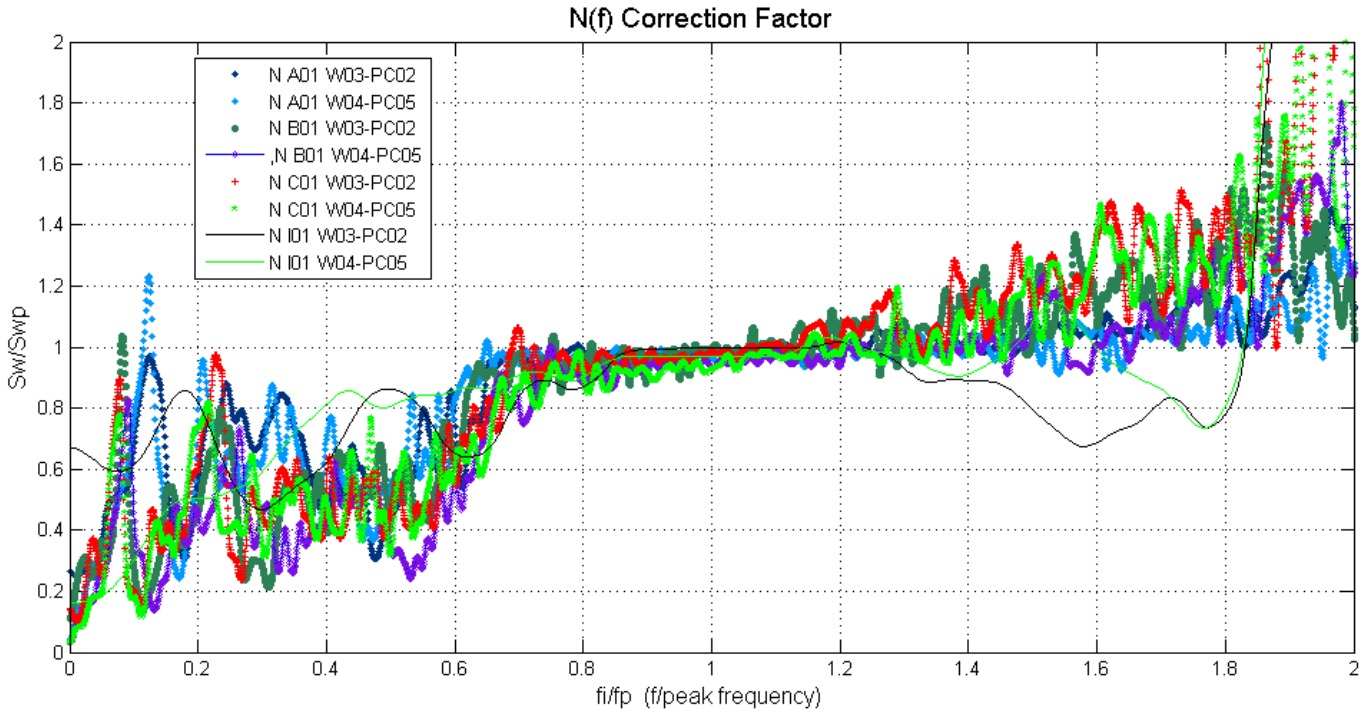

Figure 54: N correction factor as a function of normalized frequency, f/fp.

A correction factor dependant on these two limits, 0.8fp and 1.2fp is proposed. Two correction curves where obtained carrying out linear regression on the data for the zones 0fp to0.8fp and 1.2fp to 2fp. These correction curves were done using only the irregular wave conditions. Figure 55 shows the regression curves.

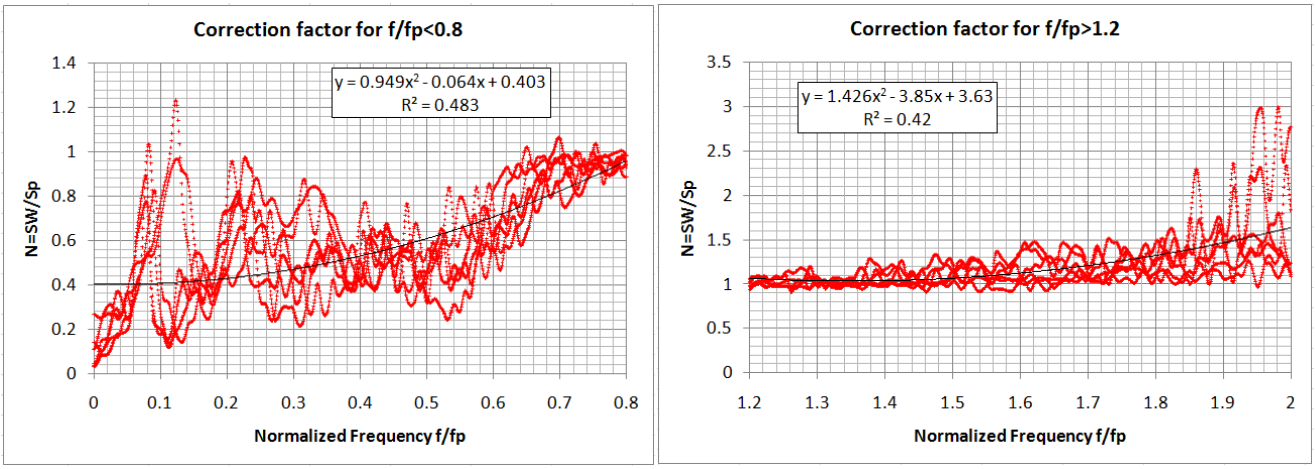

Figure 55: N correction factor as a function of normalized frequency, f/fp<0.8

3.0 Analysis of Wave Measurements

Wave measurements from 4 different locations were analyzed; the first data sets analyzed consisted of two wave measurement campaigns off the Pacific coast of Costa Rica, the second data set are wave measurements taken at the Ebro Delta in the Catalonian coast in the Mediterranean sea , the third data set analyzed are wave measurements carried out off the Atlantic coast of Costa Rica, and the fourth data set of wave measurements were from the Atlantic Coast near Cancun, Mexico during Hurricane Wilma.

All of the wave measurements were taken at intermediate waters, with water depths ranging from 3.5 to 22 meters, with peak spectral wave periods ranging from 3 to 22 seconds. For the cases of the measurements in Costa Rica and Spain, the wave measurements were carried out using submersible pressure sensors, the wave measurements in Mexico were carried out using an acoustic profiler mounted in the sea bottom.

The analyzed measurements off the Pacific coast of Costa Rica consisted of two different campaigns the first campaign consists of approximately one month of wave measurements carried out from August to October 2010, the second campaign was of *continuous* measured data started the 12th and ended the 19th of November both in 2010. These wave measurements were taken at approximately 22 meters of water depth in an exposed site. These measurements were carried by Watermark S.A for the Government of Costa Rica.

The measurements from Ebro Delta located in the Catalan Coast were carried out from the 1st to the 10th of November 1996 as part of the Ebro 96 campaign; these measurements were taken at approximately 3.5 meters of water depth. These measurements were carried by the Universidad Politecnica de Cataluna for the Ebro Delta 96 project.

The wave measurements off the Atlantic coast of Costa Rica consist of more than 1 month of wave measurements carried out from November to December 2010 at a water depth of approximately 17 meters. These measurements were taken just outside the port of Moin in an exposed site and were carried out by Watermark S.A for the Costa Rican Government.

The last data set analyzed consisted of 1 month of wave measurements in the Atlantic coast Mexico, during October 1995, when hurricane Wilma struck the coast. These measurements were carried out by the Universidad Autonoma de Mexico Professor Rodolfo Silva, outside of Puerto Morelos, Quinta Roo, Mexico, at a water depth of 22 meters.

3.1 Wave Measurements off the Pacific Coast of Costa Rica

Wave Characteristics in the Pacific Coast of Costa Rica

In the Pacific coast of Costa Rica long travelled swell is present[33]. Previously the wave climate in the Pacific coast of Costa Rica has been studied by Goda, 1983. His analysis was done using an ultrasonic buoy outside the Port of Caldera at approximately 14 meters water depth.

The swell waves are produced from storms located at a very long distance. The waves propagate from the generation zone across the Pacific Ocean, crossing the equatorial line to the Pacific coast of Costa Rica. During this propagation generally the wave height is reduced and the wave length increases, waves are dispersive. Generally the swell waves have peak spectral periods of more than 12 seconds and present low wave steepness. For the case of the waves that arrive to the Pacific Coast of Costa Rica, they are generated from large storms in the Southern Pacific in a zone of high and low pressure between 40°S to 60°S and 120° and 160°W. It is estimated, that these waves travel from 7.000 to 9.000 km or more[34]. This gives the waves very low directional spreading, and high wave grouping. This swells originating from as far as New Zeeland travel 3 to 6 days in the open ocean before they reach the Pacific coast of Costa Rica, one swell storm can affect vast a region from Chile to Mexico.

The wave field in deepwater along the pacific coast of Costa Rica is fairly uniform for a given swell because these waves were generated at such long distances. The only difference in deepwater is the time of arrival of the swells to the coast. Once these waves reach a depth of half of their wavelength they are affected by refraction, and shoaling, when they reach natural or artificial barriers they are affected by diffraction and reflection. For these swell waves, given that their periods can reach more than 18 seconds, their wavelength in deep water can be as much as 600 meters, which means they start to "feel the bottom", and get affected by refraction at depths around 300 meters.

In order to characterize the yearly average wave conditions along the Pacific coast of Costa Rica the Wavewatch III operational wave generation and propagation model from the National Oceanographic and Atmospheric Administration, NOAA, from the United States of America was used. Wavewatch III is a third generation wave model. This model has been operational since 1997. The model results are posted in monthly summaries of wave conditions every three hours, significant wave height, peak spectral period and peak spectral direction, in a 30 minute grid at ftp://polar.ncep.noaa.gov/pub/history/waves . This wave model takes the measured wind speed data from last sigma layer by satellite from the National Center of Environmental Prediction NCEP and adjusts them to a logarithmic profile to an altitude of 10 meters making the necessary correction for air and water

[33] Yoshimi Goda, "Analysis of Wave Grouping and Spectra of Long-traveled Swell", Port and Harbors Research Institute, Japan, Vol. 22, No. 1, March 1983, pp. 3 -41.

[34] F. E. SNODGRASS, G. W. GROVES,, K. F. HASSELMANN, G. R. MILLER, W. H. MUNK AND W. H. POWERS, "Propagation of Ocean Swell across the Pacific", Philosophical Transactions of the Royal Society of London. Series A, Mathematical and Physical Sciences, Vol. 259, No. 1103 (May 5, 1966), pp. 431-497

temperature. This model solves the radiation translation equation modifying the spectral parameters of the wave field. The average wave height-direction and wave-period distributions, for the “winter season” at deepwater in the Pacific coast of Costa Rica are shown in figure 56.

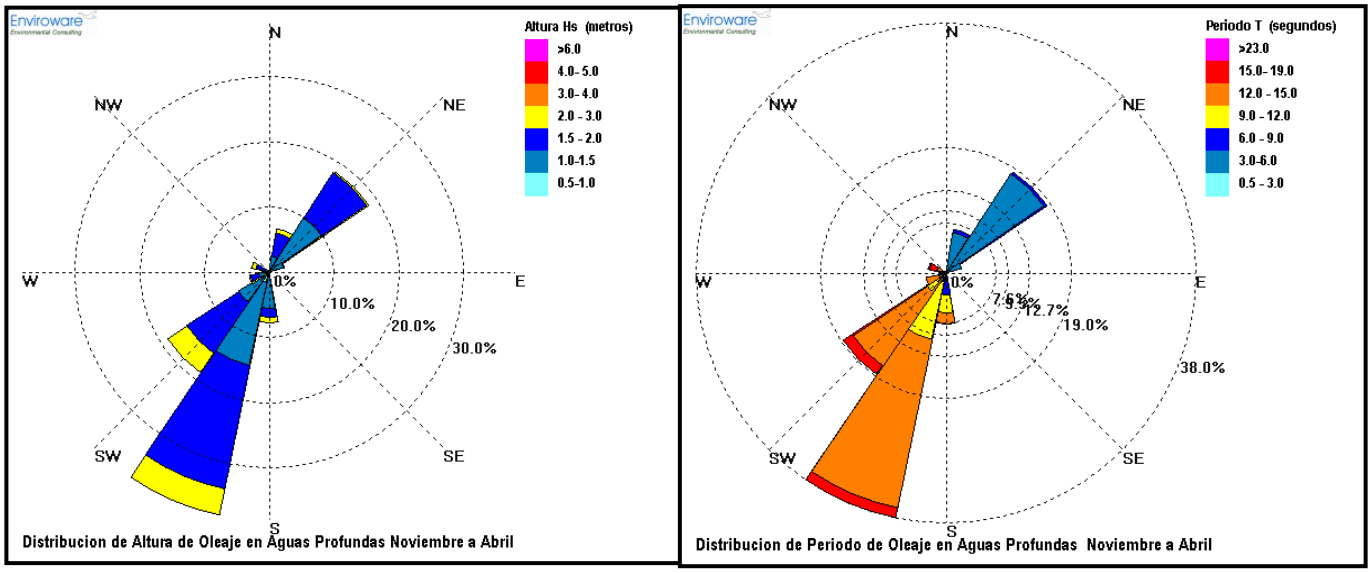

Figure 56: Wave height-direction “winter” distribution off the Pacific Coast of Costa Rica

The wave height-direction and period-direction distributions for the “summer” (May to October) from the NOAA Wavewatch III model hindcast for the Pacific coast of Costa Rica are shown in figure 57.

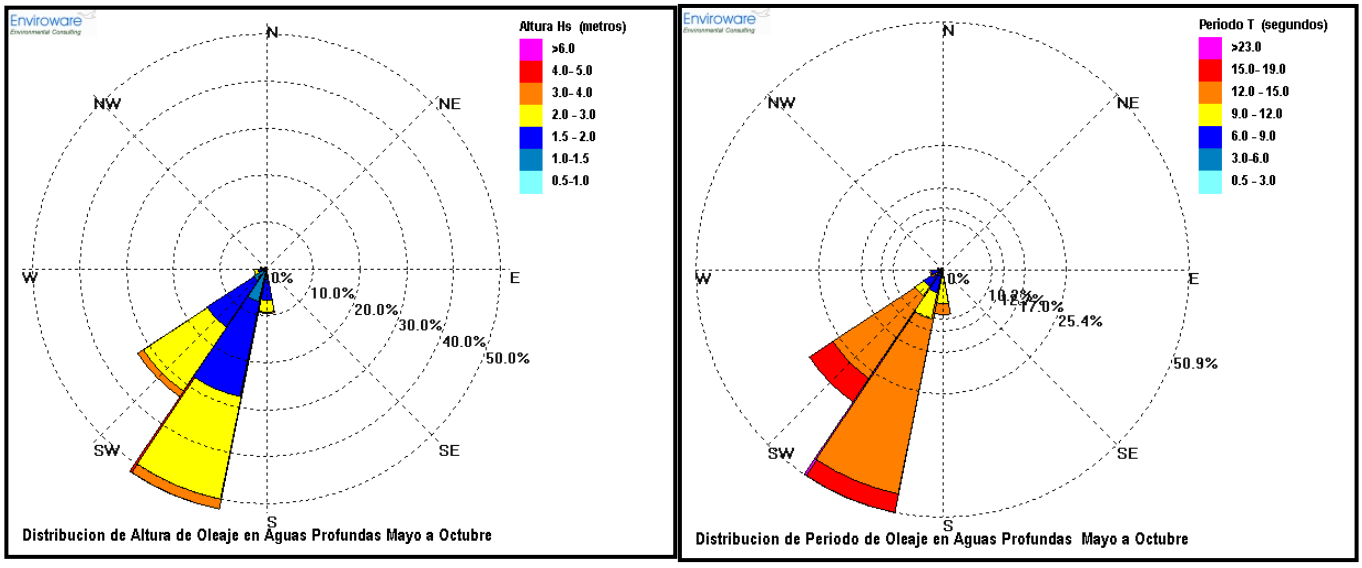

Figure 57: Wave height-direction “summer” distribution off the Pacific Coast of Costa Rica

The forecasts generated by Wavewatch III, global generation and propagation wave model, from NOAA, are used as a basis of determining the separation of the analyzed swell storms. The swell durations can vary between 2 and 5 days, with the highest periods, 21-18 seconds reaching first and then slowly decaying.

3.1.1 Location of Wave Measurements

The wave measurements were carried out off the Pacific coast of Costa Rica, at the northern part in Guanacaste. The wave measurements site was chosen because it is completely exposed to deepwater swell waves generated in the south or north parts of the Pacific. The bathymetry of the site was also investigated by means of the nautical charts and a depth sounding done in the area. Figure 58 shows the site location. The deepwater bathymetry, obtained through the digitalization of the existing nautical charts is also shown. In deep water, approximately 75 kilometers from the coast, the water depths are more than 1000 meters, then they rise quickly to a depth of 200 meters, this is because there is a large subduction zone through the whole Pacific coast of Costa Rica. At 200 meters, the continental shelf is present and there are approximately 50 kilometers of a mild slope until a more irregular bathymetry is found approximately 2 kilometers from the coast at a water depth of 20 meters. The wave gauge was located at a water depth of 22 meters, approximately 2 kilometers from the coast, outside Punta Indio between the beaches of Samara and Puerto Carrillo. The precise location of the wave gauge is shown in figure 59.

Previously, in order to compare the wave measurements with deep water wave hindcasts from the Global Wavewatch III model from NOAA a Fourier spectral type model was used to find the refraction and shoaling coefficients for wave conditions with wave periods between 8 and 20 seconds, and directions every 12.5 degrees. These transformation coefficients indicated that the expected differences between the deepwater wave height and the wave height, at the measurement location, were between 0.83 and 1.20. These means that the depending on the peak spectral wave period and its deepwater peak spectral direction the wave height can be amplified by a factor of 1.20 or reduced by factor of 0.83. However since the purpose of the present work is not to compare the measured versus modeled wave conditions at the site we will only use as a reference the deepwater wave conditions.

3.1.2 Description of Used Wave Gauge

The wave measurements were carried out using a submersible pressure type wave recorder. The pressure sensor manufacturer is RBR Ltd from Canada, and the model used was the TWR-2050P. The gauges measures temperature and has its depth channel calibrated to an accuracy of 0.05%. It uses internal Keller piezo-resistive strain gauge sensors. The sensors are absolute pressure sensors. Further details of the equipment can be consulted at http://www.rbr-global.com/products/tide-and-wave-instruments/twr-2050. At a the deployment water depth, of 22 meters wave periods of less than 6 seconds are not measured. When observing the frequency of occurrence in figures 56 and 57, wave periods per direction, it can be seen that the percentage of occurrence

of wave periods under 7 seconds is very low. The measured first campaign the gauge was at 2 Hz, with burst lengths 512 samples every 20 minutes. The second campaign the equipment was programmed at 1Hz with continuous bursts of 1024 seconds.

Figure 58: Wave Measurement Location

The equipment is deployed using divers and once per month the data is retrieved. Figure 60 shows a submarine picture of the location of the wave gauge, the turbidity of the water at the location is very low, no mayor rivers

are found near the area, and furthermore a small coral reef is found nearby, which means that the water is clear enough to maintain tropical corals at 25 meters water depth.

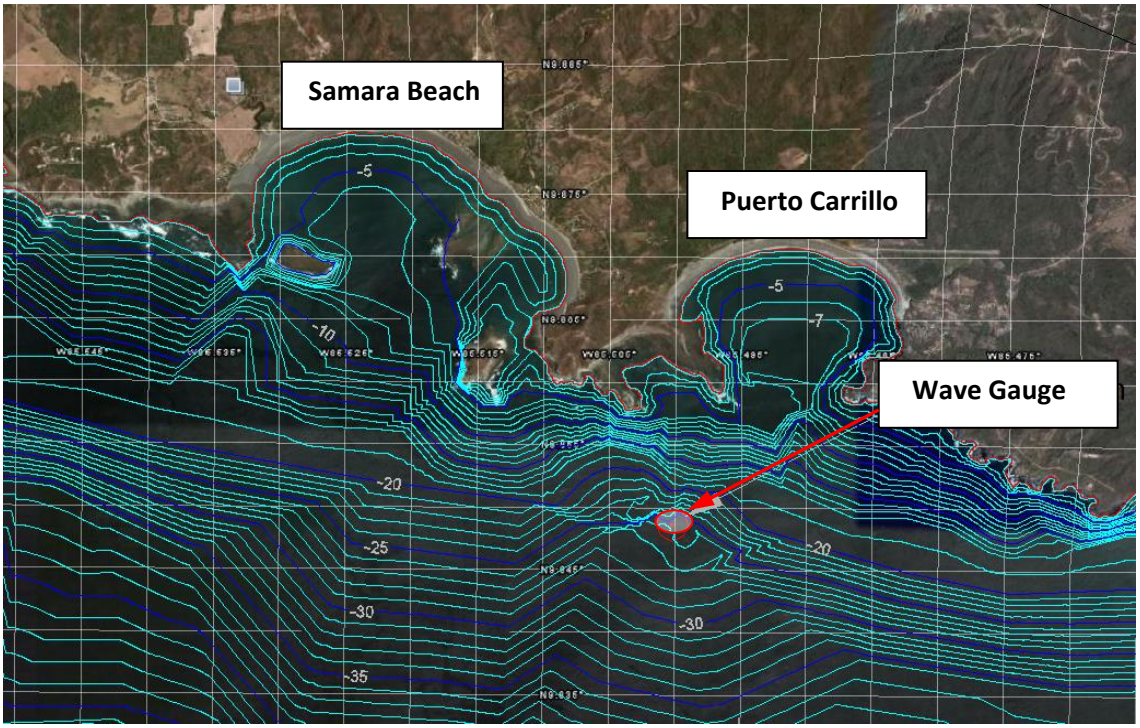

Figure 59: Site Location with depth contours @ 1 meter.

Figure 60: Pressure sensor location

3.1.3 Analysis of Wave Sources, General Comparison with Measured Waves

The sources of the measured waves were analyzed. These were determined using the Global model Wavewatch III from NOAA. To determine the origin of these long swells first a qualitative comparison between the measured significant wave height $H_{1/3}$ and reported hind casted spectral significant wave height Hs was done for the duration of the measurements. The reported hindcast peak spectral wave period was also compared with the measured peak period. Figure 61 shows the results of the comparison.

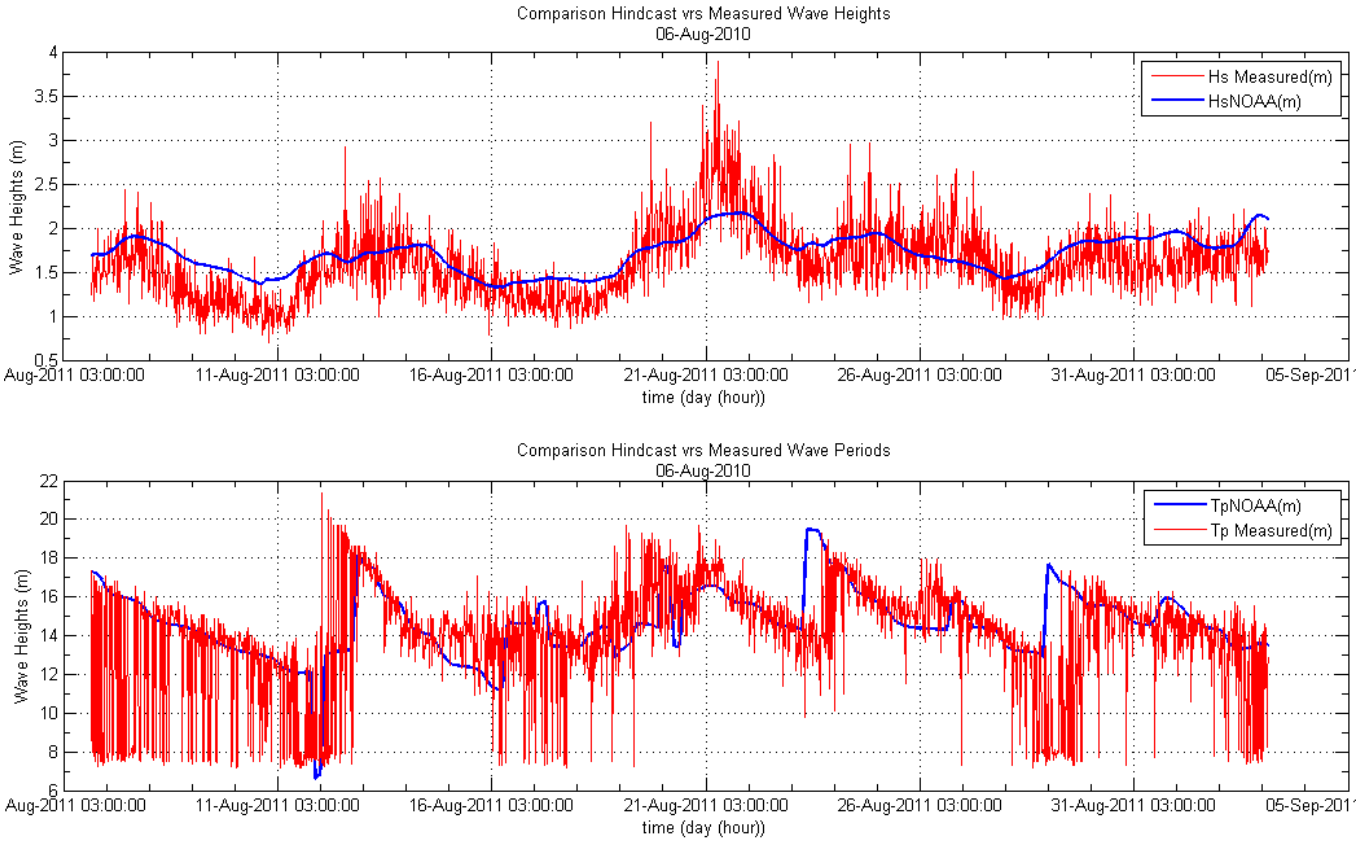

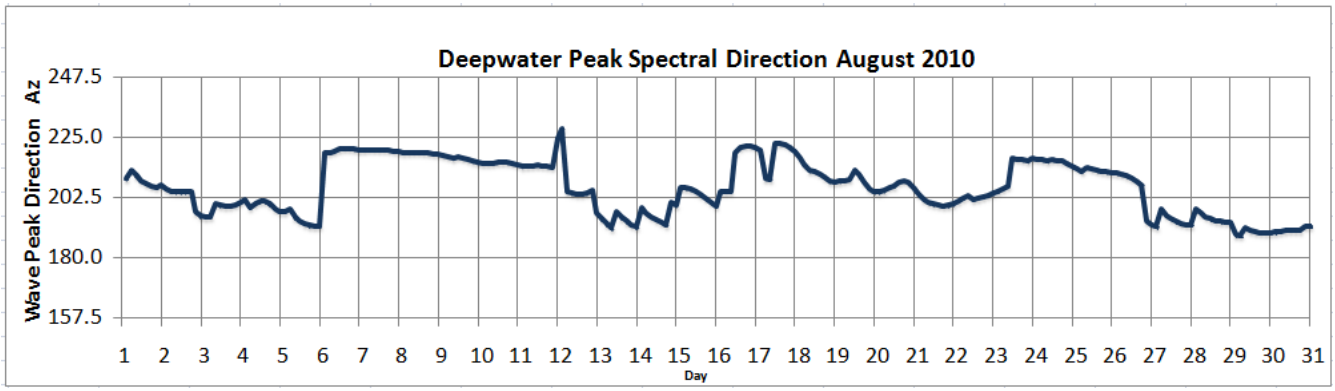

Figure 61: Deepwater Wave Hindcast and Measured Waves for Campaign Nº1 off the Pacific Coast off Costa Rica

From the figure 61 it can be seen that at least 5 swells were measured. As reference whenever there is a jump in the hind casted peak spectral period, upwards from 12-13 seconds to 17-19 seconds means the arrival of a new swell, when the fastest waves arrive. After the arrival the wave periods become smaller as slower waves arrive. The deepwater wave directions vary between 185 degrees, a Swell coming from the south and 225 degrees, a swell arriving from the southwest. The highest wave conditions measured occurred between the 20th and the 22rd, where at least two different swells arrived, one with 14 second peak spectral period and the other with 19 seconds.

The wave sources of the first campaign were studied in detail given the high wave conditions measured. For the 2nd campaign the sources were also investigated, and were of similar origin, the roaring 40's in the south pacific but of lesser energetic content.

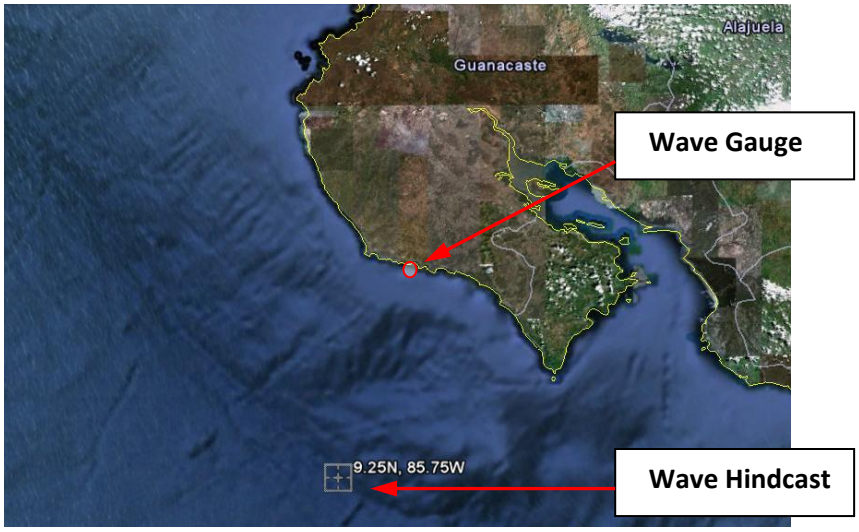

Figure 62: Wave hindcast location and measurement location, Google Earth

For the hindcast information obtained at ftp://polar.ncep.noaa.gov/pub/history/waves/ the selected output point for the comparison was latitude 9.25 North, and 85.75 West, the location of the data is shown in figure 62.

As it has been mentioned before the comparison done is qualitatively, since the objective of the present work is neither to calibrate nor corroborate the accuracy of the global model Wavewatch III by NOAA. For a quantitative comparison the transformed deepwater conditions need to be compared, which is out of the scope of the present work. Wave sources were examined by means of the monthly animation published by NOAA at http://polar.ncep.noaa.gov/waves/historic.html .

Storm from the 19th to the 23rd of August

The generation area was identified to be between latitudes 60 and 30 south and between longitudes 180 and 90 west. Figure 63 shows a large storm at latitude 60S and Longitude 120W, with significant waves over 13 meters. The area of the storm is almost the size of Australia, which means that the fetch is very long.

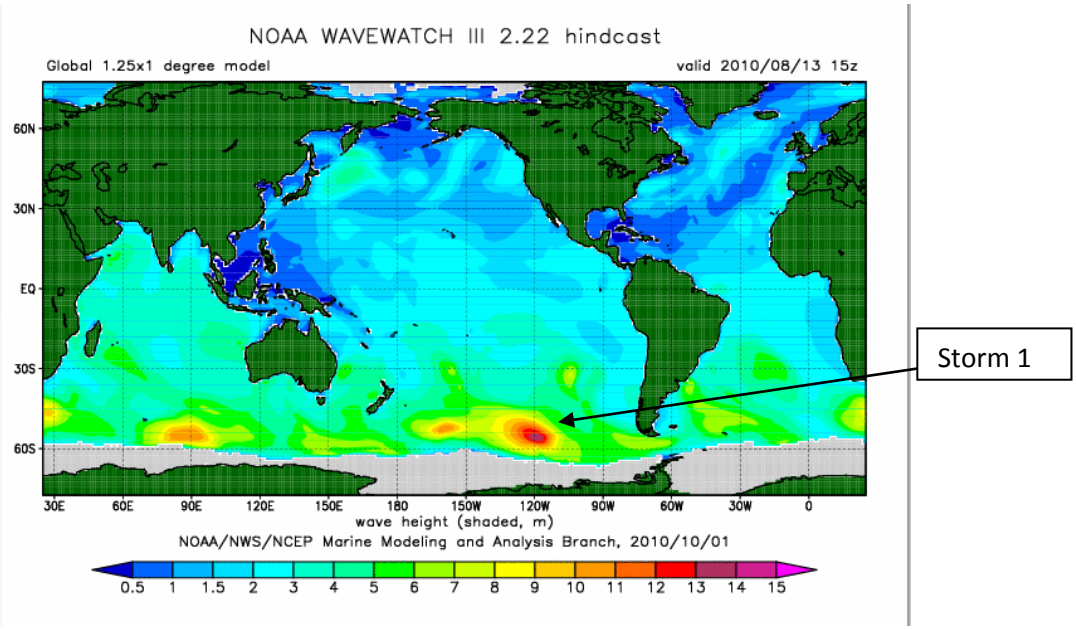

Figure 63: Large Storm at 60S and 120W during the 13th of August

The wave periods generated from this large storm were tracked until 5 days later they reached the Pacific coast of Costa Rica, and the measurement location the 19th of August. The waves travelled across the equator a distance of more than 8000 kilometers. According to the measurements waves with a significant wave height of up 3.5 meters affected the coast during 3 days and the significant wave periods were between 15 and 17 seconds.

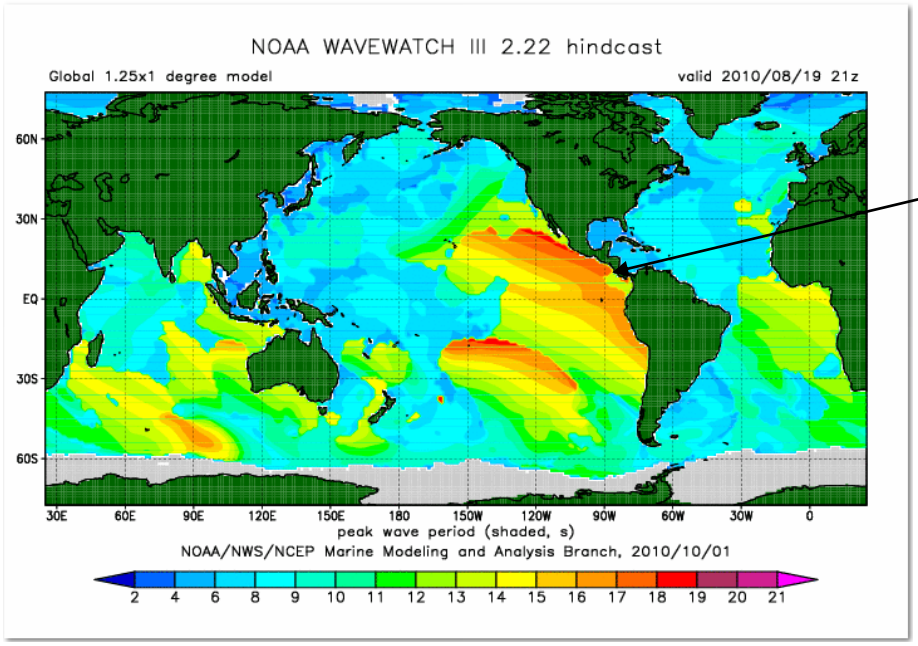

Figure 64: Swell waves reaching measuring site from large storm at 60S and 120W 5 days later.

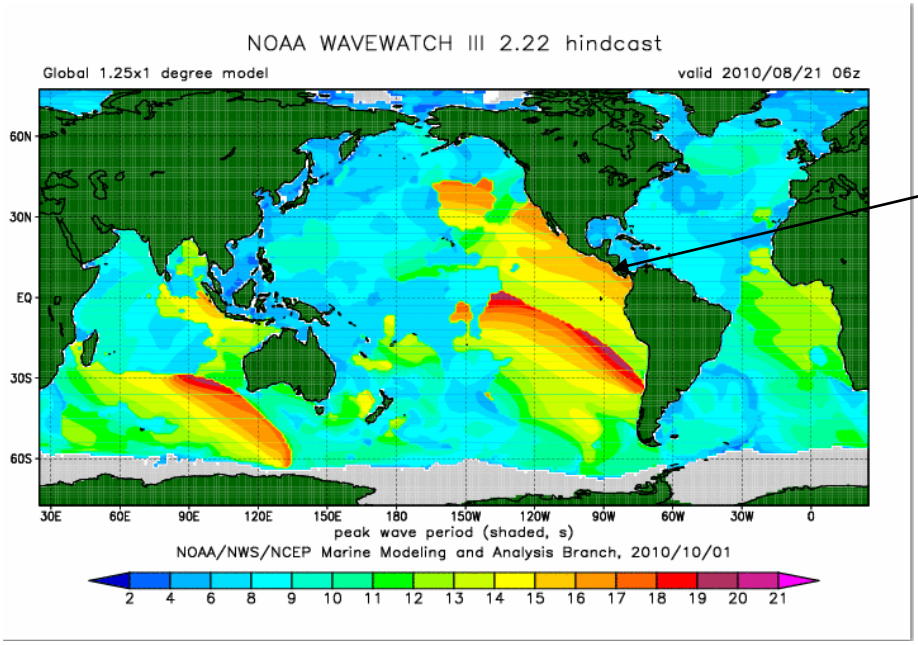

Figure 65: Swell waves peak conditions at measuring site from large storm at 60S and 120W 5 days later.

Storm from the 19th to the 23rd of August

The second storm that was analyzed corresponds to the one that was measured from the 19th to the 23rd of August. This storm is shown in figure 66; its size is larger than Australia. The waves generated by this storm were also tracked until the longer faster periods reached the wave measurements location 5 days later.

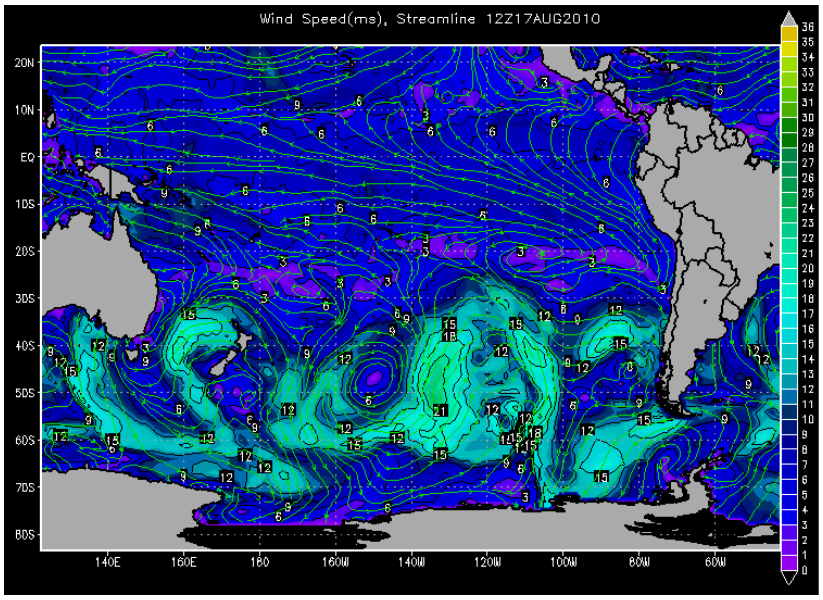

Figure 66: Wind Field in the South Pacific that originated the 2nd Storm

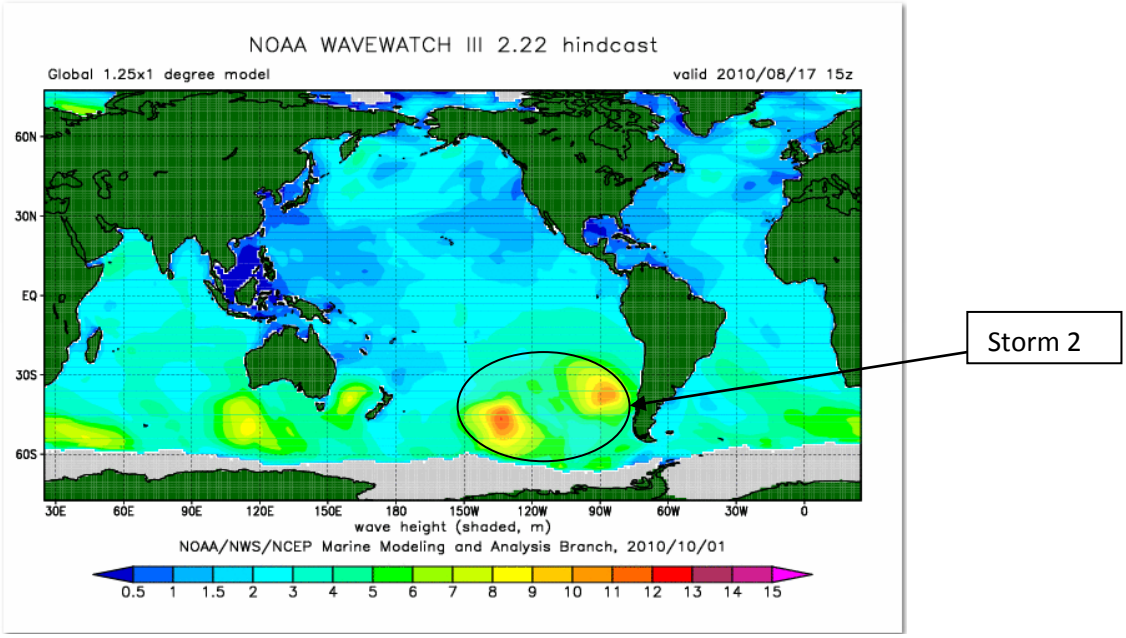

Figure 67: Large Storm between 60S to 30S and 150W to 85W during the 17th of August.

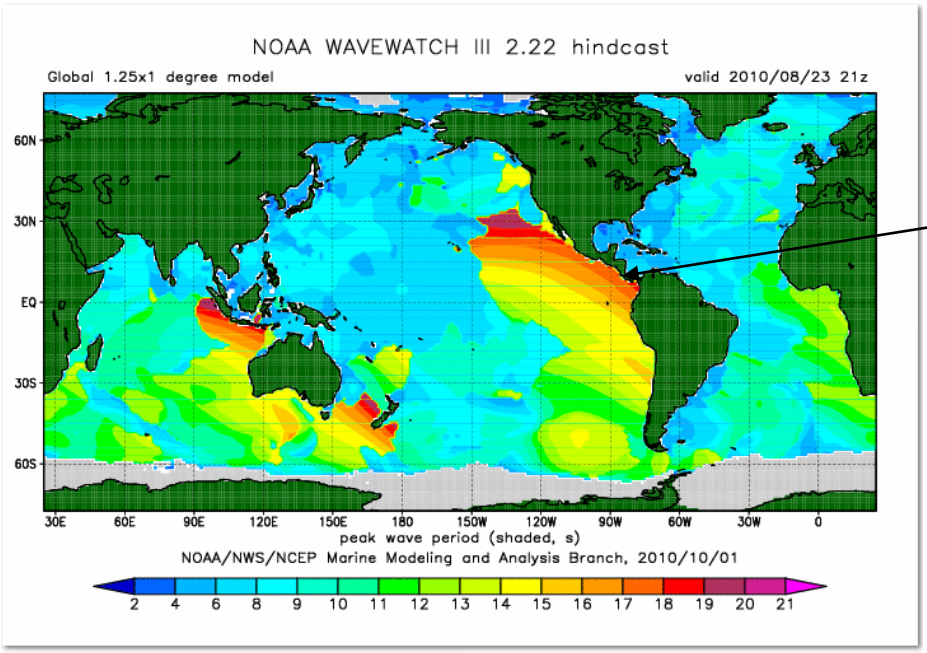

Figure 68: Swell waves reaching measuring site from large storm 5 days later.

The waves associated from this storm were present from Chile to Alaska in the northern hemisphere. The largest waves that were measured during this storm had wave periods from 17 seconds to 15 seconds. The peak spectral direction of the wave field in deep waters was 202.5 north azimuths, a south-southwest direction.

During the 2nd campaign the storms in the South Pacific Ocean had similar origins, between the latitude 30 and 60 south. However the events were much smaller than the ones measured during the first campaign. The comparison between the deepwater hindcast and the measured waves is shown in figure 69. The highest significant wave heights measured occurred during the 13th of November, considerably low periods for the location, possibly affected by waves generated by storms closer to the coast. After the 16th of November, swell waves with peak spectral periods of 17 seconds appeared, the same swell slowly decayed during the rest of the measurements. The decay shows almost a perfect correlation between the measurements and the hindcasted data with approximately losing only one second every 16 hours.

The storm origin can be also inferred by Snodgrass's et al 1966 rate of spectral shift formula,

$$D = \frac{g}{4\pi}\frac{df}{dt}$$

Eq. (65)

Where D is the travel distance and df/dt is the rate of change of the spectral peak.

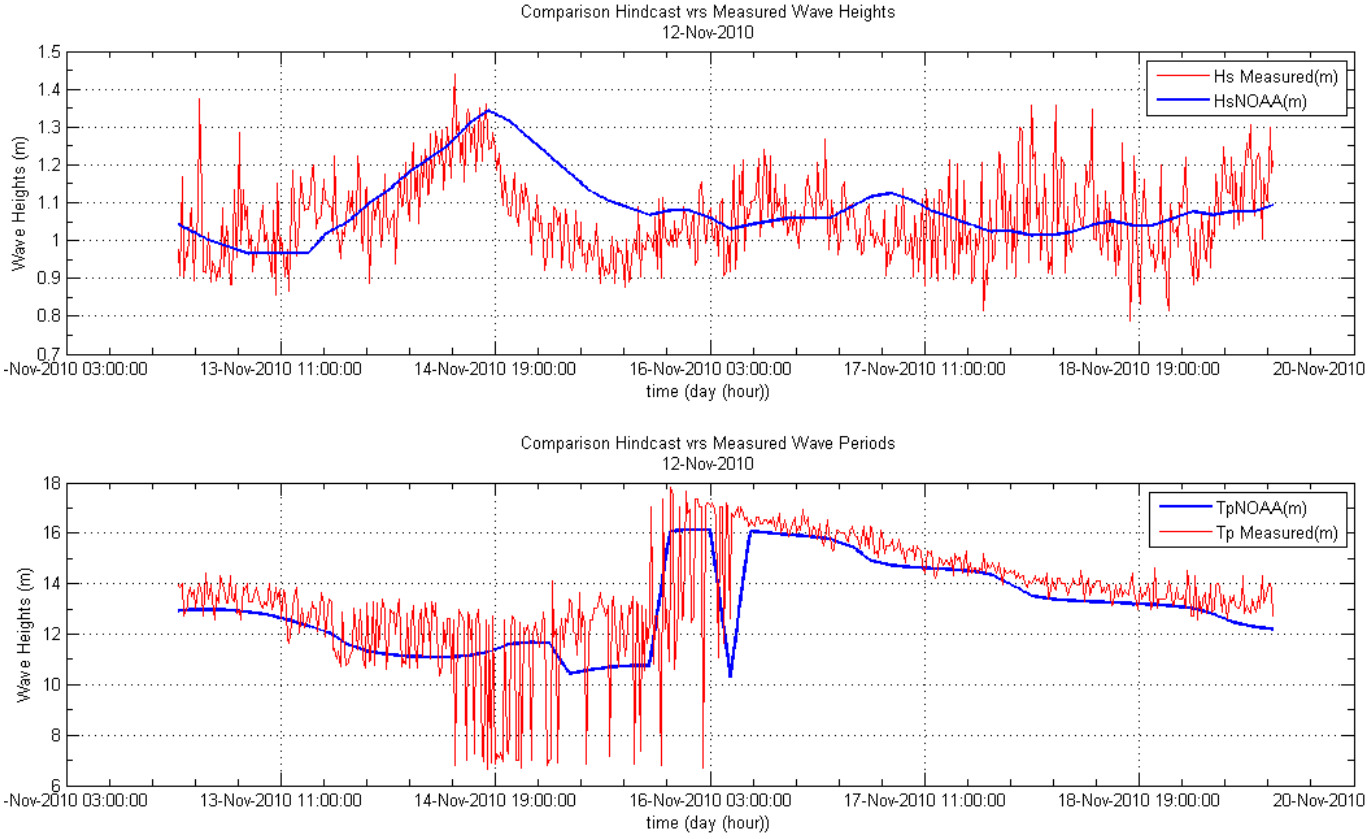

Figure 69: Deepwater Wave Hindcast and Measured Waves for Campaign Nº2 off the Pacific Coast off Costa Rica

3.1.4 Statistics Based on Zero-Down Crossing

During first wave measurement campaign, August 2010, five events were measured, and during the second measurement campaign, November 2010, two swell events were measured. In the following chapters the results of the analysis of the whole data is presented.

Figures 70 and 71 present the measured statistical values based on the zero down crossing method of the maximum, significant and root mean square wave heights and wave periods based on the zero down crossing method for the measurements during August and November respectively. The relation between these and other statistical wave heights and periods was examined for both measurements, tables 3 and 5 show the relation between these values for both measured wave campaigns. In general it can be seen that the standard deviation during the first measurements campaign was much larger than for the second one. It is estimated that the presence of several simultaneous swell events and the shorter bursts lengths is the reason for this higher standard deviations.

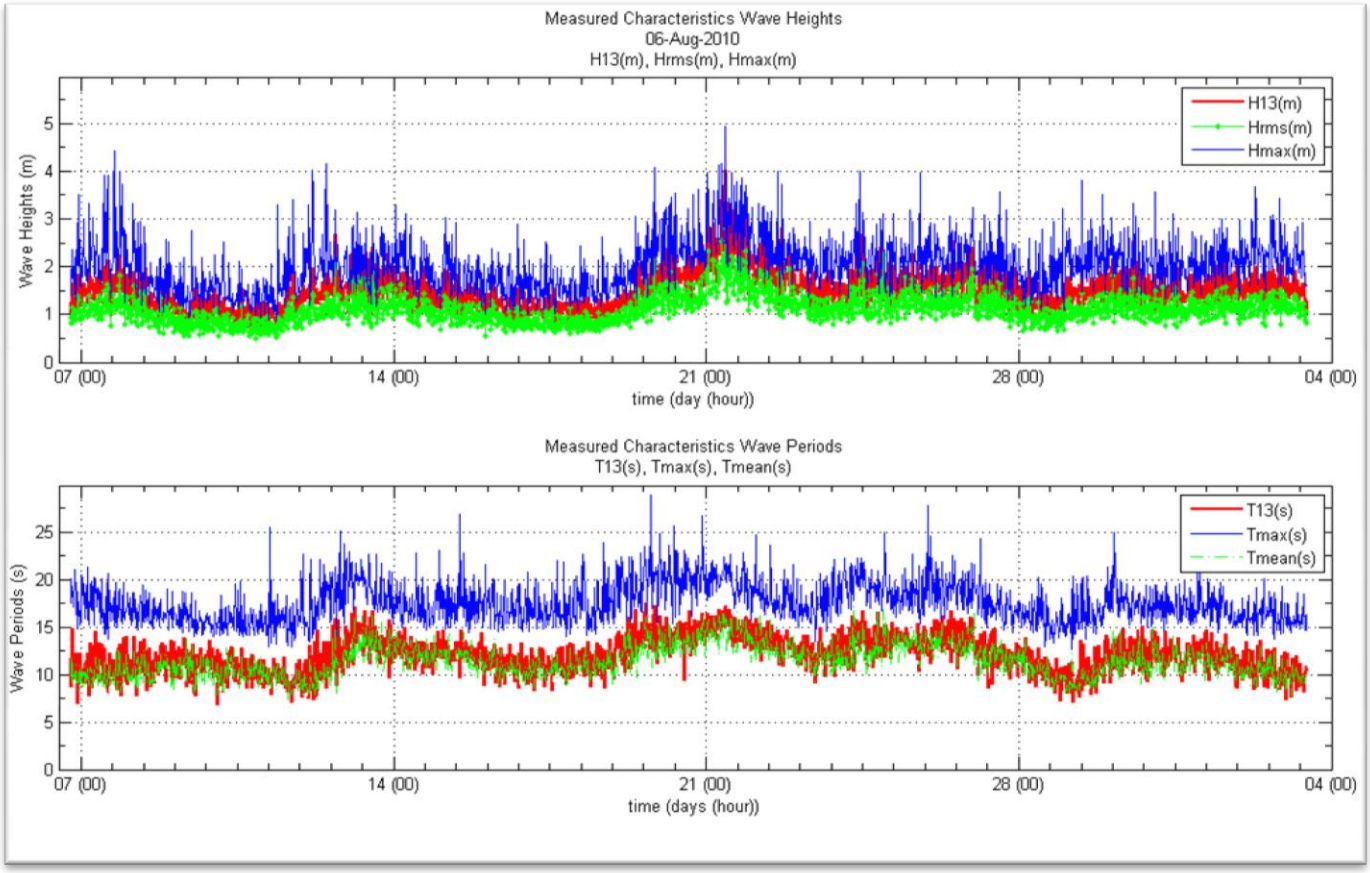

Figure 70: Temporal Variation of Wave statistical Characteristics based on zero down crossing for Long Travelled Swell August 2010.

Table 3: Ratios of the Characteristic Wave Heights and Periods based on the ZDC Long Travelled Swell August

	$H_{max}/H_{1/3}$	$H_{1/10}/H_{1/3}$	$H_{1/3}/H_{mean}$	$H_{1/3}/H_{rms}$	$T_{max}/T_{1/3}$	$T_{1/10}/T_{1/3}$	$T_{1/3}/T_{mean}$
Mean	1.379	1.035	1.477	1.328	1.484	0.800	1.056
Standard Deviation	0.196	0.218	0.123	0.073	0.227	0.211	0.106

Table 4: Skewness and Kurtosis Long Travelled Swell August 2010.

	Skewness	Kurtosis
Mean	0.04	3.15
Standard Deviation	0.21	0.95

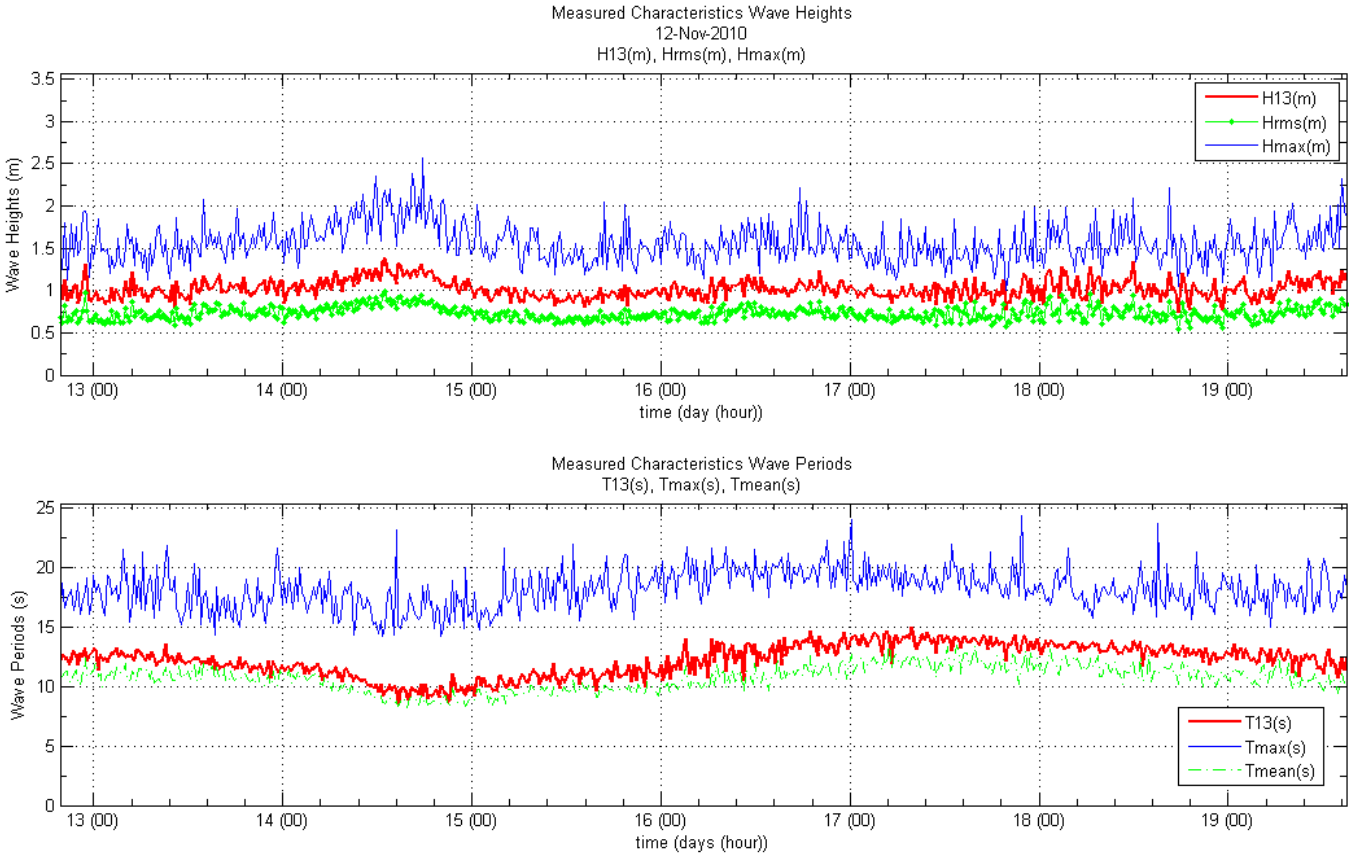

Figure 71: Temporal Variation of Wave statistical Characteristics based on zero down crossing for Long Travelled Swell November 2010.

Table 5: Ratios of the Characteristic Wave Heights and Periods based on the ZDC Long Travelled Swell November

	$H_{max}/H_{1/3}$	$H_{1/10}/H_{1/3}$	$H_{1/3}/H_{mean}$	$H_{1/3}/H_{rms}$	$T_{max}/T_{1/3}$	$T_{1/10}/T_{1/3}$	$T_{1/3}/T_{mean}$
Mean	1.546	1.199	1.545	1.385	1.506	0.964	1.133
Standard Deviation	0.169	0.059	0.056	0.029	0.179	0.056	0.055

Table 6: Skewness and Kurtosis Long Travelled Swell November

	Skewness	Kurtosis
Mean	0.02	3.00
Standard Deviation	0.09	0.29

The ratios of table 3 and 5 were obtained from 1992 and 574 wave records respectively. The ratios are much lower than the expected values predicted by the Rayleigh distribution. The reason why $T_{1/3}$ is actually lower than $T_{1/10}$ is because $T_{1/3}$ is obtained as the periods of the one third highest waves associated with the significant wave height, while $T_{1/10}$ is obtained as the mean of the one tenth highest periods. There still debates within the coastal engineering community on how to calculate $T_{1/3}$, under the author criteria the present calculation method is physically more representative of the energetic conditions, and $T_{1/10}$ should also be calculated as the associated periods to $H_{1/10}$, nevertheless scare should be taken when evaluating design formula on how the statistical period was obtained.

The maximum wave measured for both campaigns was also obtained with its given time series. Figures 72, 74 and 75 shows the maximum measured waves and the wave group where they were found. For the long travelled swell measured in August, the maximum wave occurred the 21st within a group of 3 very similar waves all with heights above 4.5 meters and zero down crossing periods of 17 seconds the group presents a discontinuity at the 4th wave with seems to be missing a crest, wave-wave interaction seems a plausible explanation for such occurrence. Such measured wave groups are constantly present during the days that these swell was measured, in which two different swells were simultaneously present.

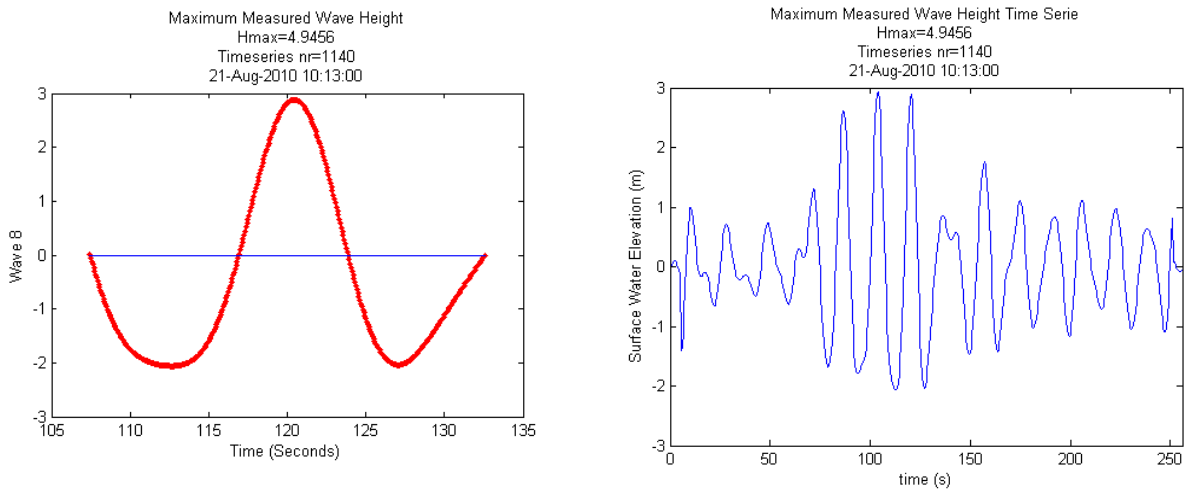

Figure 72: Maximum measured wave height and wave group based on zero down crossing for Long Travelled Swell.

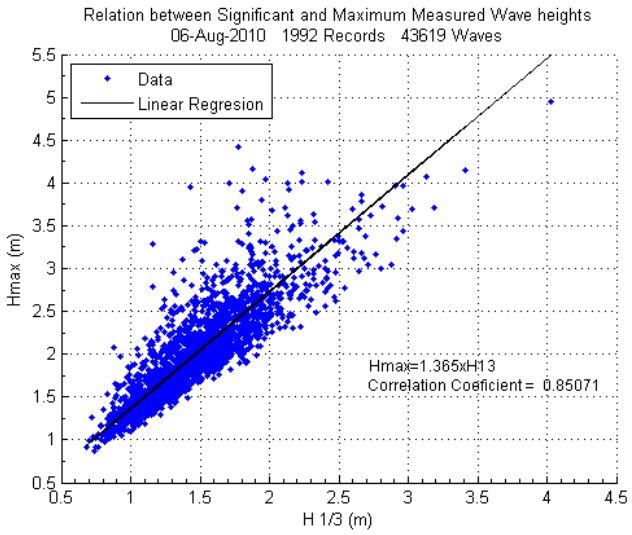

Figure 73: Regression Hmax vs $H_{1/3}$ long travelled swell August 2010.

For the case of the measured swell during the second campaign, November 2010, the highest wave measured 2.57 meters, and as seen it is composed of a deep trough but a small crest. When examining the whole time series where this wave occurred, no groups of such nature, or similar waves are found. However this wave is succeeded by relative calm short period, which is also not present in the rest of the time series. In order to evaluate the occurrence of such events the relation between the significant (H1/3) and maximum measured wave heights was further investigated by a linear regression between these values for both campaigns. The results are shown in figures 73 and 76.

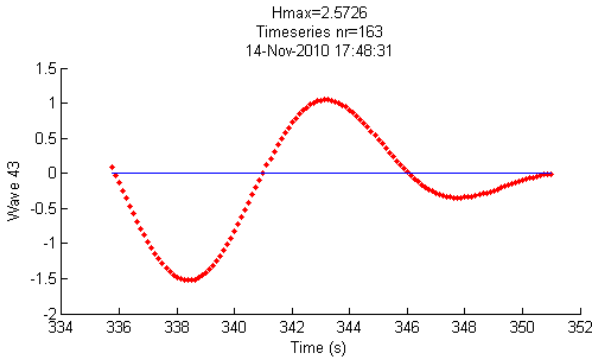

Figure 74: Maximum measured wave height based on zero down crossing for Long Travelled Swell.

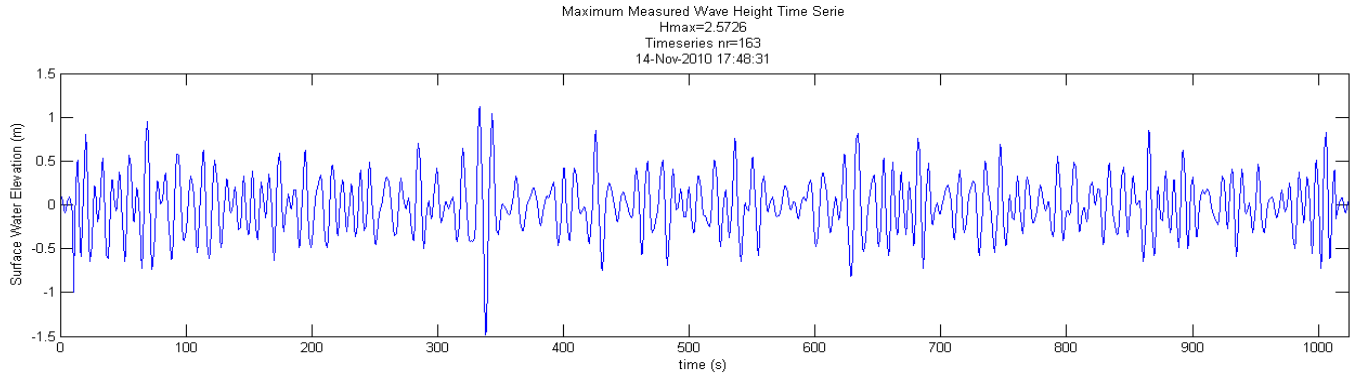

Figure 75: Group were maximum measured wave height was found.

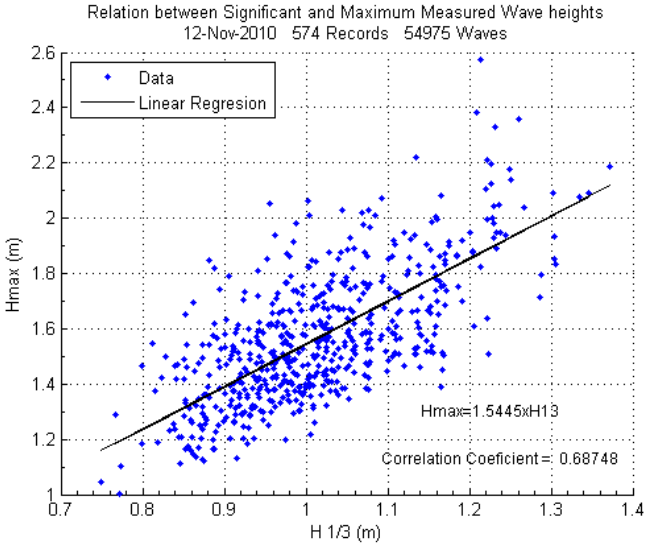

Figure 76: Regression Hmax vs $H_{1/3}$ long travelled swell November 2010.

The difference in the results between both measurement campaigns is surprising. The larger swells measured during August have a much higher correlation coefficient, 0.85, compared to the second measurement campaign,0.69. The largest measured wave during the second campaign is the highest outlier value, and in fact the outliers tend to be positive in the second regression. The reason for such a difference in between both measurements is explained from the fact that the first measurement campaign was not continuous and the sample length was short, most probably causing a miss of these high outliers. Given that the occurrence of such high waves is low, they appear in the second wave measurement campaign since the measurements were continuous. These positive outliers from close investigation of the wave records in the second measurement campaign are considered to be real and non spurious data.

The marginal probability distribution of the individual wave heights and periods was then investigated for both measurement campaigns. Figures 77 show the obtained results compared to the theoretical Rayleigh distribution

for the wave heights. A smoothed Kernel function was applied, however the fitting is not considered acceptable. The mean of the root mean square value over the whole measurement campaign was used to non dimensionalize the wave heights, while the mean period over the whole campaign was used for the wave periods. Given the fact that 5 different large swells were measured during the first campaign, the variability of the H_{rms} will affect the results.

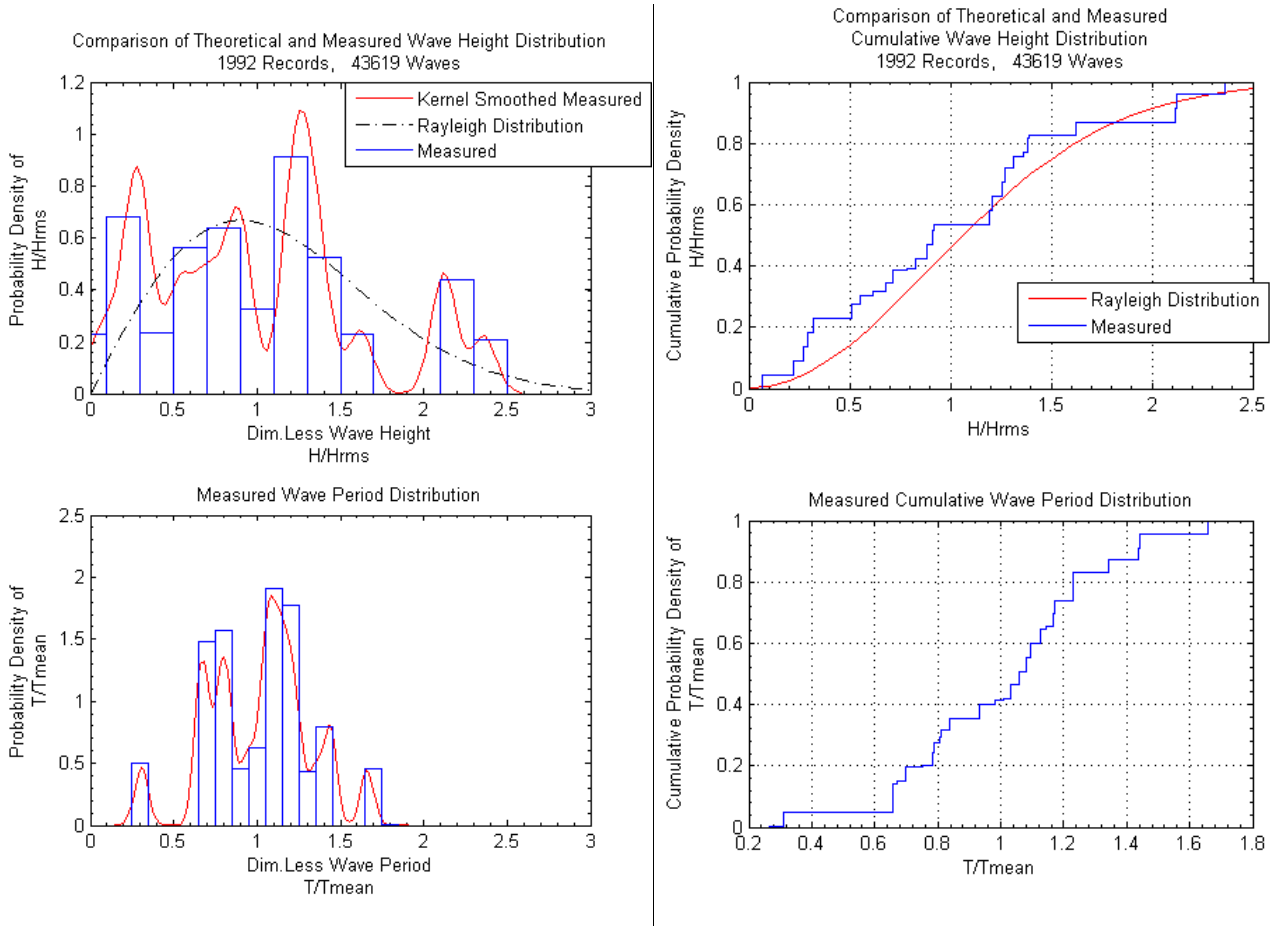

Figure 77: Marginal wave height and wave period probability distribution for long travelled swell August 2010.

The second wave campaign presents a good fit to the Rayleigh distribution, which is more clearly seen when the exceedance probability is used for comparison purposes figure 61. During the August swell measurements the lower root mean square value causes a large shift in the exceedance probability curve, figure 77. This means that individual waves will tend to be higher than what the Rayleigh distribution assumes. This effect seems more pronounced for larger swells. Goda (1983), found similar results for long travelled swell, he pointed out that the departure from the Rayleigh distribution of these long travelled swells was because the Rayleigh distribution is

based on slightly larger values of correlation coefficients than the measured ones. The measured correlation coefficient is investigated in the wave grouping chapter.

For both measurement campaigns the marginal wave period distribution is similar, with a small tendency to have more waves above the mean period. The mode tends to be 1 with a small departure from this value, almost all individual periods fall between 0.5 T/Tm and 1.5T/Tm

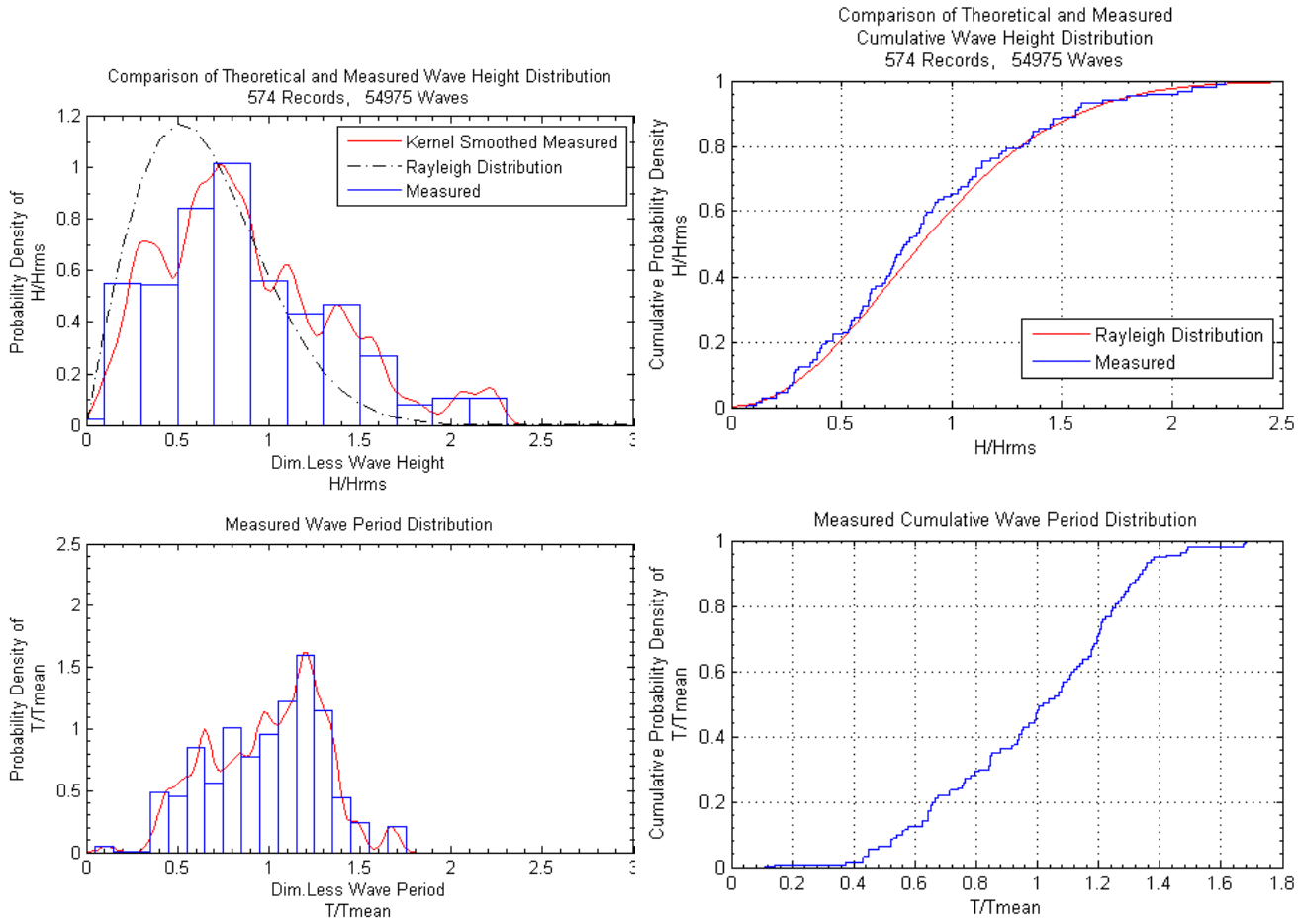

Figure 78: Cumulative wave height and wave period probability distribution for long travelled swell November 2010.

The joint distribution of wave individual wave heights and periods was then investigated, figures 79 and 80 show the measured distributions for the August and November campaigns respectively. The 1992 records, containing 43619 waves were used in the August campaign. For this campaign a strong correlation between waves in which H/H_{rms} and T/T_{mean} are equal to 1.1 is seen. The largest waves, where H/H_{rms} is above 1.5 tend to have periods between $1.3*T_{mean}$ and $1.4*T_{mean}$. For a mean period of 12.5 seconds the largest individual waves will have a period between 16.25 and 17.5 seconds, based on the zero down crossing. These values are in accordance to the highest measured wave height shown in figure 72.

The joint individual wave height and period for the second measurement campaign during November is shown in figure 80. A sharp peak, which is also present in the August campaign, is visible at the dimensionless period T/T_{mean}= 0.5-0.7 and H/H_{rms}=0.25.

Both individual joint height-period distributions show a clear bimodal distribution, with the larger waves for the larger periods, and smaller waves for shorter periods.

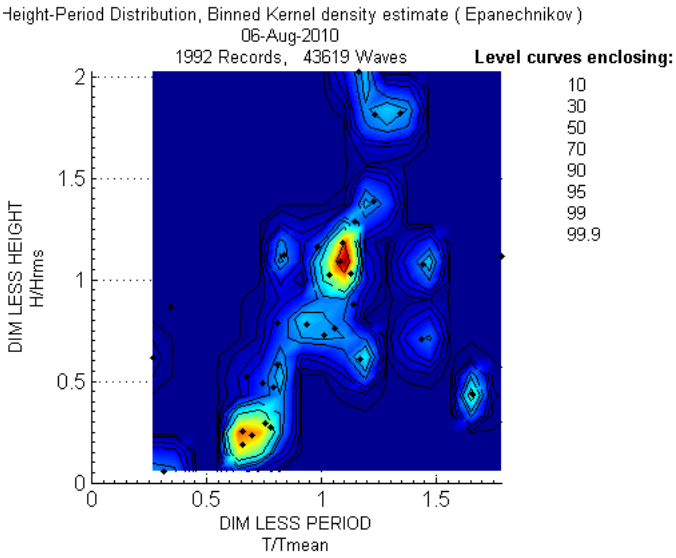

Figure 79: Joint individual wave height-period probability distribution for long travelled swell August 2010.

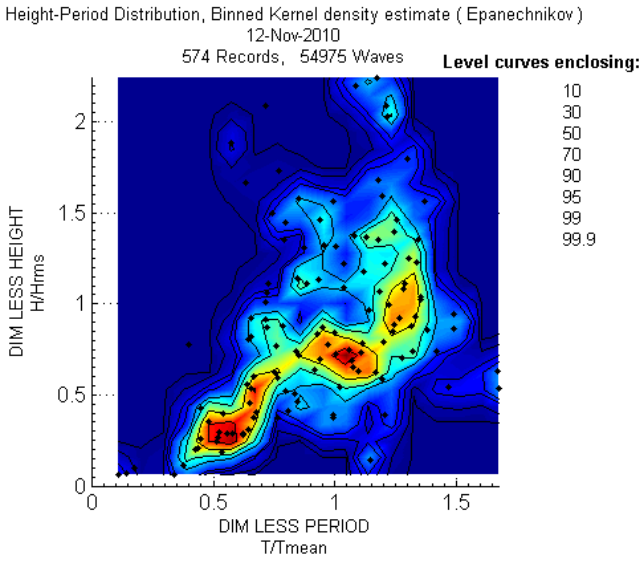

Figure 80: Joint individual wave height-period probability distribution for long travelled swell November 2010 (FFT Method and NEW Method).

3.1.5 Spectral Analysis

The detailed spectral analysis was carried on the both wave measurement campaigns. The temporal variation of the estimated spectra for each time series is present for both cases in figures 81, 82, 83 and 84. Then the temporal variation of the spectral characteristics is also analyzed. Finally the spectrum of the most energetic wave conditions and its fit to the JONSWAP spectra is presented. Again, even though TMA or Ochi-Hubble bimodal are better descriptive spectra for these waves, the JONSWAP was used for comparison and convenience purposes given its wide application within the coastal engineering community.

The temporal variation of the energetic conditions is not clearly defined when the wave time series are analyzed using the zero down crossing method, however when the spectral analysis is used the temporal variation of the wave energy is clear, as shown in figure 81. This spectrogram shows 5 clearly visible swell events. When viewed in plan view the temporal variation of the energy content per frequency component is clear. The five events measured during August arrive with frequency around 0.05, a wave period of 20 seconds, there after the period "decays" in all cases at a very similar rate. Between the 19th and the 23rd two different swells arrived at almost the same time (within 1 day of difference).

For the calculation of the spectra for both measurement campaigns the same lag was. Given that the sample length of the time series was different the number of degrees of freedom, dof, varied between both campaigns, for the first the dof used was 9 and for the second 18.

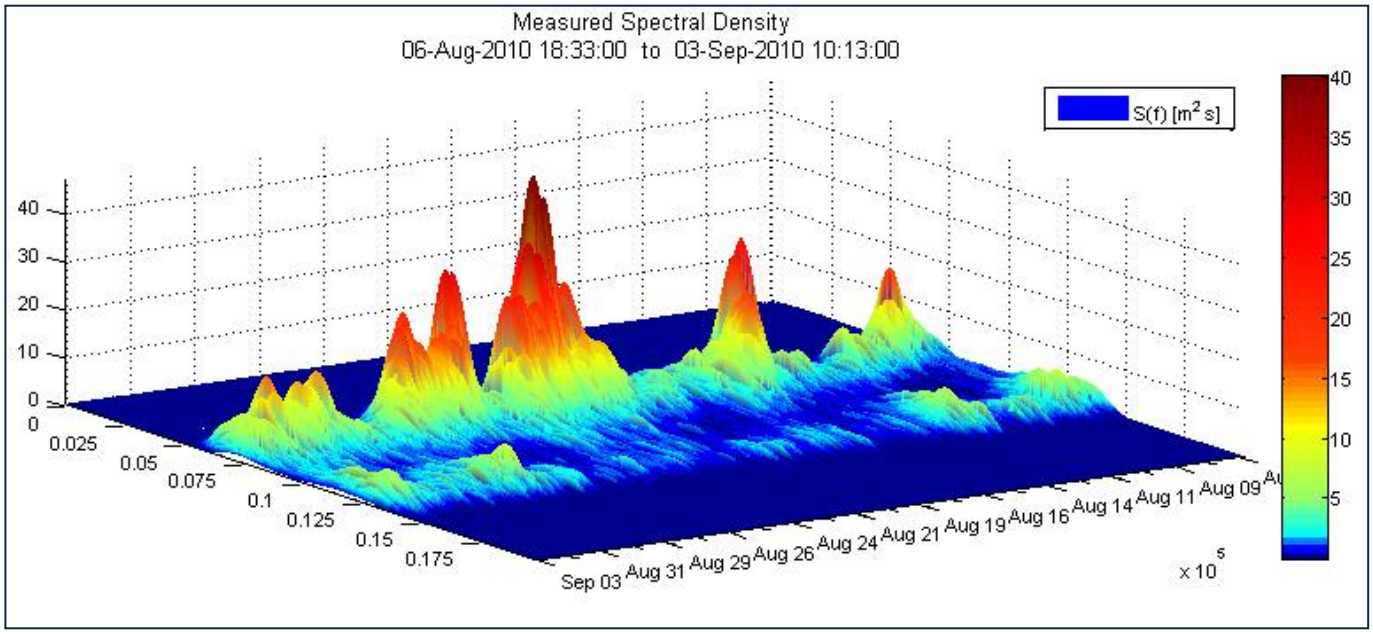

Figure 81: Spectral Temporal Variation for long travelled swell August 2010.

During the whole measurement wave energy at a frequency of 0.125Hz, wave period of 8 seconds is present. This secondary peak had been explained by (Munk 1954) as background wave energy found in the Pacific.

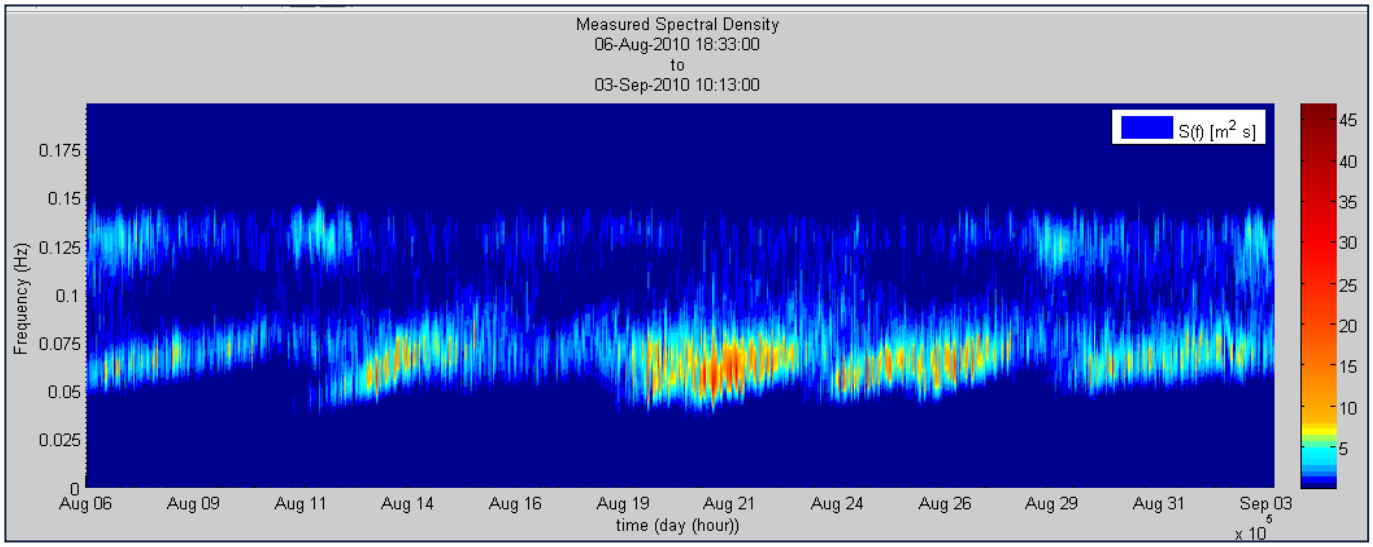

Figure 82: Spectral Temporal Variation for long travelled swell August 2010 plan view.

During the second measurement campaign, November 2010, two less energetic swell events were measured as shown in figure 83. Their peak frequency varied between 0.06 and .075 Hz, 16.7 and 13.3 second period. During the 14th a shorter period small event was measured. Again during the whole measurement a secondary smaller peak is present, this time at a frequency around 0.15Hz, 6.67 second period. This secondary peak has also been explained as a consequence of spurious harmonics by other researchers.

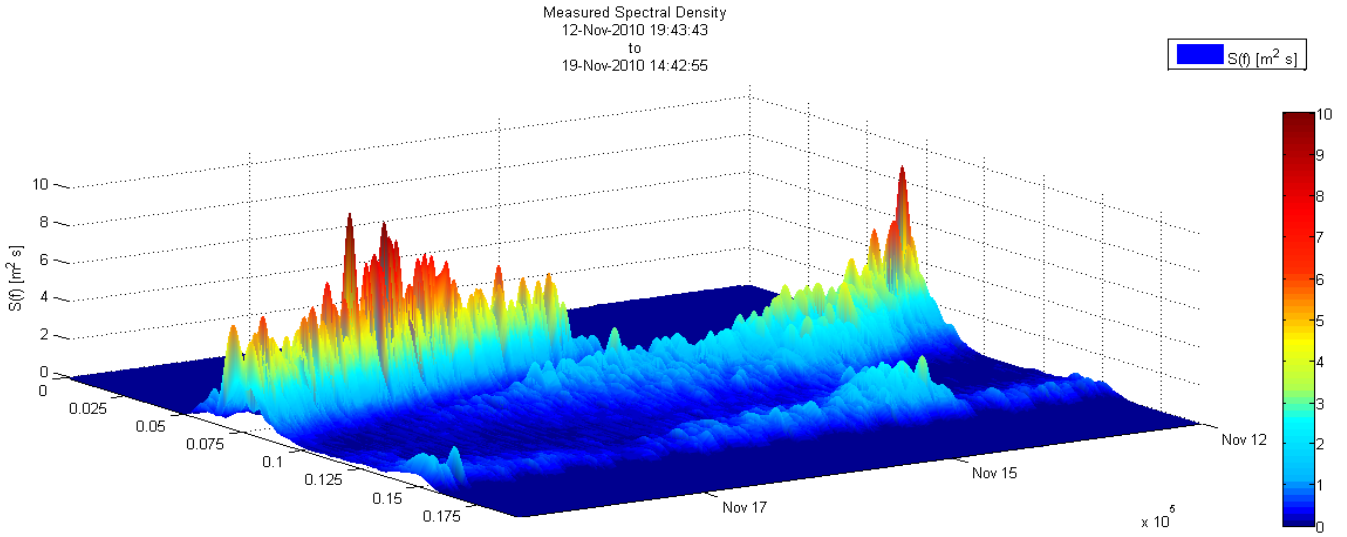

Figure 83: Spectral Temporal Variation for long travelled swell November 2010.

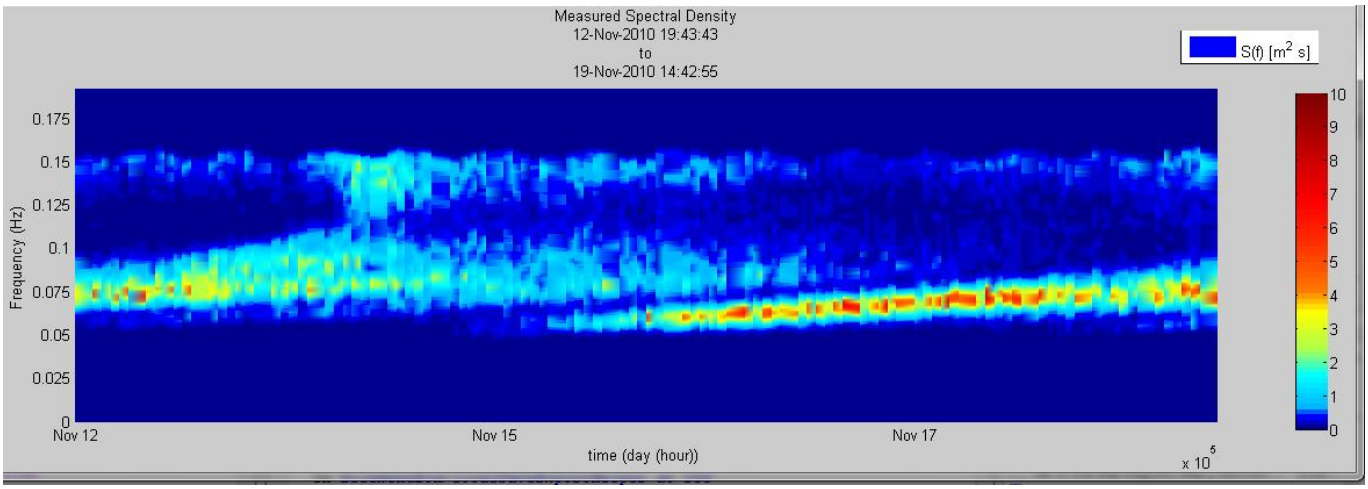

Figure 84: Spectral Temporal Variation for long travelled swell November 2010 plan view.

The obtained spectral wave height and period characteristics were compared with the statistical ones obtained through the zero down crossing. The results for both measurement campaigns are shown in tables 7 and 8

The temporal variation between the compared values for measured wave heights during August 2010 are shown in figure 85. In all cases the wave period T_{m0-1} is lower than the peak spectral period, particularly when the swell arrives and the much larger spectral peaks are measured, during the 13th of August the measured Tp was 20 seconds, whileT_{m0-1} was 14 seconds. This lower energetic period could be related to the obtained higher frequency components in the spectral calculation, and the sharp peak of the swell. This same result was also obtained for the swell waves measured in the second campaign, figure 89. Actually from this figure it seems that T_{m0-1} is almost equal to the significant period obtained from zero down crossing method.

Table 7: Ratios between Wave Spectral Parameters and ZDC Wave Parameters Long Travelled Swell August

	$H_{1/3}/H_{mo}$	H_{rms}/H_{mo}	T_{mean}/T_{mo}	$T_p/T_{1/3}$	T_{mo-1}/T_p
Mean	0.926	0.698	1.110	1.156	0.991
Standard Deviation	0.055	0.029	0.133	0.194	0.194

The relation between $T_{1/3}$ and T_{m0-1} is 1.14 and 1.03 for both measurement campaigns. All the wave period ratios are very close to 1 for both measurement campaigns; this is because of the narrow period distribution present in these long travelled swell waves.

The relation between the statistical $H_{1/3}$ and the spectral H_{mo}, "significant" wave heights was also investigated. In both cases H_{mo} was larger than $H_{1/3}$, by a factor between 1.08 and 1.05.

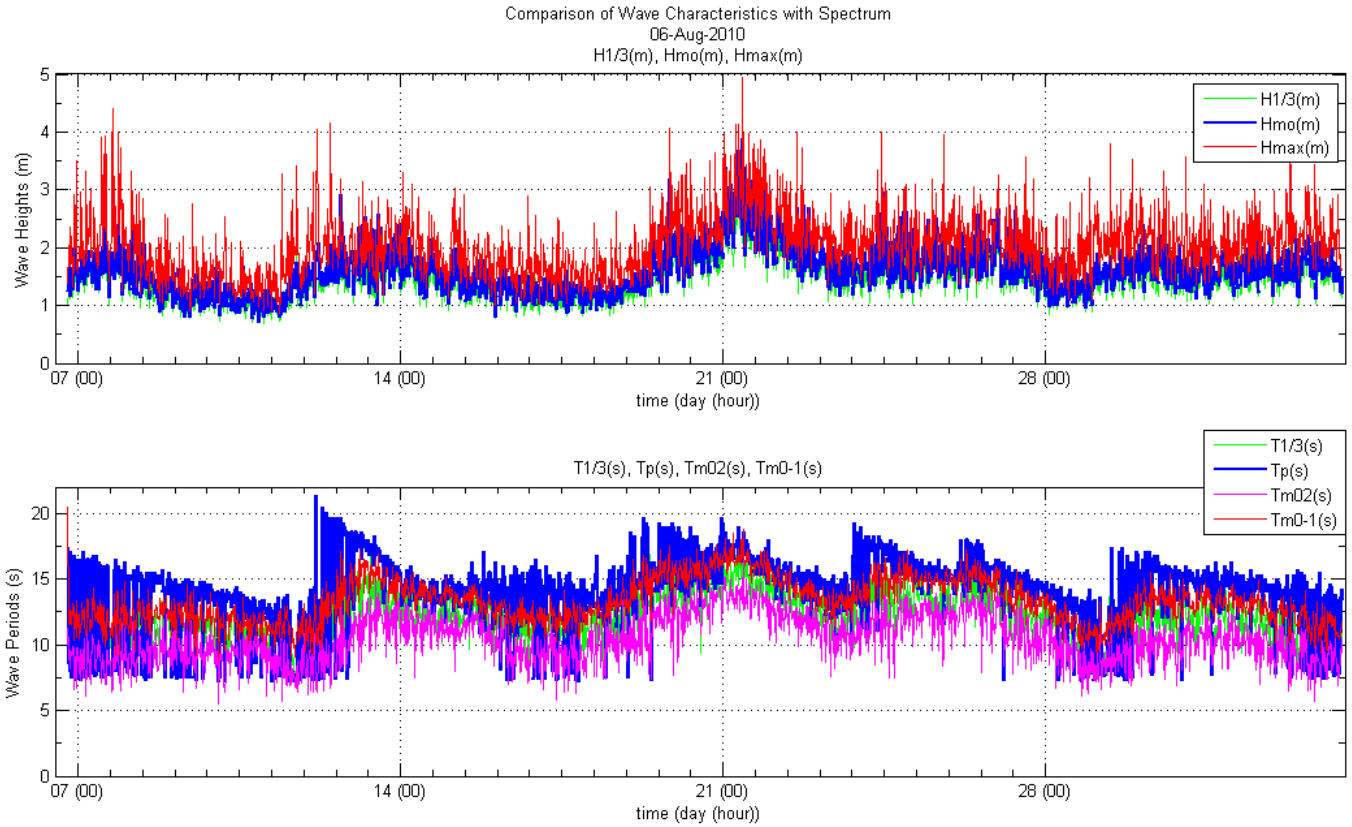

Figure 85: Temporal variation of spectral characteristics for long travelled swell August 2010.

The temporal variation of the spectral parameters Qp, ε, ν, α and κ was also calculated, the results for the first wave measurement campaign are shown in figure 86.

The spectral peakdness parameter, Qp, takes the value of 1 for white noise, the value of 2 for the Person-Moskowitz spectra, the value of 3.13 for a JONSWAP spectrum with γ equal to 3 and 5.57 for a JONSWAP spectra with γ equal to 10. During August Qp varied between 2 and 6, having the highest during the swell that arrived during the 11th of August, in which the peak period reached values of 21 seconds. It is estimated that because several swell storms where present simultaneously during the measurements from the first campaign in August, Qp tends to be smaller since the wave energy in the spectrum would be distributed between the different peaks of the present swell. The large measured variation, between 2 and 6, is attributed to the fact that since the measurements were not continues the presence of waves of the one swell or another in each individual record will cause this variability. These is also visible in the spectral narrowness parameter ε and the spectral broadness parameter ν , where both present high variability, and both parameters indicate a broad spectra, again this is attributed to the presence of simultaneous swells. The parameter α, which also describes the narrowness of the spectra takes a value under 0.5, with jumps to 0.75, these indicates an irregular wave conditions mixed with more regular (narrower) conditions.

The spectral wave groupiness parameter Ka also presents large variations, some correlation with the Goda's spectral peakdness parameter, Qp, is seen. This correlation will be examined further ahead.

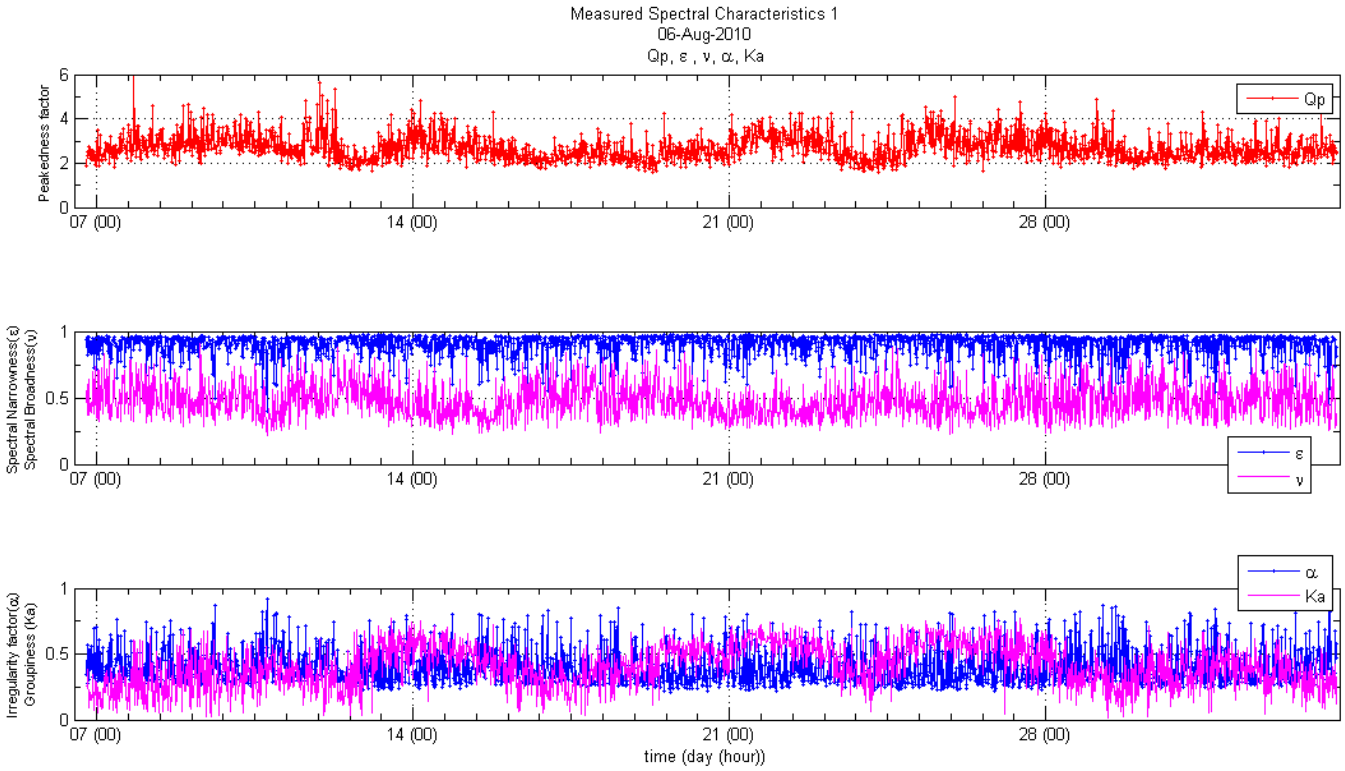

Figure 86: Temporal variation of spectral characteristics for long travelled swell August 2010.

The spectra of the five highest measured time series during the first were investigated. Figure 87 shows the highest spectra that occurred during the 21st of August. During this period of time several swells were present, however for the highest wave conditions the spectra shows only one clear peak at 17 seconds. During this period the swells that affected the site had similar wave periods, it is possible that wave-wave interaction is responsible of the high significant wave heights measured, particularly considering that the swells had very similar directions.

The broadness of the spectra of the measured swells is also represented by the fitted JONSWAP spectra. Figures 88 show the fitted JONSWAP spectra with the obtained γ value for the four highest spectrums. The peak enhancement factor γ varies between 2.3 and 4.3. These values are much lower than the previously reported ones by Goda (1983), he reported that these long travelled swells should be taken at a value between 8 and 9 on the average However he analyzed wave measurements at shallower waters. The measured difference again is attributed to the presence of several simultaneous swells during the most energetic conditions that occurred during the 21st of August.

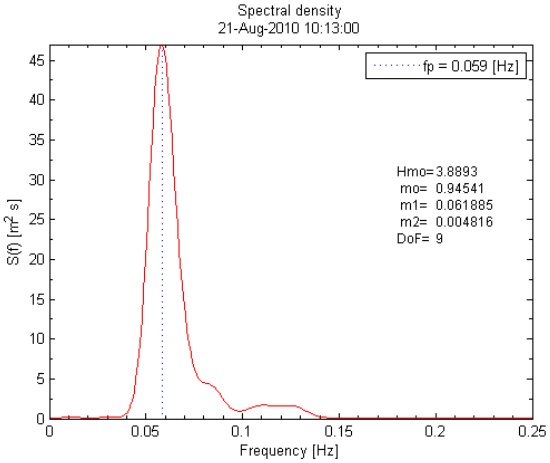

Figure 87: Spectra of the most energetic time series for long travelled swell August 2010.

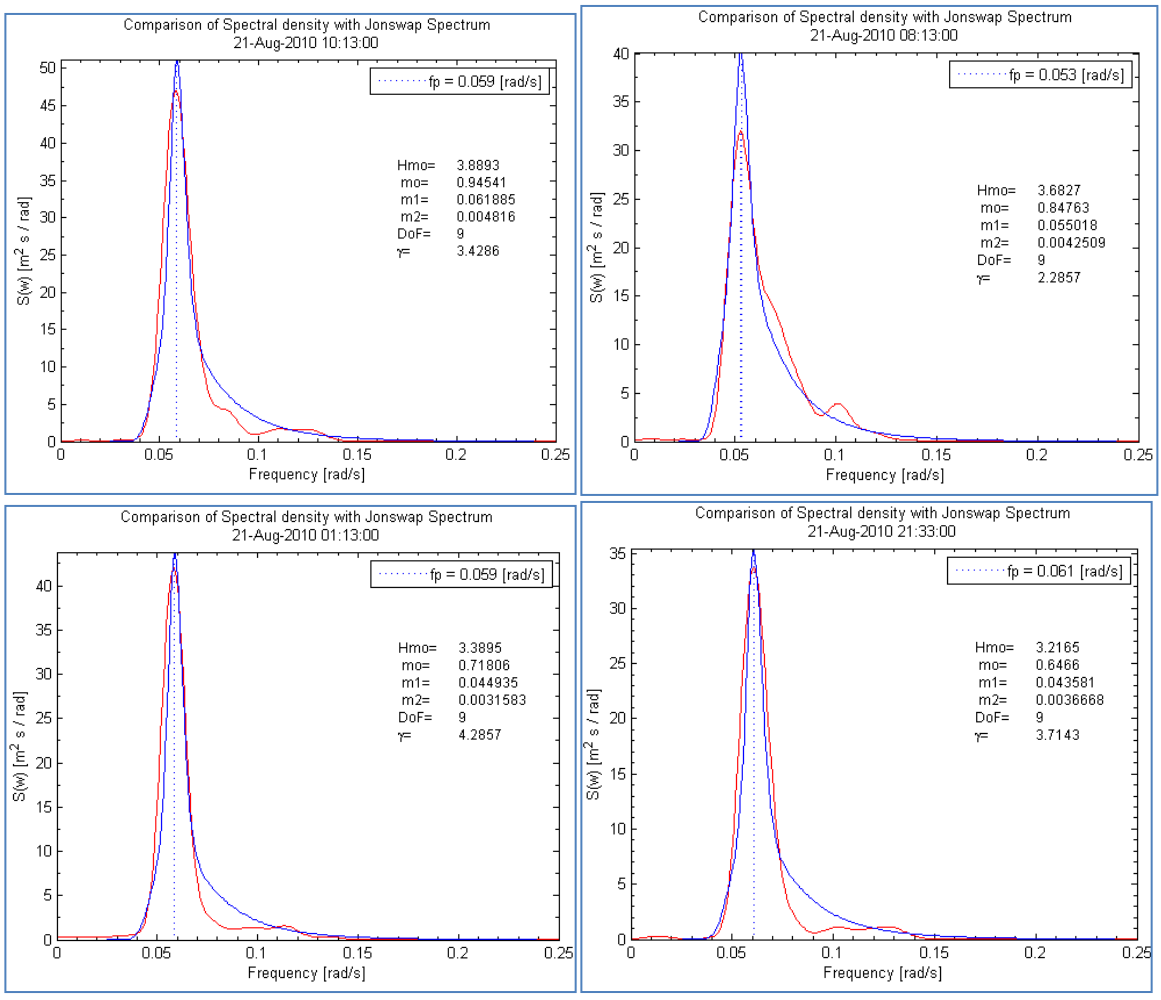

Figure 88: Fit of highest spectra to the JONSWAP spectrum for long travelled swell August 2010.

During the second measurement campaign in November 2010, the end of a swell was measured between the 13th and the 15th, with a local storm between the 14th and the 15th that produced waves with periods around 8 seconds, the 16th a low energy swell arrived with spectral peak periods around 17.5 seconds, there after the swell decayed very slowly. During this swell decay period, between the 17th and the 20th the only energy measured was due to this one swell. During this period the measured value of Qp was particularly high with values above 7.5. The associated enhancement parameter γ from the JONSWAP spectra is well above 12, and this indicates almost regular waves were present during this period. Neither the spectral bandwidth parameter ε nor the narrowness parameter ν, seem to show this spectra changes which are quite obvious. The narrowness of the spectra, α, is above0.75 through the whole period, and it also misses the presence of the short period waves that occurred the 14th and 15th, however the spectral groupiness parameter Ka, represents quite well the spectral change for this period, and its correlation with Qp is more obvious than the one observed during the first wave measurement campaign.

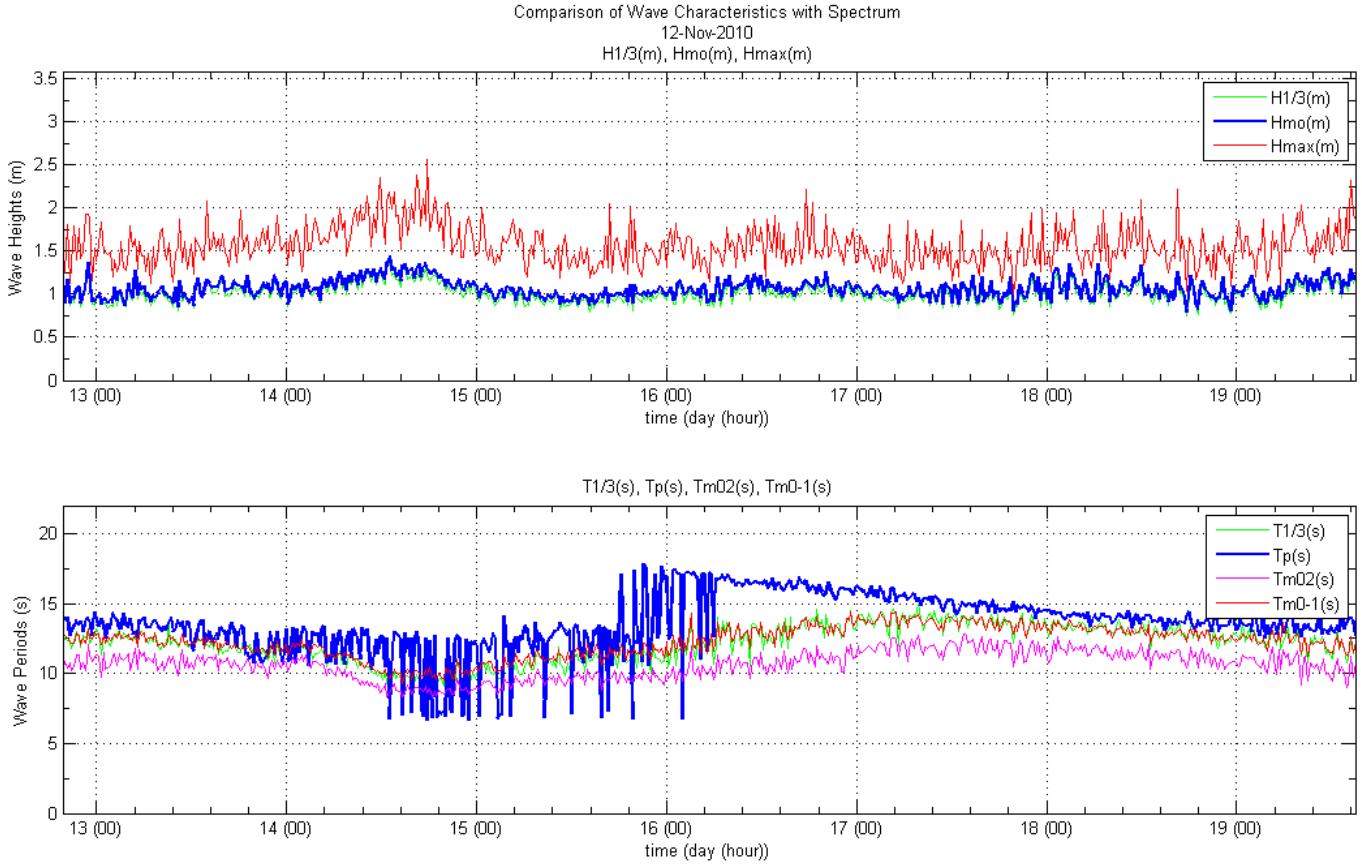

Figure 89: Temporal variation of spectral characteristics for long travelled swell November 2010.

Table 8: Ratios between Wave Spectral Parameters and ZDC Wave Parameters Long Travelled Swell November

	$H_{1/3}/H_{mo}$	H_{rms}/H_{mo}	T_{mean}/T_{mo}	$T_p/T_{1/3}$	T_{mo-1}/T_p
Mean	0.955	0.690	1.009	1.114	0.927
Standard Deviation	0.020	0.012	0.033	0.144	0.142

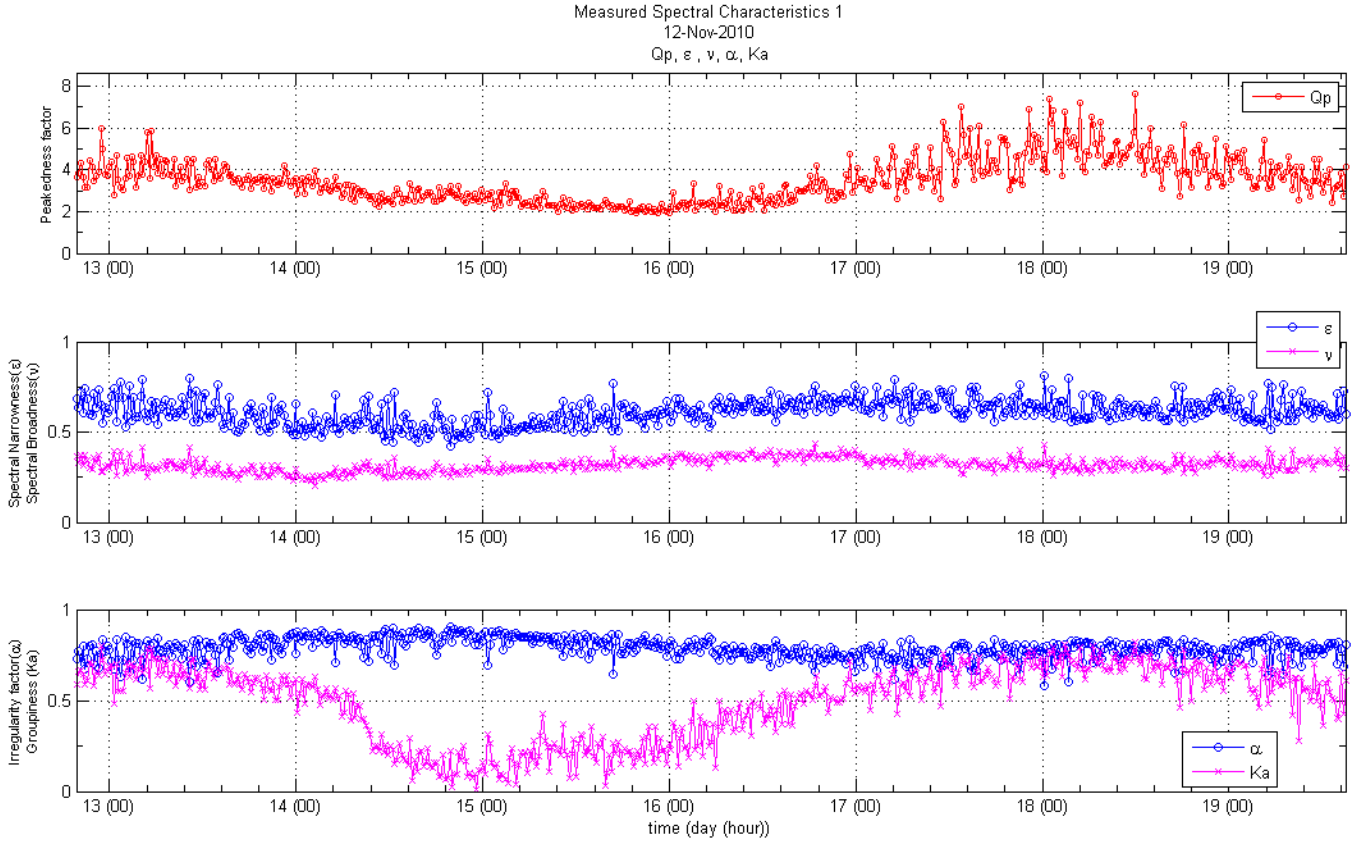

Figure 90: Temporal variation of spectral characteristics for long travelled swell November 2010.

The five highest measured spectra during the second campaign were investigated in detail. In general the wave energy content was very similar through out the whole second campaigns; the significant wave height was always around one meter. During the 14th of November lower period waves, associated with a local storm, were present and the measured wave height was slightly higher. The spectrum during this period shows clearly the double peaks from the swell and wind waves present. The wind waves had a frequency of 0.15 Hz or 6.67 second period, and the swell 0.092 Hz or 10.87 seconds, figure 91. The JONSWAP spectrum, for this mixed wind-swell conditions, presents a bad fit and should not be used. The rest of the time very regular swells were present and the peak

enhancement factor for the fitted JONSWAP spectrum varied between 10 and 16 for the most energetic conditions, with a good fit for the JONSWAP spectrum.

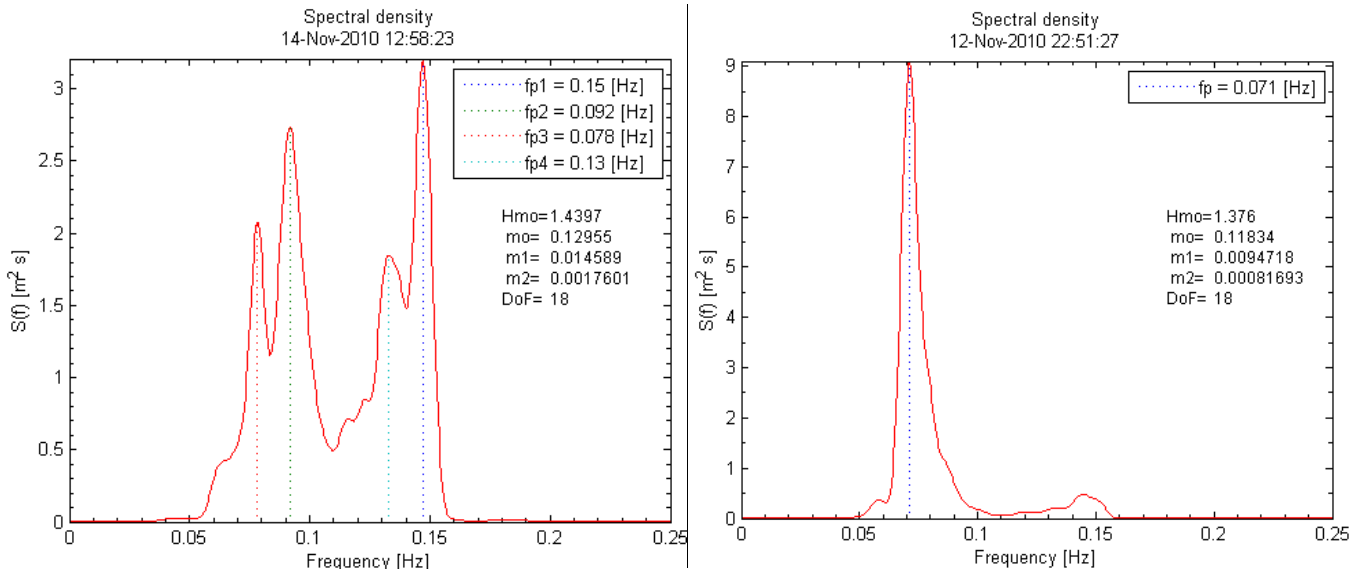

Figure 91: Spectra of the most energetic time series for long travelled swell November 2010.

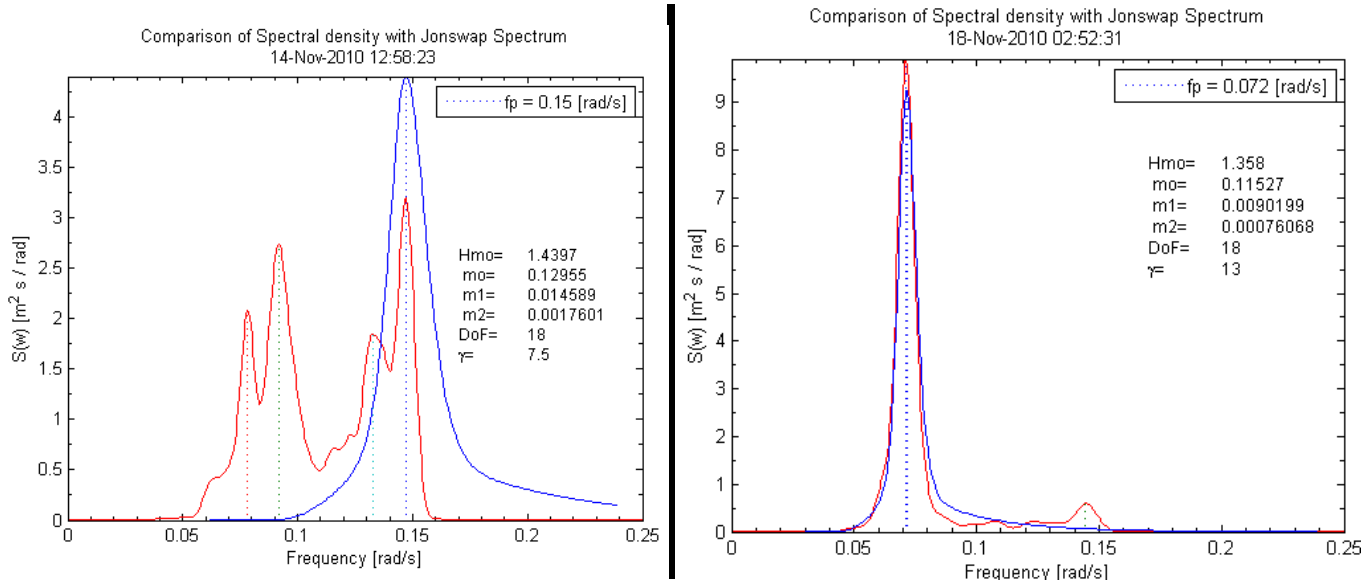

Figure 92: Fit of highest spectra to the JONSWAP spectrum for long travelled swell November 2010.

3.1.6 Wave Grouping Analysis

The grouping characteristic of the measured waves was investigated. First the correlation coefficient between successive wave heights for several lag number of waves was obtained. Figure 93 shows the obtained values for both wave measurement campaigns. The correlation coefficient for the measured waves during August is low, and presents large variability, with a mean around 0.2 for $\gamma HH(1)$. The presence of multiple swell wave conditions, and possibly the shorter wave records influenced this number. For the swell waves measured in November, the correlation coefficient is larger, with a mean around 0.35 for $\gamma HH(1)$, and positive correlation is present for 3 and 4 lag number of waves.

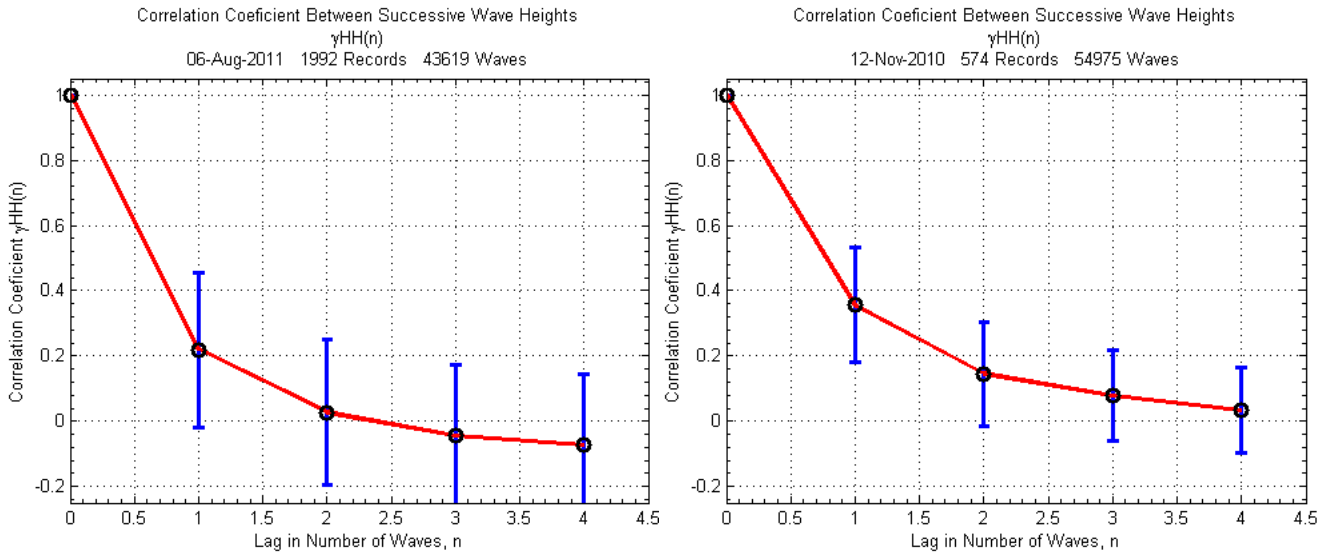

Figure 93: Correlation coefficient between successive wave heights for long travelled swell August 2010 and November 2010.

Given the large number of wave records analyzed the temporal variation of γHH (1) was investigated. The results are plotted in figure 95 with the mean run lengths.

The occurrence and exceedance run length probabilities for the wave measurements of all the records from August and November 2010 were obtained; figure 94 show the obtained results. The run lengths for waves exceeding H_{mean} and $H_{1/3}$ were obtained and compared with their theoretical values, according to Kimura's theory (1980). Even though all the individual records were included good agreement is found between the theoretical and calculated values. For August slightly longer run lengths are predicted by the theory, which is more clearly seen in the probability of exceedance curve. Goda (1983) obtained a similar result analyzing three long records, which was attributed to the deviation from the Rayleigh distribution for the measured waves.

The temporal variation of the mean run length for $H^*>H_{mean}$ and $H^*>H_{1/3}$ was also obtained per record. The results are plotted in figure 95 for the swell measured in August. Large temporal variations are observed. The correlation

between the measured mean run lengths and the individual wave correlation coefficient was examined later for the different wave measurements.

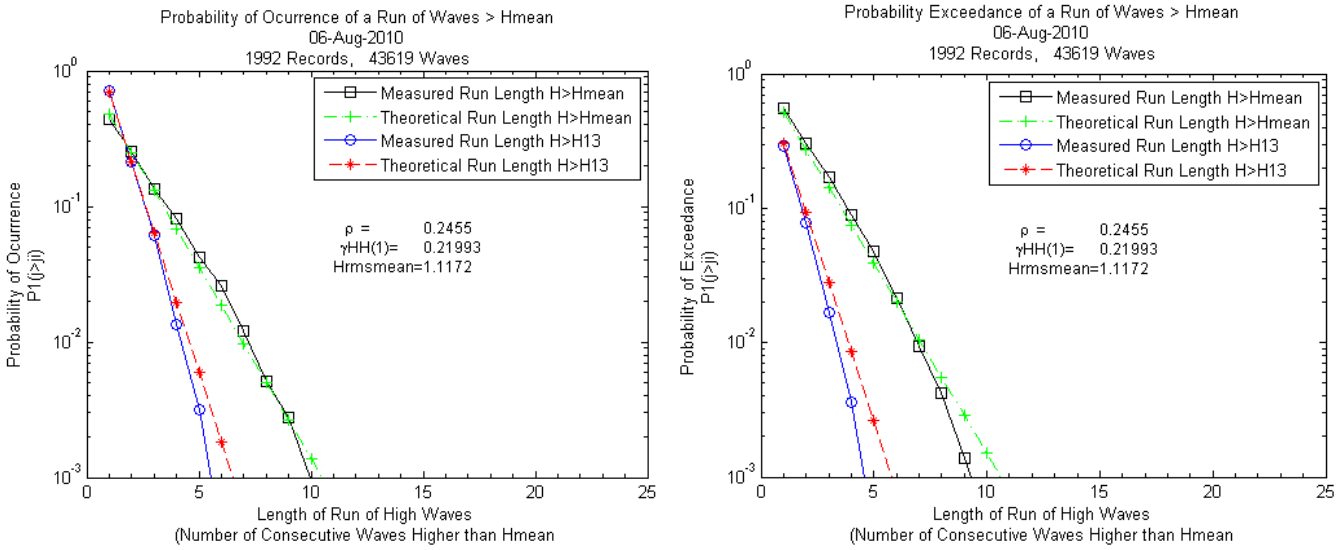

Figure 94: Occurrence and Exceedance Probability of a Run of Waves H>H* long travelled swell August 2010.

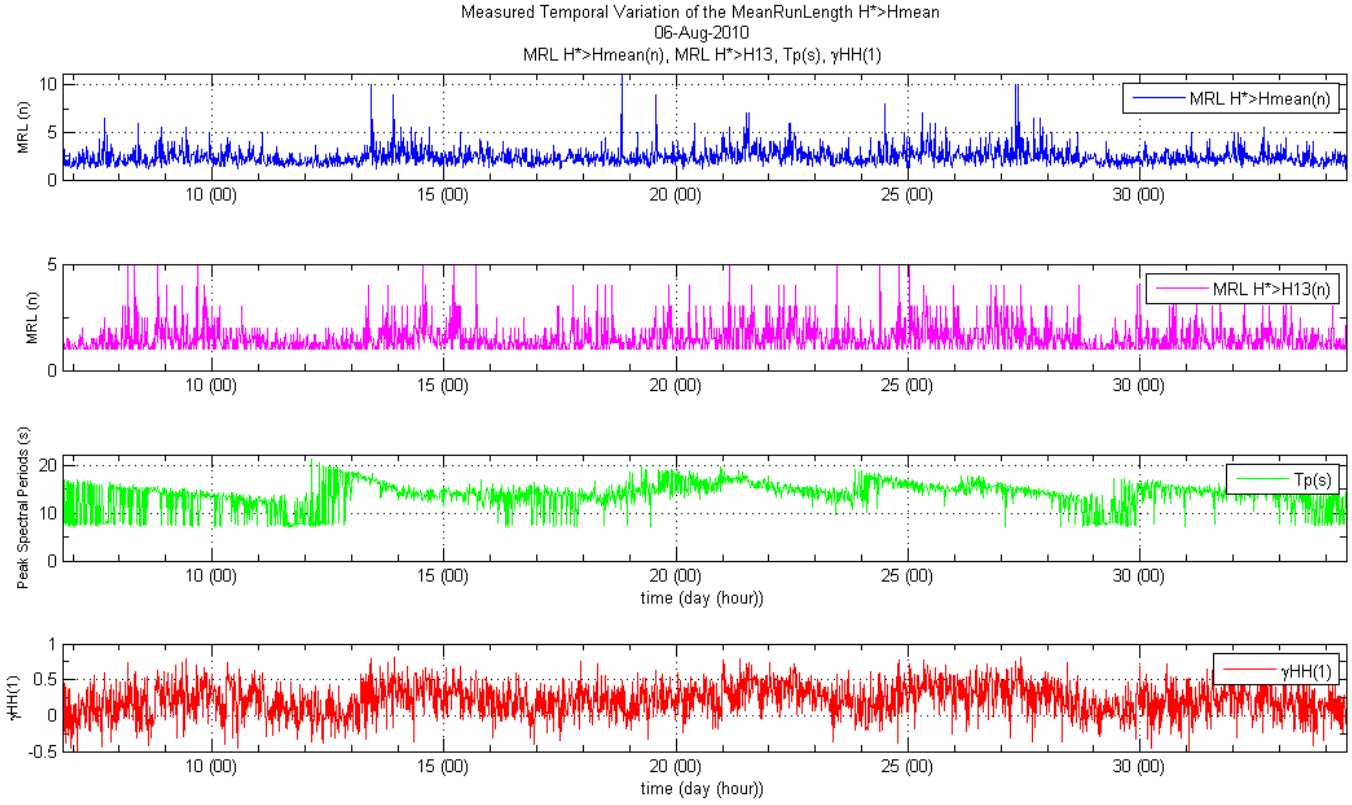

Figure 95: Temporal Variation of the mean run length H>H_{mean} and H>Hs wave heights for long travelled swell August 2010.

For the long travelled swell measurements during November 2010 the observed run lengths were higher than the measured ones in August. During these measurements the wave records were taken continuously, in samples of 1024 seconds, but for the run length analysis it was treated as one single continuous record of 54975 waves.

The calculated mean run lengths were compared to the ones predicted by Kimura's theory, figure 96. The measured values were larger than the predicted ones, particularly for run length of waves higher than H_{mean}. The reason for this deviation is not clear since the waves measured during this period fitted quite well Rayleigh's distribution. This means that longer groups of waves with heights above H_{mean} tend to appear than predicted. The regular measured wave conditions during this period would be the explanation to this deviation.

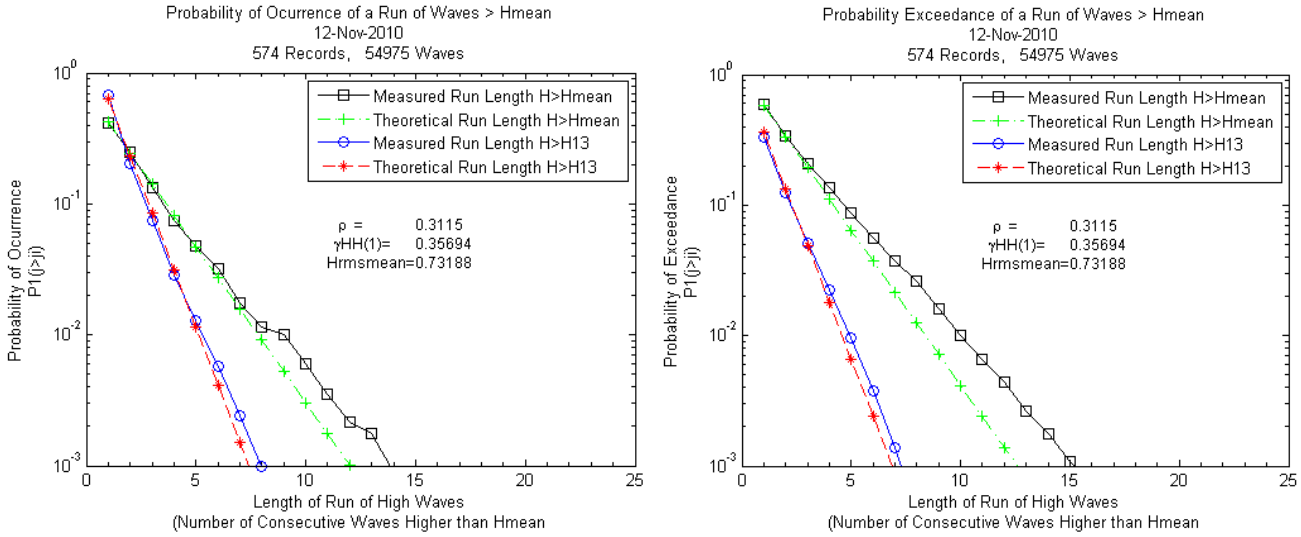

Figure 96: Occurrence and Exceedance Probability of a Run of Waves H>H* long travelled swell November 2010.

The mean run length for with H_{mean} and $H_{1/3}$ as threshold values for each wave record was obtained, figure 97 shows the temporal variation of the both calculated mean run lengths, the correlation coefficient of individual wave heights γHH(1), and the measured peak spectral period. The higher measured mean run lengths appear correlated to the higher γHH(1), and to the variability of the spectra, hence parameters such as the spectral peakdness, or the spectral grouping parameter, Ka, should be be good predictors for the measured groupiness of the record. These correlations are examined further ahead.

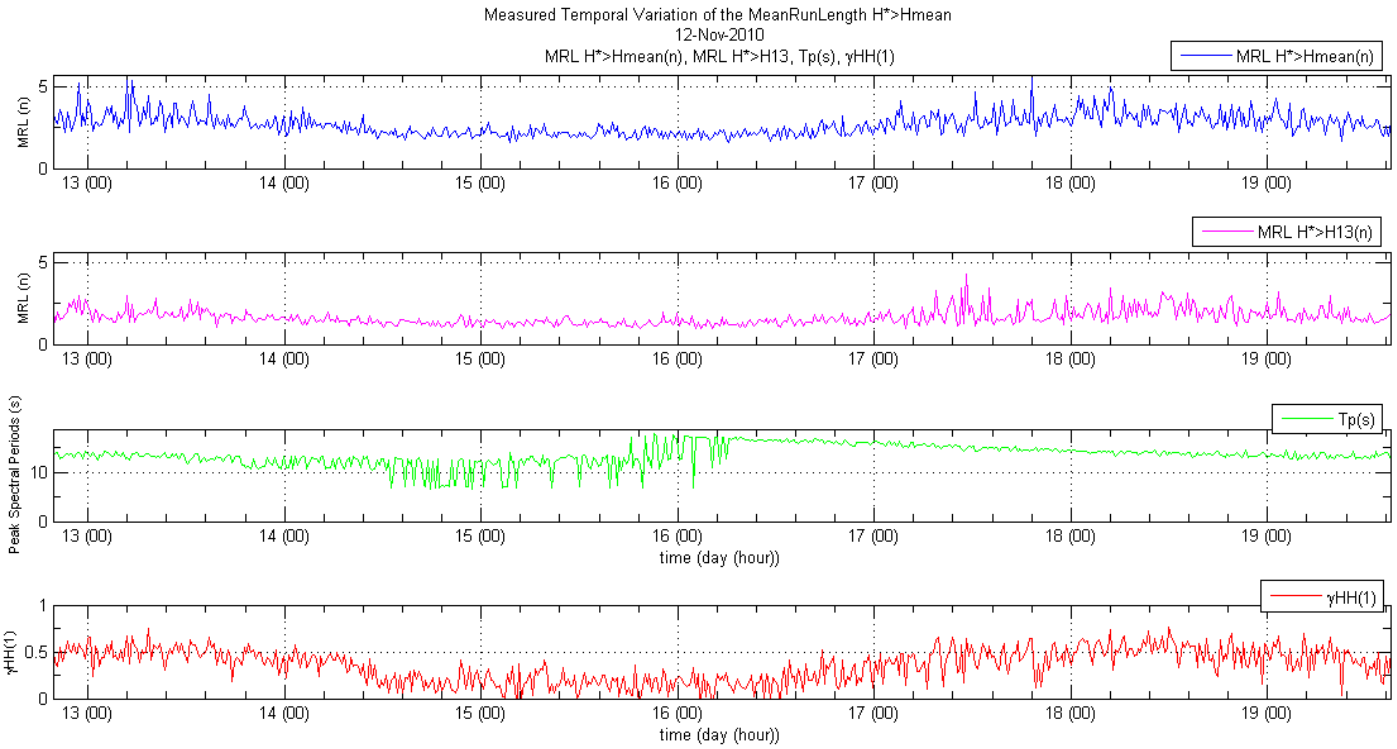

Figure 97: Temporal Variation of the mean run length H>H_{mean} and H>Hs wave heights for long travelled swell November 2010.

3.1.7 Long Wave Analysis

The presence of energy in lower frequencies area of the spectra was investigated. Two low pass filters were used to examine the energy content in all the measured records, the first was set at the maximum zero down crossing period (values around 25 seconds), and the second was set mean run length for $H^*>H_{mean}$ multipled by the T_{mean} of each individual record (values of 40 to 60 seconds). Little difference was found in the results, mainly because it was found that most of the infra gravity energy was found above 60 seconds. The first filter, T>Tmax, was used in order to incorporate all the energy above the gravity wave period definition.

Figure 98 show the filter signals for the highest infra gravity measured waves.

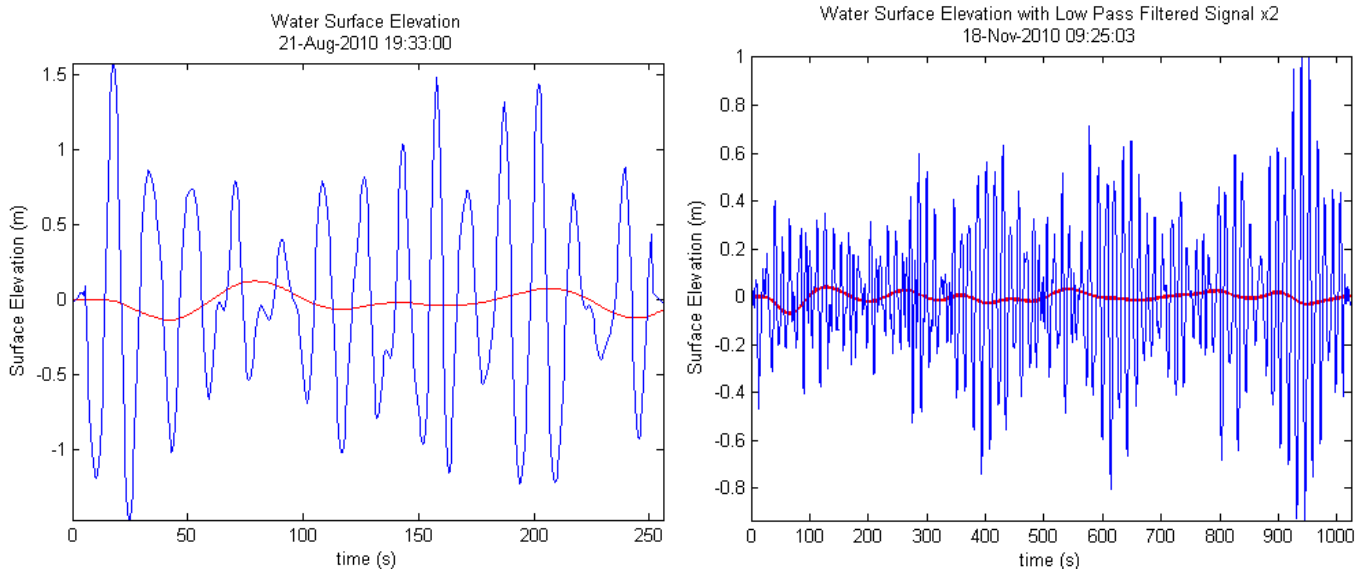

Figure 98: Filtered long wave signal for long travelled swell

The Fourier spectrum was obtained for all the filtered signals, and the long period H_{mo} and Tp was obtained for each record. Figure 99 shows the spectra of the highest infra gravity wave records of August and November respectively. The spectral resolution was increased in both cases by a factor 2. For the wave measurements during August the highest long wave height was 0.26 meters, with a wave period of 91 seconds, during November the measured long waves were less energetic, with H_{mo} of only 4 cm and a period of 128 seconds.

The five more energetic long period wave spectra obtained from the filtered records was then compared to gravity wave spectra previously obtained. Figure 100 shows this comparison for two representative records. In general the long period waves have frequencies much lower than ones found for using the whole signal. There also seems to be an area between the long wave frequencies and the wind wave frequencies where no energy is found.

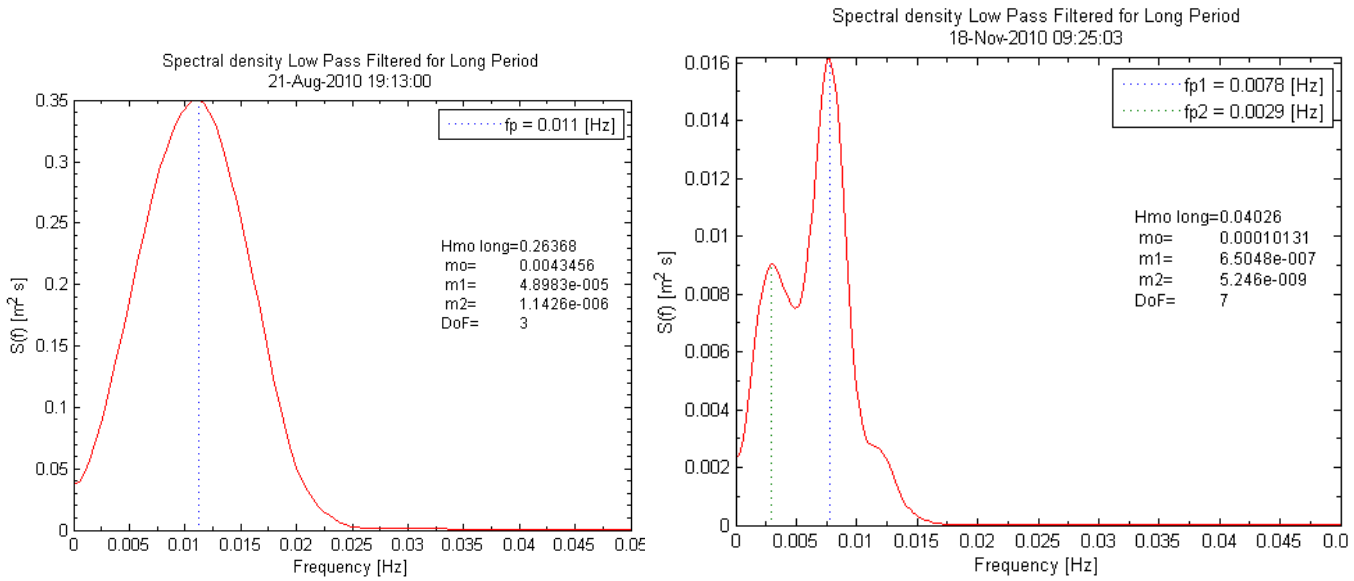

Figure 99: Long wave spectra for long travelled swell.

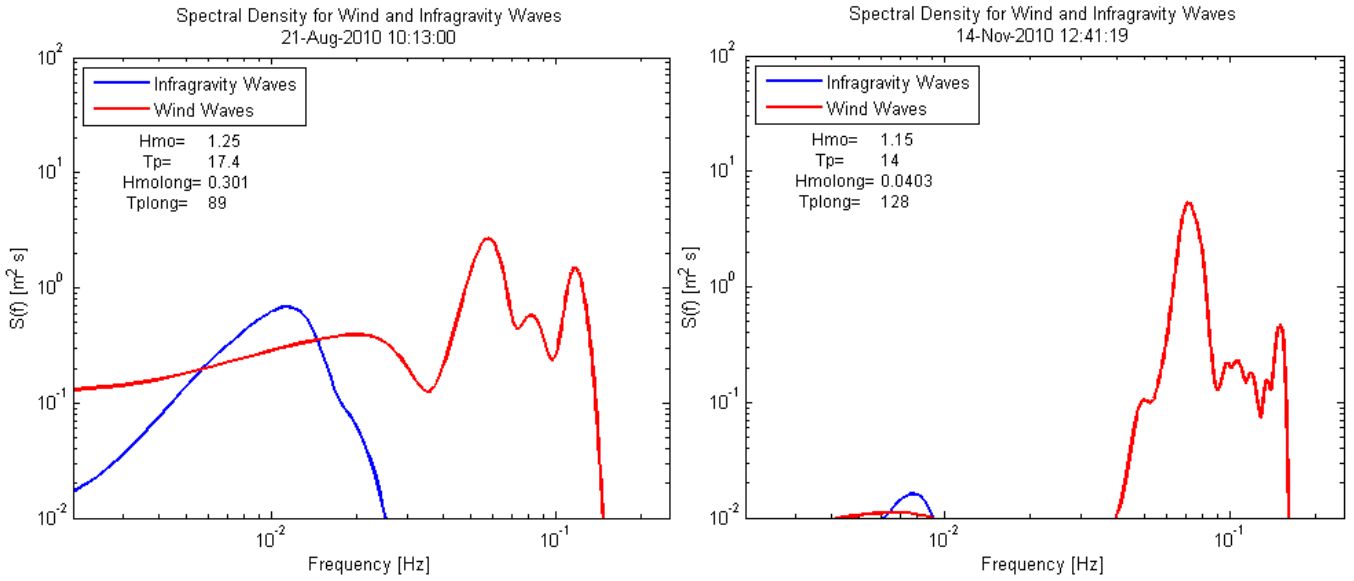

Figure 100: Long and wind wave spectra for long travelled swell

The temporal variation of the long wave energy content, described as H_{molong}, and the long wave peak period was then obtained. Figure 101, shows the results for the wave measurements of August. A very good agreement is seen between the energy content of the gravity spectrum and the long wave energy content based on the significant wave heights obtained. However no visible relation between the long wave peak spectrum periods and the peak spectral periods was observed. In general the long wave spectral period varied between 50 seconds and 250 seconds. A mean value of T_{plong} of 84 seconds was obtained.

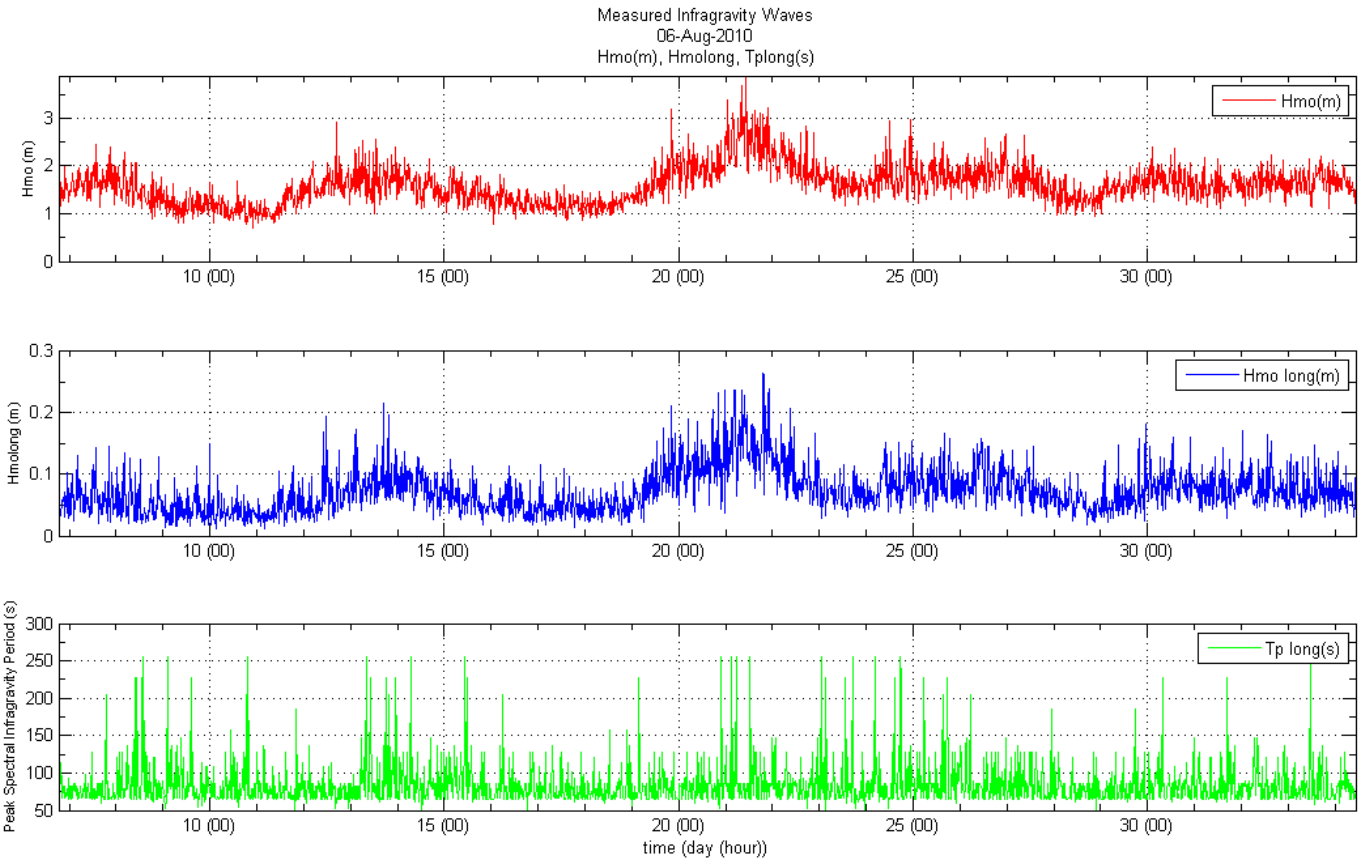

Figure 101: Temporal variation of the long wave height for long travelled swell August 2010.

For the wave measurements carried out during November measured the long wave energy was much smaller than the one measured in August, figure 102, shows the temporal variation H_{molong} and T_{plong} with the measured significant wave height. No simple correlation is visible between Hmo and H_{molong}, one reason is that the most energetic wave conditions measured were associated with the presence of shorter period waves, with T_p=6.67 seconds, and during this event the amount of measured long wave energy is lower. The long wave peak spectral period was higher than the measured in August, with a mean T_{plong} of 174 seconds. During the 16th and 18th, when the near regular waves were the measured, the T_{plong} is in larger. In general the measured long period was well above 100 seconds. The longer wave record explains this difference. More continuous data of the energetic swells is required for this analysis.

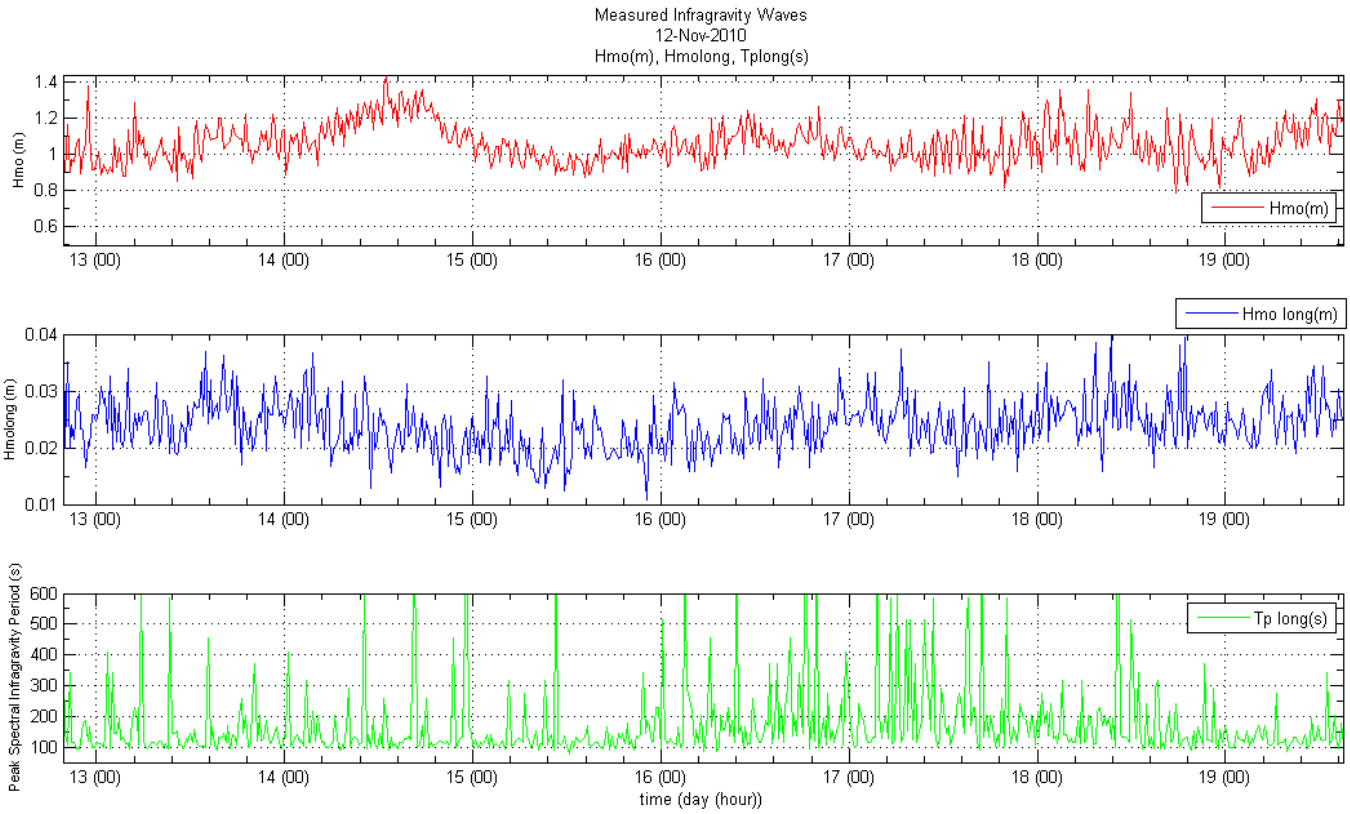

Figure 102: Temporal variation of the long wave height for long travelled swell November 2010.

3.1.8 Analysis using the Hilbert Huang Spectrum

The most energetic measured conditions during the first and second wave measurement campaigns were analyzed in detail using the Hilbert Huang transform. The Hilbert time dependant spectra was then represented as a interpolated surface of the instantaneous water surface level squared of each intrinsic mode function with its obtained instantaneous frequency. Figure 103 shows the most energetic time series for the measured waves during August in the Pacific coast of Costa Rica. The time series most important group is also shown in figure 72, where one clear group of waves is visible, and is also shown in the with the HHT spectra. The specific group where the highest measured wave occurred now shows its instantaneous frequency with the HHT spectra. Figure 104 shows a plan view of the same HHT, where it is easier to distinguish the instantaneous frequencies of the waves, the most energetic waves oscillated between 0.04 and 0.08 Hz, instantaneous periods between 12.5 and 25 seconds approximately. The black dots are seen in the figure correspond to the intrinsic mode functions determined using the empirical decomposition method. The most energetic groups correspond to a decrease in instantaneous frequency.

The energy content obtained in the intrinsic mode functions with low frequencies was in general low compared to the energy obtained within the 0.1 and 0.04 Hz frequency bands.

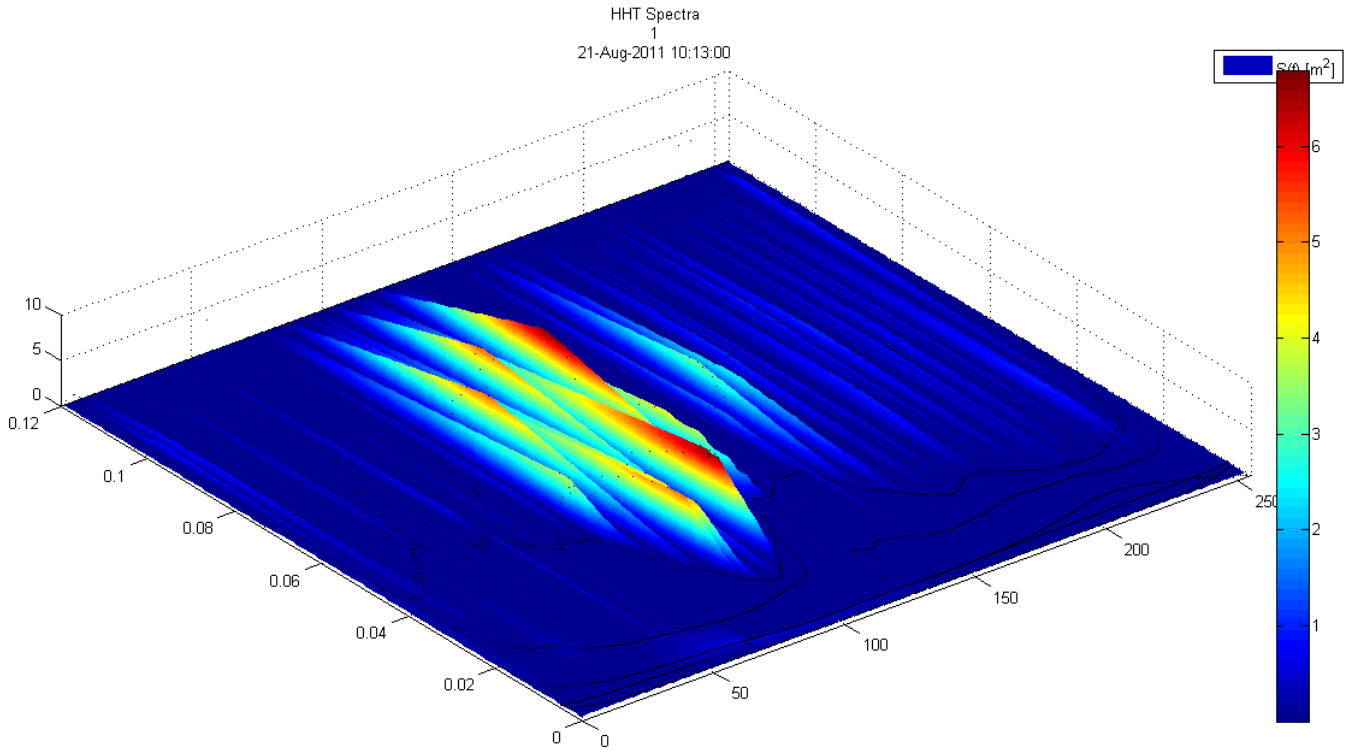

Figure 103: HHT Spectrum for most energetic time series long travelled swell August 2010.

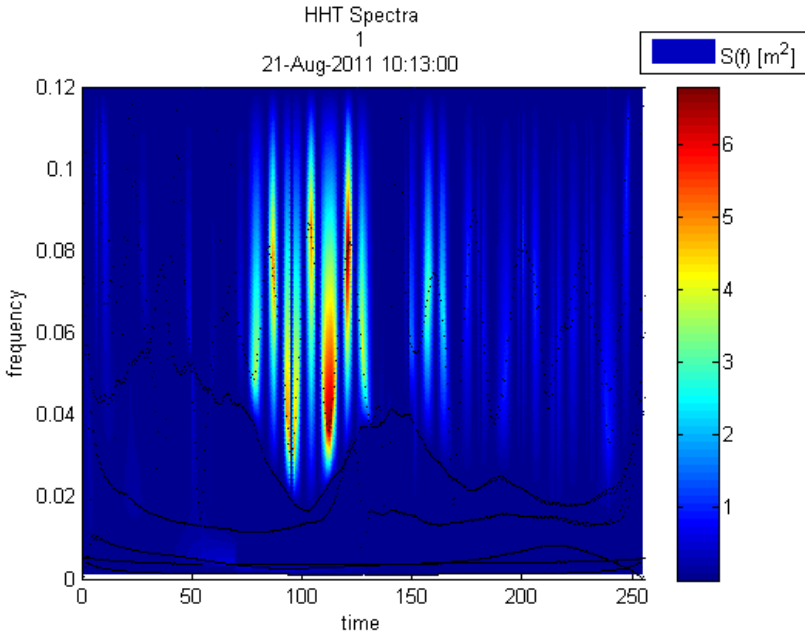

Figure 104: HHT Spectrum 1 for long travelled swell August 2010.

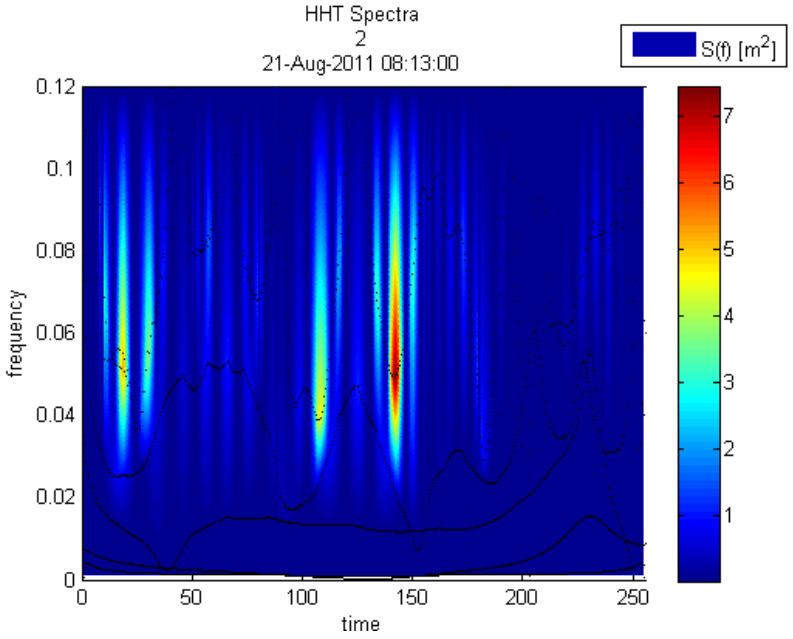

Figure 105: HHT Spectrum 1 for long travelled swell August 2010.

The marginal Hilbert Huang spectra were obtained for the most energetic wave conditions. The marginal spectrum corresponds to the integration over the time of the energy content per instantaneous frequency. Its meaning as has been mentioned is different from the Fourier spectra where the energy obtained corresponds to a permanent frequency that existed through out the whole time series; hence the units could be argued to be

different since the reconstruction of the time series is impossible with the HHT Marginal spectra. Nevertheless a comparison was made between the spectra in order to show the differences obtained in total frequency energy content through out the time series obtained depending on the assumptions of each method. Figure 106 shows the comparison of the four most energetic measured events. A broader spectrum is obtained in all case, for the most energetic time series, the HHT marginal spectra shows the energy distribution between 0.04 and 0.08 Hz observed before, and the single peaked obtained with the FFT spectra at 0.06 Hz. The second largest spectra, also shown above, do show one single peak at 0.05 for both HHT and FFT spectra but the distribution is completely different, with a very sharp peak for the HHT. The low frequency energy content in the HHT for all is much higher.

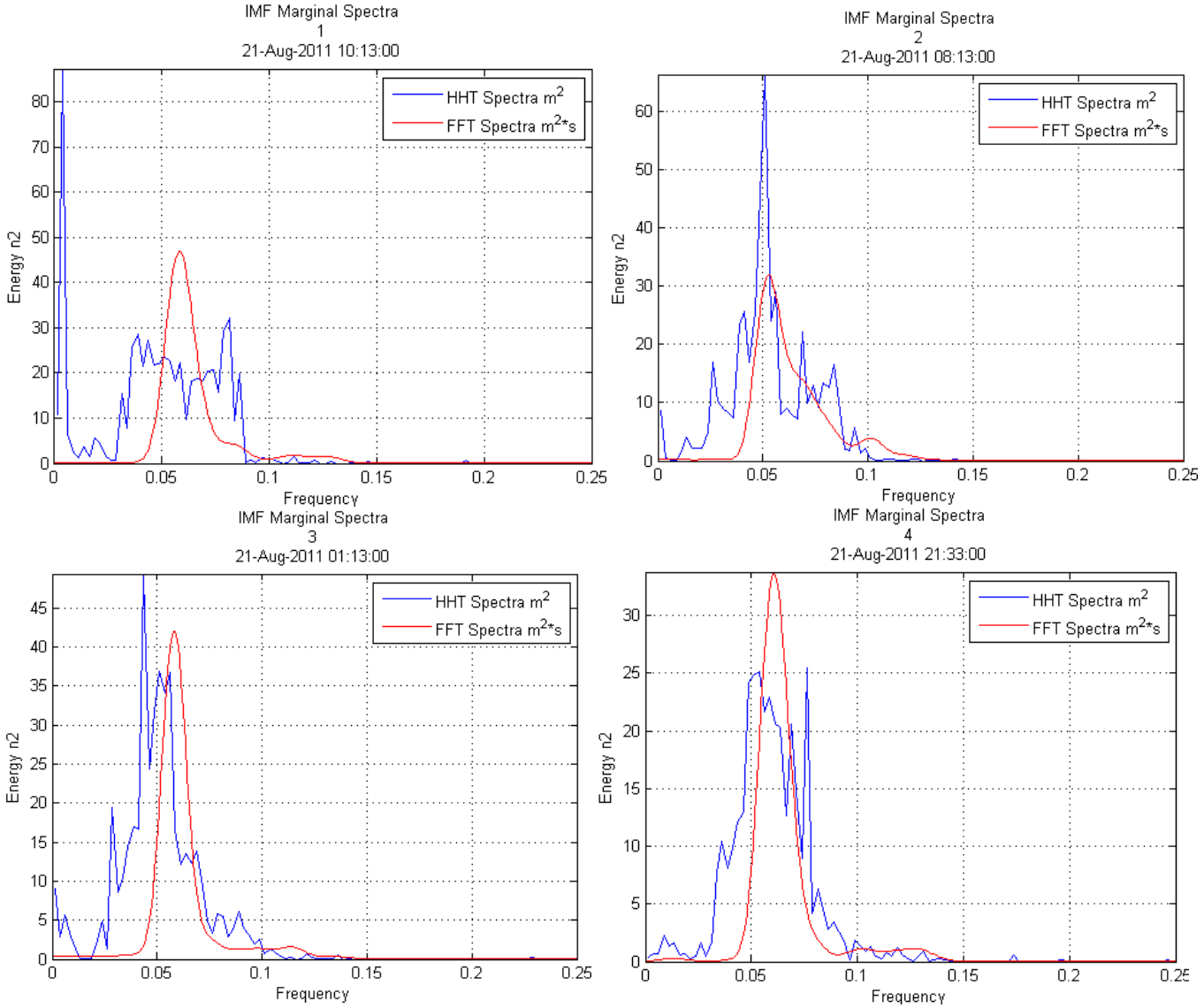

Figure 106: HHT marginal spectrum for long travelled swell August 2010.

The difference in the higher energy content of the HHT than the FFT comes from difference of the defined energy, in the FFT one single low frequency cosine component wave, with one amplitude a ,contributes only a^2 through out the time series, while in the HHT spectra the instantaneous amplitude and instantaneous frequency are integrated over time; then the continuous amplitude of the long low frequency waves contribute a_n^2 as it is integrated over time showing a considerable higher amount of "energy".

The HHT spectrum for the most energetic time series, measured during November in the Pacific Coast of Costa Rica, is shown in figure 107. As has been mentioned the wave conditions during these period consisted of almost regular swell waves with little variation in the peak spectral period through out the 7 days of continuous measurements, except for the small period where shorter period waves were measured during the 14th, shown in figure 108. The instantaneous frequency varies between 0.05 and 0.13 Hz, 7.7 and 20 seconds. The highest energy shown in the HHT spectra corresponds to the shorter period waves during the 14th, where wave grouping as defined by Veltcheva (2002) is not appreciated since packets of high wave energy seemed to be randomly distributed.

Figure 109 shows the third most energetic time series measured which occurred during the 12th of November. Wave grouping is very clear around t=800 seconds. During this period very regular wave conditions were measured.

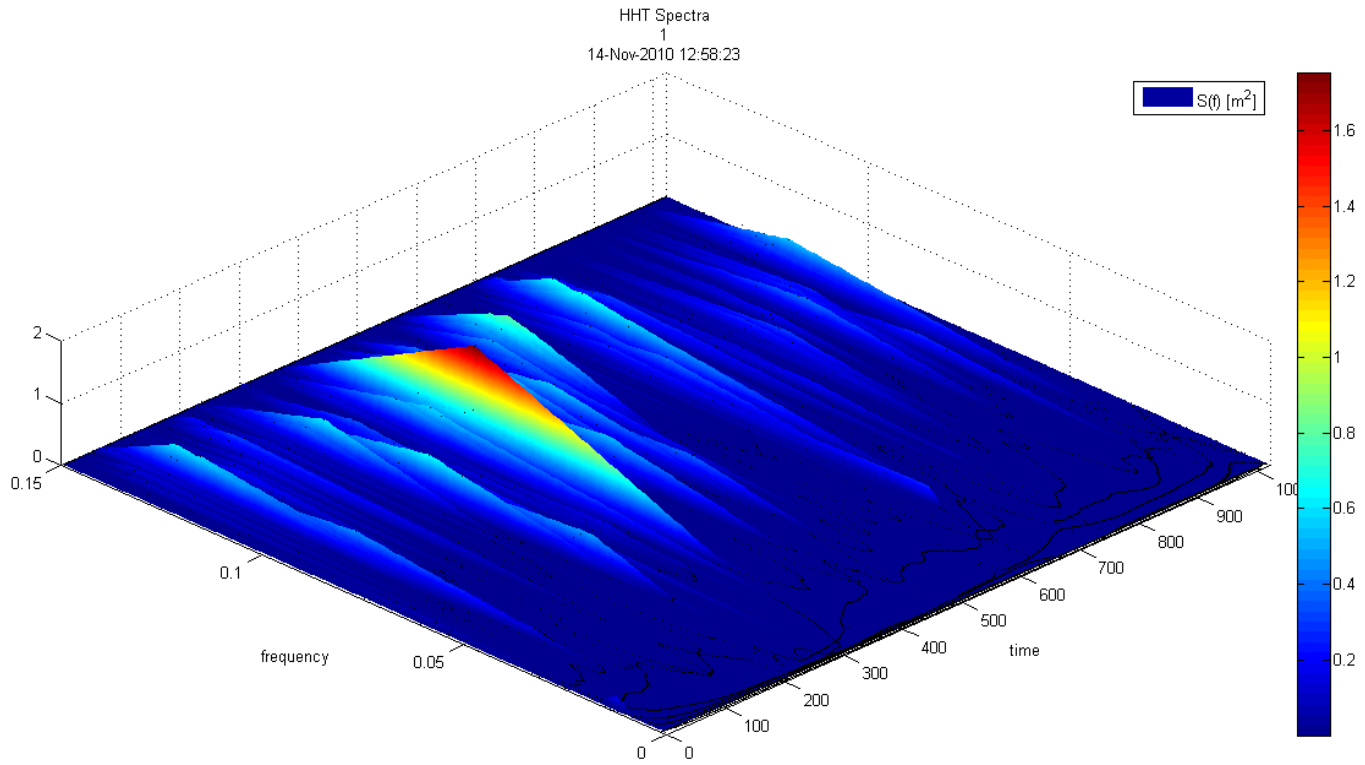

Figure 107: HHT Spectrum 1 for long travelled swell November 2010.

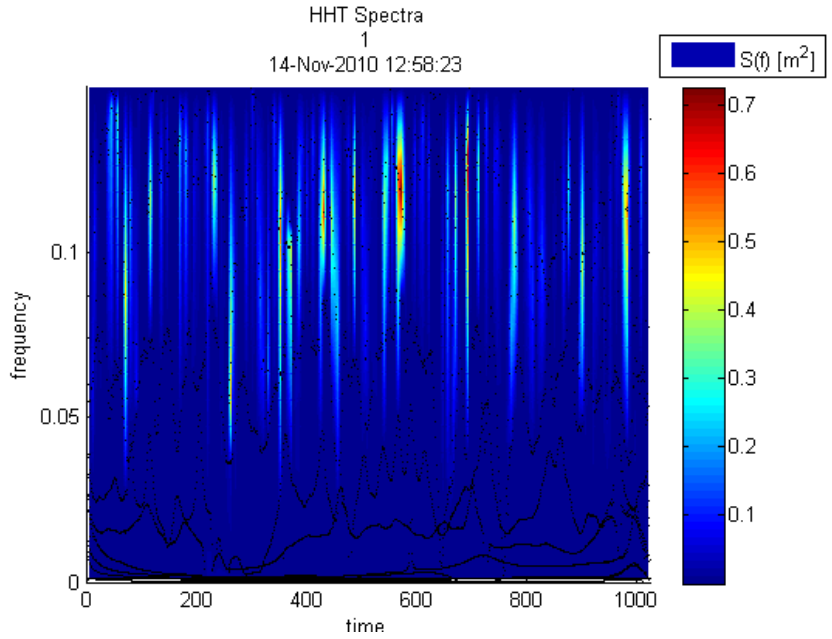

Figure 108: HHT Spectrum 1 for long travelled swell November 2010.

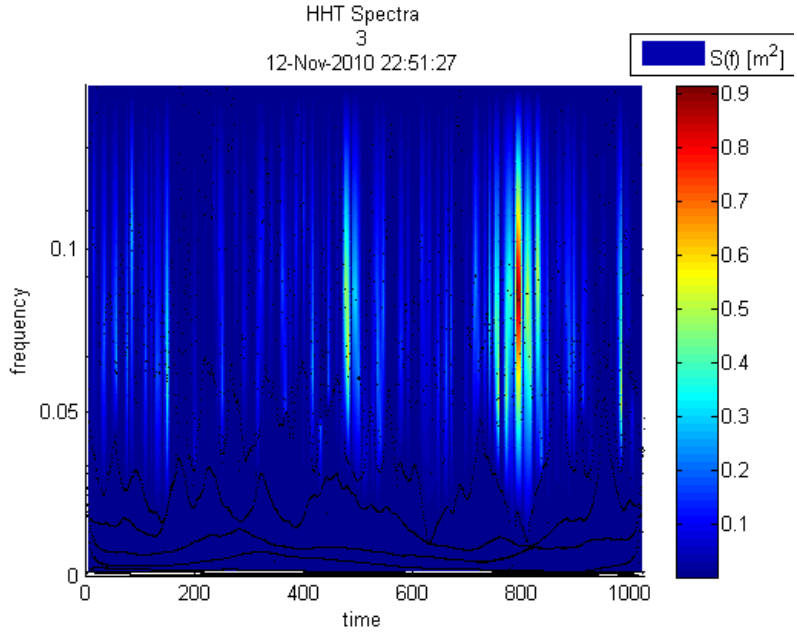

Figure 109: HHT Spectrum 1 for long travelled swell November 2010.

The marginal HHT spectra for the four most energetic wave conditions, based on H_{mo}, are shown in figure 110 with the corresponding FFT spectra. The energy distribution, based on the square of the amplitude, seen in the HHT spectrum of the most energetic condition shows a very different behaiviour than the FFT spectrum. While the FFT spectra interprets the signal as the occurrence of sinusoidal waves with two different frequency

peaks ,0.15 and 0.092Hz, (6.67 and 10.87 seconds) the HHT interprets it as an almost single peaked energy in the middle, at 0.12Hz, 8.33 seconds. The same is observed for the second most energetic spectra which corresponded to the previous time series measured. For the third highest measured spectra, the HHT shows a much broader energetic distribution than the FFT spectra which shows a very narrow single peaked spectrum at 0.072 Hz, 13.88 seconds.

The entire HHT spectrum shows much higher energy content within the very low frequencies, which is a consequence of the nature of the HHT marginal spectra amplitude integration over time.

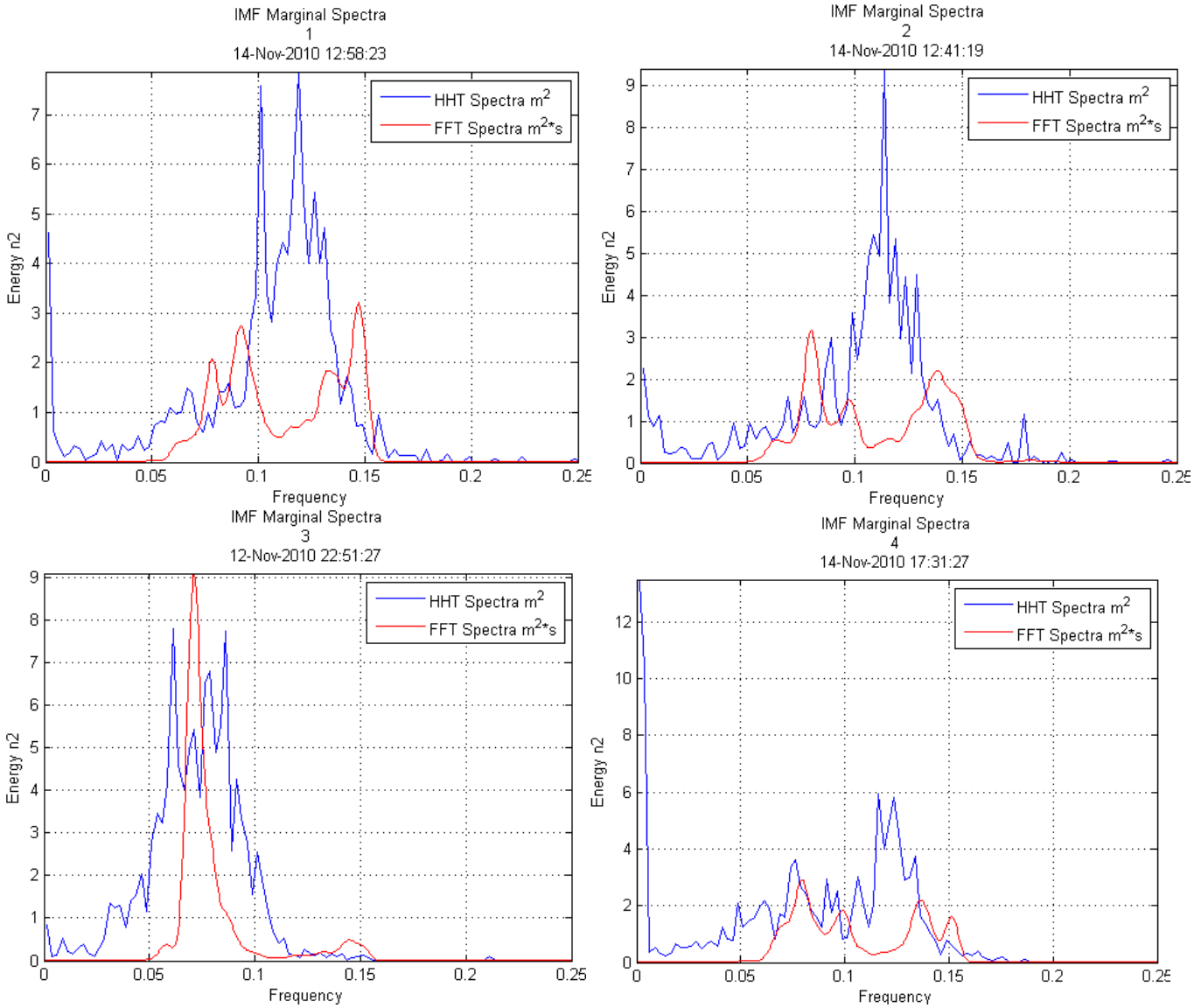

Figure 110: HHT Marginal Spectrum for long travelled swell November 2010.

3.2 Wave Measurements at the Ebro Delta

Wave measurements from the Catalonia coast in the Mediterranean Sea were analyzed in detail. The wave measurements were located at Ebro Delta, in Catalonia, Spain, and were carried out as part of the European project, FANS-Delta 96. The field campaigns included video recording of the wave transformation, wave measurements along the beach profile and current measurements. The purpose of the campaign was part of a study of the beach zone hydrodynamics and they were carried out by Universitat Politecnica de Catalunya, Spain. The analyzed wave measurements consisted of 10 days, from the 1st to the 10th of November 1996, carried using a pressure sensor at a water depth of approximately 3.5 meters. The measured waves are considered to represent calm wave conditions in the Mediterranean Spanish coast.

3.2.1 Location of Wave Measurements and Equipment used

The wave measurements were carried at playa Barra del Tabucador, in the delta del Ebro. The location of the Ebro delta is shown in figure 111. The Delta del Ebro is located approximately 150 kilometers southwest from Barcelona.

Figure 111: Location of the delta del Ebro, Google Earth.

The wave measurements were carried out using a PUV-S4DW pressure sensor with a sampling rate of 2 Hz, at a depth of 3.5 meters.[35] The samples were taken for 35 minutes every hour.

The measured waves at Barra del Tabucador were compared qualitatively with the deep water measured wave characteristics by the Catalonian meteorological network XIOM, (http://www.xiom.cat/captortosa.aspx). The

[35] Mosso C., Pau Sierra J., Rodriguez A., Gracia V., Barnadas J., "Estudio experimental de la evolución del espectro del oleaje en una playa", Ingeniería hidráulica en México, vol XXII, num1 pp.47-61, enero-marzo de 2007.

deepwater wave conditions at Cap de Tortosa measured by XIOM are done using a DATAWELL wave rider at a water depth of 60 meters, 5 kilometers offshore. The deepwater and site wave measurements are shown in figure 112. Calm wave conditions were present during the wave measurement campaign at Barra Tabucador, with significant wave heights of less than 1 meter, and peak spectral periods between 3 and 9 seconds.

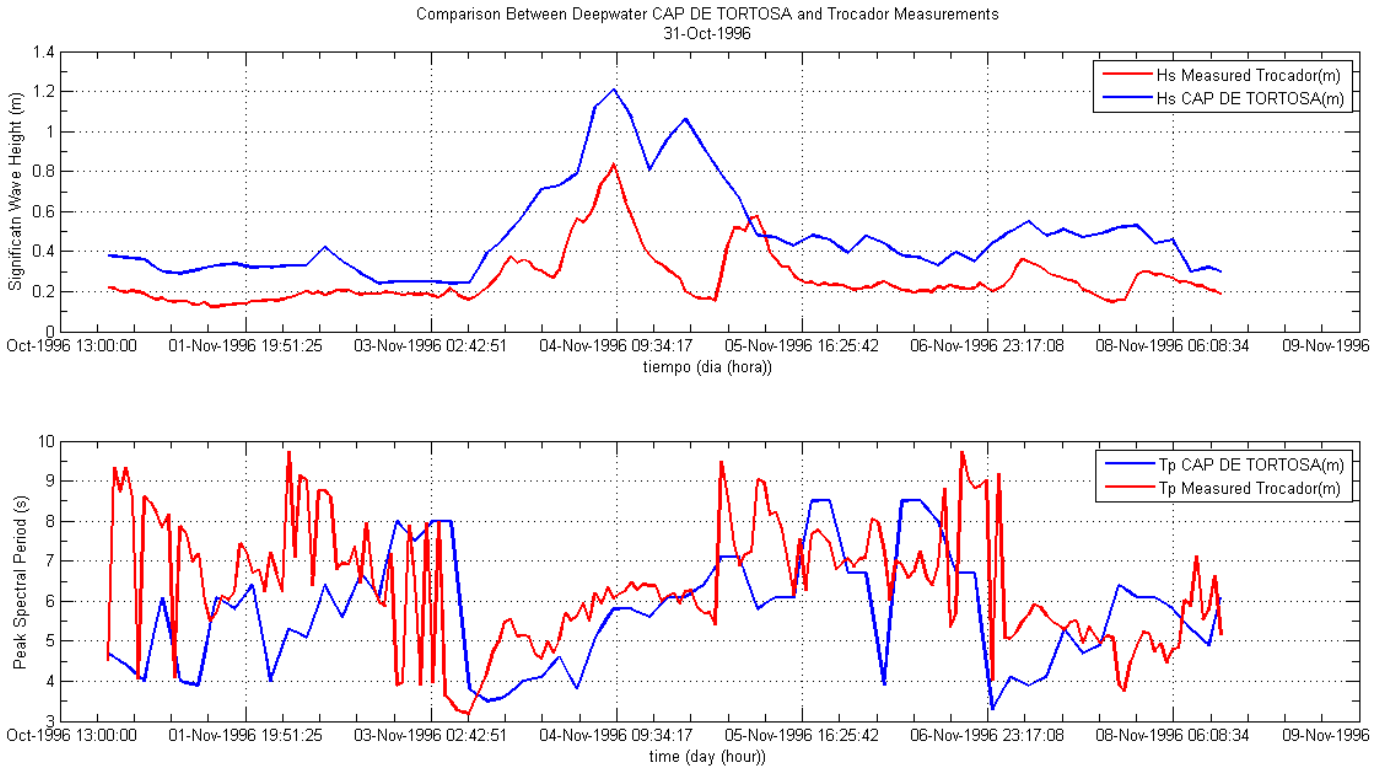

Figure 112: Comparison between deepwater measured waves and site measurements Ebro Delta

3.2.2 Statistics Based on Zero-Down Crossing

The results from the analyzed time series, using the zero down crossing method, are shown in figure 113. One small storm was measured during the 4th of November 1996, where $H_{1/3}$ was 0.75 meters, with a maximum wave height of 1.28 meters. The significant period, $T_{1/3}$, was very constant with values around 5 seconds through out the whole measurements, which means that the more energetic waves defined by the zero down crossing period have individual periods around 5 seconds during this wave measurement period. The maximum measured zero down crossing period was around 10 seconds, except for some time series where T_{max} reached values of 22 seconds, all within the limits of gravity waves.

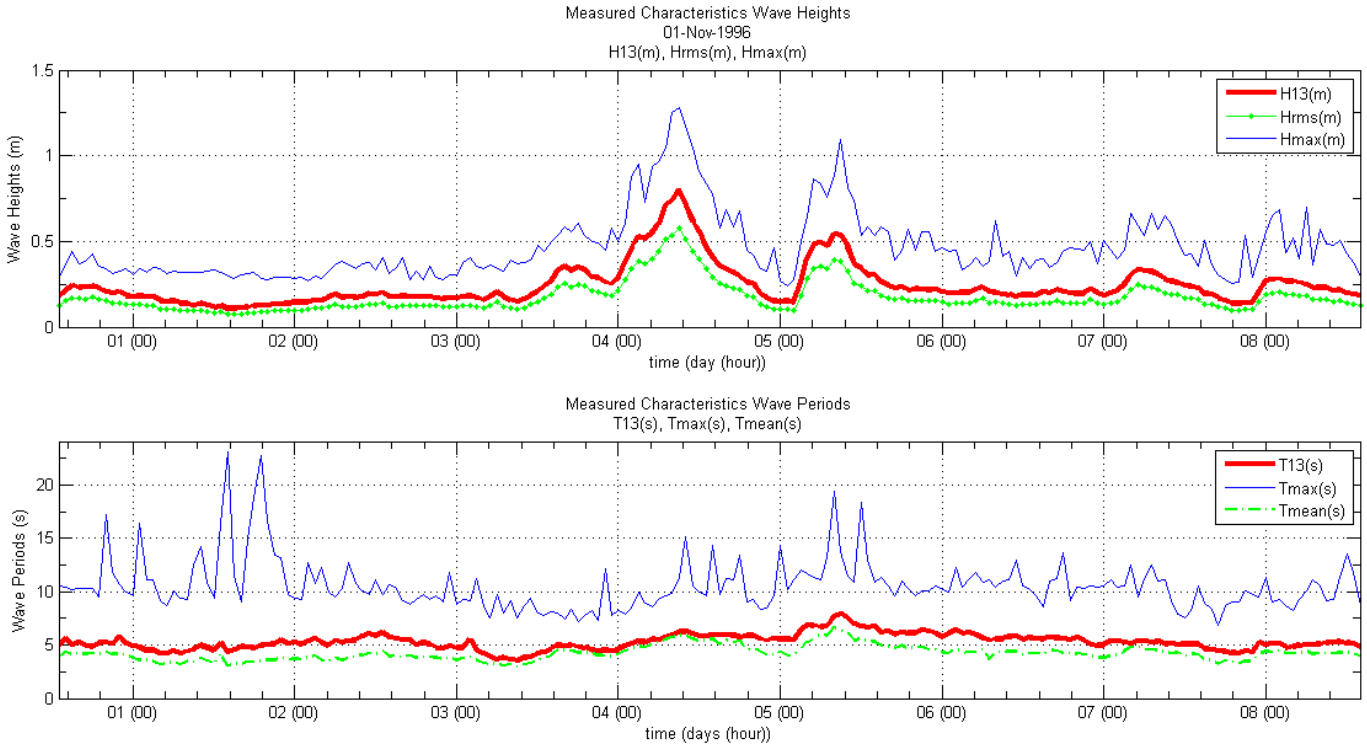

Figure 113: Temporal Variation of Wave statistical Characteristics based on zero down crossing Ebro Delta.

The maximum wave height, based on the ZDC method, measured during the whole period was obtained, figure 114. The wave with a measured height of 1.28 meters and individual period of 7 seconds, presents a sharp crest and a longer trough, typical of a wave near to its breaking condition, which does not follow a harmonic function.

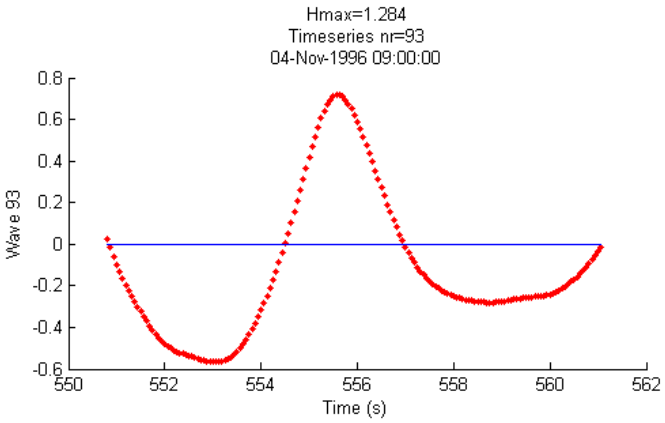

Figure 114: Maximum measured wave height based on zero down crossing Ebro Delta.

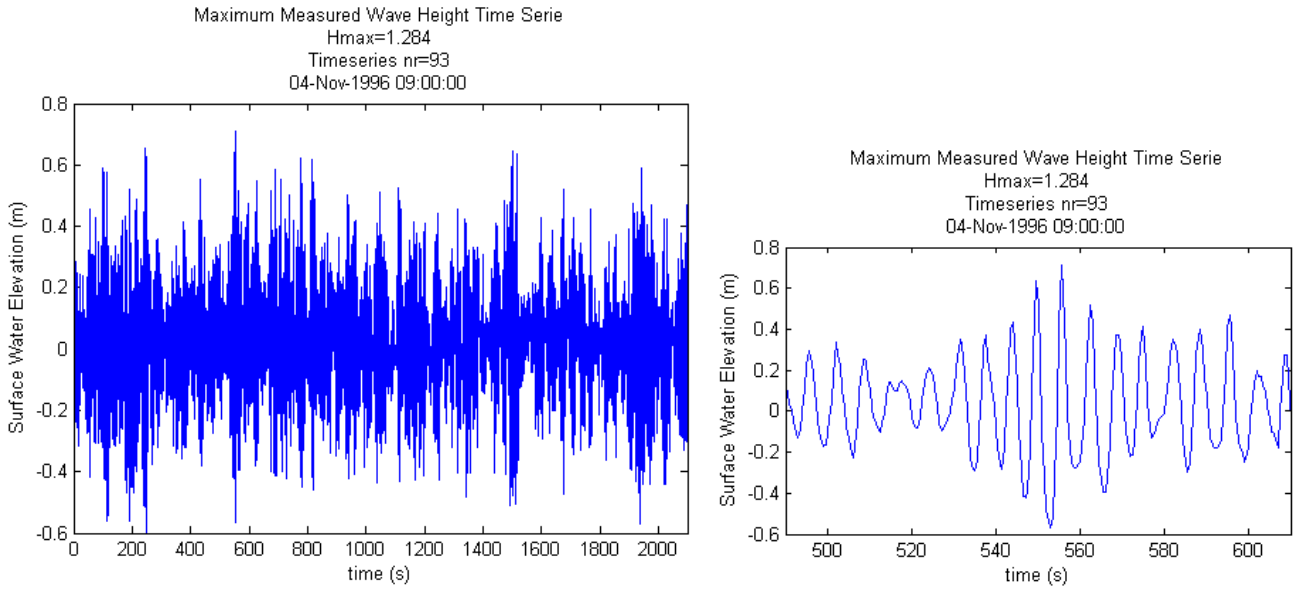

Figure 115: Time series of maximum measured wave height based on zero down crossing Ebro Delta.

The time series where the wave occurred is shown in figure 115 with the specific wave group where this wave was found. This time series shows a very irregular wave profile, characteristic of short period waves. The wave group where the maximum wave was measured was composed of 6 high waves.

The ratios between the different characteristic wave heights and periods for these wave measurements are shown in table 9. Given the shallow water conditions and the broad spectra of short period waves, it would be expected to find a deviation from Rayleigh distribution, however surprisingly the wave height values appear to be very close to the ones predicted by the Rayleigh distribution, $H_{1/10}/H_{1/3}$=1.27 and $H_{1/3}/H_{mean}$=1.6.

Table 9: Ratios of the Characteristic Wave Heights and Periods based on the ZDC for Ebro Delta

	$H_{max}/H_{1/3}$	$H_{1/10}/H_{1/3}$	$H_{1/3}/H_{mean}$	$H_{1/3}/H_{rms}$	$T_{max}/T_{1/3}$	$T_{1/10}/T_{1/3}$	$T_{1/3}/T_{mean}$
Mean	1.985	1.272	1.615	1.415	2.019	0.996	1.264
Standard Deviation	0.353	0.048	0.062	0.025	0.492	0.039	0.109

Table 10: Skewness and Kurtosis Ebro Delta

	Skewness	Kurtosis
Mean	0.17	3.69
Standard Deviation	0.21	1.04

The relation between the $H_{1/3}$ and the H_{max} is shown in figure 116, using 193 wave records with 98768 waves. These regression shows that the expected maximum wave height is 1.82*$H_{1/3}$, a ratio much higher than the one found for long travelled swells.

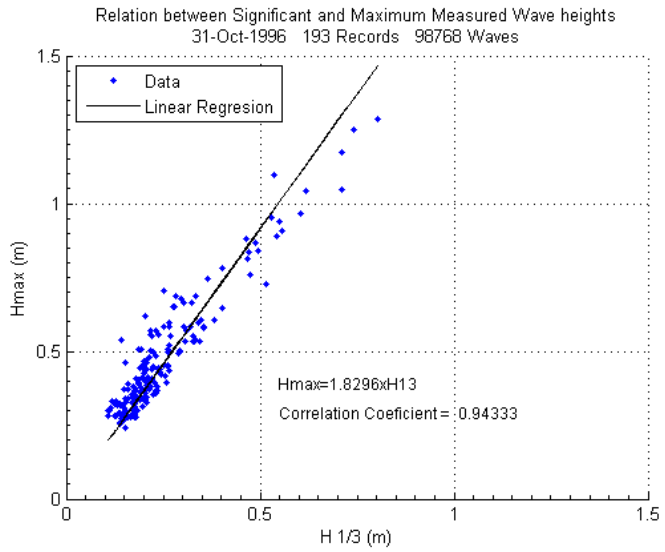

Figure 116: Relation between maximum and significant (H1/3) wave heights

The ratios between the characteristic wave periods show a larger spread between the individual wave periods. This larger spread in individual wave heights and wave periods is characteristic of highly irregular short period waves, which contrast with the previously analyzed long travelled swell where almost regular wave conditions were measured.

The spreading in the occurrence of individual wave periods is shown in its marginal distribution. The marginal individual wave height and wave period distributions are shown in figure 117. The normalized individual wave height distribution shows good agreement with the Rayleigh distribution, with a small tendency of smaller waves to occur. This effect is more clearly seen in the cumulative occurrence distribution.

The joint individual wave height-period distribution shows that the larger waves, H=2*H_{rms}, tend to have periods at 1.25*T_{mean}, figure 118. A strong correlation between heights and periods of small waves is visible, which is characteristic of wind waves. For the mode found at T/Tmean 1.15 shows a positive skewness with w higher occurrence of individual waves of larger period than shorter periods for waves higher than H_{rms}.

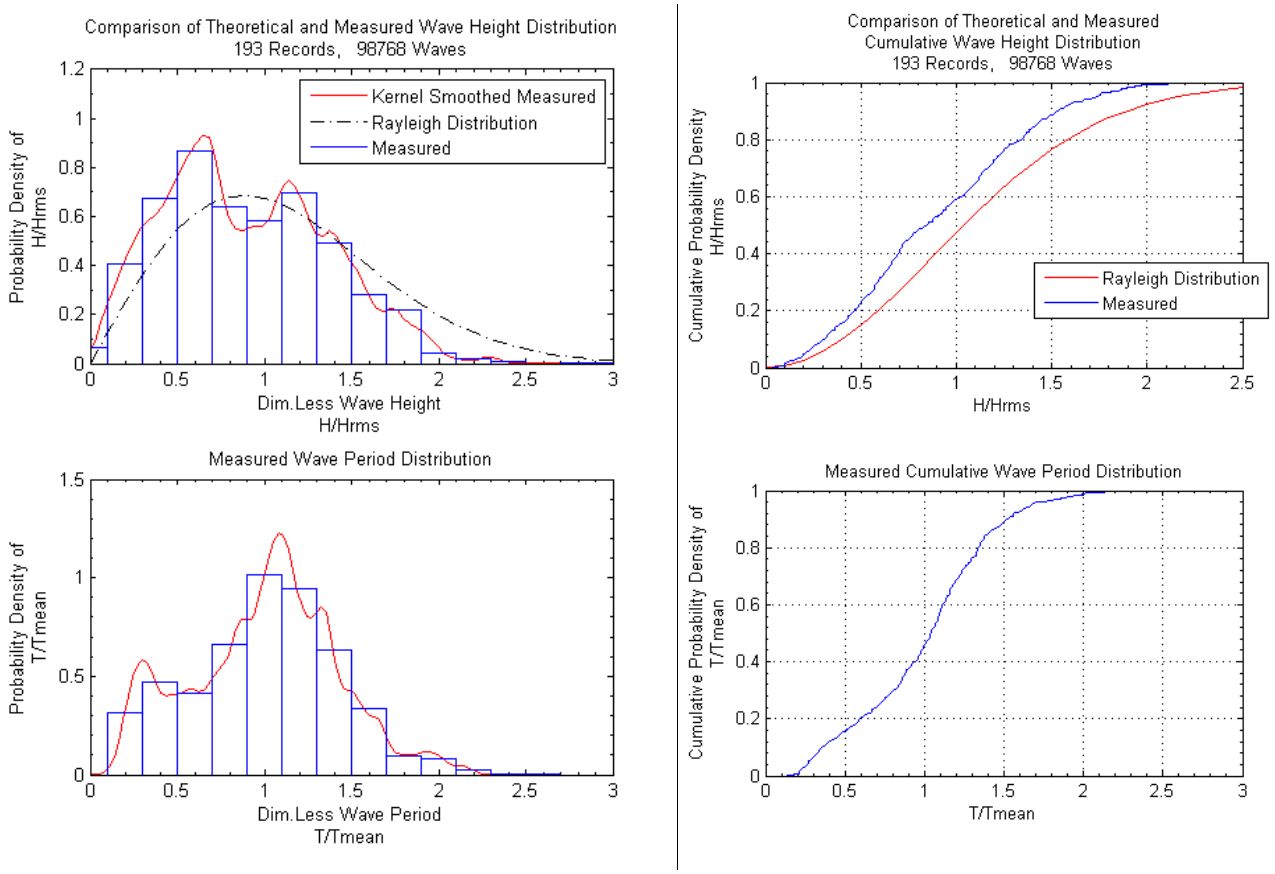

Figure 117: Measured wave height and wave period marginal distributions Ebro Delta.

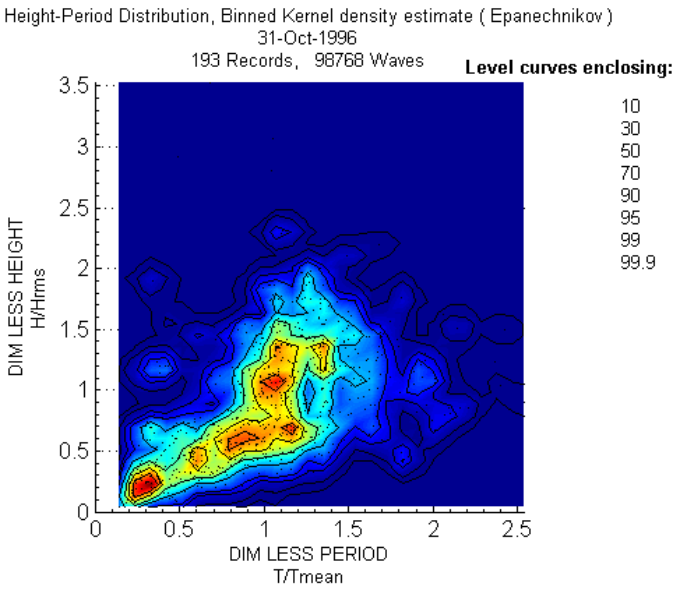

Figure 118: Measured joint distribution of individual waves Ebro Delta

3.2.3 Spectral Analysis

A detailed spectral analysis was done to all the measured time series. The temporal spectral variation of the measured data set is shown in figure 119. Two relative larger energetic events are clear seen in this representation, which occurred the 4th and the 5th of November 1996, during the rest of measurements very calm conditions were measured. The frequency distribution of the energy content is seen clearer in figure 120. The first event that occurred during the 4th shows a peak condition at frequencies around 0.15Hz, 6.667 seconds, while the second one shows a slightly lower frequency at approximately 0.1 Hz, or 10 seconds.

In general the energy is found to be between 0.09 and 0.3 Hz, 11.1 and 3.33 seconds. Very low frequency energy is visible during the two more energetic events. The fact that the wave measurements were carried at very shallow water, a depth of 3.5 meters, and very close to shore and the breaker zone can be the reason for the observed low frequency energy, also given the fact that very calm conditions were measured, makes it easier to observe the low frequency energy, which otherwise would be hidden due to scale effects. This low frequency energy will be examined further in the long wave chapter.

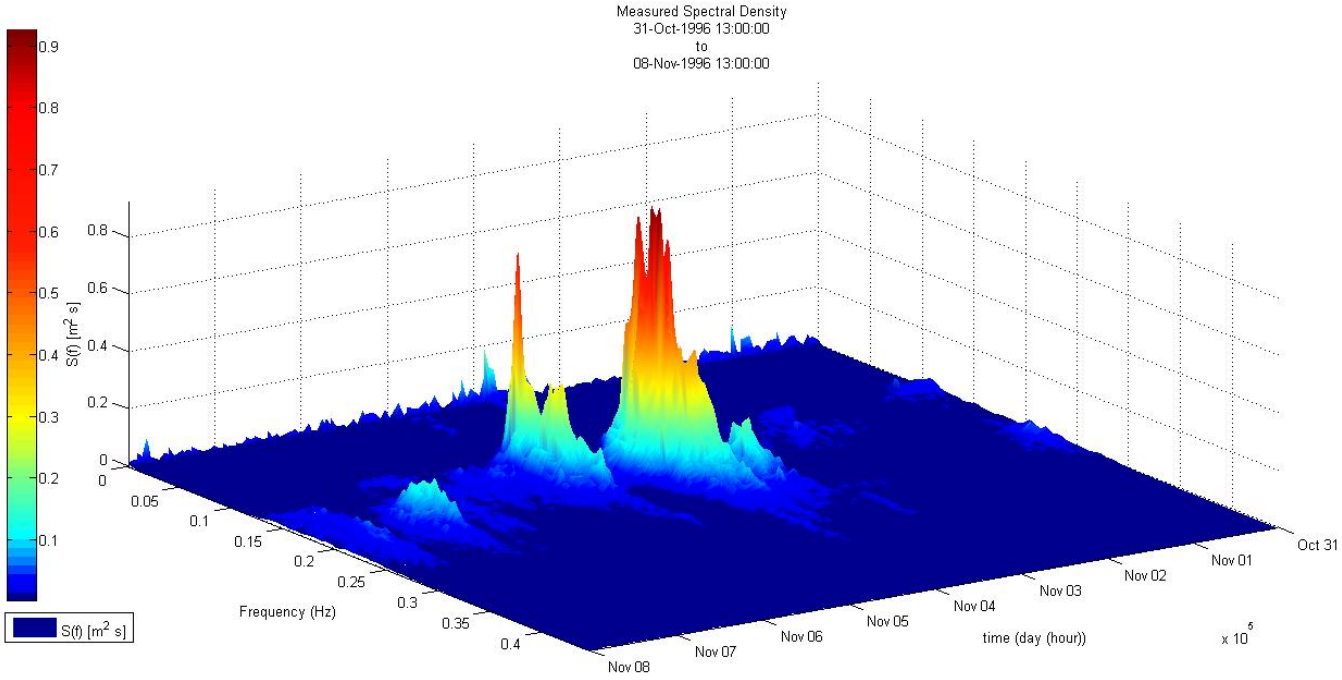

Figure 119: Temporal spectral variation Ebro Delta.

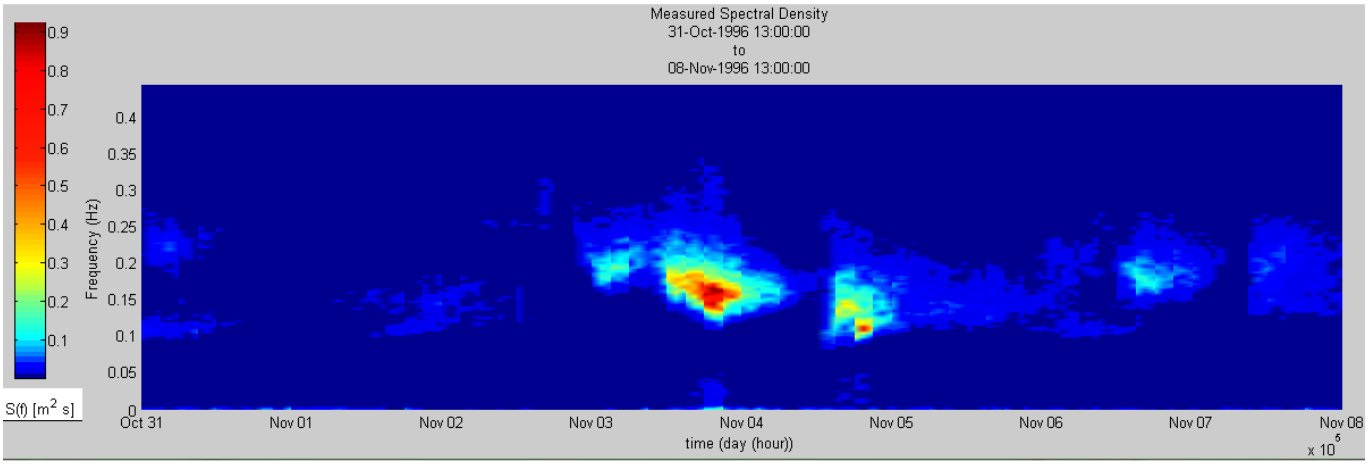

Figure 120: Temporal spectral variation Ebro Delta.

The spectral wave heights and periods derived from the spectra were obtained; figure 121 shows the temporal variation of these characteristics compared to the statistical values derived from the zero down crossing method. The relation between H_{mo} and $H_{1/3}$ shows that the significant wave height derived from the ZDC is lower by a factor 0.93. The energetic period, T_{m0-1}, seems to be unstable due to the relatively large low frequency energy content, it is 3.7*Tp, with a standard deviation of 3.

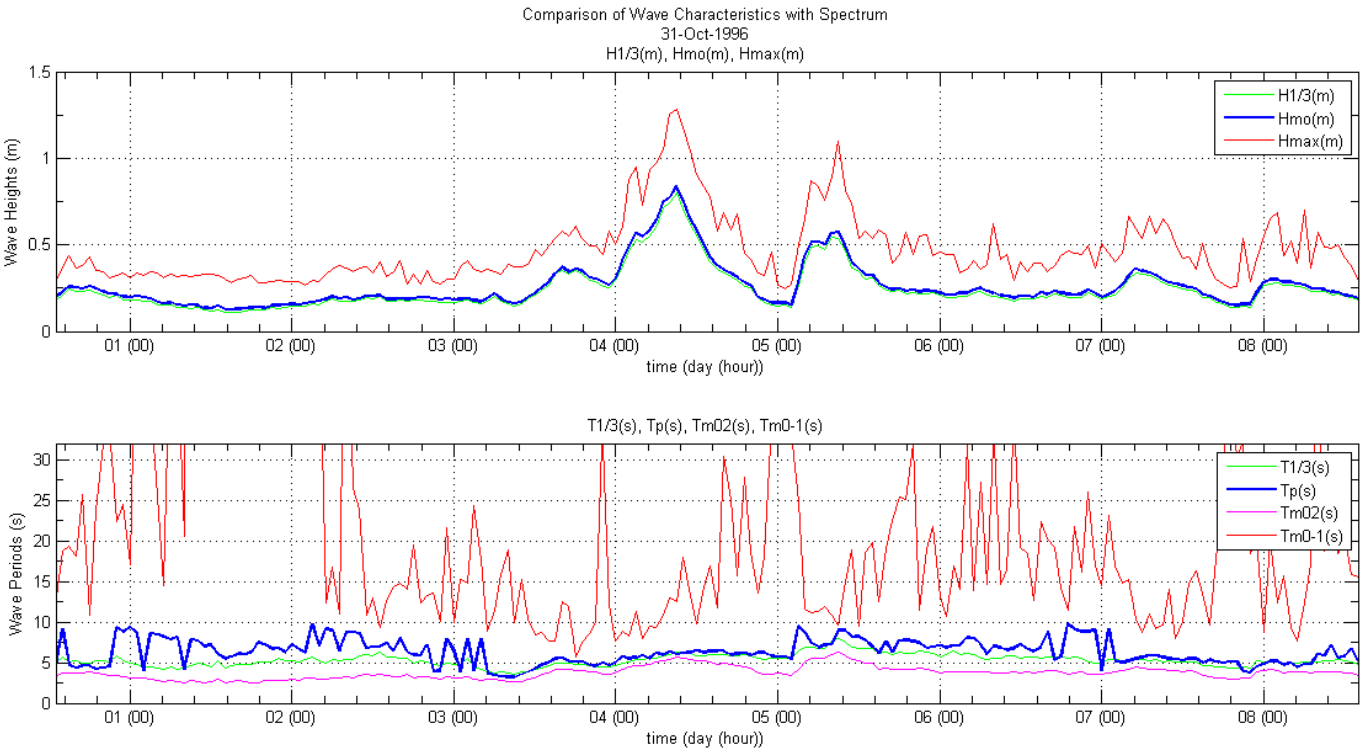

Figure 121: Temporal variation of wave spectral characteristics Ebro Delta.

Table 11: Spectral wave ratios Ebro Delta

	$H_{1/3}/H_{mo}$	H_{rms}/H_{mo}	T_{mean}/T_{mo}	$T_p/T_{1/3}$	T_{mo-1}/T_p
Mean	0.930	0.658	1.141	1.187	3.709
Standard Deviation	0.023	0.020	0.080	0.264	3.014

The spectral parameters to characterize the spectra for the measurement period are shown in figure 122. The spectral peakdness parameter Qp, varies between 0.5 and 2 during the most of the time, which is characteristic of such short period waves, during the most energetic events, Qp becomes larger with values reaching 4. During the calm conditions the spectra is close to a white noise, very broad.

The spectral bandwidth parameter, ε, is close to 1 during the whole measurements, and again it misses the changes in the spectra. The narrowness parameter ν, correlates inversely with Qp, showing how the observed changes in the measured spectra. The second narrowness of spectra parameter α, is an almost constant value of 0.5, missing the measured spectral changes. The spectral grouping parameter Ka, does correlate with Qp, and higher values are observed according to measured spectral changes. It is concluded that Qp, ν and Ka represent the spectral changes observed, while the other parameters miss the clear changes observed.

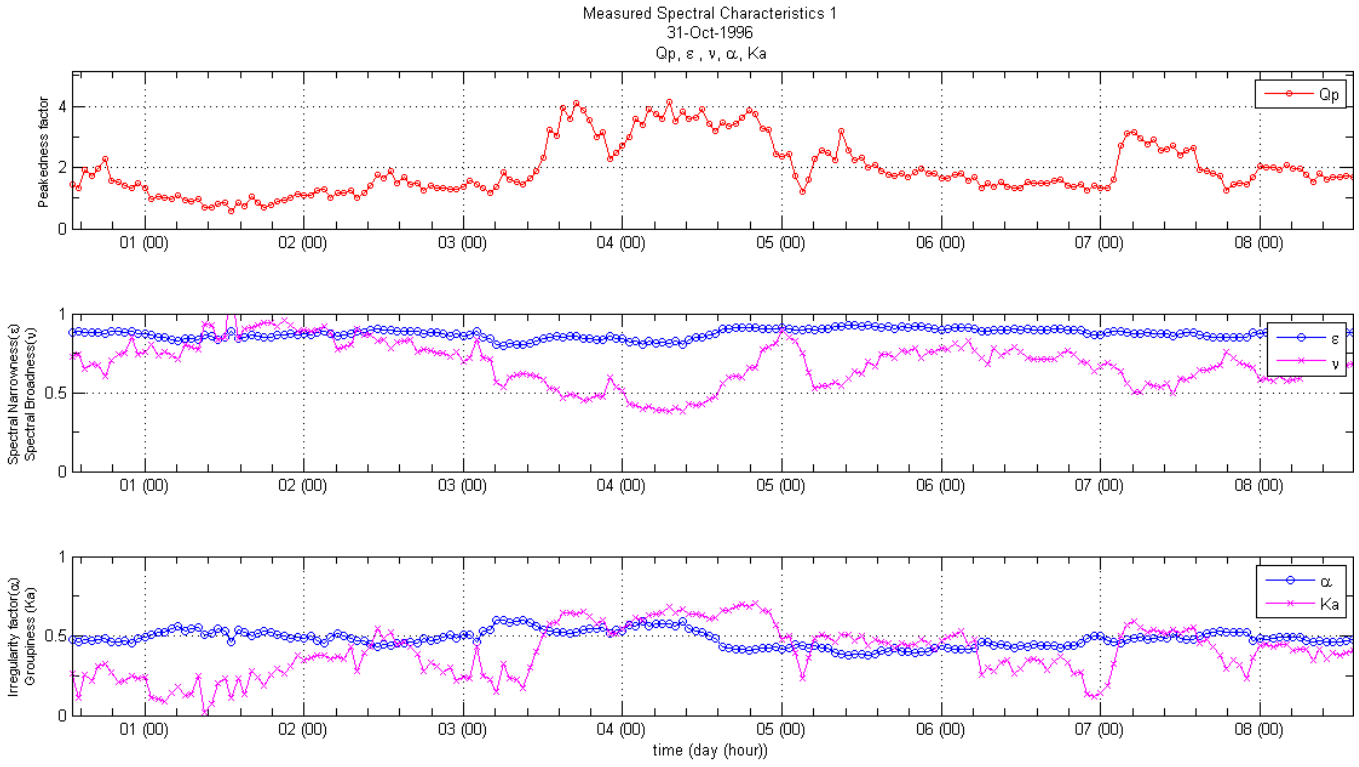

Figure 122: Temporal variation of wave spectral characteristics Ebro Delta.

The spectra of the most energetic condition were investigated in detail. The spectra of the five highest wave conditions were obtained, and compared with the JONSWAP spectra. The spectra showed several peaks around the maximum measured frequency, varying between 0.14 and 0.18 Hz, 5.56 and 7.14 seconds. This characteristic of the irregular short period wind waves. The peak enhancement factor, γ, obtained from the fitted JONSWAP spectrum varied between 4 and 4.8 for these most energetic conditions.

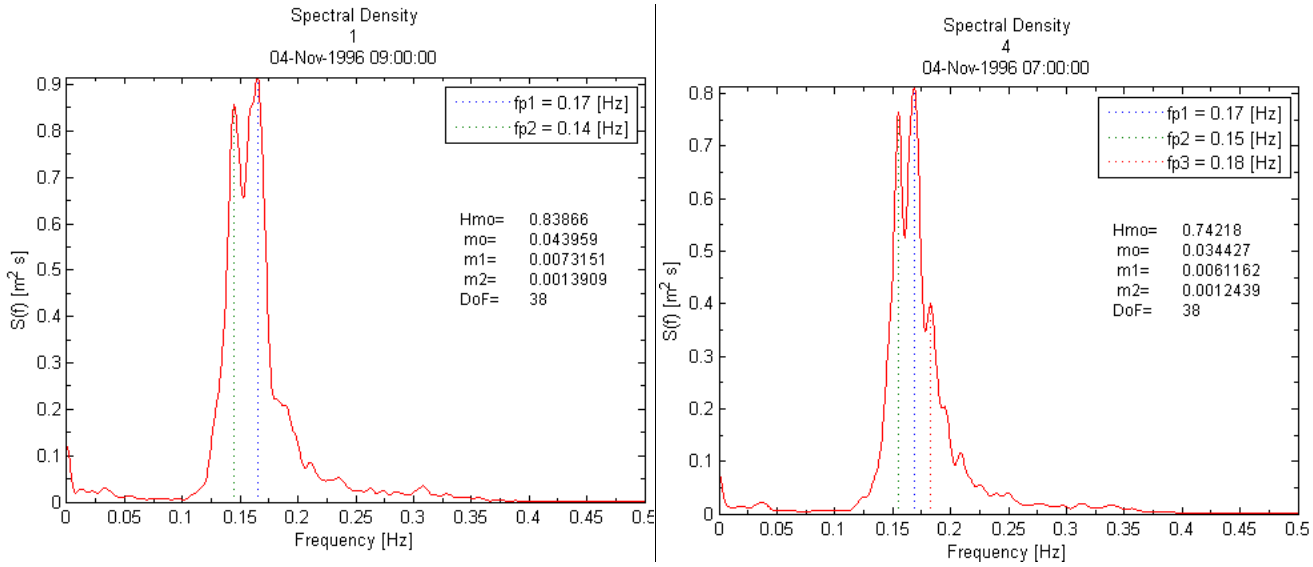

Figure 123: Spectra for most energetic wave time series Ebro Delta.

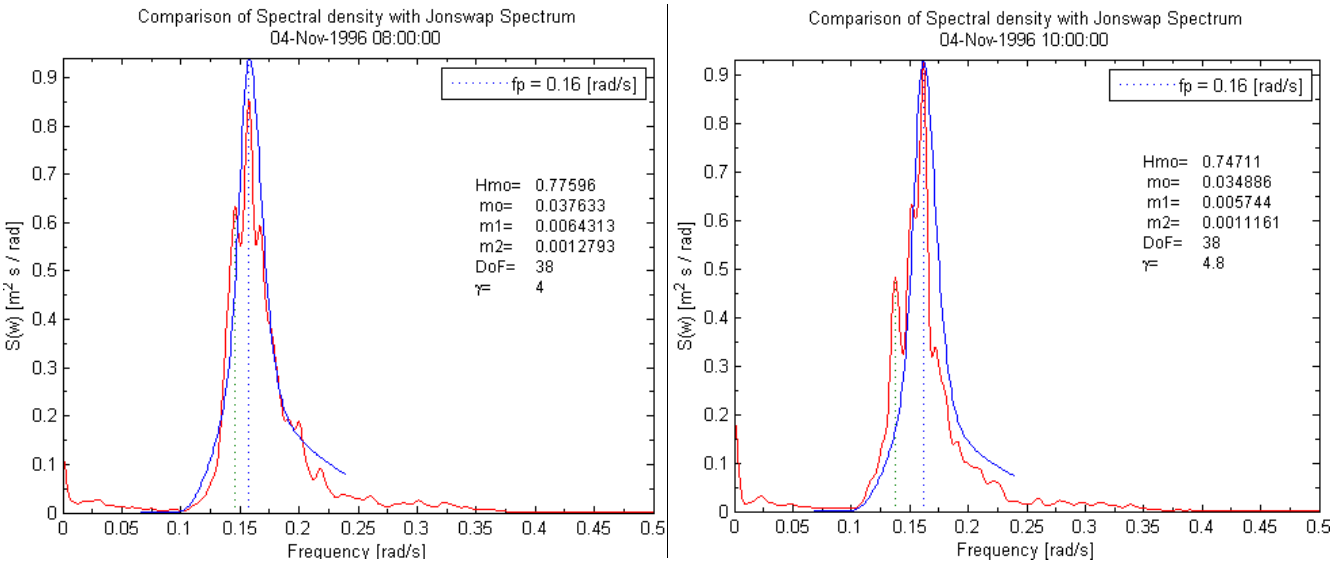

Figure 124: JONSWAP fit for the spectra for most energetic wave time series Ebro Delta.

3.2.4 Wave Grouping Analysis

The wave grouping characteristics of the all the wave records were analyzed. The correlation coefficient between individual wave heights defined by the zero down crossing method was obtained for the 193 individual records, which contained 98768 wave, and average of 511 waves per record. Lag number of waves of 1, 2 3 and 4 were evaluated. The results average with its standard deviation from all the records is shown in figure 125. The average correlation coefficient between two consecutive waves was 0.25, lower than the average value of 0.3 reported for wind waves by Rye 1974, which suggest that there is a very low correlation between individual waves. However the values do present large variability for a lag number of one wave, which is expected given the different sea states measured during the whole period. The temporal variation of the correlation coefficient between to successive waves, $\gamma HH(1)$, is shown in figure 127. During the calm $\gamma HH(1)$ is low, however, during the more energetic wave conditions, the $\gamma HH(1)$ increases to values of up to 0.5, which suggests that the groupiness of the waves increased during these period.

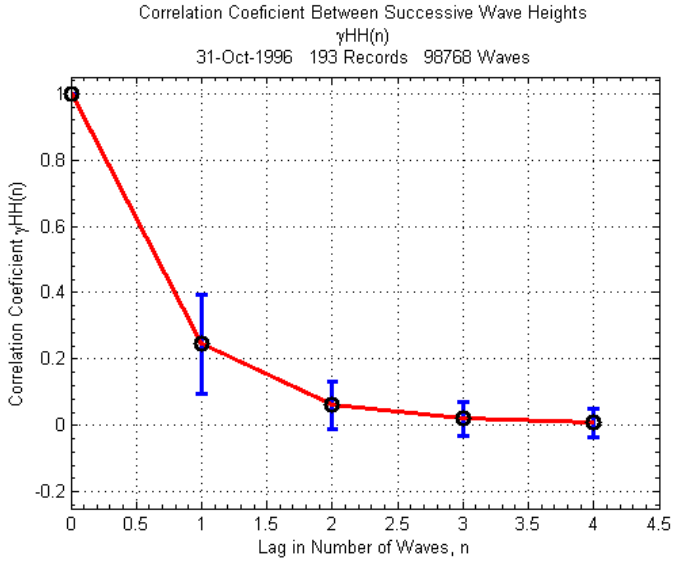

Figure 125: Correlation coefficient between successive wave heights Ebro Delta.

The run length for individual waves above $H_{1/3}$ and H_{mean} was investigated. Figure 126, shows the occurrence probability and exceedance probability for these run lengths compared to the predicted values by Kimura's theory. The theory predicts very different values than the measured ones, mainly because the mean on the Hrms, and the mean of $\gamma HH(1)$, during the measurement period are not representative through out the whole period. The validity of the theory is only for stationary wave conditions.

The mean run length for H*>H1/3 and H*>Hmean was then obtained for each wave record. Figure 127 shows the temporal variability of these two parameters with the measured peak period and $\gamma HH(1)$. The higher measured mean run lengths, occur when groups of successive waves appear. It is seen that during the most energetic events

the measured mean run lengths increases from 2 waves in average to 3 waves for H*>Hmean, and from 1 to 1.5 for H*>H1/3, which means that the groupiness increased during these period, which can be correlated to changes in the spectral characteristics previously analyzed.

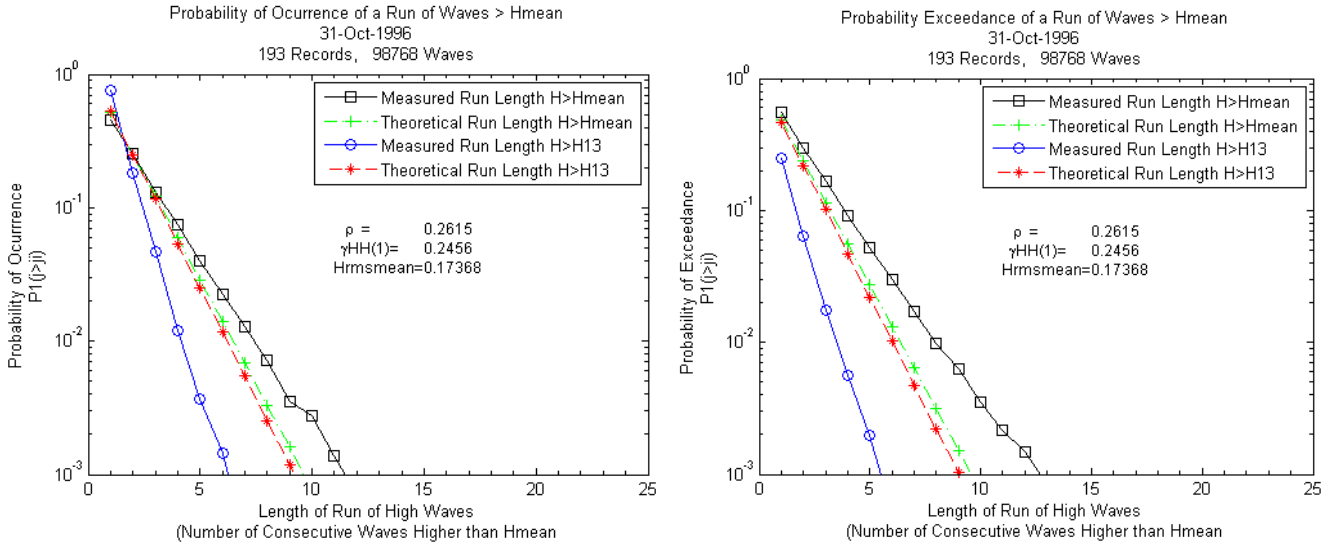

Figure 126: Occurrence and Exceedance Probability of a Run of Waves H>H*.

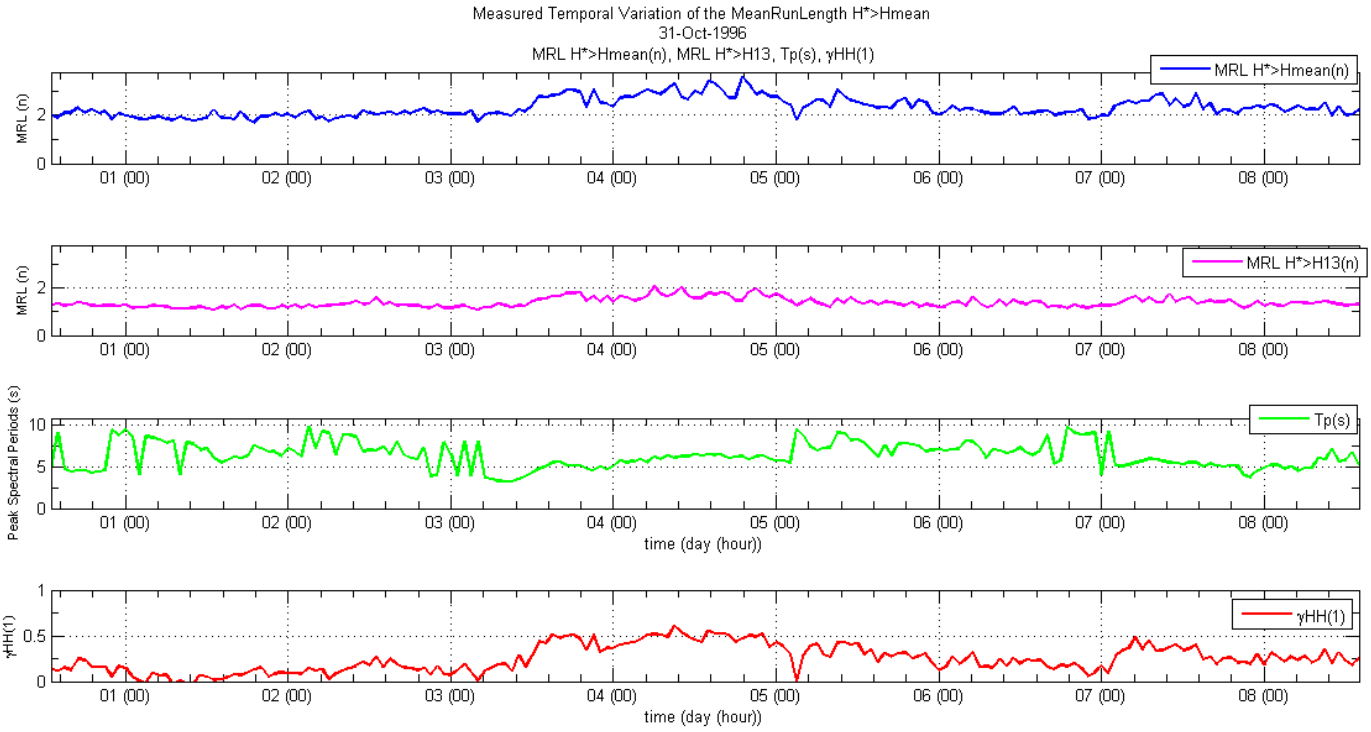

Figure 127: Temporal Variation of the mean run length H>H_{mean} and H>Hs wave heights Ebro Delta.

3.2.5 Long Wave Analysis

The energy content in the low frequency bands was investigated in the 193 measured wave records. As it was mentioned during the spectral analysis, relative large amount of energy in the lower frequencies was observed. The wave records were filtered using a low pass filter programmed at the maximum zero down crossing period. Then the spectra was obtained, with which the long wave spectral significant wave height, H_{molong} was obtained. The spectra for the highest measured long waves are shown in figure 128. The long wave energy for the highest conditions represented around 20% of the total energy, however for the calm conditions it represented up to 25%, with H_{mo}=.20m and H_{molong}=0.05m. Another noticeable characteristic of these measured long waves is that their period was very long, of more than 1000 seconds.

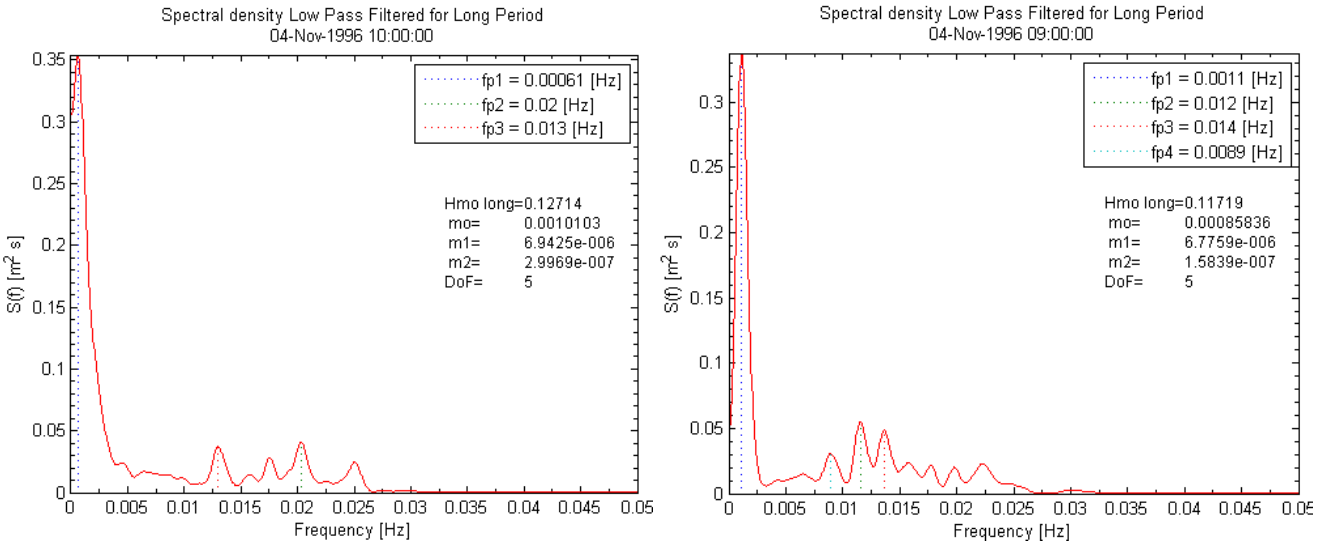

Figure 128: Long wave spectra Ebro Delta.

The spectra were the highest gravity waves where measured were compared with the obtained long wave spectra, figure 129. Again a zone with almost no energy is found where the lowest gravity wave frequencies end and the long wave a spectrum begins.

The very low frequencies measured were investigated by looking at the time series of original signal with the filtered signal. Figures 130 and 131 show the time series where the long wave spectra shows a sharp peak at 1086 seconds period and 1639 seconds period. The long modulation is visible in the time series at the same long period. It is estimated that the proximity of the breaker zone, and the shallow water conditions are responsible for such long waves, interaction between the breaking waves and the reflected waves from the beach can produce such long wave modulation.

The temporal variation of the long wave spectral wave height and its peak period was then investigated. The results are shown in figure 133. The very long period was found to occur through out the whole measurements.

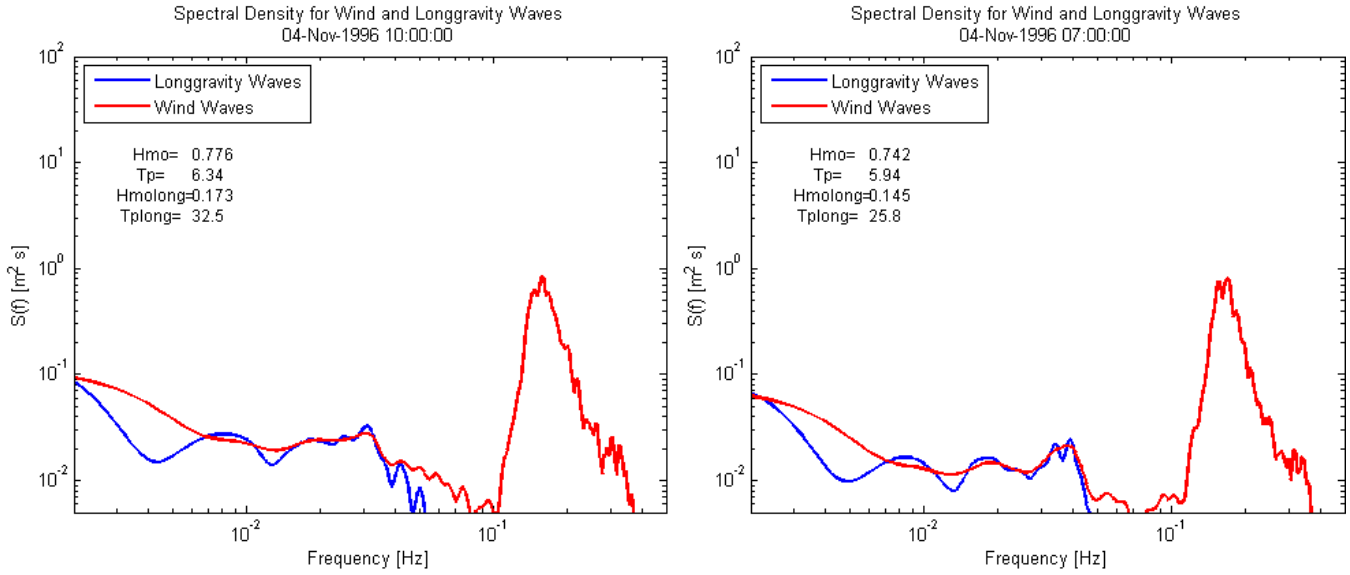

Figure 129: Long and wind wave spectra Ebro Delta.

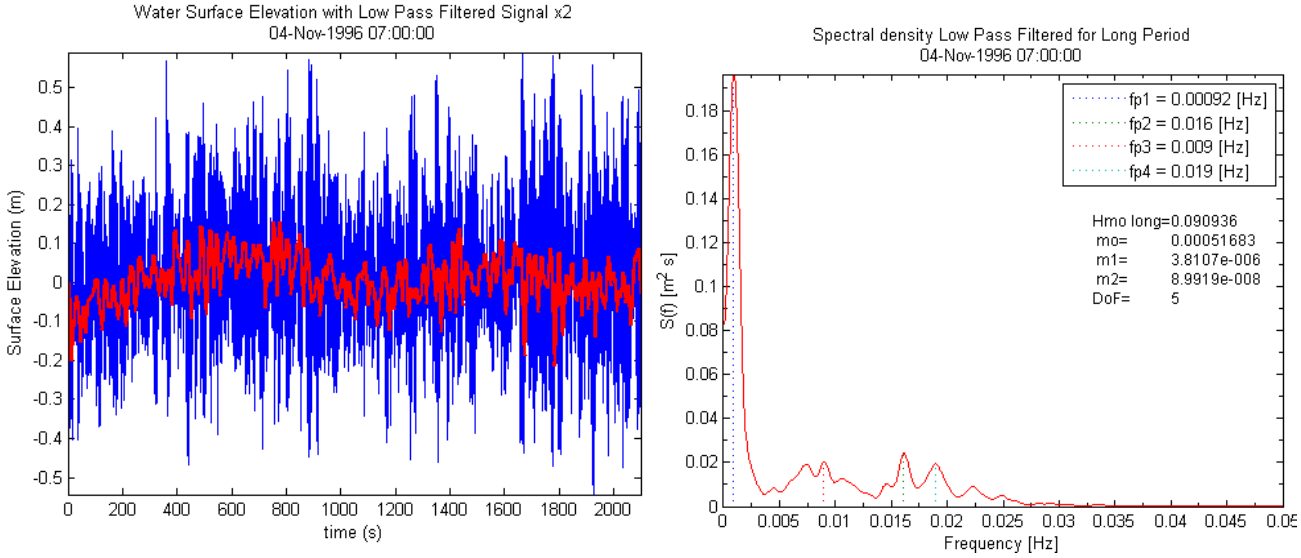

Figure 130: Filtered long wave signal Ebro Delta.

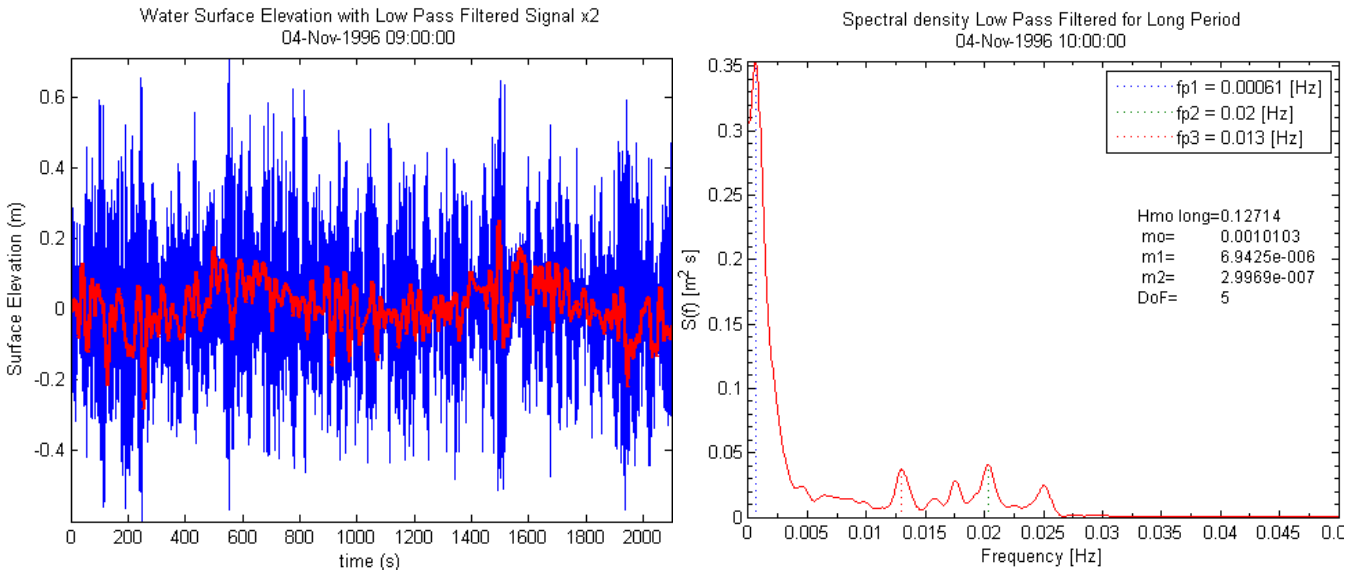

Figure 131: Filtered long wave signal Ebro Delta.

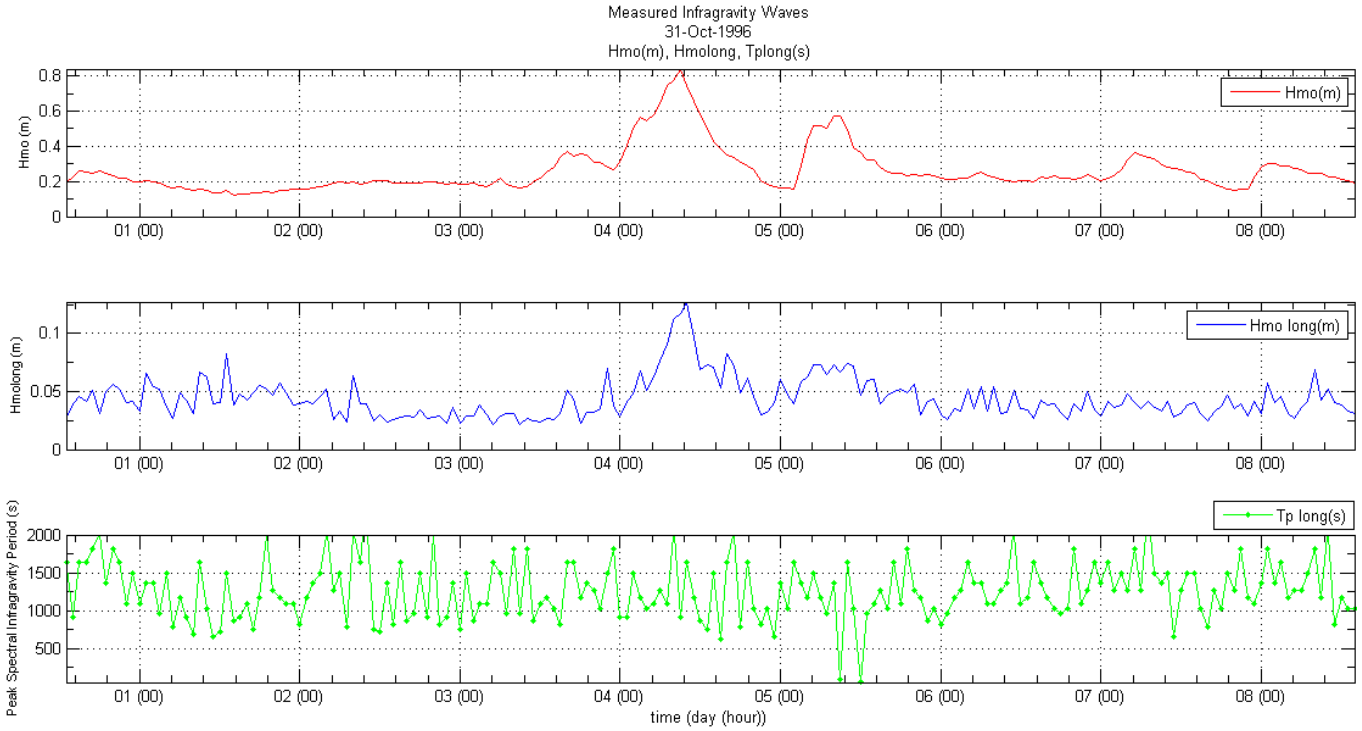

Figure 132: Temporal variation of the long wave height and peak period Ebro Delta.

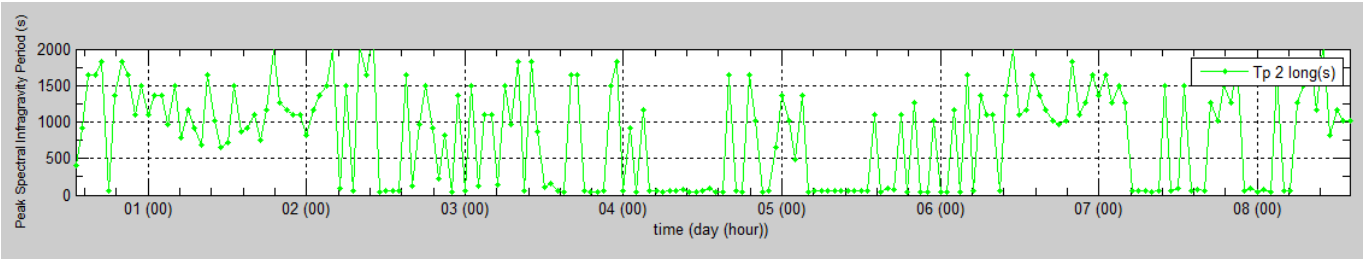

Figure 133: Temporal variation of the long wave secondary peak period Ebro Delta.

3.2.6 Analysis using the Hilbert Huang Spectrum

The HHT spectrum for the most energetic time series measured at the Ebro Delta campaign is shown in figure 134. The highly irregular wave conditions with no apparent grouping are very clear from this figure. The energy distribution over the instantaneous frequencies is also very broad with energy content found from 0.05 to 0.25 Hz, 4 to 20 seconds. Figures 135 and 136 also show the same irregular wave conditions both are consecutive time series. The low frequency energy content is clearly visible in figure 136. The low frequency energy is only found the first 500 seconds of the time series, with frequencies between 0.005 and 0.05. These would correspond to wave periods between 20 and 500 seconds, though they are not constant through out the whole time series. The corresponding time series with the low pass filter clearly shows a positive increase in the water surface elevation from the 0^{th} to the 400 second; hence the low frequency oscillation is real.

The marginal HHT(ω) spectra are shown in figure 137 for the four most energetic wave conditions. The differences with the FFT are clear for this highly irregular sea condition, a much broader frequency distribution of the energy is obtained in the HHT and the low frequency energy content obtained is much higher. Again the interpretation of the HHT and FFT is completely different, HHT shows the total energy contained through out the whole time series.

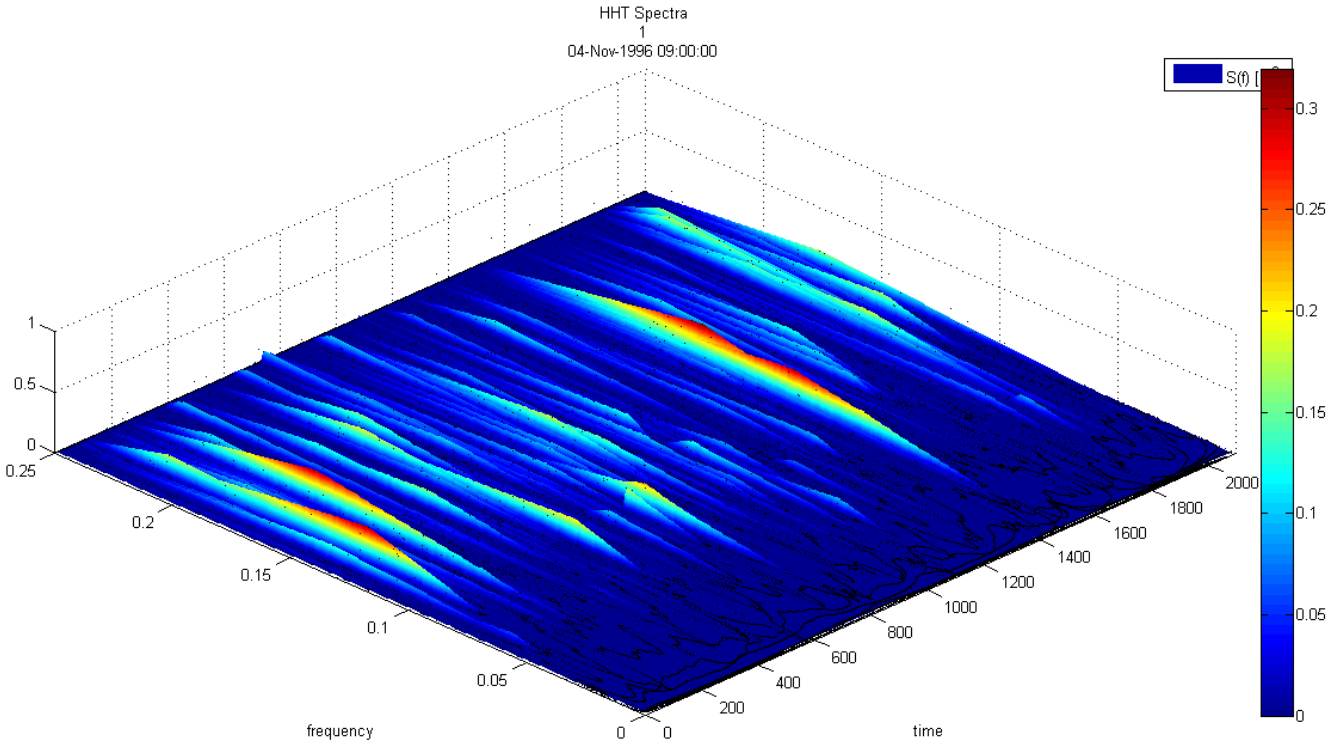

Figure 134: HHT Spectrum for most energetic time series Ebro Delta.

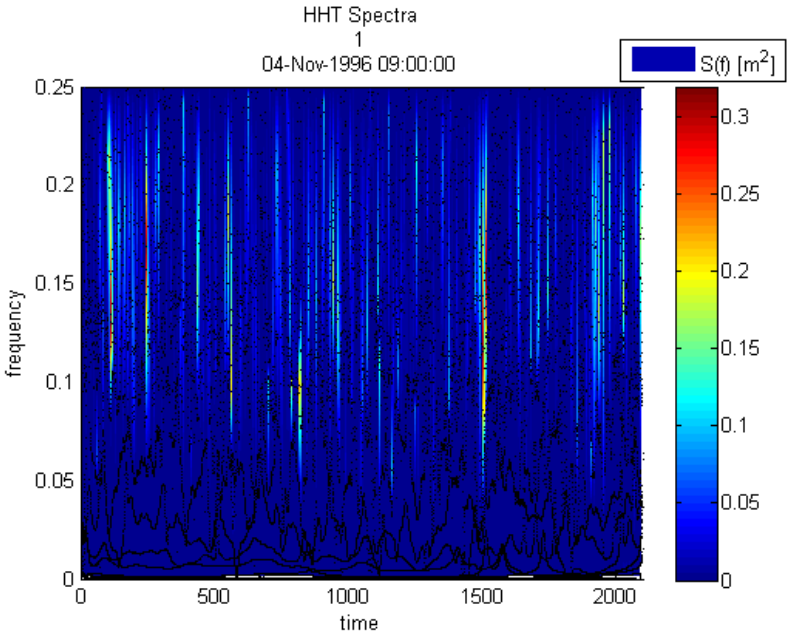

Figure 135: HHT Spectrum for most energetic time series Ebro Delta.

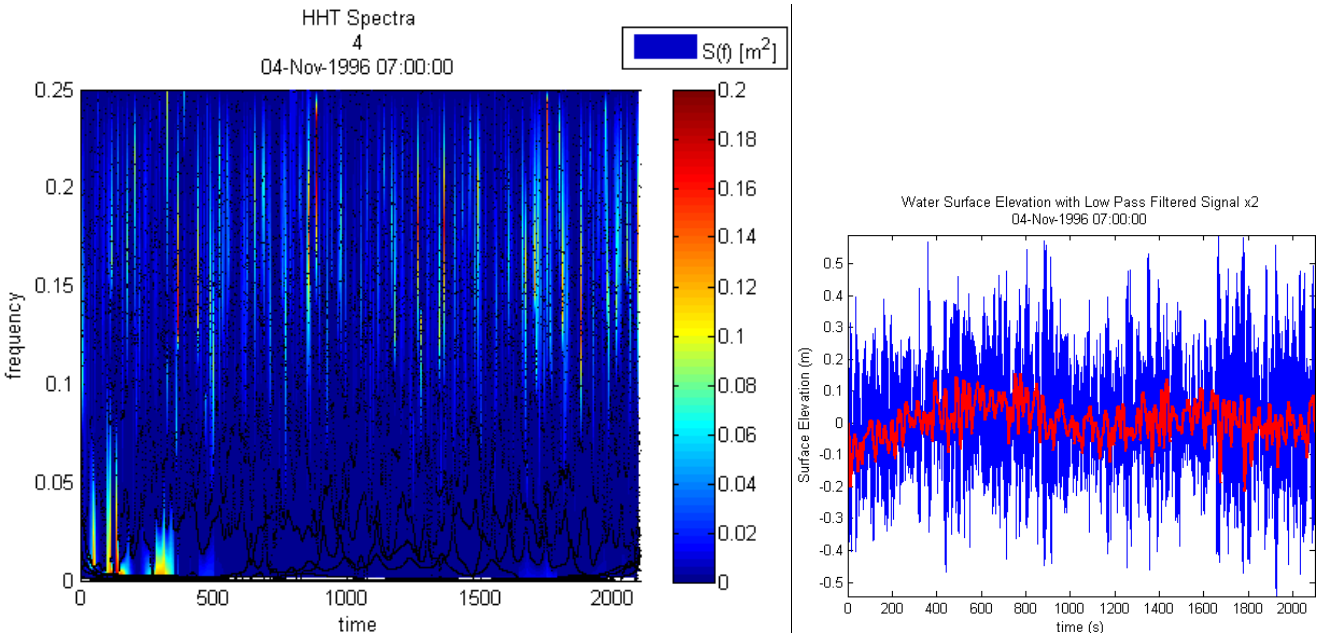

Figure 136: HHT Spectrum time series Ebro Delta.

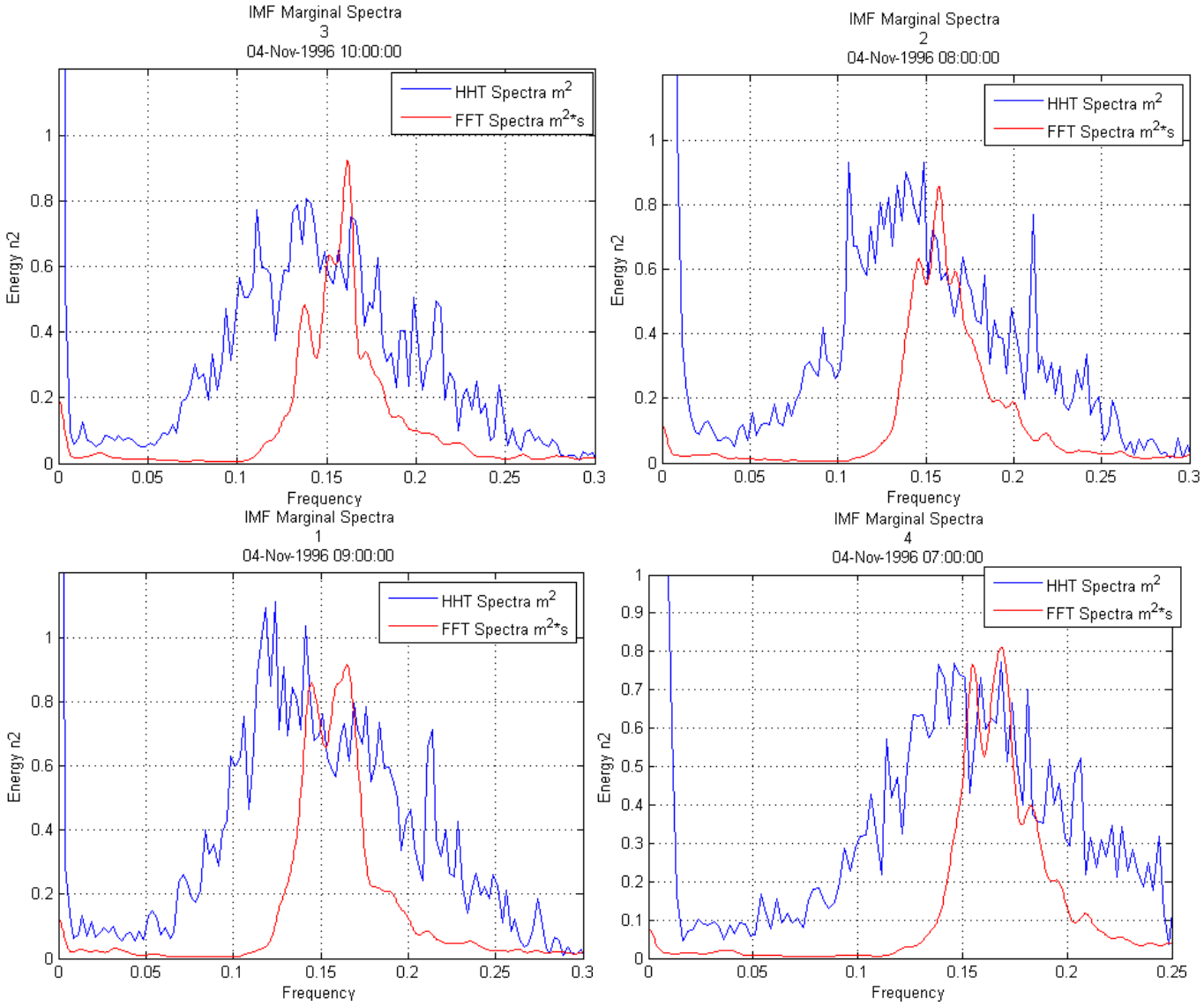

Figure 137: HHT Marginal Spectrum for time series Ebro Delta.

3.3 Wave Measurements off the Atlantic Coast of Costa Rica

Wave measurements, from the Atlantic coast of Costa Rica, were analyzed. These wave measurements were taken outside Port of Moin at a water depth of 17 meters using a submersible pressure gage. The wave measurements were carried out by Watermark S.A. for the government of Costa Rica, as part of a monitoring campaign. The wave conditions in the Atlantic coast of Costa Rica are dominated by events with deepwater directions from north to east, with wave periods between 7 and 10 seconds, being the most predominant the east-northeast direction as seen in figure 138 which shows the yearly wave height and period occurrence probability per direction in deepwater.

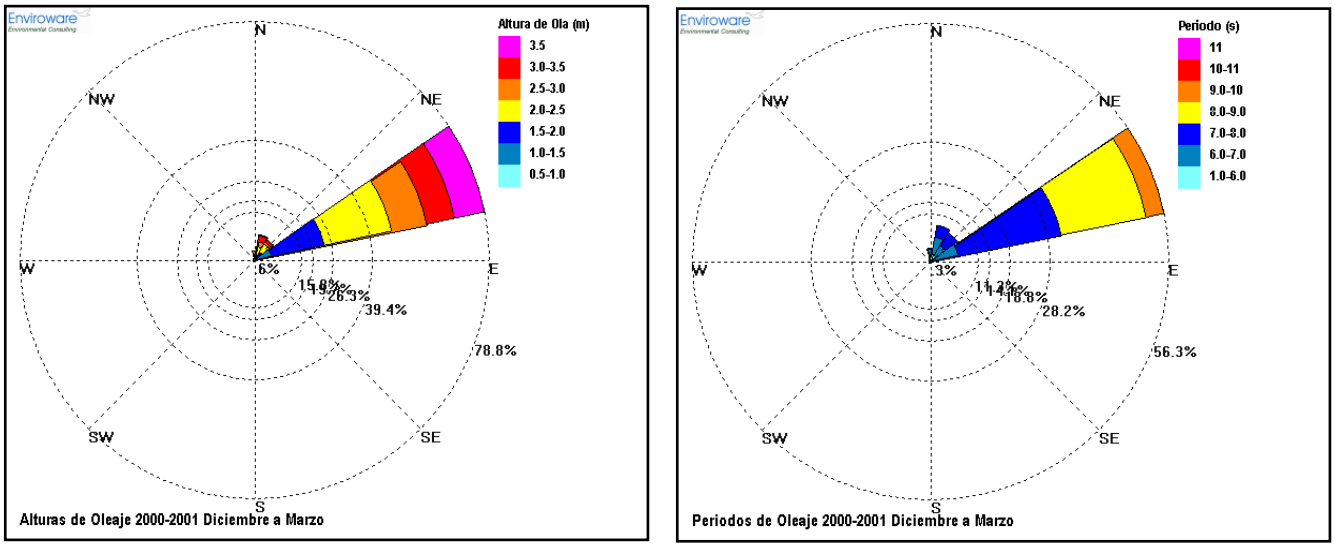

Figure 138: Yearly wave height and wave periods for the measurement site.

3.3.1 Location of Wave Measurements and Equipment used

The location of the wave measurements is shown in figure 139. They were carried out at 17 meters water depth outside of the port of Moin, which is largest port in Costa Rica. This port suffers from large operation downtimes due to agitation conditions in the harbor of Moin port. The wave measurements were carried out using a submersible pressure sensor, TWR-2050 from RBR. The same equipment as the one used to measure the waves in Pacific Coast of Costa Rica. The equipment measures pressure, and temperature.

The wave measurements were registered at 1 Hz in continuous samples of 512 seconds. The tidal variations at location are considered low, less than 40cm, with a semidiurnal cycle.

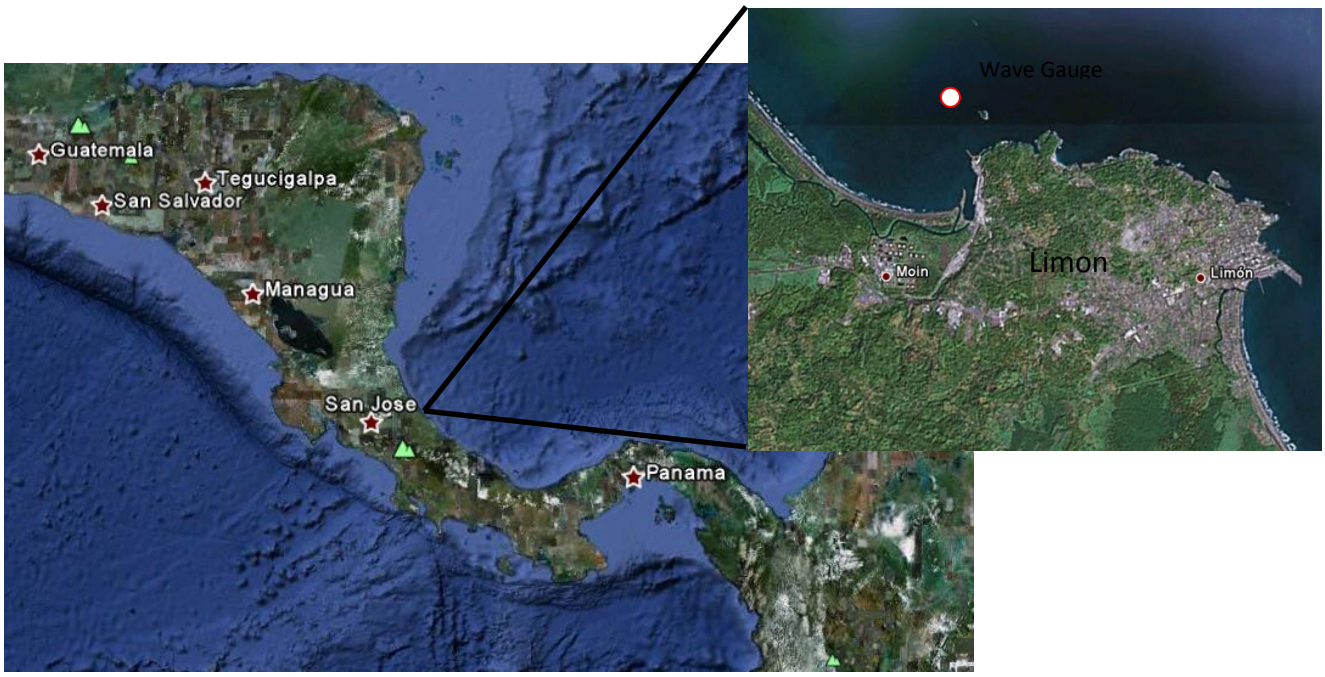

Figure 139: Atlantic coast wave measurements location Google Earth.

The deepwater wave conditions during the analyzed wave measurements are shown in figure 140. These deepwater wave conditions were obtained from the NOAA hindcast from the operational model Wavewatch III. In figure 140 the measured wave conditions in the coastal waters are shown as a qualitatively comparison. The deepwater waves suffer from refraction and shoaling and in order to carry out a quantitative comparison they should be transformed accordingly, however this is out of the scope of the present work.

Even though the comparison is done as a qualitatively one, the measured and hindcasted waves are in good agreement. The wave periods varied between 10 and 6 seconds, and four events were measured with significant wave heights above 2 meters. The deepwater wave direction during the most energetic events the waves had a east northeast direction. These waves are the product of the north trade winds which affect the site during the winter of the northern hemisphere. These the period of time when the Port of Moin presents the highest down time operations due to excessive agitation in the harbor. Several accidents during dredge operations have occurred, in two occasion during these storms two different trailing suction hopper dredgers have drifted to shore, in one occasion stranding the ship in old coral formations. This is also where the petroleum terminal of Costa Rica is located.

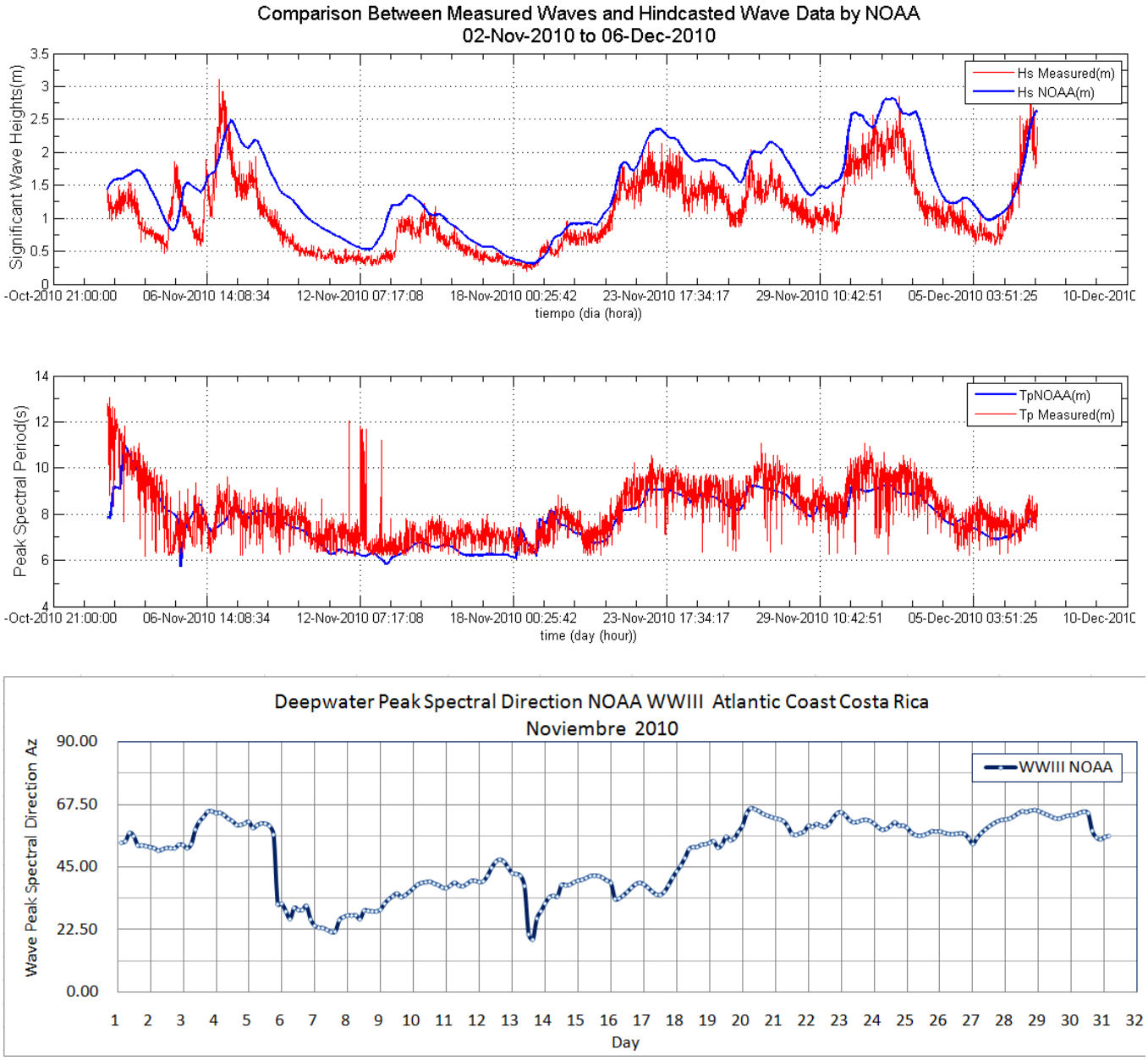

Figure 140: Comparison of deepwater hind casted conditions and measured conditions.

3.3.2 Statistics Based on Zero-Down Crossing

The statistical stability of the wave measurements was analyzed first. The analysis included the temporal variation of the characteristic statistical wave heights and periods, the ratios between them, the marginal occurrence and exceedance probability of the individual waves, and their fit to the Rayleigh distribution, and the joint probability occurrence of individual wave heights and periods, all derived from the zero down crossing method. A total of 2942 wave records, containing 191430 individual waves were analyzed.

Figure 141 shows the temporal variation of the characteristic wave heights and periods derived from their statistical analysis based on the zero down crossing method. Maximum wave heights of 5 meters were measured, and the maximum zero down crossing period had a mean of 12 seconds, with maximum values of up to 25 seconds, all well within the periods defined for gravity waves. The significant and mean periods were both very similar through out the whole measurements; an almost constant value of 7.5 seconds was measured, with no significant changes between the calm conditions and the storm conditions measured.

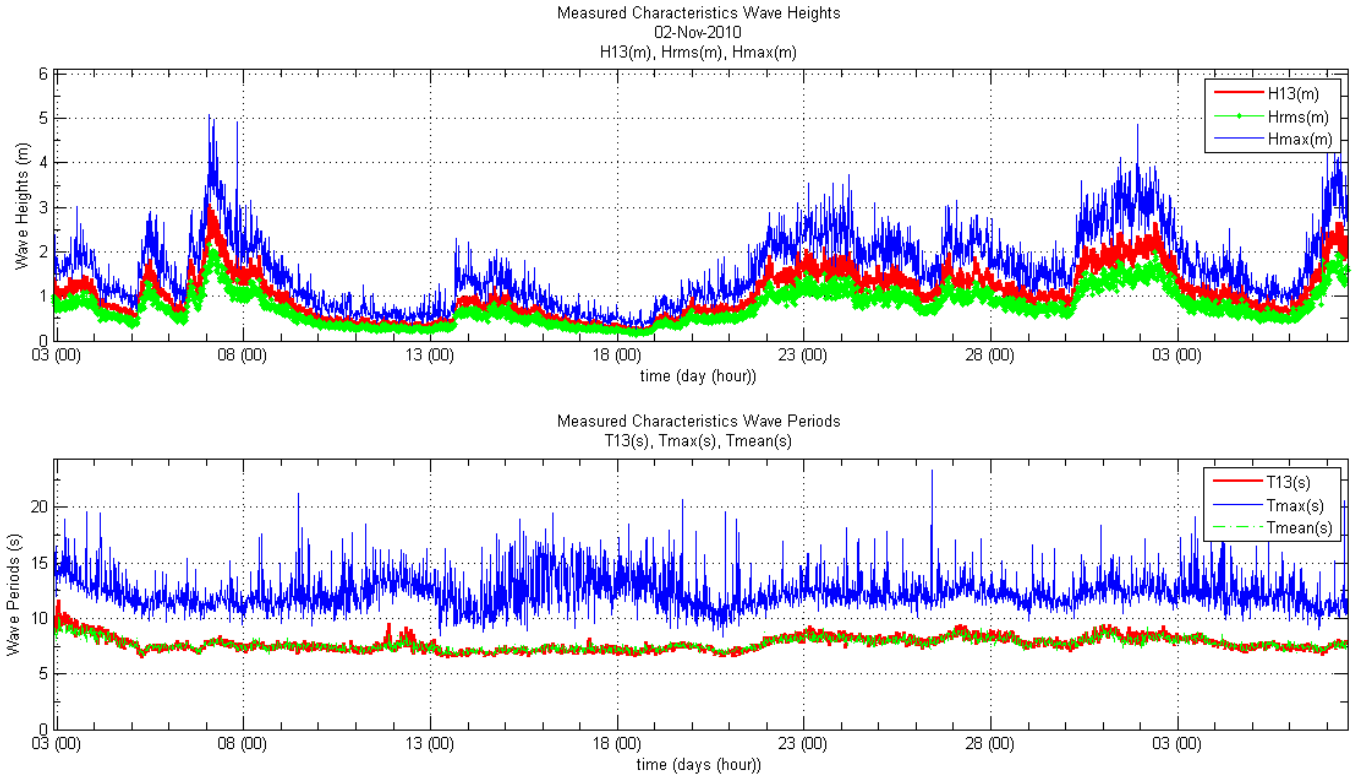

Figure 141: Temporal Variation of Wave statistical Characteristics based on zero down crossing Moin.

The ratios between the characteristic wave heights and periods are shown in table 12. The values are slightly lower than the ones predicted by the Rayleigh distribution for the wave heights. For the wave periods the ratio between the significant and mean period of 1, with a standard deviation of only 0.037 shows that the most energetic waves occur for the mean waves. Such a low standard deviation shows a strong correlation given the fact that 2942 records are considered in the obtained results.

Table 12: Ratios of the Characteristic Wave Heights and Periods based on the ZDC for Moin

	$H_{max}/H_{1/3}$	$H_{1/10}/H_{1/3}$	$H_{1/3}/H_{mean}$	$H_{1/3}/H_{rms}$	$T_{max}/T_{1/3}$	$T_{1/10}/T_{1/3}$	$T_{1/3}/T_{mean}$
Mean	1.537	1.195	1.558	1.387	1.606	0.936	1.003
Standard Deviation	0.205	0.084	0.072	0.036	0.230	0.057	0.037

Table 13: Skewness and Kurtosis Moin

	Skewness	Kurtosis
Mean	-0.02	3.12
Standard Deviation	0.07	0.58

The maximum measured wave height was investigated in detail. Figure 142, shows the maximum measured wave, with a height of 5.09 meters with the wave group where the wave occurred. The wave had an individual period of 7.5 seconds, and a two wave groups are seen were separated by 3 conspicuous small waves. The relation between the $H_{1/3}$ and H_{max} was the investigated. Figure 143 shows the linear regression between them.

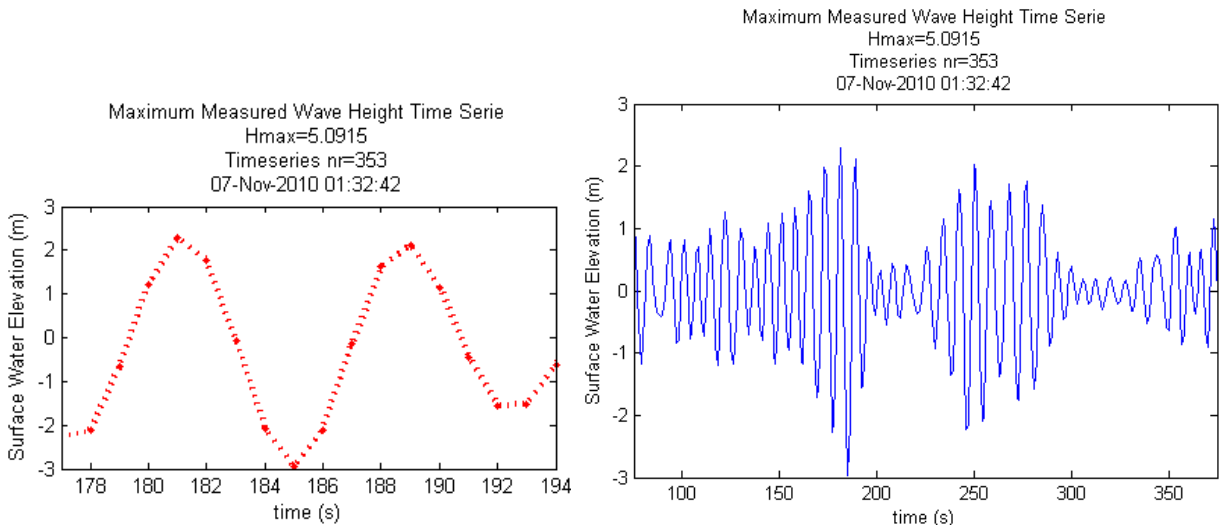

Figure 142: Maximum measured wave height based on zero down crossing Moin.

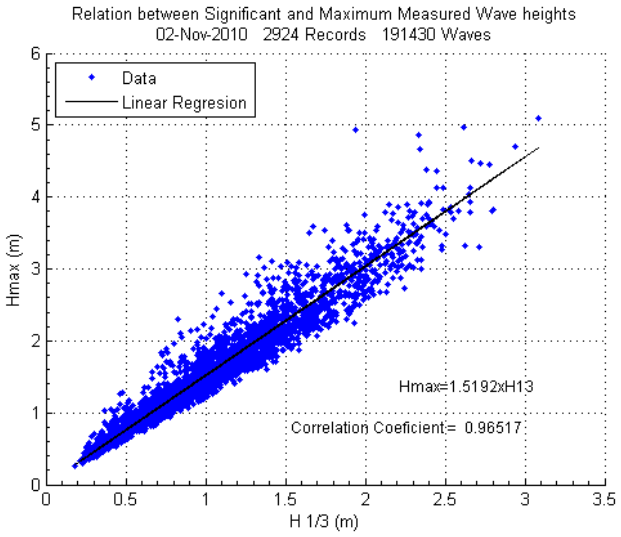

Figure 143: Relation between maximum and significant (H1/3) wave heights

Certain scatter is visible for the highest measured waves, such high waves don't follow the Rayleigh distribution and their appearance is supposed to have occurred due to transfer energy between individual waves.

The marginal individual wave heights and periods were then investigated. Figure 144 shows the occurrence probability and exceedance probability of individual waves. More individual waves higher than the predicted Rayleigh distribution are clearly seen in the occurrence probability curves. This is clearer when the measured waves are compared in the exceedance probability curve. Nevertheless the departure from the Rayleigh distribution is small.

The occurrence probability of individual periods shows a very narrow distribution. Such narrowness is odd given the low wave periods, and explains the reason why the significant and mean period is practically the same. Such narrow distribution has been previously supposed to occur for swell wave conditions and not for wind waves of with Ts =7.5 seconds.

The joint probability occurrence distribution for individual waves and periods shows even more clearly the narrowness on the occurrence of individual periods (defined by the ZDC method). The mode is found for $T/T_{mean}=1$ and the individual wave heights are distributed evenly around this mode, with small waves having a larger period distribution, but the higher waves, $H/H_{rms}>1$, are all clearly associated to wave periods equal to T_{mean}. This behavior was then investigated by means of the Fourier spectral analysis.

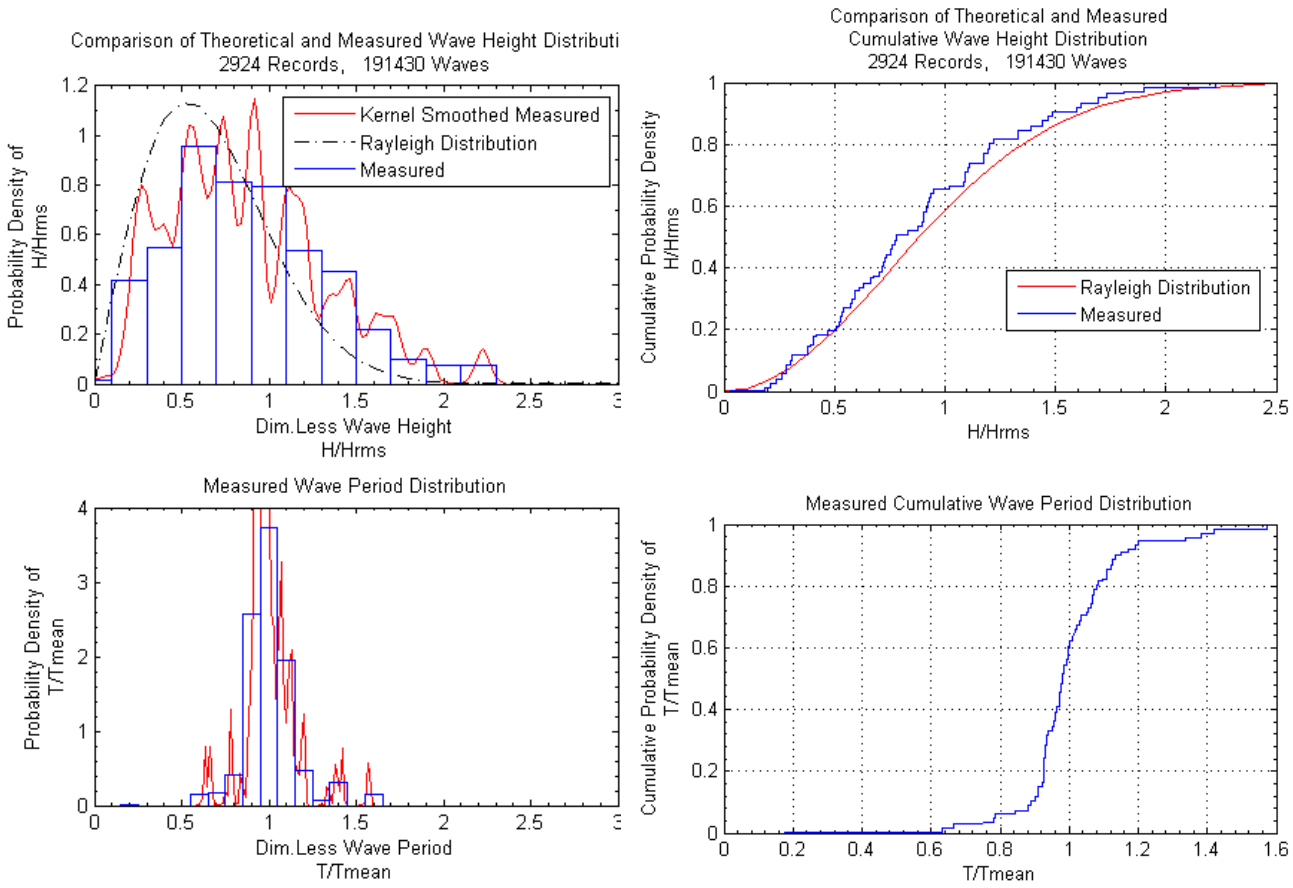

Figure 144: Measured wave height and wave period distribution Moin.

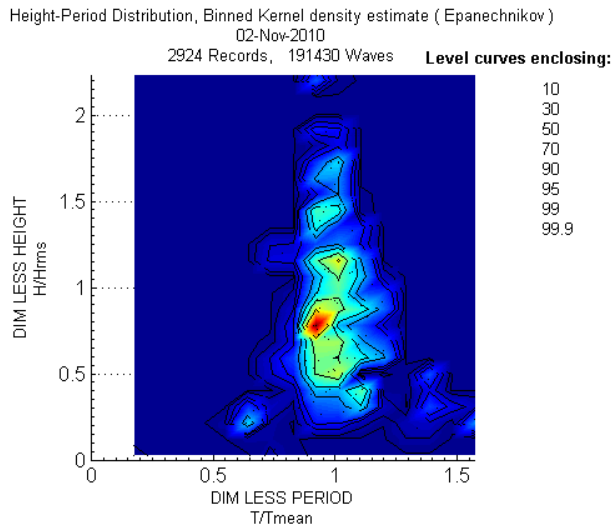

Figure 145: Measured joint distribution of individual waves Moin.

3.3.3 Spectral Analysis

For the measured waves it was found that using the zero down crossing method their individual period distribution was very narrow. A detailed spectral analysis was then carried out in order to assess the precise frequency distribution. Wave energy distributed with several frequencies can be found within one zero down crossing wave.

The temporal variation of the wave energy is shown in the spectrogram of the measured wave conditions show in figures 146 and 147. Most of the measured energy lies with the frequency bands of 0.075 and 0.16 Hz, 13.3 and 6.67 seconds. The for the wave measurements at 17 meters of water depth wave periods lower than 6 seconds cannot be measured accurately, which can explain why a cut off frequency is shown around these frequency, the amount of energy within these frequencies for the measured waves is low, the peak energy is found between 7.5 and 10 seconds. Nevertheless this cut off frequency could affect spectral characteristics such as the second, third or fourth moment, which depend on the spectral shape.

The most energetic wave conditions occurred during the 7th , then calm wave conditions are clearly visible between the 10th and 20th. From the 21st of November to the 6th of December several smaller storms were measured. In general when comparing the spectra with the long travelled swell conditions a more irregular spectra with multiple peaks is observed for this shorter period waves.

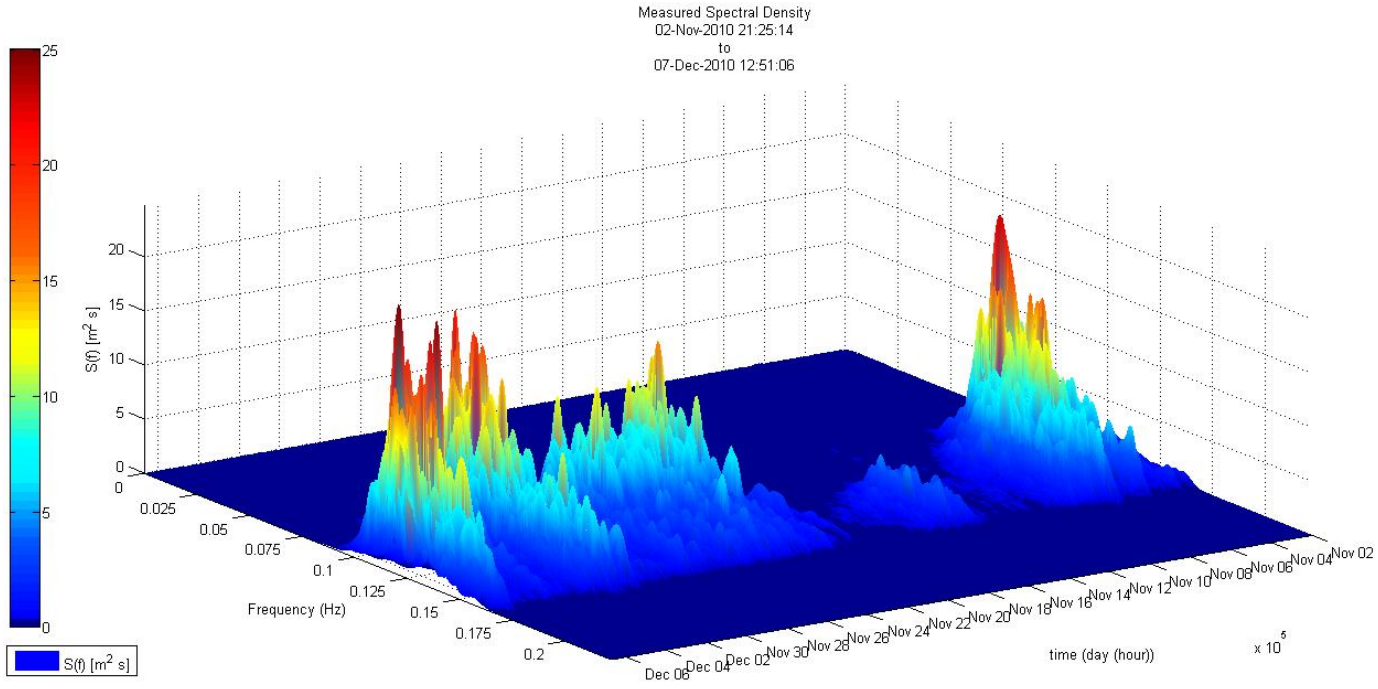

Figure 146: Temporal spectral variation Moin.

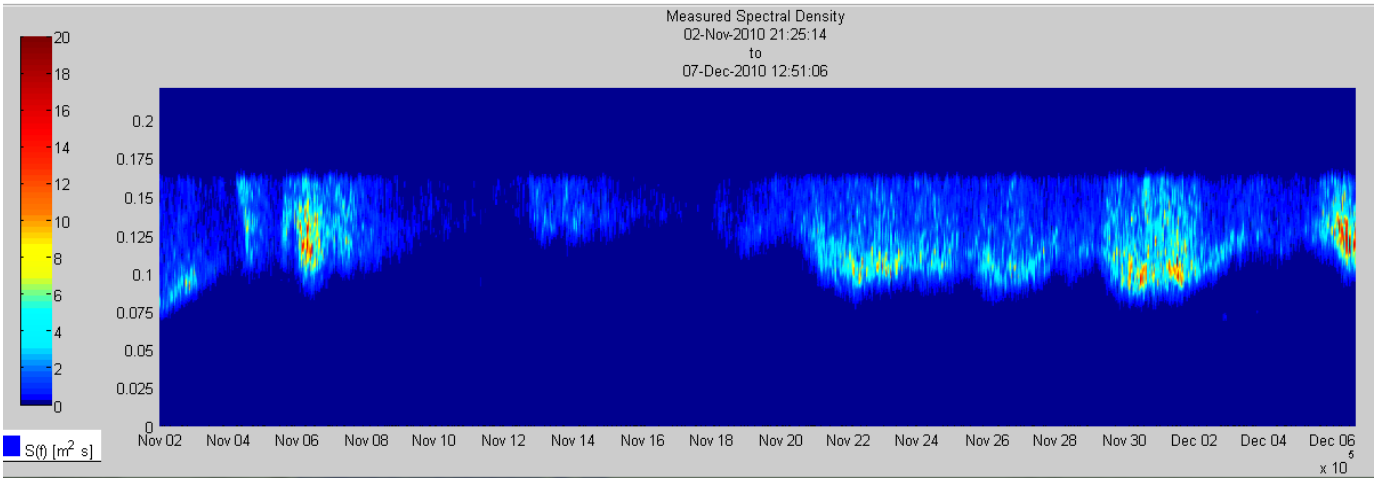

Figure 147: Temporal spectral variation Moin.

The temporal variation of the spectral significant wave height, H_{mo}, and the spectral periods compared with the ones obtained with the zero down crossing are shown in figure 148. The $H_{1/3}$ and H_{mo} are almost the same through out the whole measurements. This relation is also shown in table 14, where $H_{1/3}=0.973*H_{mo}$ with a standard deviation of 0.027.

Table 14: Ratios between Spectral and Zero Down Crossing Wave Characteristic Heights and Periods Moin

	$H_{1/3}/H_{mo}$	H_{rms}/H_{mo}	T_{mean}/T_{mo}	$T_p/T_{1/3}$	T_{mo-1}/T_p
Mean	0.973	0.701	1.004	1.049	1.060
Standard Deviation	0.027	0.010	0.028	0.093	0.099

The narrowness of the wave period distribution is again seen with the spectral periods, where all are very close to the peak spectral period, also seen in table 14. Between the 22nd of November and the 3rd of December the wave periods were slightly larger with peak spectral periods between 9 and 10 seconds associated with the more energetic wave conditions during these period.

The characteristics of the measured spectra were then analyzed through the peakdness, Qp, broadness and narrowness, ε and ν, regularity and spectral grouping, α and Ka parameters. The temporal variation of these parameters is shown in figure 149.

The measured spectral peakdness parameter, Qp, was high through out the whole measurementswith values between 3 and 6 for the most energetic wave conditions. During the calm conditions, particulary from the 14th to the 22nd of November Qp was very large with Qp around 8. These large values of Qp indicate that during the calm wave conditions a very sharp peaked spectra is found with associated JONSWAP peak enhancement parameter γ higher than 10.

The spectral bandwidth parameter ε shows a high dispersion through out the whole measurement with values between 0.25 and 0.6, and it does not show the spectral changes seen with the spectral peakdness parameter Qp. The narrowness parameter ν seem to be constant with a value of 0.2.

The other narrowness parameter a, also shows a constant value of 0.8 to 1, which means that the measured wave conditions are very regular. This is in accordance to the observed wave period distribution. This regularity parameter is larger than the one observed for the long travelled swell conditions.

The spectral wave groupiness parameter Ka receives high values almost through out the whole measurements particularly during the measured calm conditions. This is in accordance to the values given by the spectral peakdness parameter Qp. This high groupiness parameter is associated with narrow wave period distribution obtained with the zero down crossing method.

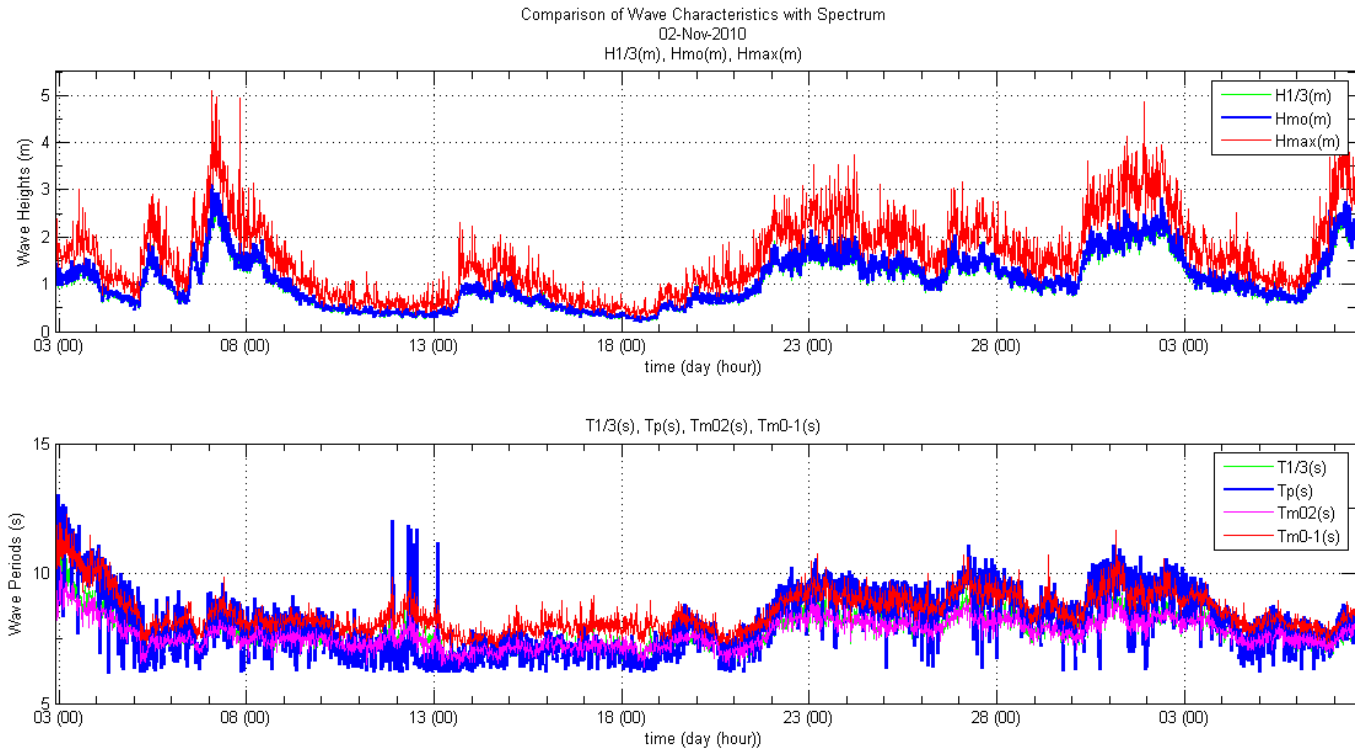

Figure 148: Temporal variation of wave spectral characteristics Moin.

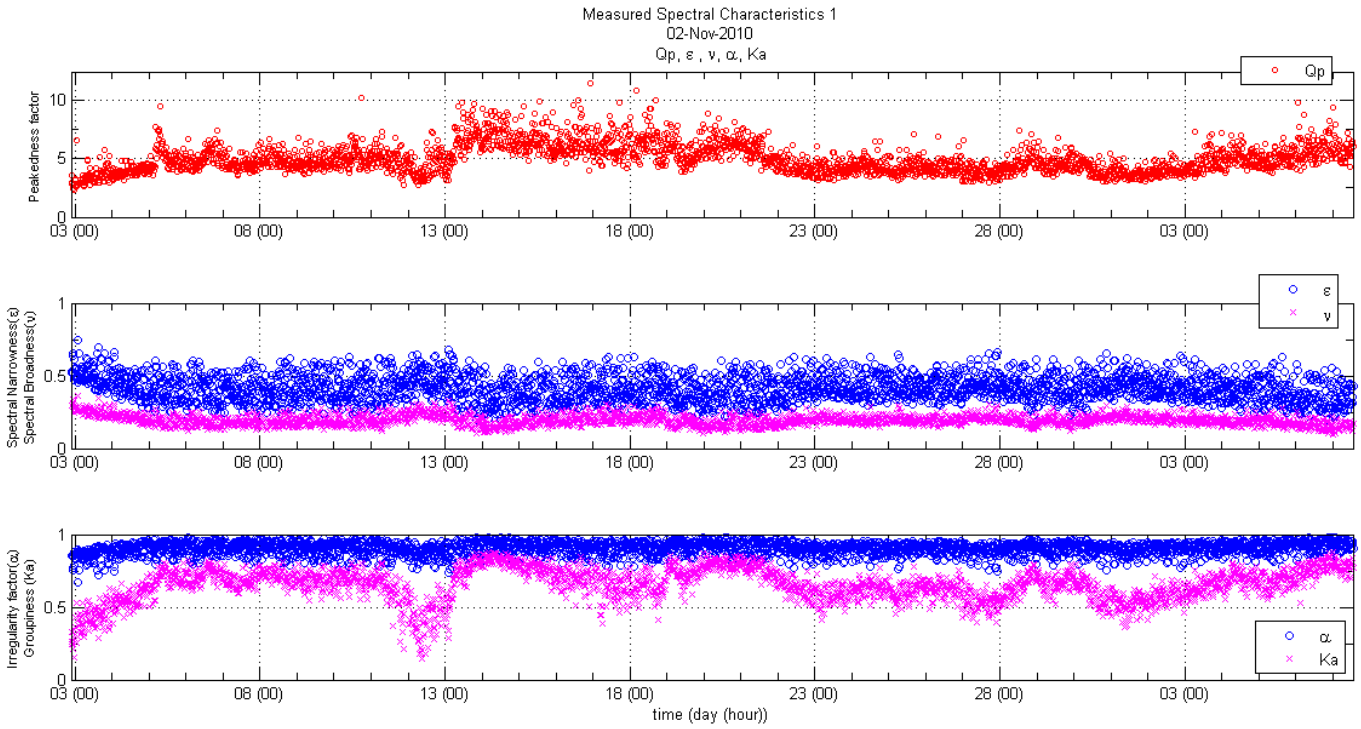

Figure 149: Temporal variation of wave spectral characteristics Moin.

The spectra of the highest wave conditions were analyzed in detail. The five highest measured spectra were plotted and compared with the JONSWAP spectrum. The most energetic wave conditions occurred during the storm of the 7th of November, and the 2nd of December. Figure 150 shows the two most energetic measured spectra. Multiple peaks are seen around the peak frequencies, these had peak frequencies between 0.12 and 0.13 Hz, 7.69 and 8.3 seconds.

The peak enhancement parameter g, from the JONSWAP parameter was obtained for the five highest spectra. Figure 151 shows the fitted JONSWAP spectra against the 3rd and 4th highest spectra. Three of these largest spectra had a γ of 5.3, the third 6.56 and the fifth 4.37. These values are in accordance to the values found for the peakdness parameter Qp.

These spectrums present a sharp decay towards the lower frequencies, and multiple peaks around the maximum measured frequencies.

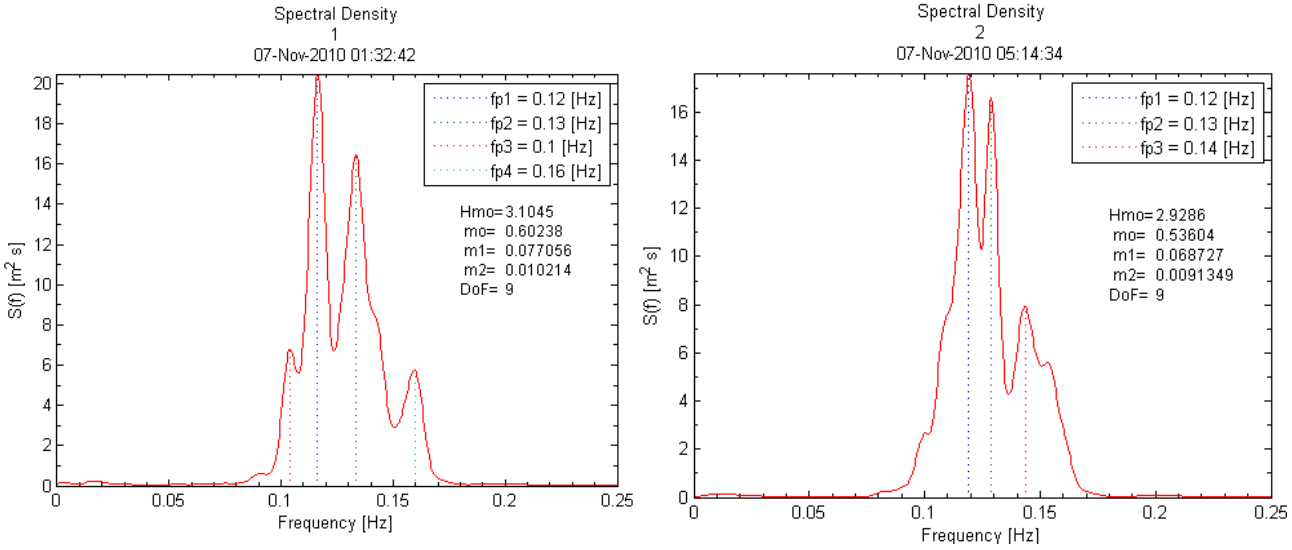

Figure 150: Spectra for most energetic wave time series Moin.

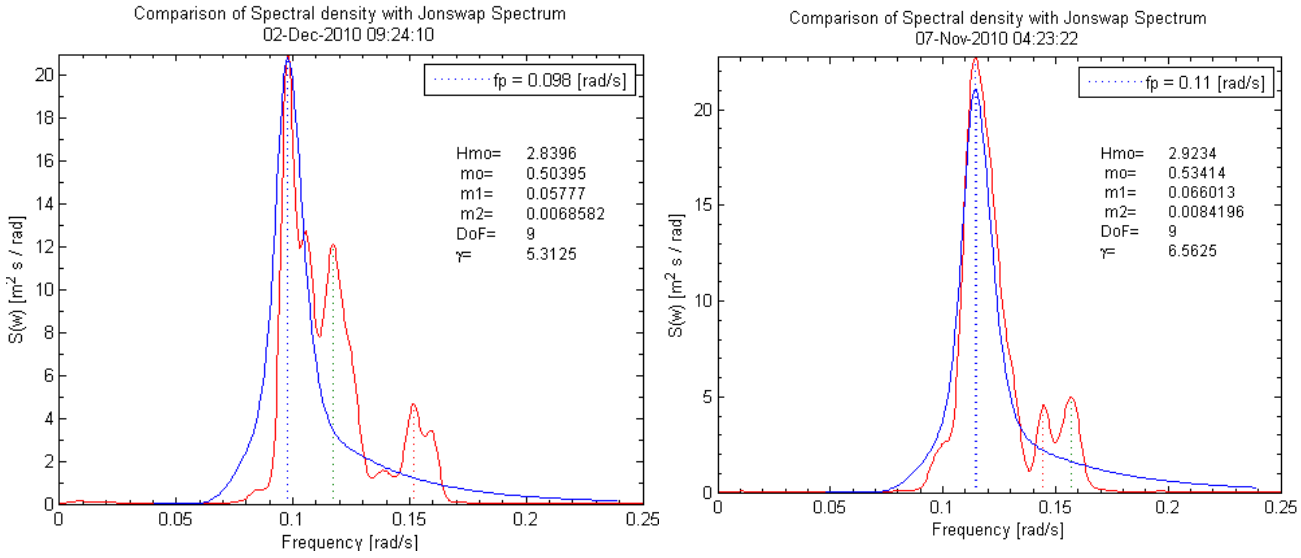

Figure 151: JONSWAP spectrum fit Moin.

3.3.4 Wave Grouping Analysis

The wave grouping characteristics of the measured waves in Moin were analyzed. The spectral parameters, Ka and Qp, showed waves with high groupiness characteristics. The correlation coefficient between individual waves was obtained for lag number of waves up to 4 for the 2924 records containing 191430 individual waves. The correlation coefficient between two successive waves, γHH(1), obtained was 0.47, with values of up to 0.8. These value is considered to be high, Rye (1974,1982), Arhan and Ezrady (1978) and Su et al, (1982) had reported values with an average of 0.3 for wind waves.

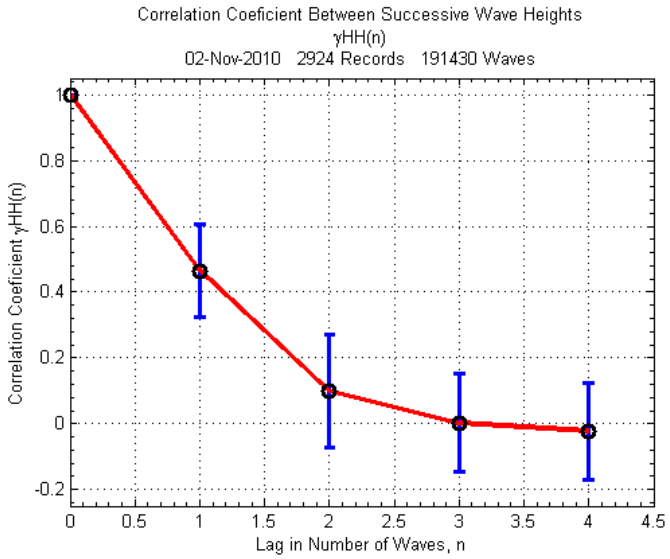

Figure 152: Correlation coefficient between successive wave heights.

The run lengths for the wave height threshold values of H*>Hmean and H*>H1/3 were obtained and the occurrence probability and exceedance probability was then compared to the predicted values by Kimura's theory. The obtained run lengths are lower than the predicted values, which are clearly seen in the exceedance probability. The mean run length for H*>Hmean and H*>H1/3 were obtained for the 2924 wave records, the temporal variation of these values are shown in figure 154, with the measured peak spectral period and correlation coefficient between two individual waves. Higher mean run lengths are observed during the calm conditions that occurred between the 13th and the 21st of November, with measured mean run lengths H*>Hmean, higher of 5 consecutive waves. These higher values during this period are in accordance with the observed higher spectral peakdness parameter, Qp, and spectral groupiness parameter Ka.

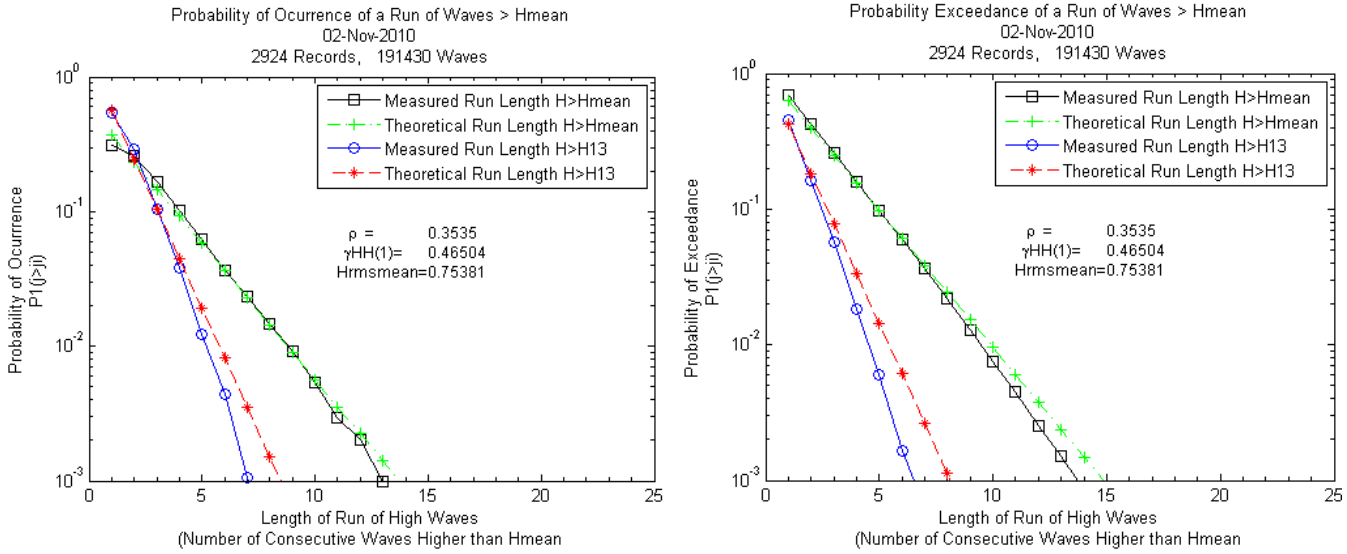

Figure 153: Occurrence and Exceedance Probability of a Run of Waves H>H*.

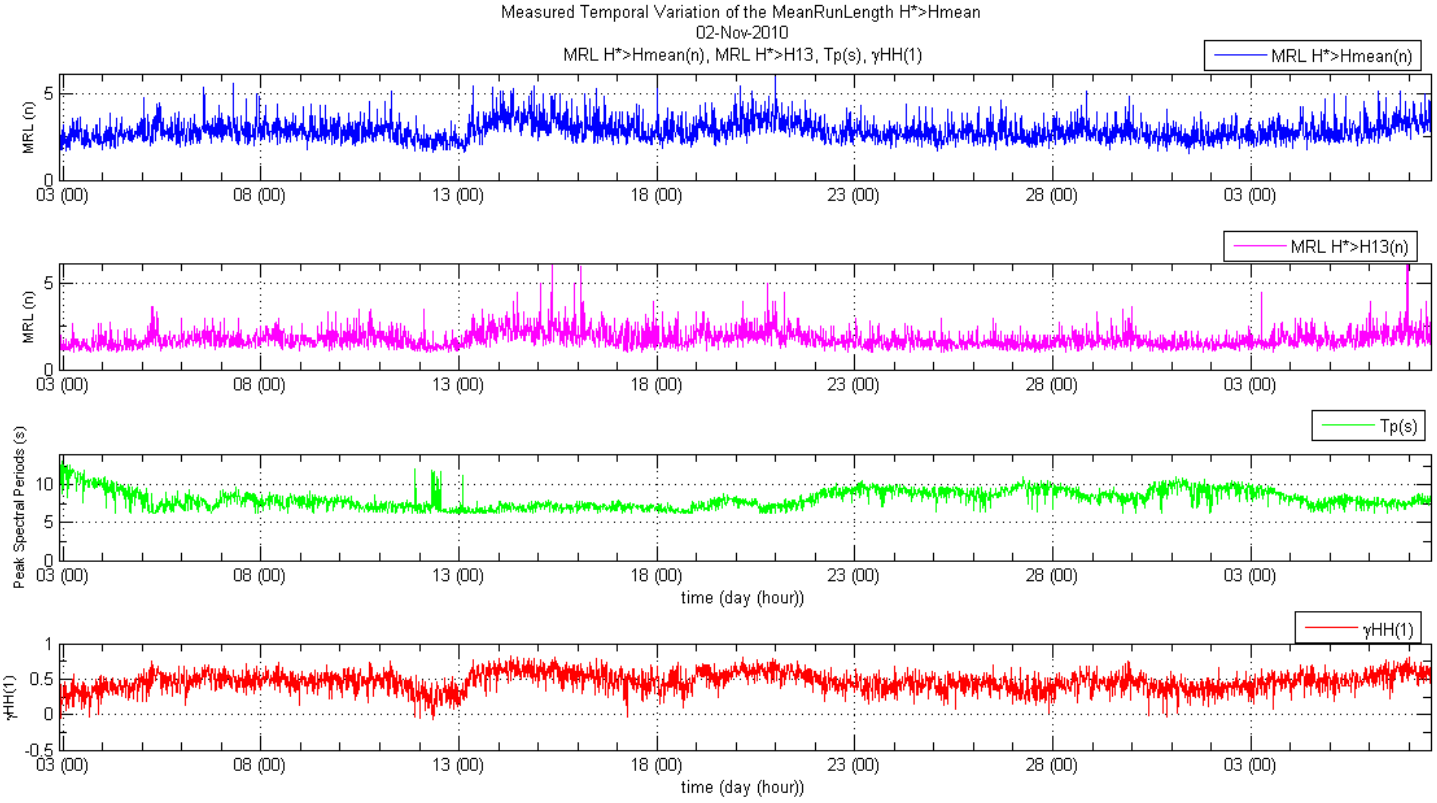

Figure 154: Temporal Variation of the mean run length H>H_{mean} and H>Hs wave heights for Hurricane Wilma.

3.3.5 Long Wave Analysis

The long waves were analyzed using the low pass filter on the 2924 wave records. The cutoff low frequency for the filter used was set at the highest measured period obtained with the zero down crossing method. A spectral analysis was then carried out on the filtered wave records, obtaining the significant long wave height and peak spectral periods. Figure 155 shows the most energetic long period wave spectra measured with the filtered wave signal, with a significant wave height, Hmolong of 0.141 meters and a peak spectral period of 227 seconds.

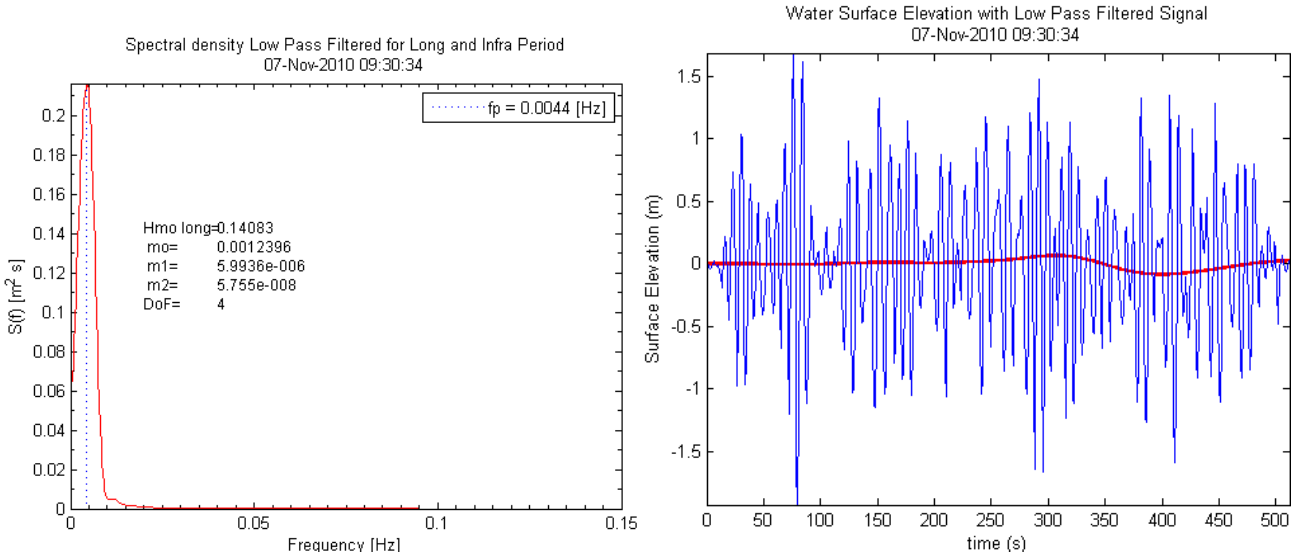

Figure 155: Long wave spectra Moin.

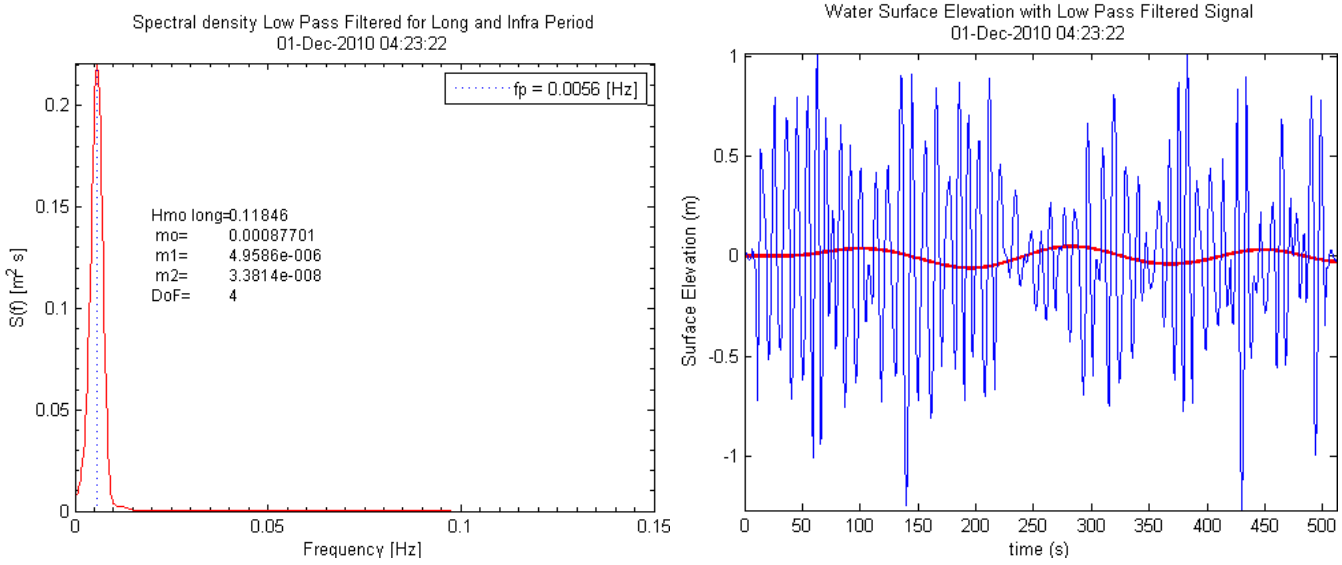

Figure 156: Filtered long wave signal Moin.

The obtained long wave spectra were then compared with the whole spectra for the highest wave records. Figure 157 shows the comparison for the most energetic wave record.

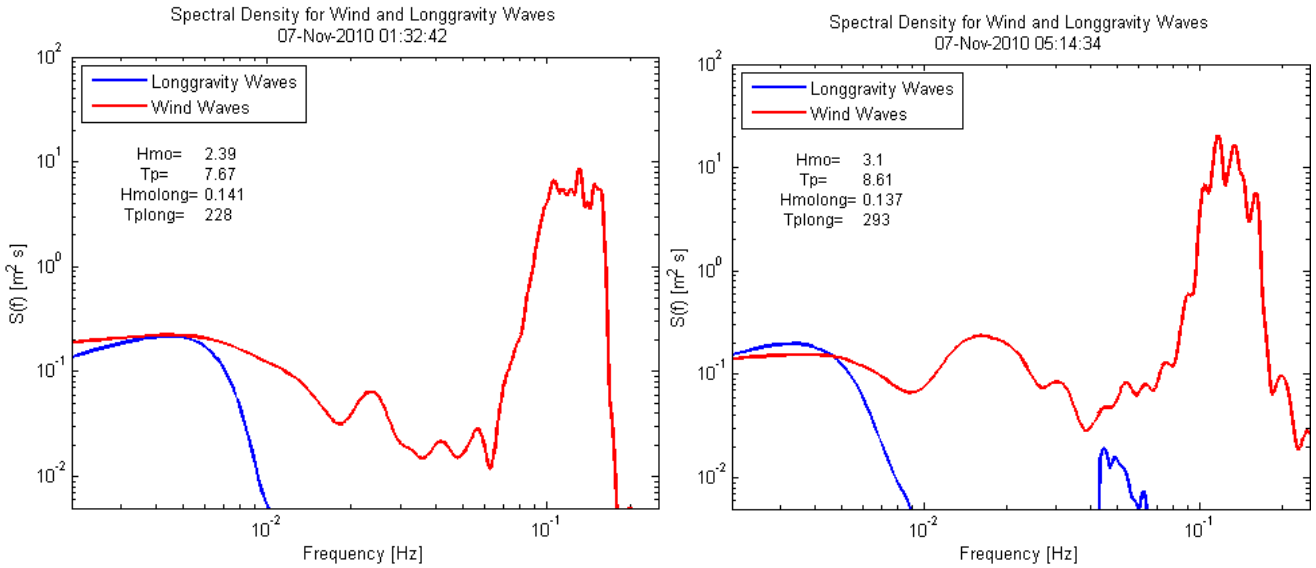

Figure 157: Long and wind wave spectra Moin.

The temporal variation of the long wave height and period are shown in figure 158 with the significant wave height. Good agreement is seen between the observed gravity wave height and the long wave height, however no correlation was observed for the long wave period. The long wave period seems to have clear defined mean at 190 seconds, however large dispersion is seen, the standard deviation is 112. The most energetic long wave spectra showed peak periods between 294 and 178 seconds.

This long wave period is of sum importance when calculating harbor resonance problems like the one than the port of Moin suffers. However the energy content found at 17 meters of water depth of the long waves is considered low, representing in average only 2% of the total wave height. Nevertheless for the highest condition it represented up to 6%.

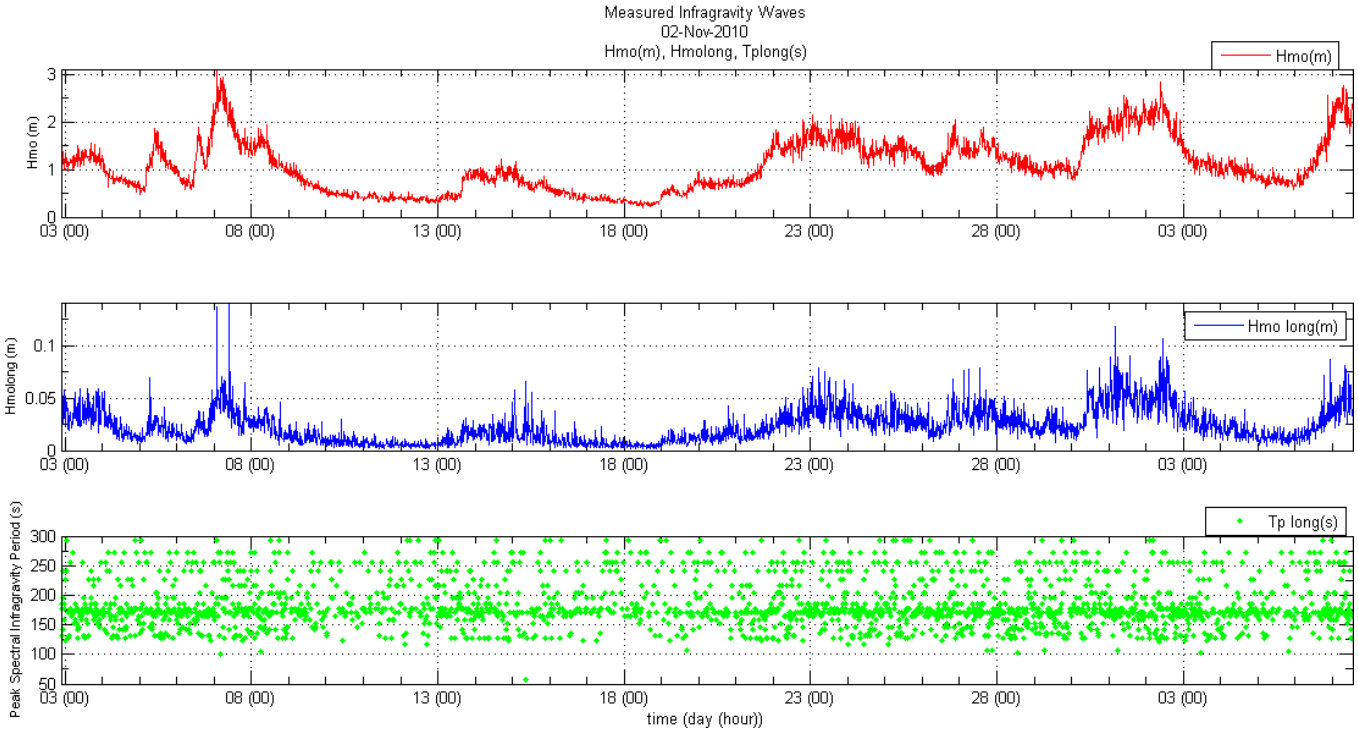

Figure 158: Temporal variation of the long wave height Moin.

3.3.6 Analysis using the Hilbert Huang Spectrum

The HHT (ω,t) spectra and its marginal H(ω) were obtained for the most energetic wave conditions measured at Moin. Figure 159 shows an isometric view of the frequency-energy content through the most energetic time series defined as the one with the highest H_{mo}. Three main energetic peaks were obtained, all within a narrower frequency band, with a clear peak at 0.125 Hz, 8 seconds.

The higher wave grouping, is clearly visible in the HHT spectra, figures 160 to 161, with groups of shown as higher energy areas in the HHT spectra. In all cases the grouping was associated with the same narrower instantaneous frequency distribution.

This narrow instantaneous frequency distribution is also visible in the HHT marginal distribution, figure 162. A shaper higher peak is obtained with the with the H(ω) spectra, in most cases, than with the FFT spectra. This is a very different result than in the other wave measurement sites, where typically a wider frequency distribution was obtained. For all the analyzed spectra a very clear peak at 0.125 Hz was obtained. The low frequency energy obtained was also lower than in the measurements carried out at the different sites, nevertheless it is always higher than the one obtained through the FFT spectra.

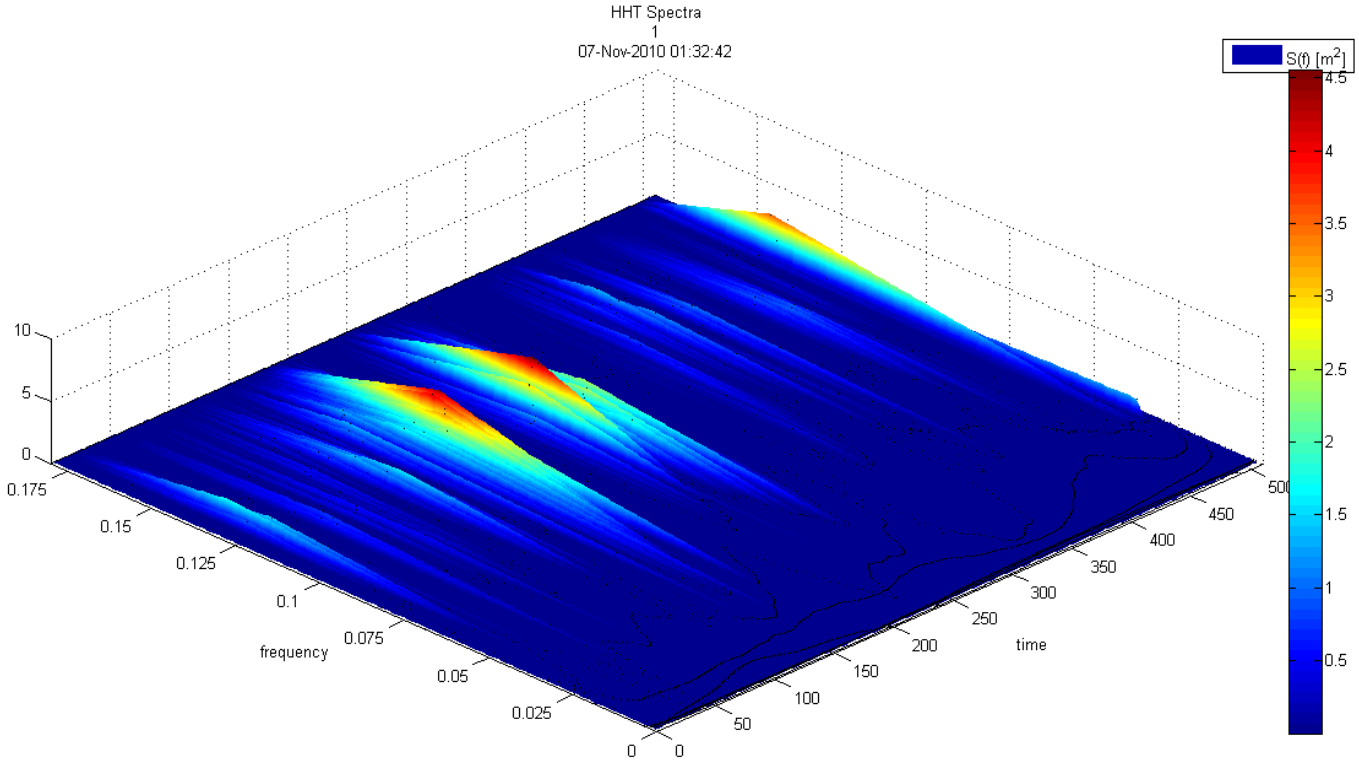

Figure 159: HHT Spectrum for most energetic time series Moin.

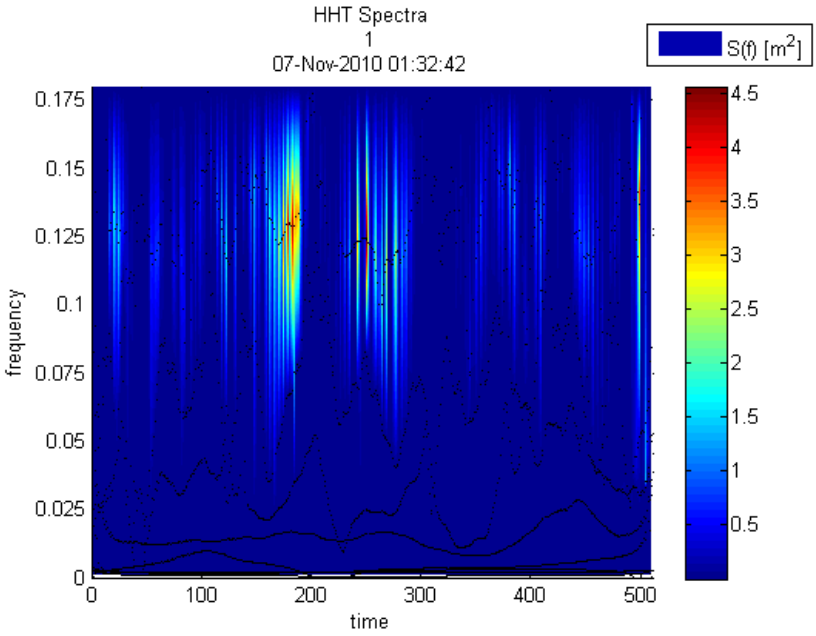

Figure 160: HHT Spectrum for most energetic time series Moin.

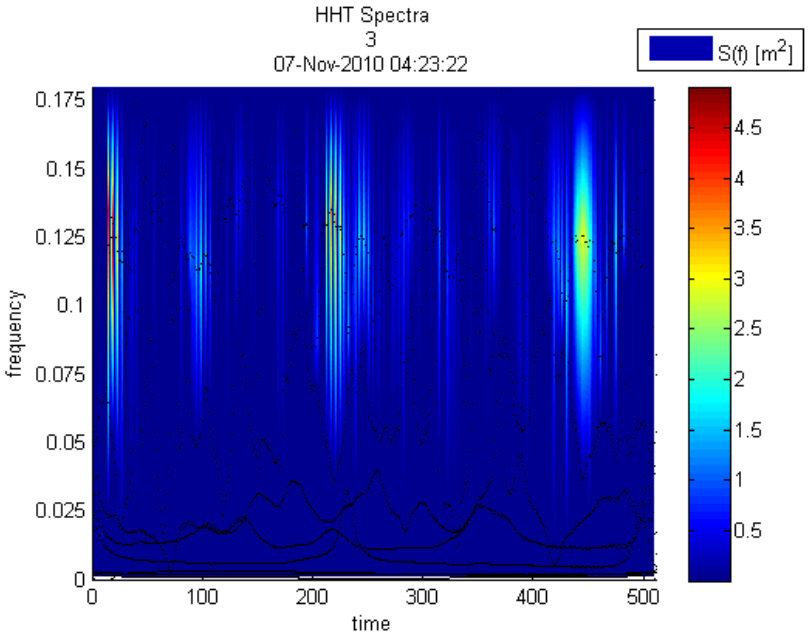

Figure 161: HHT Spectrum for Moin.

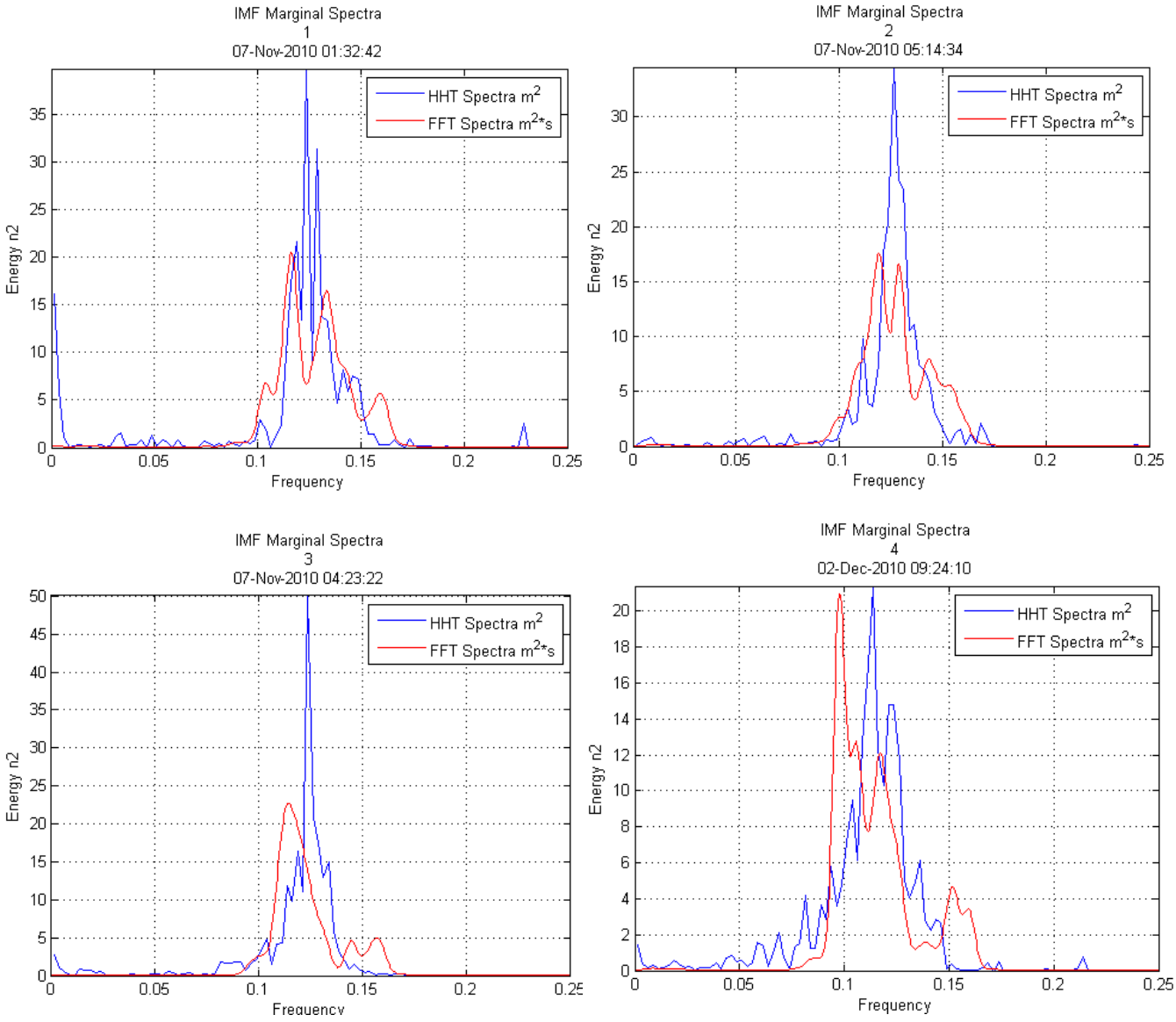

Figure 162: HHT Marginal Spectrum for most energetic time series Moin.

3.4 Wave Measurements at Puerto Morales Cancun (Hurricane Wilma)

Hurricane waves in coastal waters are very different from the previously measured waves. High winds and pressure changes produce large set ups and oscillations which are clearly not related to the long wave process under investigation. Nevertheless these waves show other long wave processes which are worthwhile studying.

Wave measurements carried out near Cancun, in Puerto Morales, at the southeast of Mexico were analyzed using the developed software WES. These wave measurements were carried out by Rodolfo Silva, of the Universidad Autonoma de Mexico, from the August to November 2005, the analyzed data corresponds to the period when the zone was affected by Hurricane Wilma, from the 17th to the 26th of October. The eye of Hurricane Wilma passed over the measurement zone the 21st of October, giving the opportunity to measure the wave characteristics of such an extreme event. Understanding in detail the wave characteristics of such an extreme event is of sum importance in order to design and plan coastal infrastructure in zones affected by cyclones. Forecasting tools should take into account the particular spectral characteristics that these events present.

Hurricane Wilma has been one of the strongest recorded Hurricanes with several records. The 19th of October 2005, when it was 520 kilometers from Quintana Roo, Mexico, it had sustained winds of 280km/h with the lowest recorded pressure of Atlantic Hurricanes 882 mb. When the hurricane passed over the measurement site it had sustained winds of 220 km/h with gusts of 270 km/h, it was a category 5 hurricane in the Saffir-Simpson scale[36]. The wave measurements include the swell waves approaching the site while the hurricane was in the ocean, later the waves within the generation zone, and finally the period after the hurricane has passed the site. The hurricane passing over the south-eastern part of Mexico is shown in figure 163, the size of the hurricane, affecting the northern Caribbean see is clear.

Figure 163: Hurricane Wilma over measurement location. www.hurricane-facts.com

[36] Silva R.C., Mendoza E.B, Escalante E.M, "Oleaje inducido por el huracán Wilma en Puerto Morelos Quintana Roo, México", Ingenieria hidráulica en México, vol.XXIV, pp.93-109, abril-junio de 2009.

Hurricane Wilma caused severe damage in the northeastern Yucatan Peninsula, including Cancun, widespread damage in southern Florida and flooding in Cuba. Twenty two deaths were attributed directly to Wilma[37]. The waves from Hurricane Wilma produced coastal damage, including severe erosion in Cancun

3.4.1 Location of Wave Measurements

The wave measurements carried by Silva were done in front of Puerto Morales, Quintana Roo, Mexico. This is located in the Yucatan Peninsula, 35 kilometers south of Cancun, in a zone known as the Mayan Riviera. Figure 164 shows the location of the wave gage. The measurements were carried out at a mean water depth of 20.7 meters. The tides at the location are small with mixed tide with predominance of a semi diurnal tide.

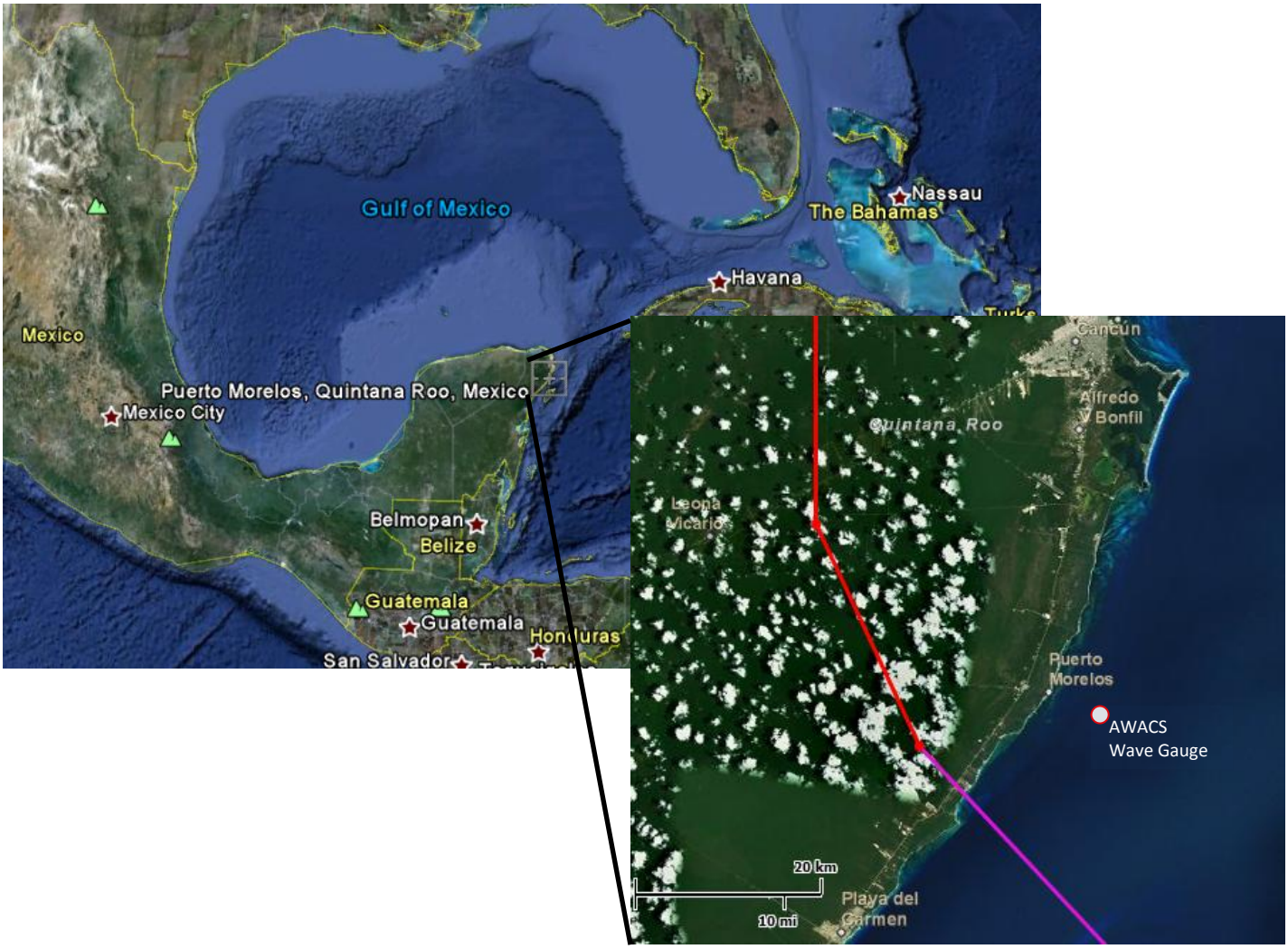

Figure 164: Wave measurement location Puerto Morales Mexico.

[37] Huricane History NOAA, http://www.nhc.noaa.gov/HAW2/english/history.shtml#wilma.

3.4.2 Description of Wave Gauge Equipment

The wave gage used was an autonomous acoustic wave and current profiler (AWAC), of 1 MHz from NORTEK. The equipment registers the free water surface and orbital velocities using 4 different acoustic beams, it also measures temperature and pressure and water currents at different depths. The wave gage was setup to register 2048 seconds every two hours at a sampling frequency of 2 Hz. The analyzed data in this report corresponds only to the free water surface measured without consideration of the directional properties of the wave field.

3.4.3 Analysis of Wave Sources, General Comparison with Measured Waves

The measured wave conditions, from the 17th to the 26th of October 2005 were affected by Hurricane Wilma. Hurricane Wilma is the most intense in the Atlantic basin, and was the thirteenth hurricane of the 2005 season. It formed in the Caribbean Sea near Jamaica the 15th of October as a tropical depression; it became hurricane the 18th of October. The storm travelled northwest and reached the Yucatan Peninsula between the 20th and 21st of October. The complete path of the storm is shown in figure 165.

Figure 165: Path of Hurricane Wilma NOAA.

The north Atlantic Hurricane Model of NOAA, based on the model Wavewatch III indicates that the waves when impacting the coast were above 15 meters, figure 166. This is the significant wave height. Using Mitch´s wave breaking criteria we would should have a breaking water depth for this waves as $h_b = 2*H_s$, this means that the

waves would be breaking at the measuring location, since 2*Hs=32 meters! Even though the waves measured indicate that they were breaking, they were in intermediate waters.

The measured period covers the full extent of the effect of Hurricane Wilma and a detail observation into the long wave energy, grouping and spectra provides invaluable information to help in the understanding of this extreme storms.

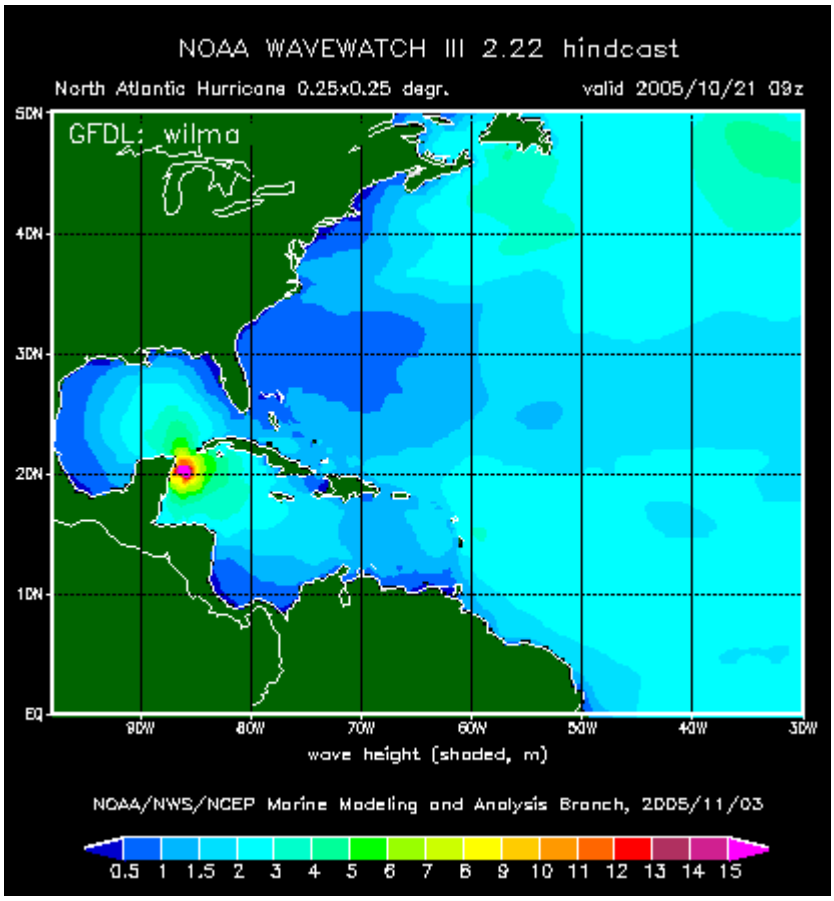

Figure 166: Hind casted wave heights for Hurricane Wilma NOAA.

3.4.4 Statistics Based on Zero-Down Crossing

The basic static analysis based on the zero down crossing method was done for the whole wave measurement period. The temporal variation of the characteristic wave heights and wave periods obtained through the zero down crossing method are shown in figure 167. Hurricane Wilma passed over the measurement site during the night of the 21st, however its effects are visible starting the 19th with a sharp increase in the significant wave height. The wave periods were relatively long as the hurricane approached the site, as swell waves from the Hurricane as it was over the Caribbean reached the site. When the Hurricane stroked there was a dramatic shift in the wave periods, the high winds at the site produced short period waves. The large maximum period measured is most probably associated with the surge produced by the hurricane and or breaking waves at the site.

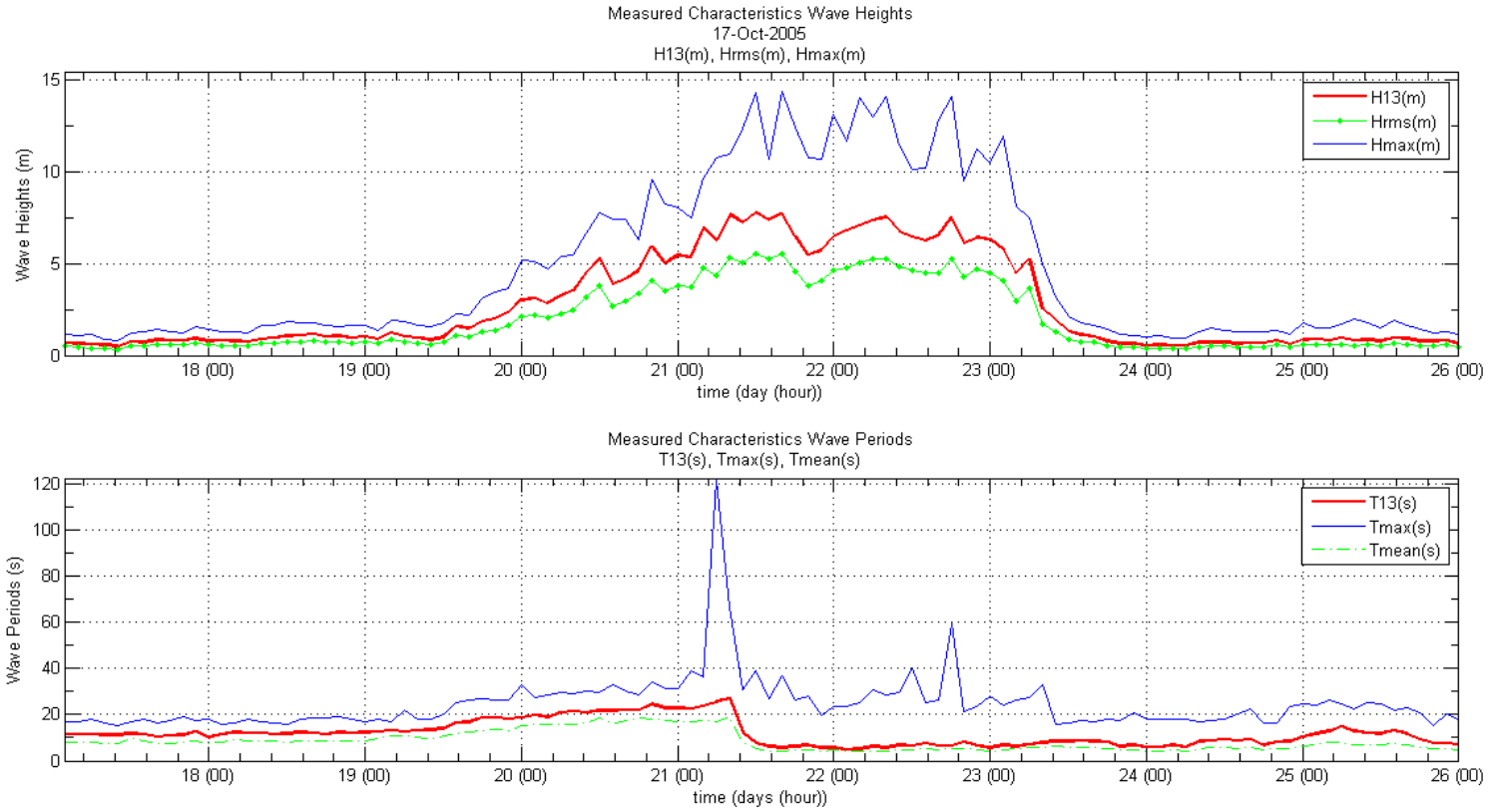

Figure 167: Temporal Variation of Wave statistical Characteristics based on zero down crossing for Hurricane Wilma.

Figure 168 shows the more clearly the observed temporal variation of the significant period. From the 17th to the 19th waves with periods of 12 seconds affected the site, then a dramatic increase in the significant wave period, T13 is observed, reaching values of up to 26 seconds, with a significant height of more than 7 meters and maximum wave heights of more than 11 meters. Then when the winds affect the site the significant wave period

drops to 7 seconds, however the wave heights continuo to increase. The high waves are measured during two days.

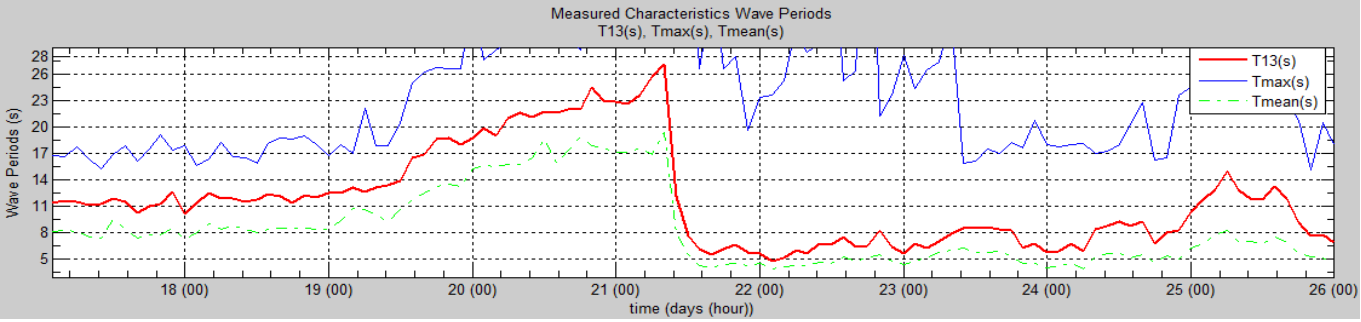

Figure 168: Temporal Variation of Wave statistical Characteristics based on zero down crossing for Hurricane Wilma.

Table 15: Ratios between Characteristic wave heights and period based on ZDC Hurricane Wilma

	$H_{max}/H_{1/3}$	$H_{1/10}/H_{1/3}$	$H_{1/3}/H_{mean}$	$H_{1/3}/H_{rms}$	$T_{max}/T_{1/3}$	$T_{1/10}/T_{1/3}$	$T_{1/3}/T_{mean}$
Mean	1.725	1.264	1.655	1.432	2.423	1.095	1.424
Standard Deviation	0.183	0.054	0.070	0.027	1.384	0.129	0.143

The ratios between the different characteristic wave heights were then obtained and are shown in table 15. The wave heights exhibit ratios that similar to the ones predicted by the Rayleigh distribution, $H_{1/3}=1.6H_{mean}$ and $H_{1/10}=1.27H_{1/3}$. The wave period ratios show larger dispersion in the measured periods.

The relation between the significant and maximum wave height was then investigated in detail. The maximum measured individual wave is shown in figure 171. The height of this individual wave is 14.38 meters, but the period of the individual wave is a little more than 2 seconds, this is physically impossible. This measured wave occurred the 21st at 16:00:00, around 4 hours before the eye of the Hurricane passed over the measurement site. The time series where this wave was measured was then investigated. Large waves with a very high crest and low troughs are visible in the record. The measured significant period for the time series was 7 seconds. The skewness of the measurements was then investigated. The temporal variation of the skewness through out the measurements is shown in figure 154. A positive skewness, above 1, is associated with the most energetic conditions, however it is followed by low skewness, such a behavior in the skewness of the other wave measurements was not observed.

Table 16: Measured Skewness and Kurtosis Hurricane Wilma

	Skewness	Kurtosis
Mean	0.09	3.11
Standard Deviation	0.37	0.65

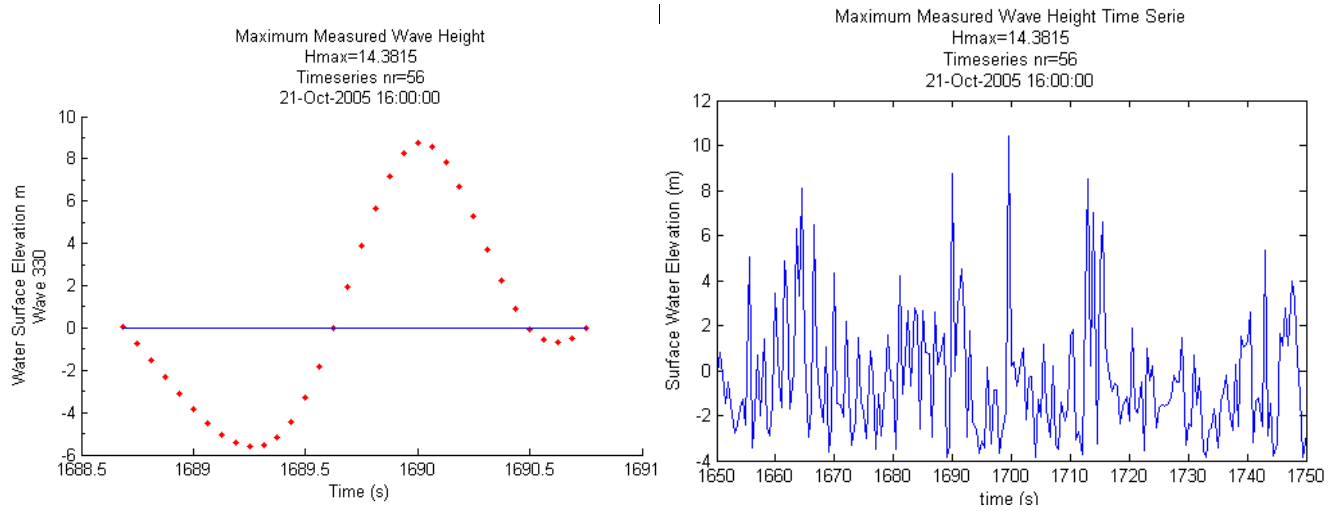

Figure 169: Maximum measured wave height based on zero down crossing for Hurricane Wilma.

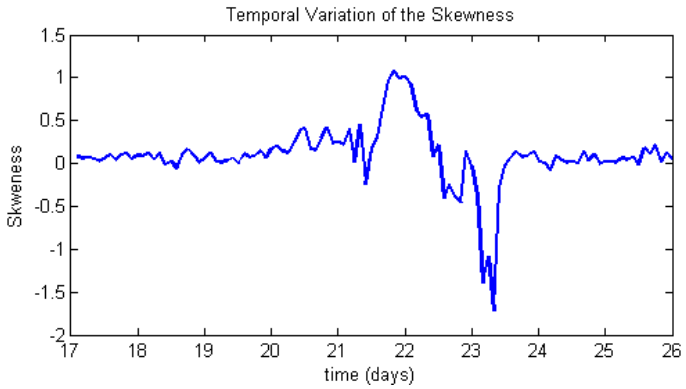

Figure 170: Temporal variation of the skewness from each time series for Hurricane Wilma.

The relation between the significant and maximum measured wave height was then investigated to determine whether the measured maximum waves corresponded to spurious or real data. A linear regression between the maximum measured waves in each record with its given maximum measured wave for the record is shown in figure 171. A good correlation is seen with a correlation coefficient of 0.986, though certain dispersion is seen in the higher waves. The regression shows maximum wave heights of almost 15 meters, given the fact that the measurements were taken at 20 meters of water depth, clearly this waves correspond to breaking conditions. Larger waves could have existed further offshore but most certainly they would have broken before reaching the site. These breaking waves explain the long periods, and high positive skewness observed. Furthermore the dispersion in the tail of the regression could be explained by the broken waves as well. However the short 2 second period is still hard to explain due to the breaking of waves. The low skewness in the signal after the 23rd is also hard to explain. This negative skewness means that the troughs of the waves were larger than the crests, a possible explanation are high currents which interacted with the waves because of the hurricane.

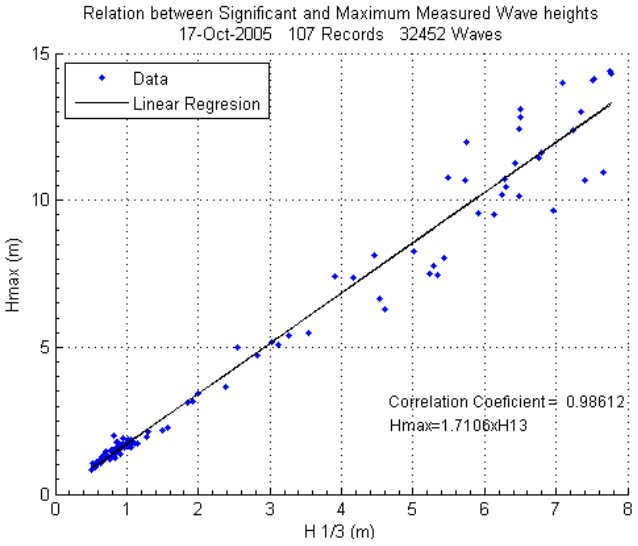

Figure 171: Relation between maximum and significant (H1/3) wave heights.

The marginal distributions for the individual wave heights and periods defined by the zero down crossing were obtained for the 107 records, containing 32452 waves. The wave heights fitted a Rayleigh distribution with a small departure. This departure could be due that the Rayleigh distribution was obtained for narrow spectra, and as it will be shown below, during the period of direct influence of Hurricane Wilma very broad spectra was measured. However the fit is surprisingly good, and it was checked by revising the temporal variation of the ratio $H_{1/3}/H_{mean}$. The Rayleigh distribution predicts a value 1.6, and no major departure was observed even the days of direct influence of the Hurricane.

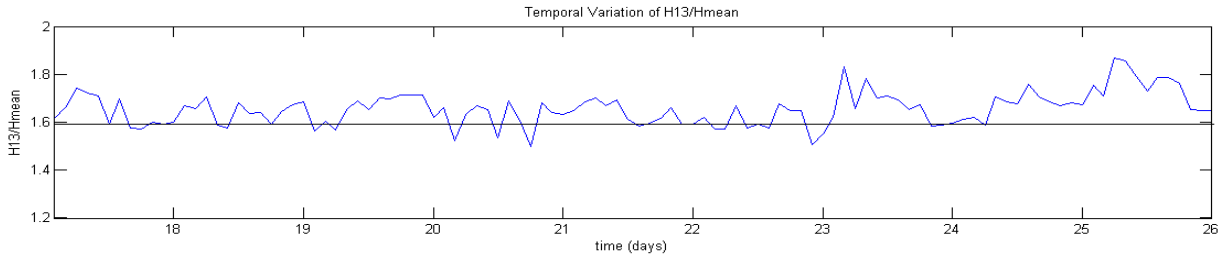

Figure 172: Temporal Variation of $H_{1/3}/H_{mean}$ ratio for Hurricane Wilma.

The wave period marginal distribution shows a large spread in the values, a clear mode is not visible, and waves with periods of up 4 times the mean period are present. These high spread in the period distribution is associated with the high winds and the wave generation process.

The joint individual wave height period distribution, figure 174, shows that the smaller waves are all associated with wave heights below Hrms. The larger waves, H>2*Hrms have wave periods from 1 to 3 times Tmean, which means that the large measured waves are all associated with longer periods than the mean period. The maximum measured wave height, with the 2 second period is most probably a spurious breaking wave.

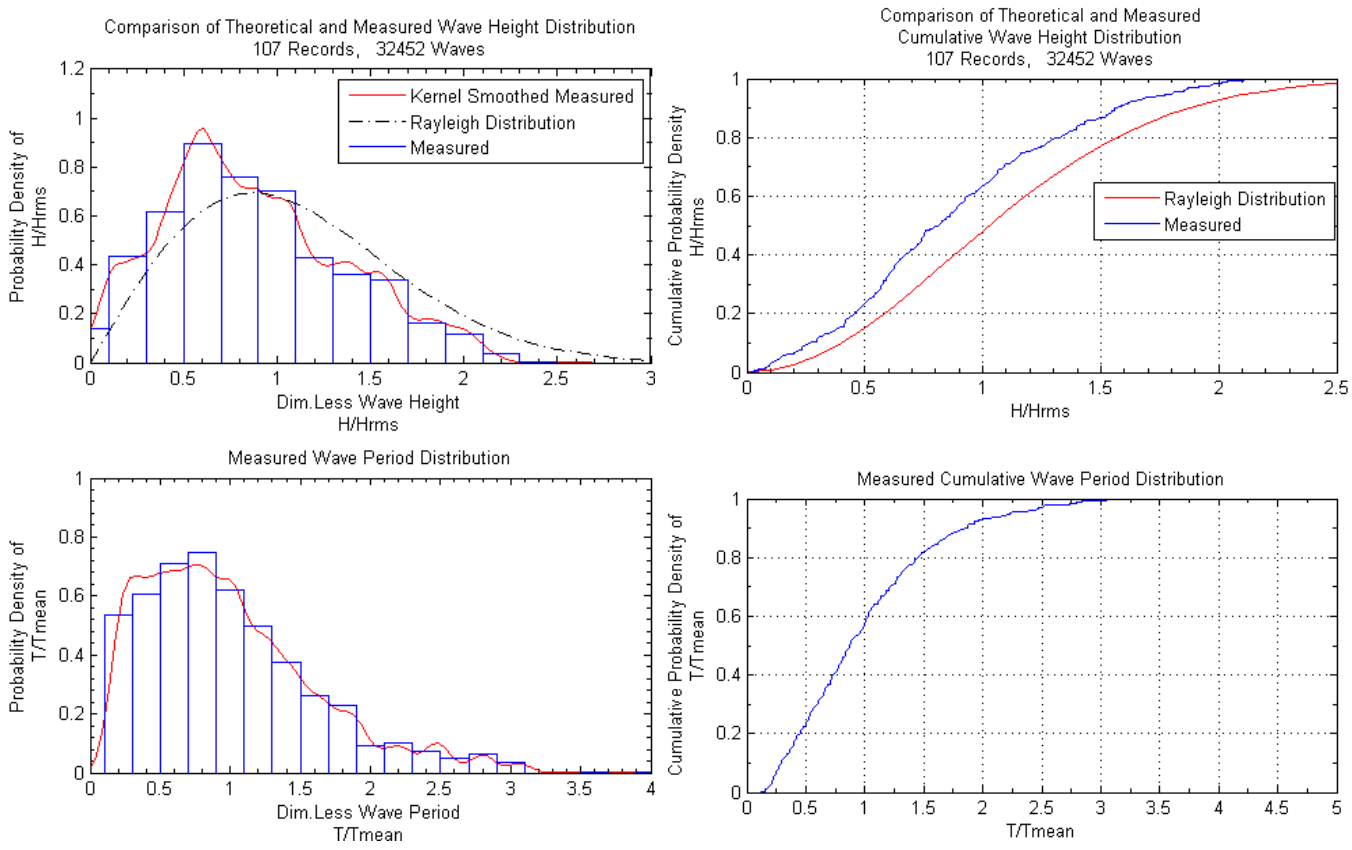

Figure 173: Measured wave height and wave period occurrence and exceedance distribution for Hurricane Wilma.

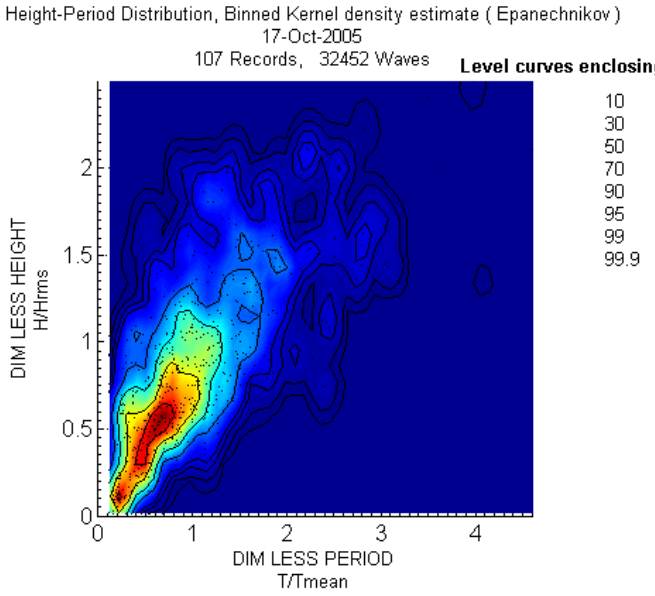

Figure 174: Measured joint distribution of individual waves for Hurricane Wilma.

3.4.5 Spectral Analysis

A detail spectral analysis was carried out on the 107 wave records taken at Puerto Morales. The temporal variation through out the wave measurements is shown in spectrogram in figure 175. The spectrogram shows the measured energy content at the site due to the waves. Because of the scale only the energy due to Hurricane Wilma is visible in figure 175, during the days is it affected the site, from the 21st to the 23rd of October. Spectral peaks above 400 m^2s are visible and the frequency distribution the energy goes from very low frequencies, less than 0.025 (40 seconds) to high frequencies of 0.2 (5 seconds). During the 22nd a broad spectrums are visible.

Figure 176 shows more clearly the energy frequency distribution during the wave measurements. The energy scale was cut off at 30m^2s in order to get more resolution on the periods before and after the passing of the Hurricane. It can be appreciated clearly how from the start of the measurements, the 17th of October the wave peak frequency starts to decrease from 0.075 Hz, 13.3 seconds, until it reaches a value of 0.04 Hz, 25 seconds, the 21st of October, almost 20 hours before the eye of the Hurricane passes over the site. From the 21st to the 23rd of October the direct influence of the Hurricane winds produced affected the site. The spectra turns almost into a white noise spectrum with important wave energy found from the high frequencies all the way int the lowest frequency where peak energy is found. During the first hours the 23rd the energy decreases and lower energy waves with peak periods of 15 seconds affect the site.

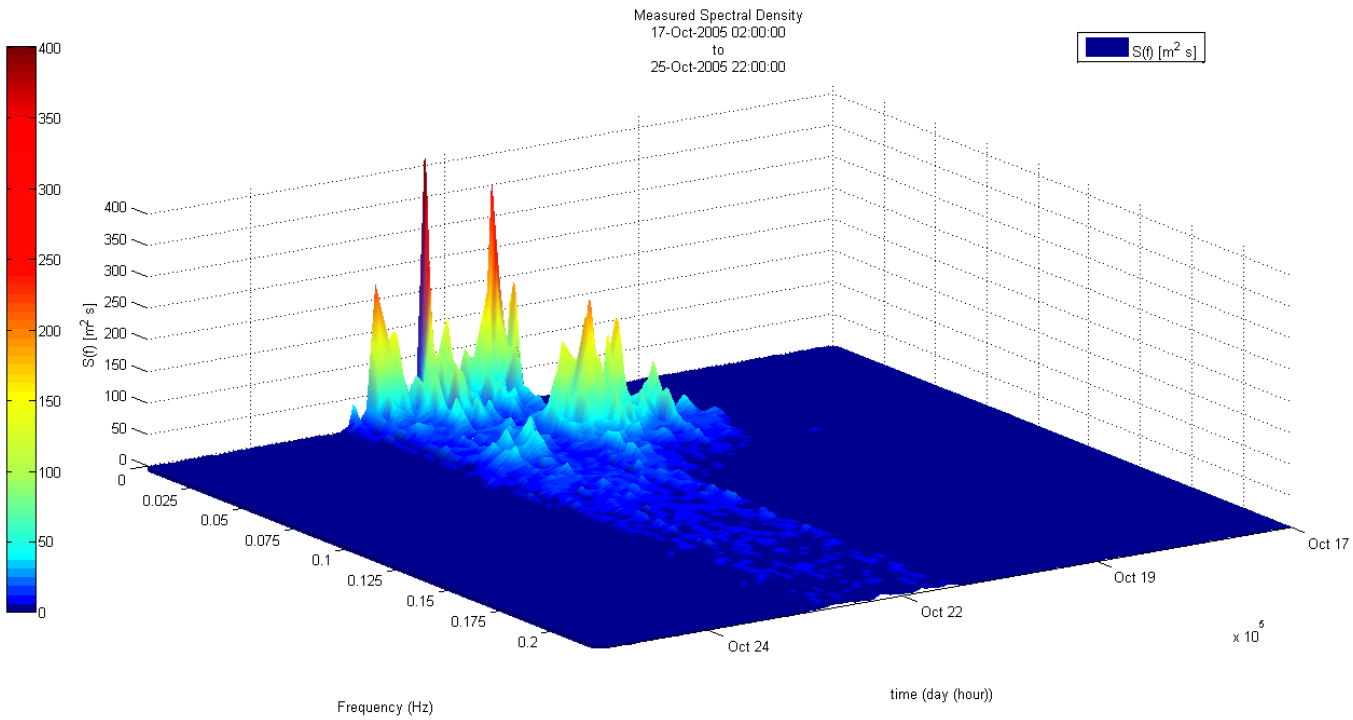

Figure 175: Temporal spectral variation for Hurricane Wilma.

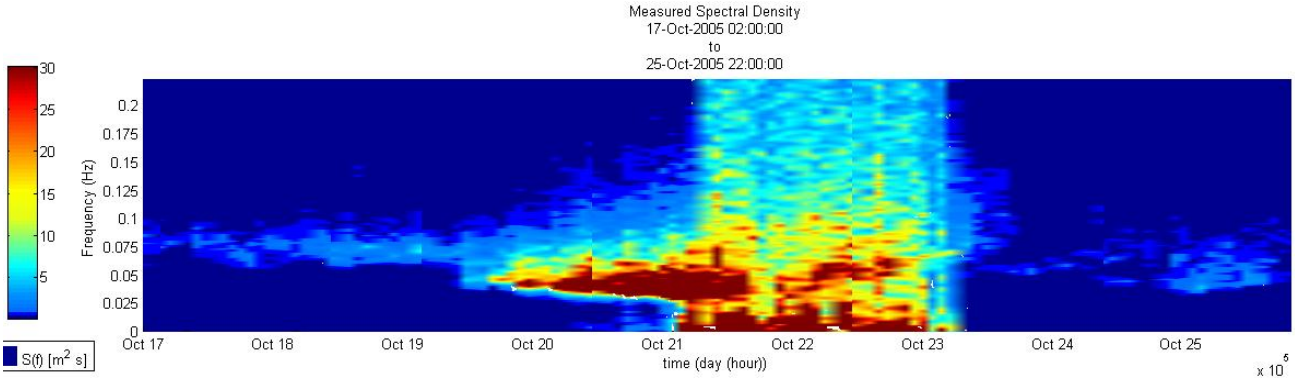

Figure 176: Temporal spectral variation for Hurricane Wilma.

The very low frequency peaks during the passing of the Hurricane are investigated in more detail further ahead in the long wave chapter analysis. The surge and changes in the sea level due to the atmospheric pressure changes could have produced large low frequency oscillations. As well wave breaking is expected to have played a major role. Given the wave heights, with values of Hmo above 7.5 meters, and maximum waves between 10 and 14 meters, some breaking of the largest waves would be expected at 20 meters water depth since H/h=0.7 according to Miche criteria. Furthermore, the high winds that occurred during the passing of the Hurricane, with wind speeds, measured in Cancun, of up to 35 m/s, until the anemometer stop recording the 21st of October at 20:00, should have produced a very irregular sea state, with lots of white capping and breaking of the waves.

Figure 177 shows the temporal variation of the ratio between the spectral significant wave height, Hmo and the ZDC significant wave height H 1/3. The peak spectral period T_p, the energetic period T_{m0-1}, the mean period T_{m02} and the significant period, Ts obtained from the zero down crossing method and wave heights temporal variation are shown in figure 178. During the direct influence of Hurricane Wilma, from the 21st to the 23rd, the peak spectral period jumped to several occasions to values of up to 455 seconds. Figure 179 shows the temporal variation of the highest peak period, the longest peak period and the shortest peak period. These jumps of such low frequencies mean that the most energetic waves were long waves during these particular time series. The shorter peak period during 21st to 23rd has values between 12 and 24 seconds, which represent the gravity waves as a secondary peak of energy.

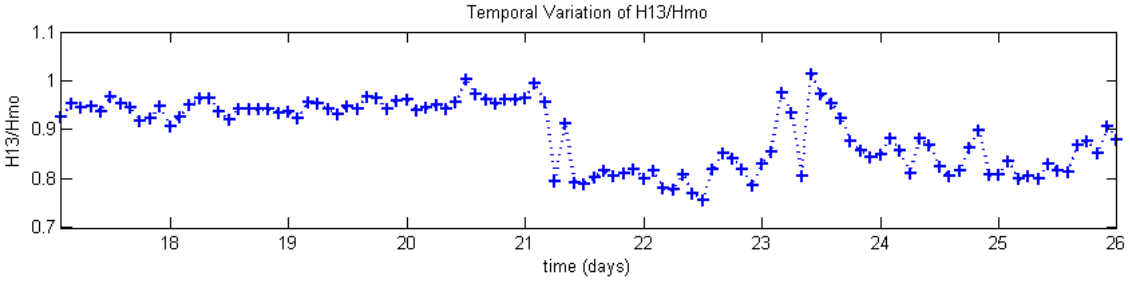

Figure 177: Temporal variation of wave spectral characteristics for Hurricane Wilma.

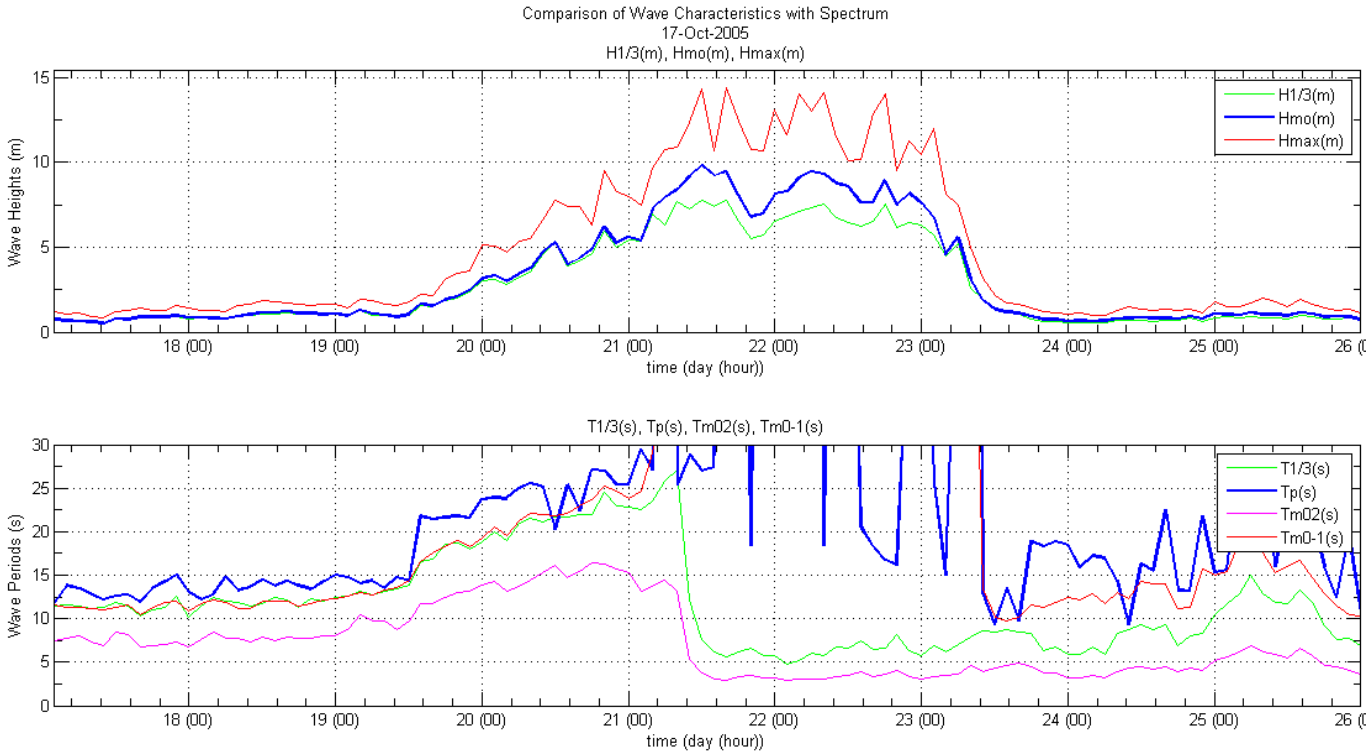

Figure 178: Temporal variation of wave spectral characteristics for Hurricane Wilma.

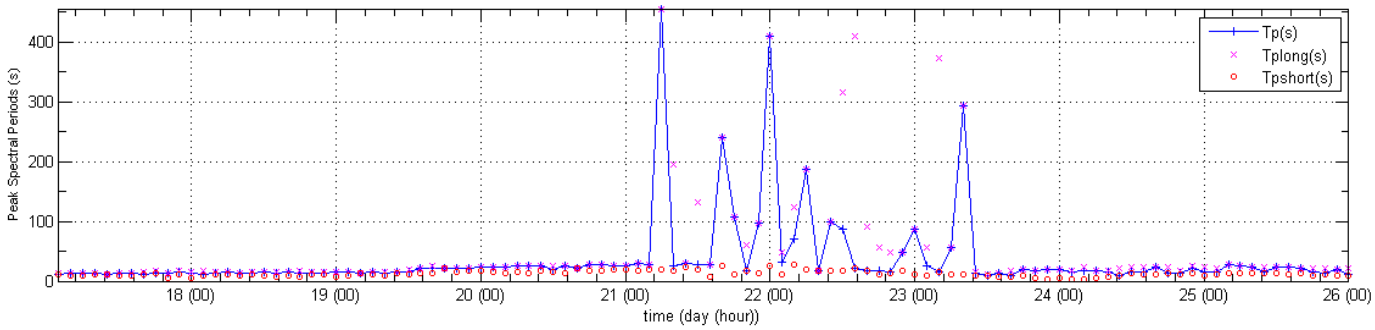

Figure 179: Temporal variation of wave spectral peak periods for Hurricane Wilma.

The ratios H_{13}/H_{mo} and the T_p and the $T_{1/3}$ where investigated. It is clear that T_p differs greatly from the significant wave perid defined by the zero crossing. The zero down crossing will miss long period oscillations when analysis the signal. The large spread in the wave period distribution, and long period waves affect the ratios significantly. Even the ratio between $H_{1/3}$ and H_{mo} is affected by the fact that the ZDC method misses the long wave energy and it is clear that H_{mo} is much larger during the days that that the long wave energy was present from the 21st to the

23rd, because the spectral density is taking into account these long period oscillations in the signal from wave breaking.

Table 17: Ratios between Wave Spectral Parameters and Zero Down Crossing Wave Parameters Hurricane Wilma

	$H_{1/3}/H_{mo}$	H_{rms}/H_{mo}	T_{mean}/T_{mo}	$T_p/T_{1/3}$	T_{mo-1}/T_p
Mean	0.891	0.623	1.212	4.325	1.297
Standard Deviation	0.067	0.048	0.142	9.416	1.490

The temporal variations of the spectral parameters, describing the spectra, are shown in figure 180. The spectral peachiness parameter Q_p, shows low values between 2 and 4, with a mean of 3 before the direct impact of Hurricane Wilma, this would correspond to a JONSWAP spectrum with a peak enhancement parameter g of 3.3, and close to the Pierson Moskowitz spectrum. From the 21st to the 23rd during the direct influence of Hurricane Wilma, this parameter is less than 1, which corresponds to a white noise spectrum, these irregular spectrum are seen for the rest of the measurements. Clearly the JONSWAP spectra is not a good fit during this conditions and its use is not recommended.

The spectral bandwidth parameter, ε takes the value of 1 through out the measurements, which should represent white noise as well. The narrowness parameter n takes the value of 0.75, and above 1 after the 21st . these two parameters have been shown not to depict accurately spectral changes. The parameter a, which should show the narrowness of the spectra has values between 0.2 to almost 0.5, a sharp change is seen when the Hurricane affects the site. The spectral groupiness parameter Ka, has values above 0.5 before the Hurricane and below during the influence of the Hurricane.

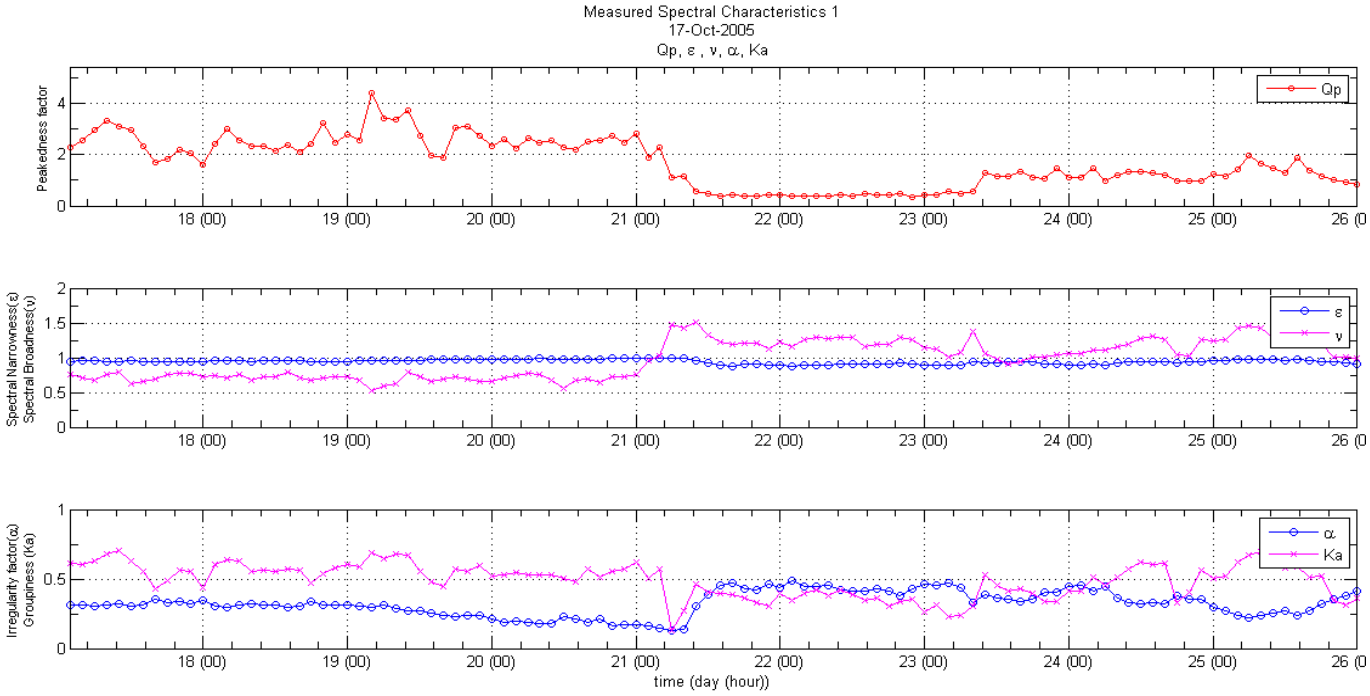

Figure 180: Temporal variation of wave spectral characteristics for Hurricane Wilma.

The spectra during the highest wave conditions were examined in detail. The five highest spectra were examined in detail. In all of these spectra long wave energy was found to be the component with the highest energy. Figure 181 shows the spectra of the most energetic wave condition measured, the peak energy was 0.037 Hz, 27 seconds. Wave energy is spread through out almost all measured wave frequencies in important levels, with energy levels of more than 40m^{2}s in the low frequency range of 0.0076 Hz, 131 seconds. The presence of these low frequency waves is also shown in figure 182, where a wave with almost 800 seconds of period, and height above 4 meters is clearly seen in the time series. Such waves have the potential to flood large areas, reaching deep inside land. Their potential to erode and stir the sediment generating important currents in the coastal zone is very high.

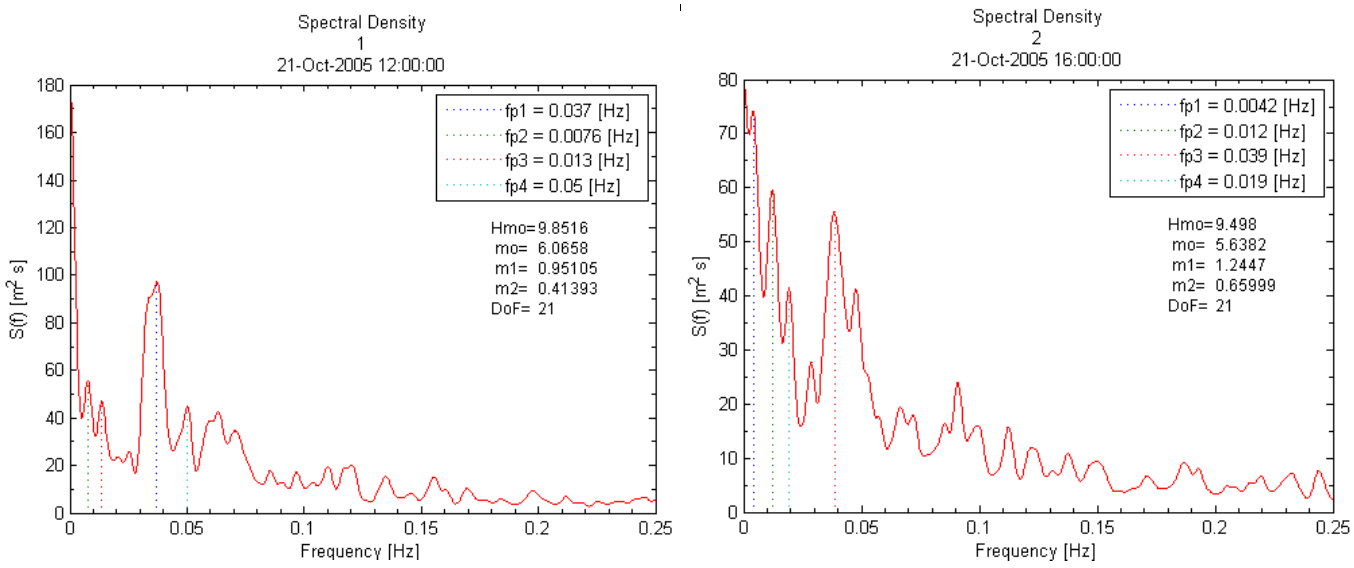

Figure 181: Spectra for most energetic wave time series Hurricane Wilma.

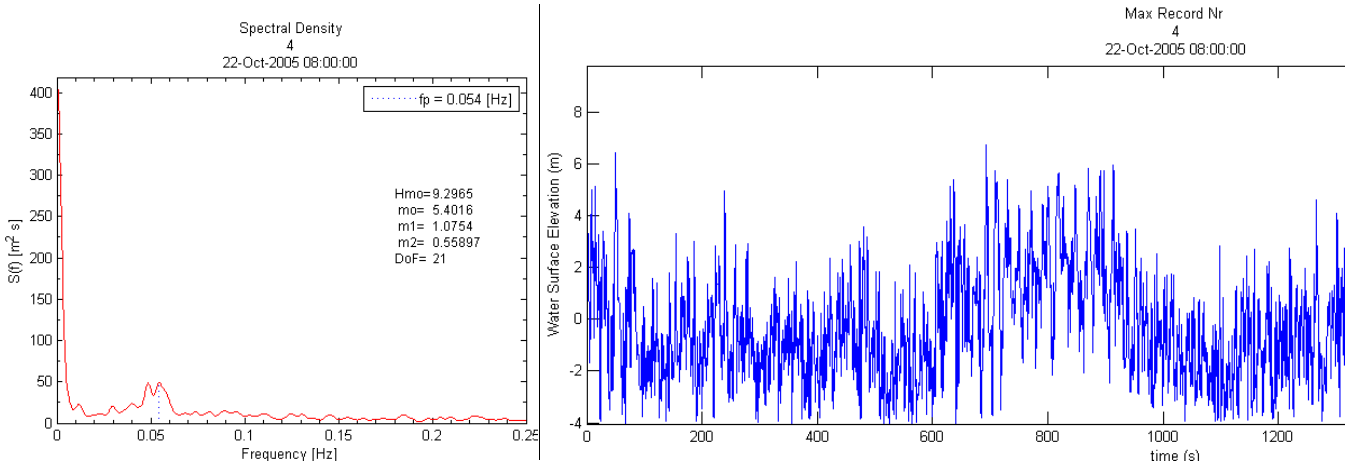

Figure 182: Spectra with wave time series Hurricane Wilma.

3.4.6 Wave Grouping Analysis

The wave grouping characteristics of the wave measurements were investigated. The correlation coefficient between successive wave heights for lag numbers of 1 to 4 were obtained for the 107 records containing 32452 waves, figure 183. Correlation between two successive waves is low with a mean of 0.228. For lag number greater than 1 the correlation is practically null. The temporal variation coefficient of two successive waves, $\gamma HH(1)$, is shown in figure 185. $\gamma HH(1)$ took values between 0.25 and 0.5 before the 21st of October, then there after the values were under 0.2. these means that there was some low groupiness before Hurricane Wilma arrived, however after the Hurricane passed over the site the irregular sea condition showed no groupiness at all.

The occurrence and exceedance probability of runs of number of waves with $H^*>H_{mean}$ and $H^*>H_{13}$ shows good agreement with the theory, and a low probability of large runs in the data. The temporal variation of mean run of waves exceeding $H_{1/3}$ and H_{mean} is shown in figure 185. In average no more than two waves exceeding H_{mean} occurred after the 21st and the number of consecutive waves above $H_{1/3}$ was less than two. Hence there was practically no clear defined wave groups of waves with heights above the two threshold values defined.

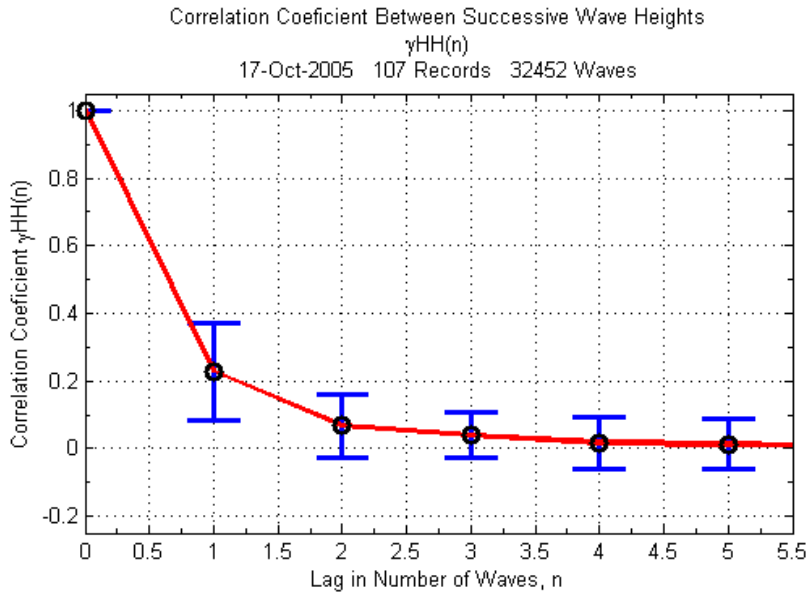

Figure 183: Correlation coefficient between successive wave heights for Hurricane Wilma.

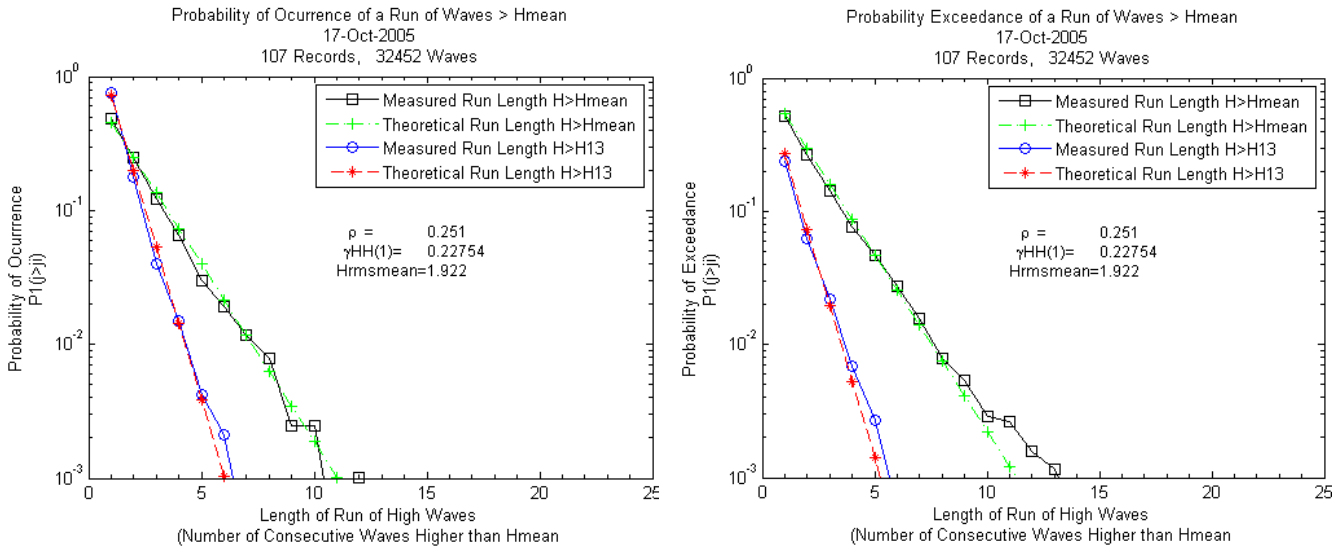

Figure 184: Occurrence and Exceedance Probability of a Run of Waves H>H*.

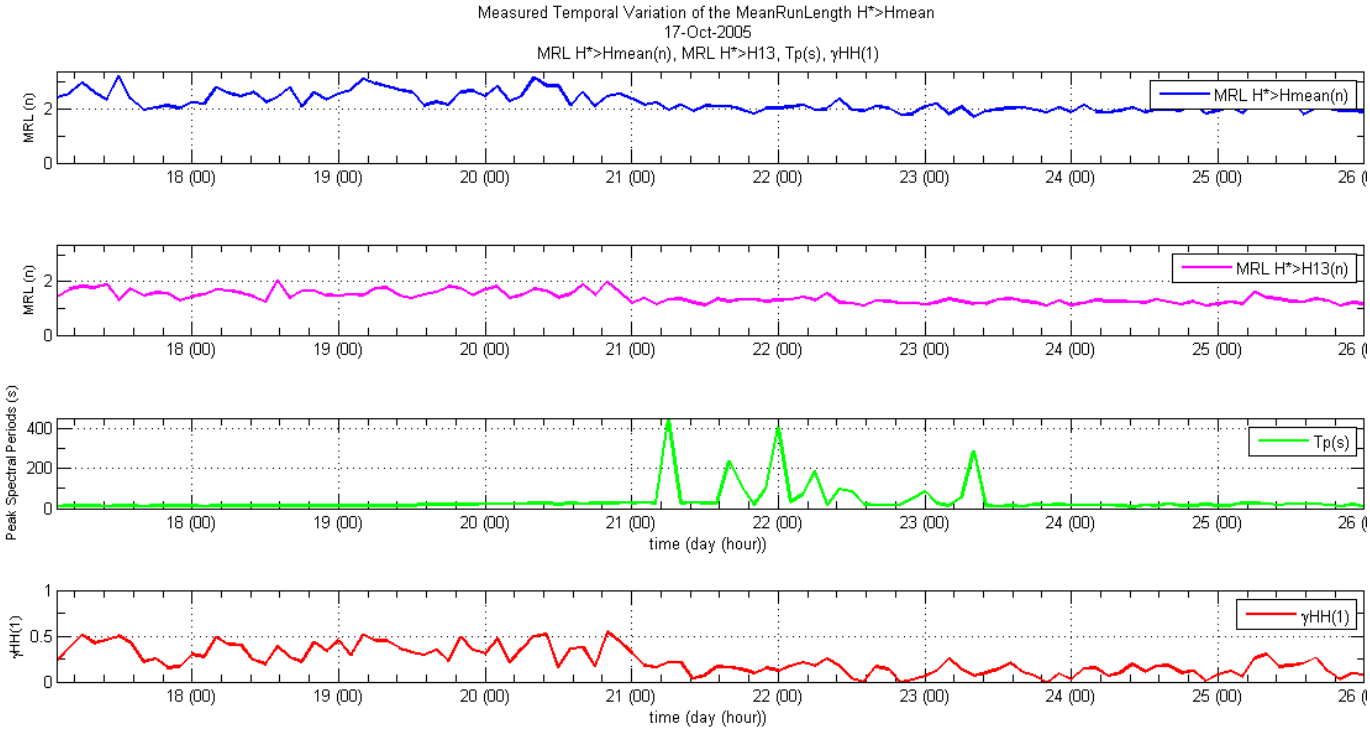

Figure 185: Temporal Variation of the mean run length H>H_{mean} and H>Hs wave heights for Hurricane Wilma.

3.4.7 Long Wave Analysis

In the spectral analysis it was observed that the long wave energy content during the direct influence of Hurricane Wilma was very large. The 107 time series were analyzed for the presence of the these long waves using a low pass filter with a cut off frequency set at the maximum period obtained from the zero down crossing method. The filtered wave signal was then analyzed using the Fourier transform to obtain the long wave significant wave height, H_{molong} and the long wave peak period. Figure 186, shows the most energetic long period time series with the filtered signal in red. In this time series a long wave with more than 4 meters in height and a period of almost 800 seconds is visible.

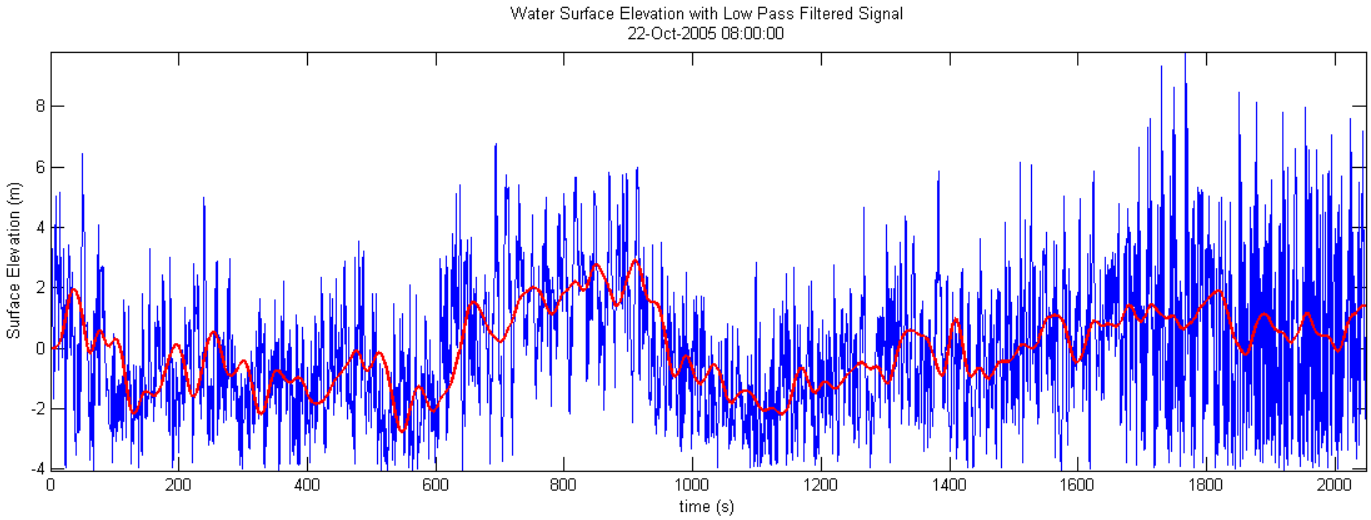

Figure 186: Filtered long wave signal for Hurricane Wilma.

The four highest measured long wave spectra are shown in figure 187, they all occurred the 22nd of October during the morning, between 4 and 10 am. In all cases the measured long wave height is above 4 meters, however their peak frequency varies. In three cases the peak frequency lies between 0.011 and 0.014, 71 and 90 seconds peak period, in one the measured peak frequency was 833 seconds.

The spectra of the most energetic wave conditions measured were compared with their long wave spectral estimate, figures 188. In these cases the long wave energy composed from 50 to 55 percent of the total measured energy. These means that during the most intense wave conditions almost half of the wave energy measured was composed of waves with periods above 100 seconds.

The temporal variation of H_{molong} and the long wave peak period was then compared with the H_{mo}, figure 189. From the 20th till the 21st, when the wave period increased and swell waves were arriving the measured long wave height increased from 0.16 meters to 0.50 meters. The significant wave height increased from 3 to 6 meters during this same period. After the 21st the long wave energy jumps from 1 meter to 4 meters in less than 2 hours,

the significant wave height goes from 6 meters to 8 meters. Then while the significant wave height, H_{mo}, is above 7 meters the measured long wave height, H_{molong}, is above 3 meters. This condition was maintained through put the 21st and the 22nd. During the 23rd as the significant wave height decreased the long wave height decreased very fast.

It is estimated that the long waves measured during the 21st and the 22nd were produced due to wave breaking of very high waves, at the wave measurement site. These long waves are not associated to bound long waves, wave grouping during the measurements was very low.

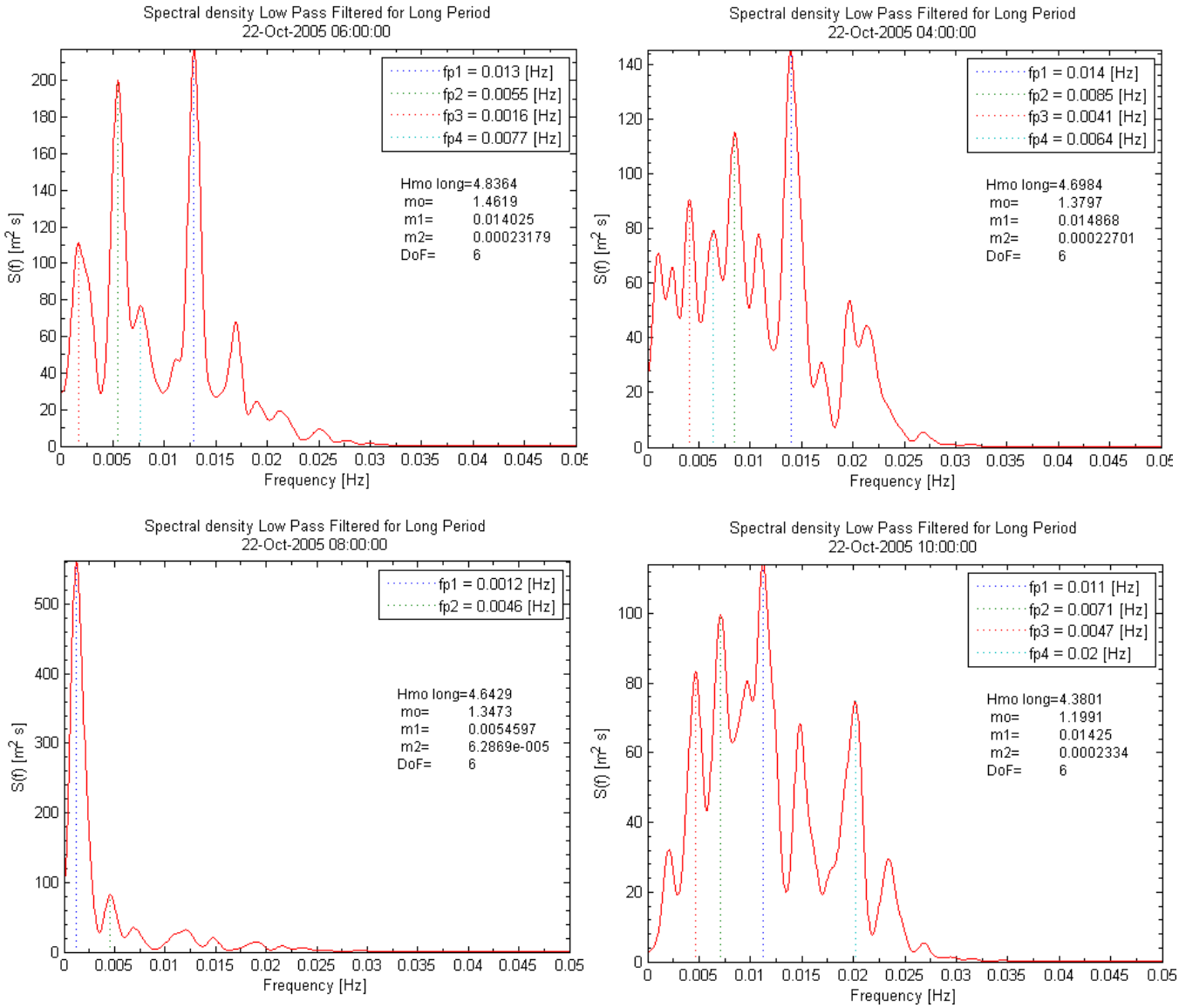

Figure 187: Long wave spectra for Hurricane Wilma.

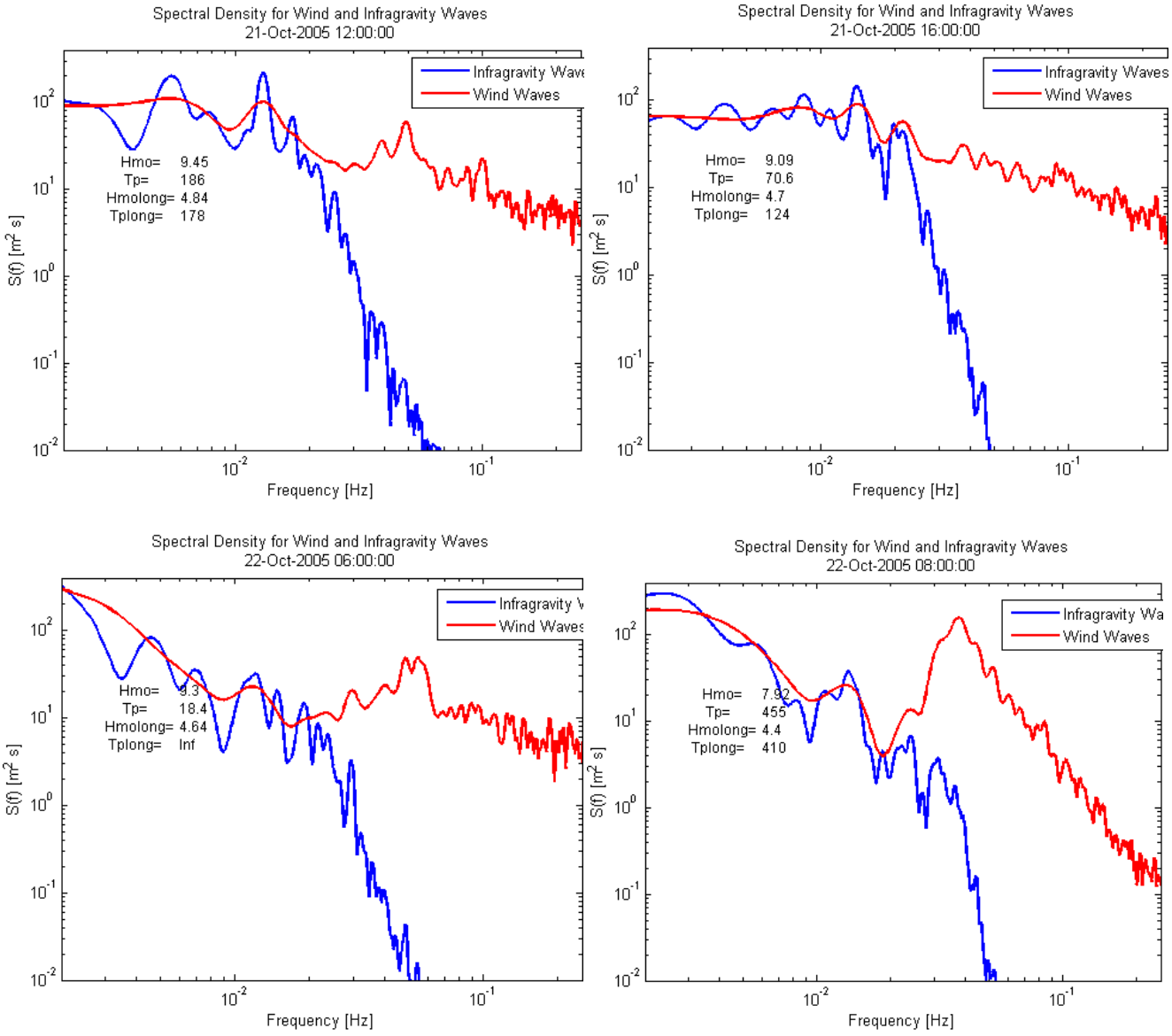

Figure 188: Filtered long wave signal for Hurricane Wilma.

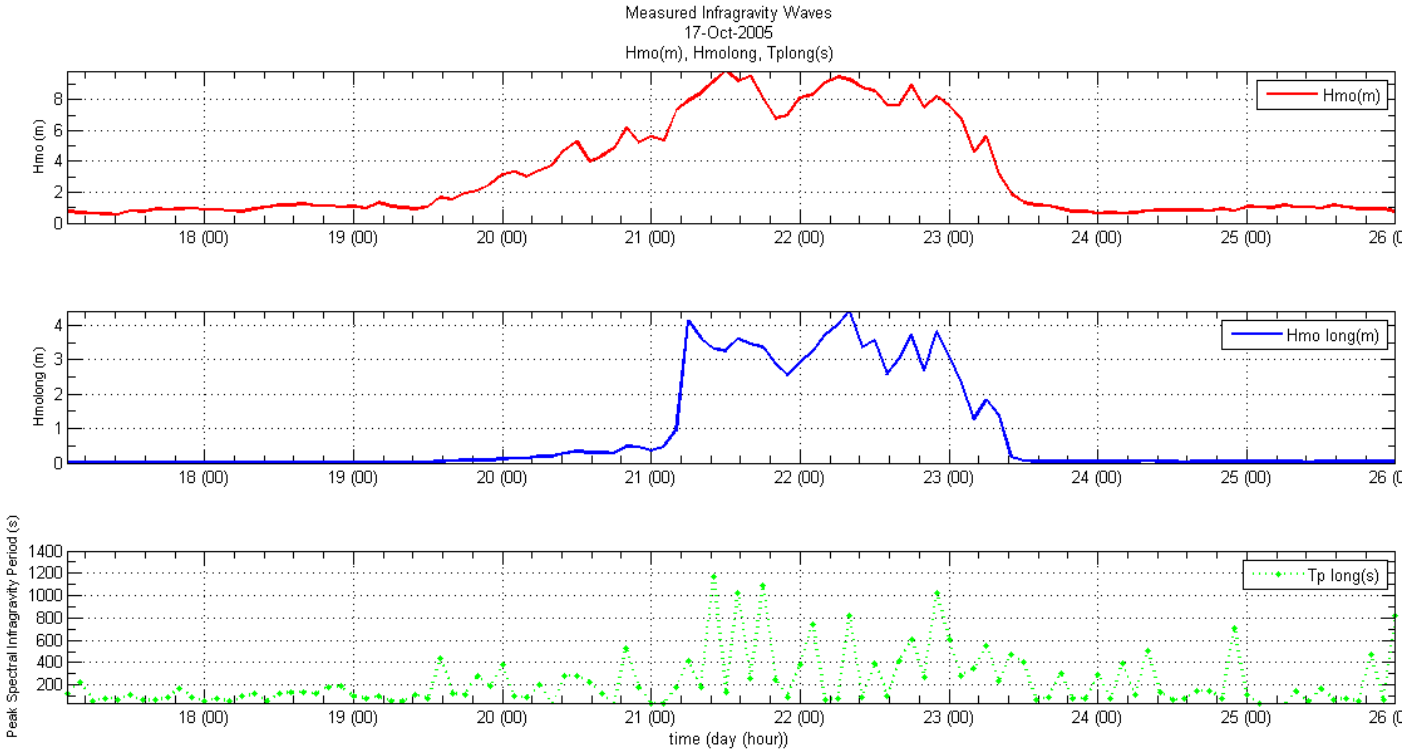

Figure 189: Temporal variation of the long wave height for Hurricane Wilma.

3.4.8 Analysis using the Hilbert Huang Spectrum

The HHT(ω,t) spectra for the most energetic wave records, defined as the ones with the largest H_{mo}, were obtained. Figure 190 shows the HHT(ω,t) spectrum for most energetic wave record which occurred during noon of the 21st of October. A very highly irregular sea is visible, with high amounts of energy distributed almost through out all instantaneous frequencies. Low frequency energy components are also visible in figure 191. The marginal HHT(ω)spectra are shown in figure 192, compared with the FFT spectra. Both show a startling resemblance, with a secondary frequency peak at 0.05Hz, 20 seconds or lower, and a primary peak very low frequency peak, under 0.01; hence the FFT spectra is capable of representing such an irregular low frequency content signal. The HHT(ω,t) provides a in depth view of the temporal frequency variation.

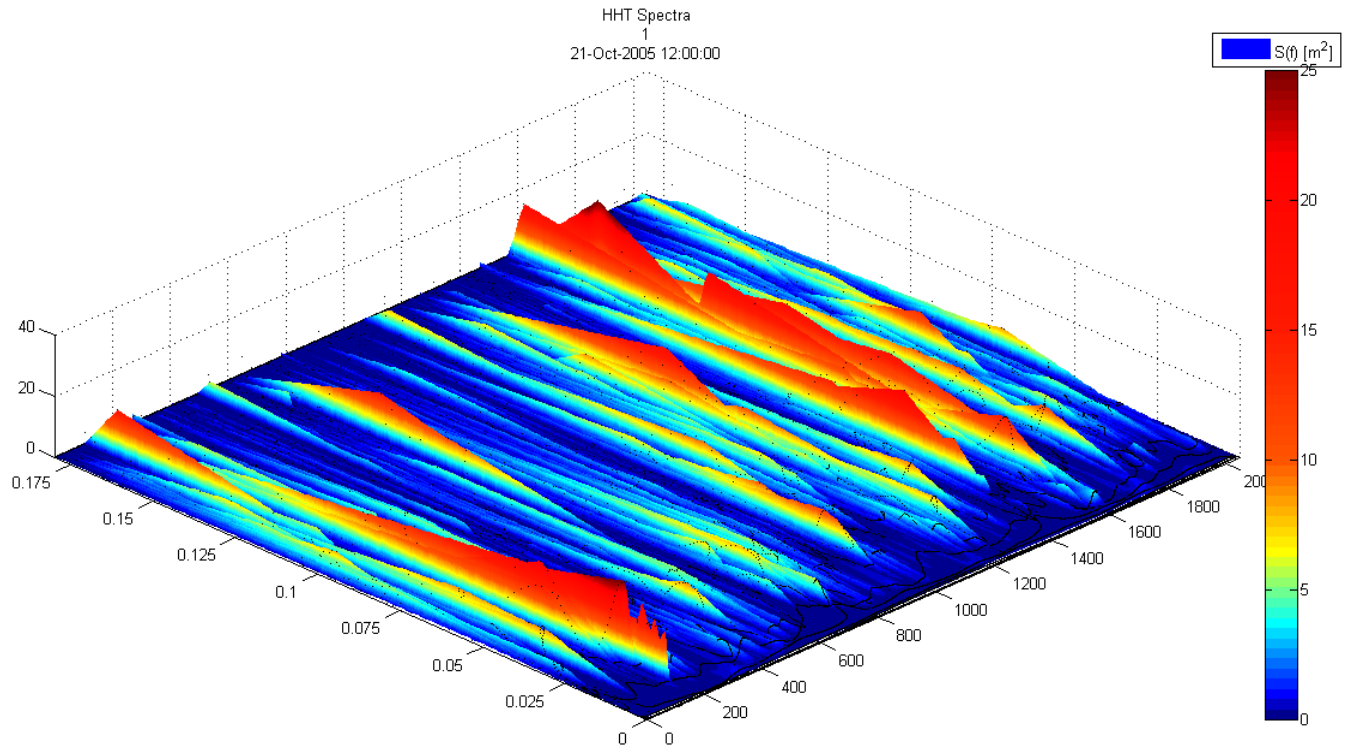

Figure 190: HHT Spectrum for most energetic time series Hurricane Wilma.

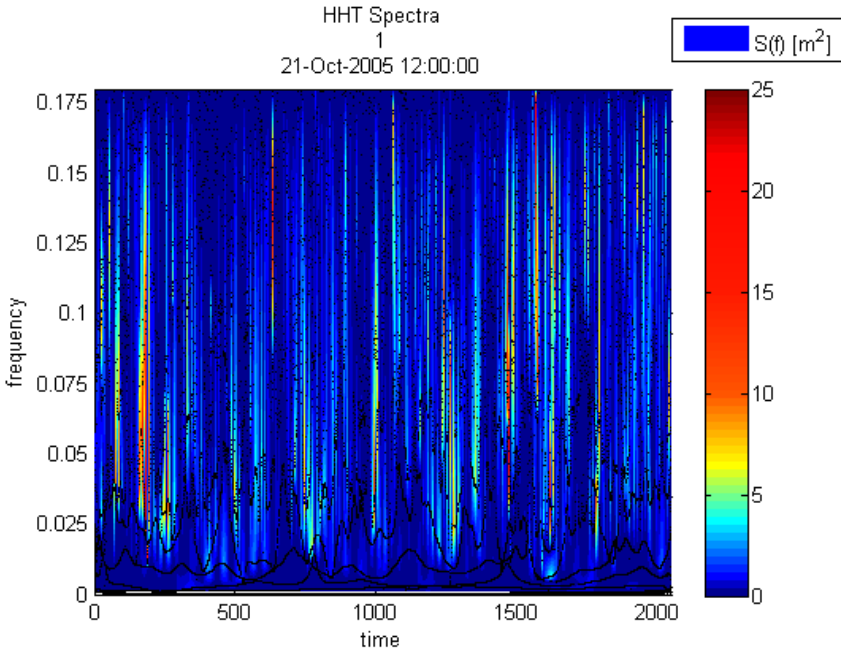

Figure 191: HHT Spectrum for most energetic time series Hurricane Wilma.

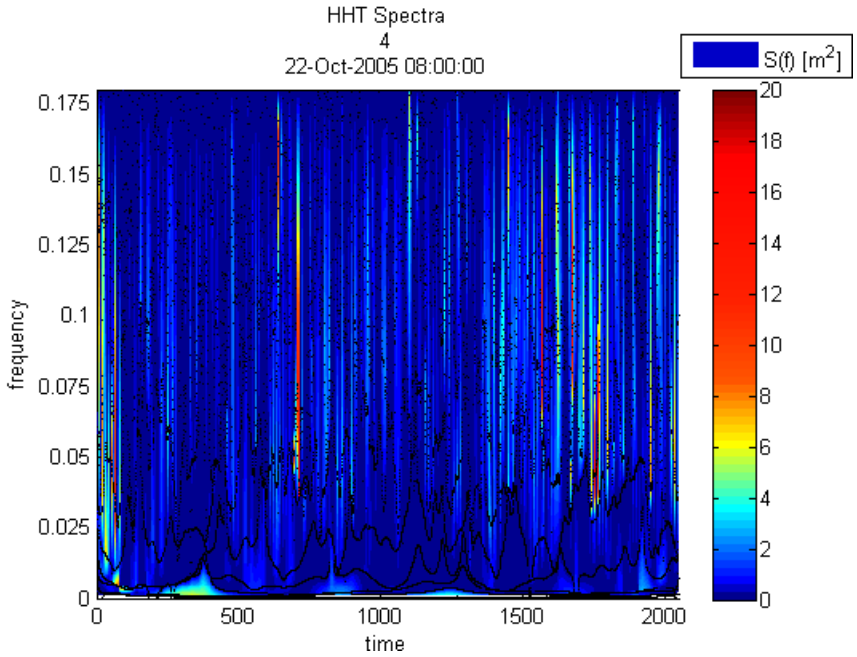

Figure 192: HHT Spectrum for most energetic time series Hurricane Wilma.

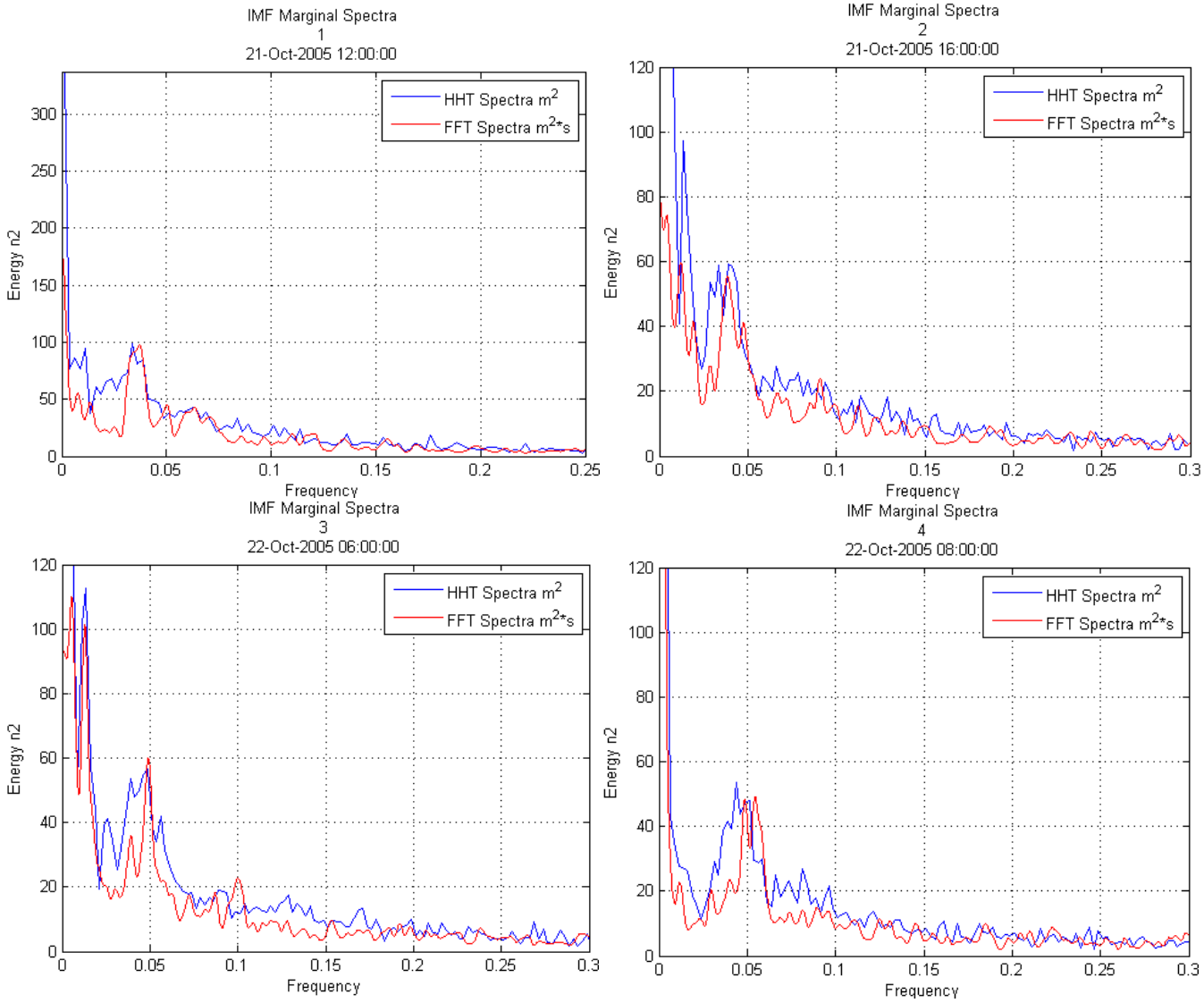

Figure 193: HHT Marginal Spectrum for most energetic time series Hurricane Wilma.

4.0 Summary of the Results of the Wave Analysis

4.1 Analysis of the Spectral Characteristics

The spectra of the different wave measurements analyzed were very different between each site. The long travelled swell presented regular single peaked spectra, with peak periods between 14 and 20 seconds. The wind waves off the Atlantic coast of Costa Rica presented several spectral peak periods between 7 and 10 seconds. The measured waves at Barra Troncador in the Delta del Ebro had spectral peak periods between 4 and 6 seconds, and presented smother spectra. The waves from Hurricane Wilma presented almost a white noise spectrum during the direct influence of the Hurricane, wave breaking and extreme wind conditions certainly played a role generation very long waves in a rippled white capping sea conditions.

Among the several spectral parameters analyzed it was noted that the spectral peakdness parameter Qp, represented quite well the observed spectral characteristics. Ka, the spectral groupiness parameter also seemed to represent the temporal changes, on the other hand the other parameters, of broadness, and narrowness missed clear temporal spectral changes, these parameters will not be analyzed any further.

The relationship between the spectral peakdness parameter, Qp, and spectral groupiness parameter Ka, is shown in figure 194. Even though the data sets come from very different wave conditions measured at different water depths a good agreement is shown; large values of Qp are related with high values of the spectral groupiness parameter.

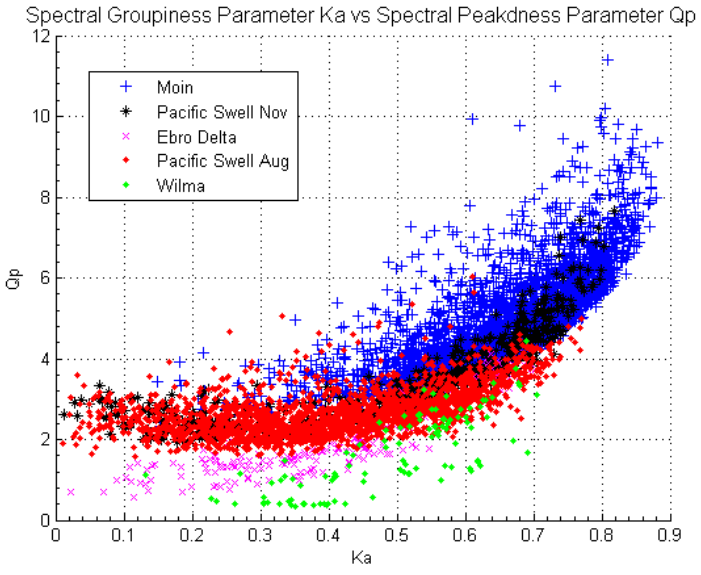

Figure 194: Relation between Qp and Ka.

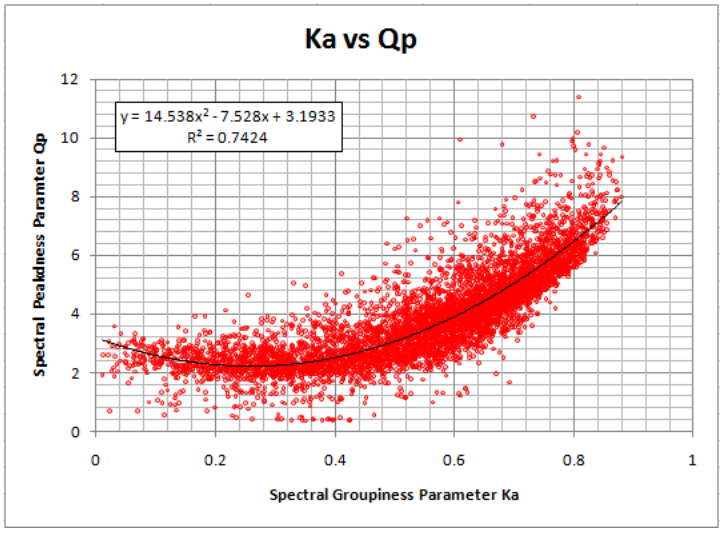

Figure 195: Relation between Qp and Ka.

A regression between Qp and Ka was made using the all data from the 5796 wave records from the wave measurements at the 4 locations analyzed. Figure 195 shows the results from the regression analysis. A clear polynomial trend is observed with a determination coefficient of 0.74.

The spectral peakdness parameter intends to describe the spectral shape and how peaked it is, the spectral grouping parameter Ka attempts to measure to what extent high local extremes come in groups. It is related to the envelope behavior of the signal. A clear correlation between the peakdness of the spectra and the envelope behavior of the signal has been obtained from the regression analysis.

The relation between Qp and the peak enhancement parameter from the JONSWAP spectrum has been previously shown, (Goda 1983). The spectra of the highest measured wave conditions from each location were fitted to the JONSWAP spectrum. Good fits were found for the long travelled swell waves, with peak enhancement parameters from 3.5 to 4.5 for very energetic swells and up to 13 for very regular wave conditions, but less energetic. For the measured wave conditions in the Atlantic Coast of Costa Rica, in Moin the peak enhancement parameter varied from 4.5 to 6.5 for the most energetic conditions, however the fit was not as good since multiple peaks were obtained around the peak frequency, nevertheless it shows that lower period waves can also present peaked spectral shapes. For the wave conditions measured at Ebro Delta the peak enhancement parameter took values between 4 and 4.8 and the shape fitted fairly. For the measured waves outside Puerto Morales during Hurricane Wilma the spectral shape did not show any resemblance to the JONSWAP spectra. Spectral Peaks at much lower frequencies and energy distributed along all of the measured frequencies showed that the JONSWAP spectra does not represent the energy distribution observed during the most energetic conditions of Hurricane Wilma. The fact that wave breaking could have been occurring is a possible explanation for this bad fit, care is advise when using spectral numerical models.

4.2 Analysis Wave Grouping Characteristics

The wave groupiness of the different records was analyzed by means of the correlation coefficient between two successive waves, γHH(1), and the mean run length of waves higher than the threshold values of $H_{1/3}$ and H_{mean}. These parameters were obtained after getting the individual waves with the zero down crossing method. The mean values of these parameters were shown to have a high temporal variation depending on the wave conditions at each site. The correlation between these values, the spectral peakdness parameter Qp and the spectral groupiness parameter Ka is examined below.

4.2.1 Correlation between Qp and Ka with the correlation coefficient between two successive wave

First the correlation between the spectral peakdness parameter, Qp, and the correlation coefficient between two successive, γHH(1), waves was investigated. Figure 196-1, shows the relation of these two parameters for the different wave measurement sites. No clear relation is visible and the parameters seem to be site dependant. Then the relationship between the spectral groupiness parameter Ka and the γHH(1) was also investigated. Figure 196-2 shows the scatter of points of these two variables for all the measurement sites. It was noted that the measurements from the August Pacific swell measurements were the most scatter, with many negative values of γHH(1). These negative correlation is high given the fact that the samples were probably too short for the measured period, the number of waves per samples becomes low and the correlation coefficient is then affected since complete wave groups cannot be measured.

Figure 197 shows the regression analysis carried out between the correlation coeffiecient between successive waves gHH(1) with Qp and Ka. Because of the dispersion when using the correlation coefficient of two successive waves for the August Pacific swells these data was not used for the regression analysis.

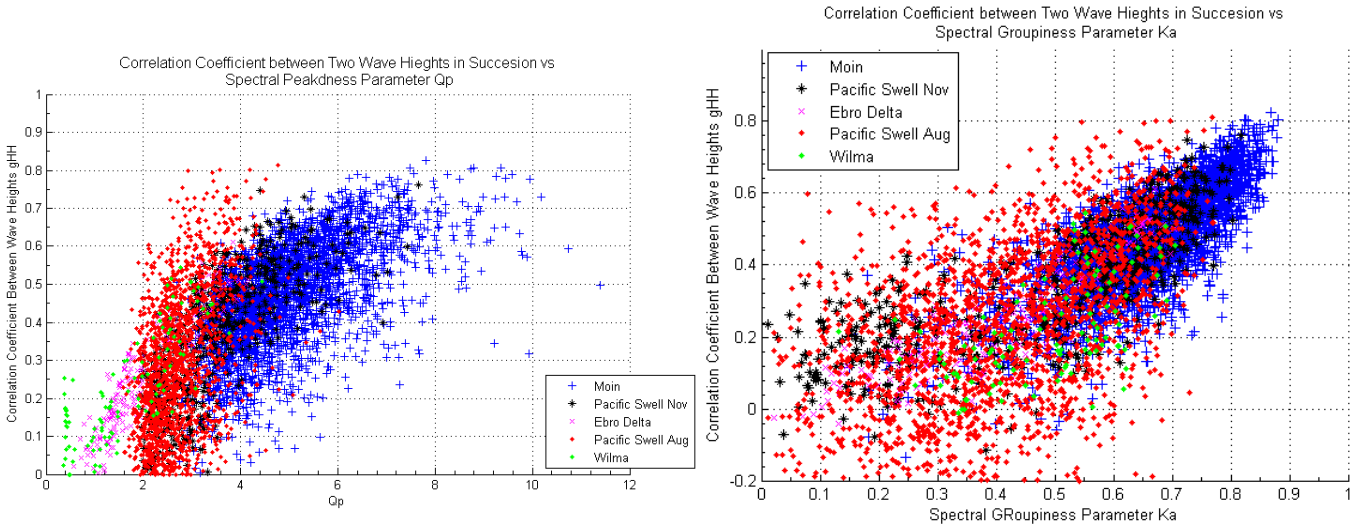

Figure 196: Relation between Qp and Ka with the correlation coefficient between two successive waves.

The regression analysis shows that the spectral groupiness parameter Ka, has a higher correlation with γHH(1)than Qp. This was the case even when considering the August swells data. The determination coefficient is also higher when using the Ka, with r^2=0.66, which is considered very high given the difference of the measured wave conditions and the locations. The best regression found when analyzing the spectral peakdness parameter against the correlation coefficient of successive waves was a linear one, however when analyzing the spectral groupiness parameter against the correlation coefficient between two successive waves a cubic regression showed to have the best fit, this was expected since the relation between Ka and Qp was also found to be polynomial of second order.

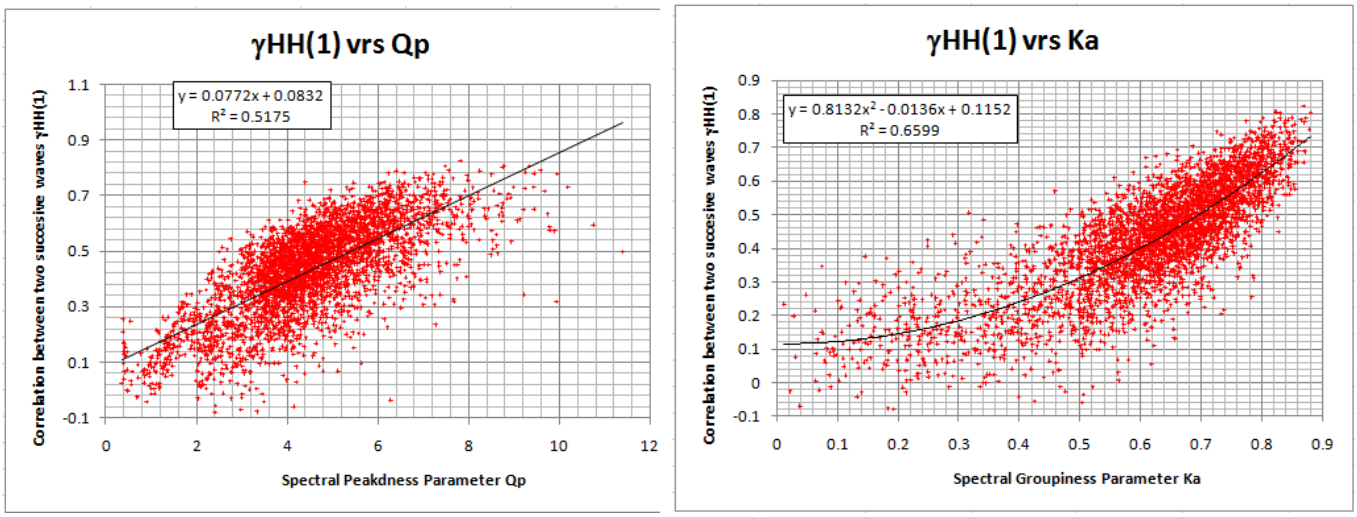

Figure 197: Relation between Qp and Ka with the correlation coefficient between two successive waves.

4.2.2 Correlation between the mean run length and the correlation coefficient between two successive wave

The relation between γHH(1) and the measured mean run lengths was then investigated. Figure 198-1 shows the data scatter plot for the mean run length of waves higher than H_{mean} for all the different measurements. Again certain scatter is visible in the August swells data, however in general the data follows a clear tendency, with the longest runs for the high γHH(1) values. Figure 198-2 shows the relation when setting the threshold value of runs at the significant wave height. Again a clear tendency to have the longer runs in the wave samples where the highest γHH(1) was measured is visible.

Regression analysis were carried using the whole data and without the August swell measurement data. The results of the regression were very similar; the main difference was the higher determination coefficient when

the values from the August swells were not incorporated into the analysis. Figure 199 shows the results from the regression analysis. The dispersion in the data is not surprising since 5976 wave records were used. The best fit found corresponded to second order polynomial regression; in this case the determination coefficient was lower, 0.48 and 0.46 for the run lengths of waves higher than H_{mean} and H_{13} respectively. These values represent regression correlation coefficients of 0.66 and 0.63, which when considering the large number of records used show a fit between the data. The figure also shows the values predicted by Kimura's theory, with an even better fit.

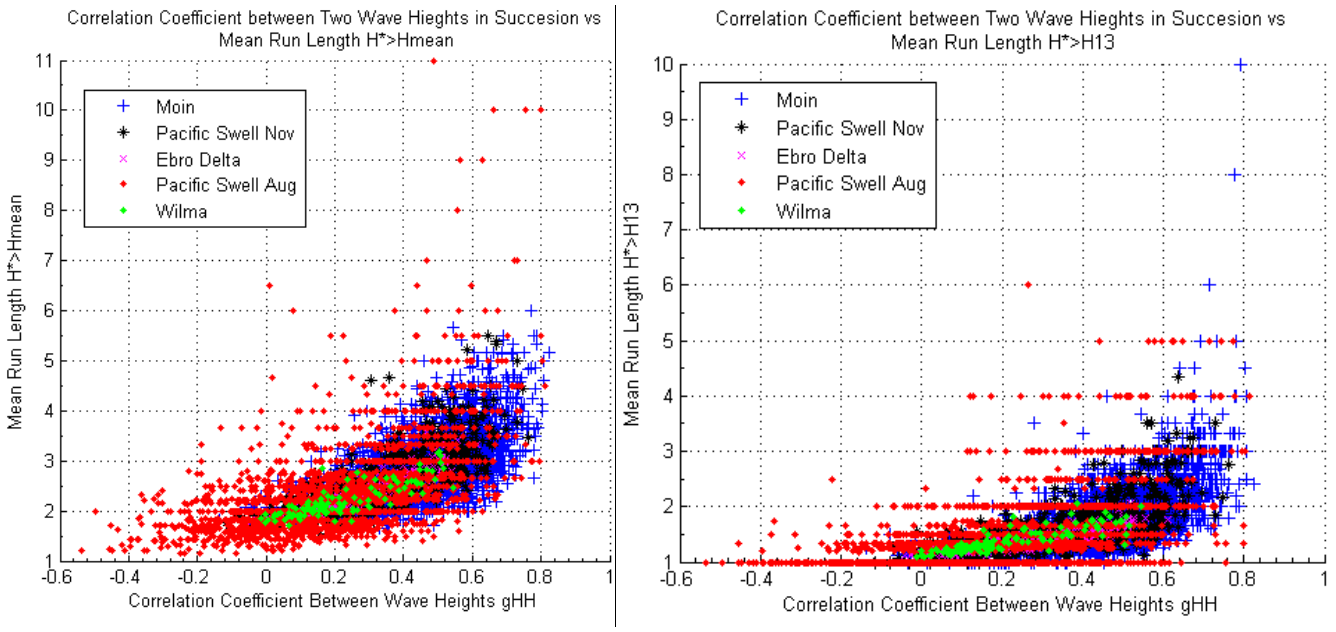

Figure 198: Relation between correlation coefficient between two successive waves and the mean run length.

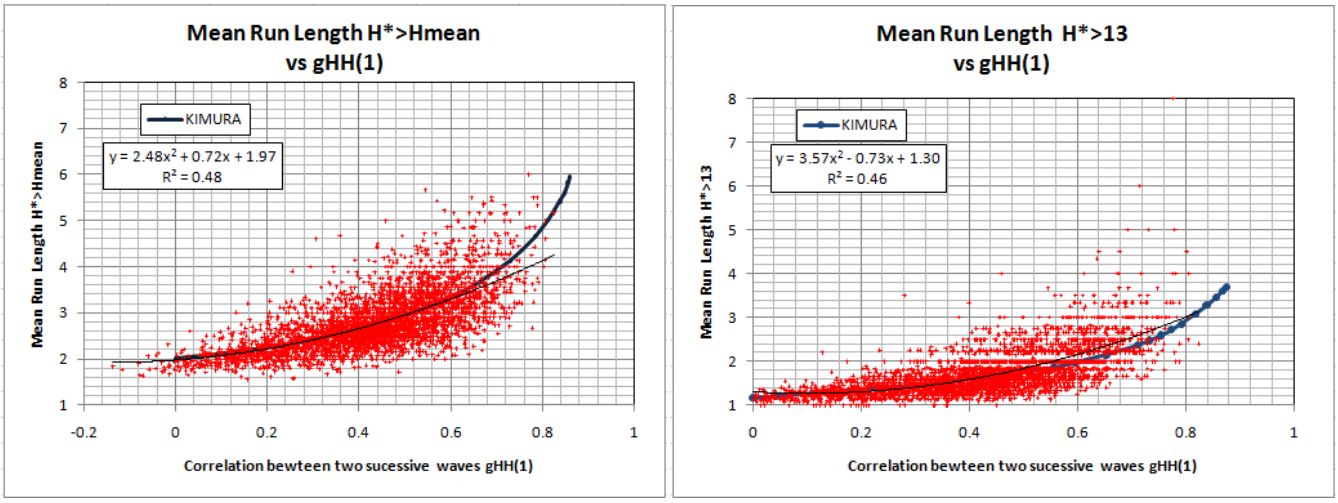

Figure 199: Relation between correlation coefficient between two successive waves and the mean run length.

4.2.3 Correlation between the mean run length and the spectral groupiness parameter Ka

The relation between the spectral groupiness parameter Ka and the mean run lengths for H*>Hmean and H*>H13 is shown in figure 200 for all the 5976 wave records from the 4 different sites. Again certain dispersion in the August swell data is present; nevertheless it is included in the analysis due to significance because it incorporates spectra of combined swell events. The data shows a clear trend, increasing the run length of consecutive waves with an increase in the spectral groupiness parameter Ka. The measured mean run lengths for the data from the August swells present in average larger number of waves, except for the data from the Atlantic coast of Costa Rica, Moin, where mean run lengths of 8 and 10 consecutive waves higher than $H_{1/3}$ were measured, this values are correlated with Ka values of more than 0.8. These long runs of waves occurred for very calm wave conditions.

The regression analysis was done for two cases, one considering the long travelled swell from August and the other without, figures 201 and 202 show both cases. The regression shows a correlation between both parameters. The regression had a better fit for the case when the August swell was not considered.

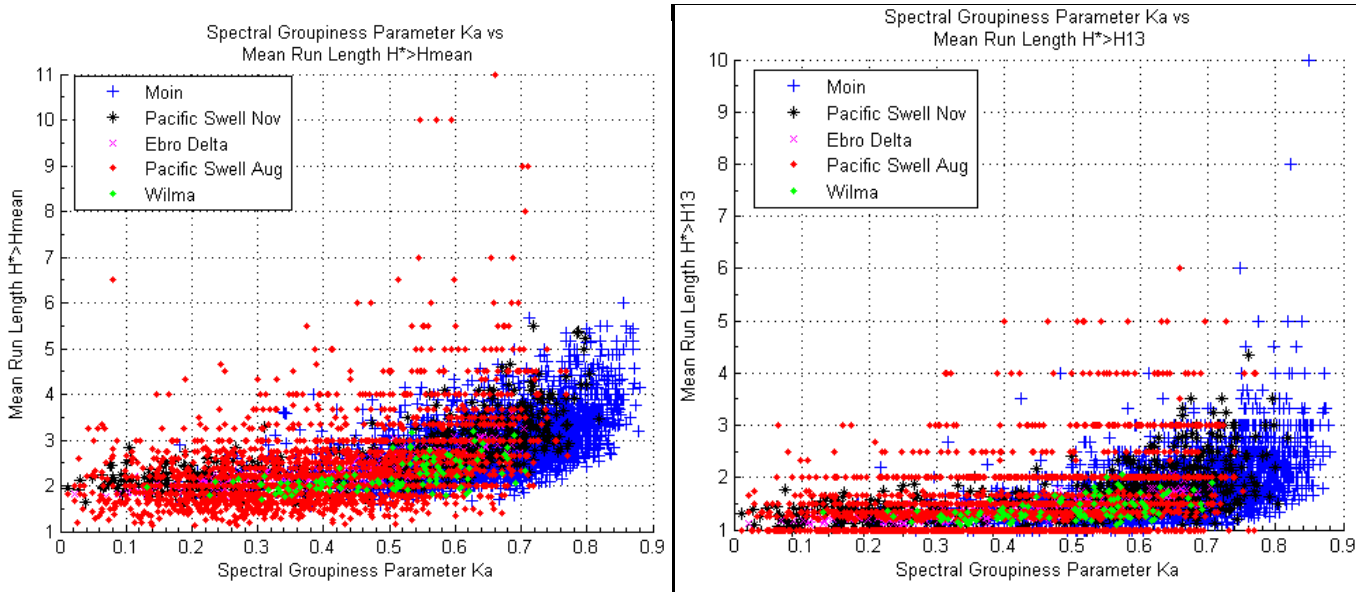

Figure 200: Relation between Ka and the mean run length.

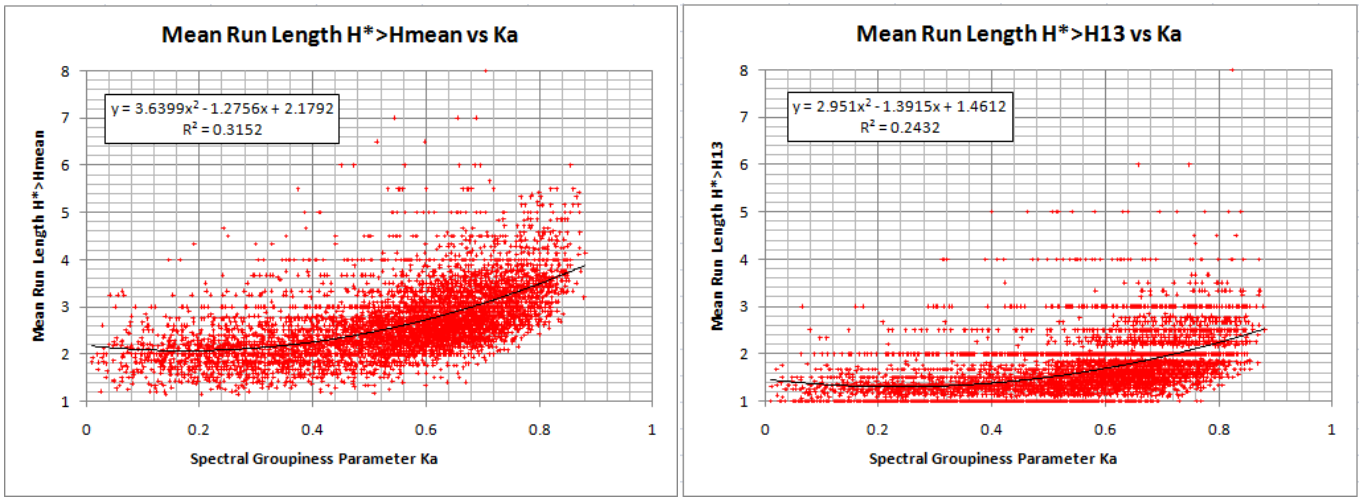

Figure 201: Relation between Ka and the mean run length.

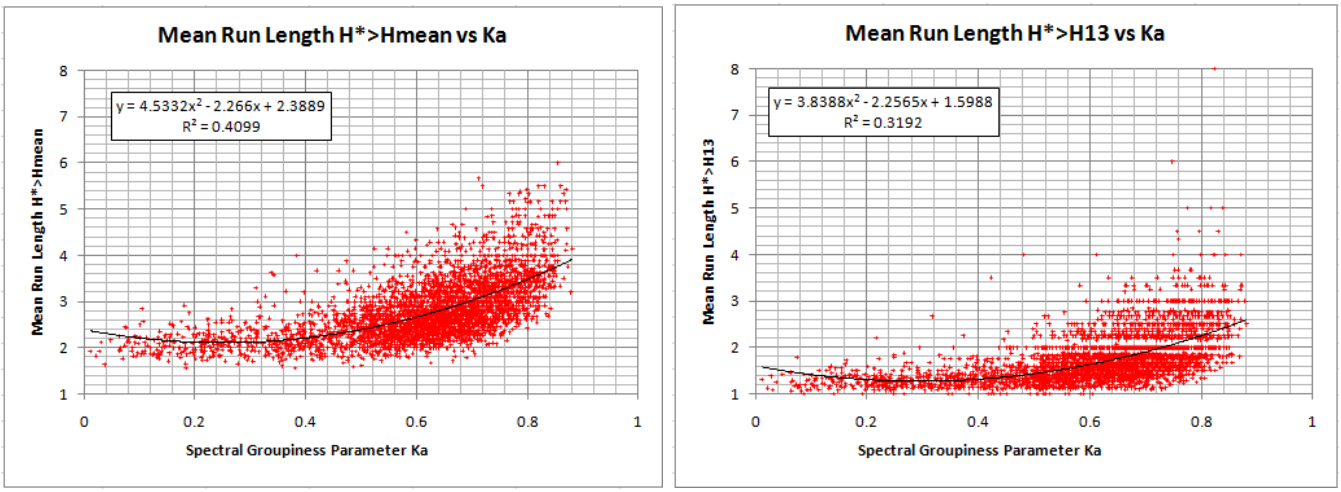

Figure 202: Relation between Ka and the mean run length without August Pacific swell.

4.2.4 Correlation between the mean run length and the spectral peakdness parameter Qp

The correlation between the spectral peakdness parameter, Qp, and the measured mean run lengths was investigated. The scatter plot of all the measured data is shown in figure 203. The relation is not as clear as the previously analyzed correlations. The long travelled swell tends to have high run lengths, but the measured spectral peakdness is always under 5. The longest run lengths for H*>H13 for the measurements at Moin had spectral peakdness values of 8, while other spectra with higher spectral peakdness parameter had mean run lengths of less than 2. The regression analysis of the data didn't show a good correlation either, with determination coefficients of 0.24 and 0.19. Clearly the spectral groupiness parameter is a better representation of the grouping characteristics than the spectral peakdness parameter.

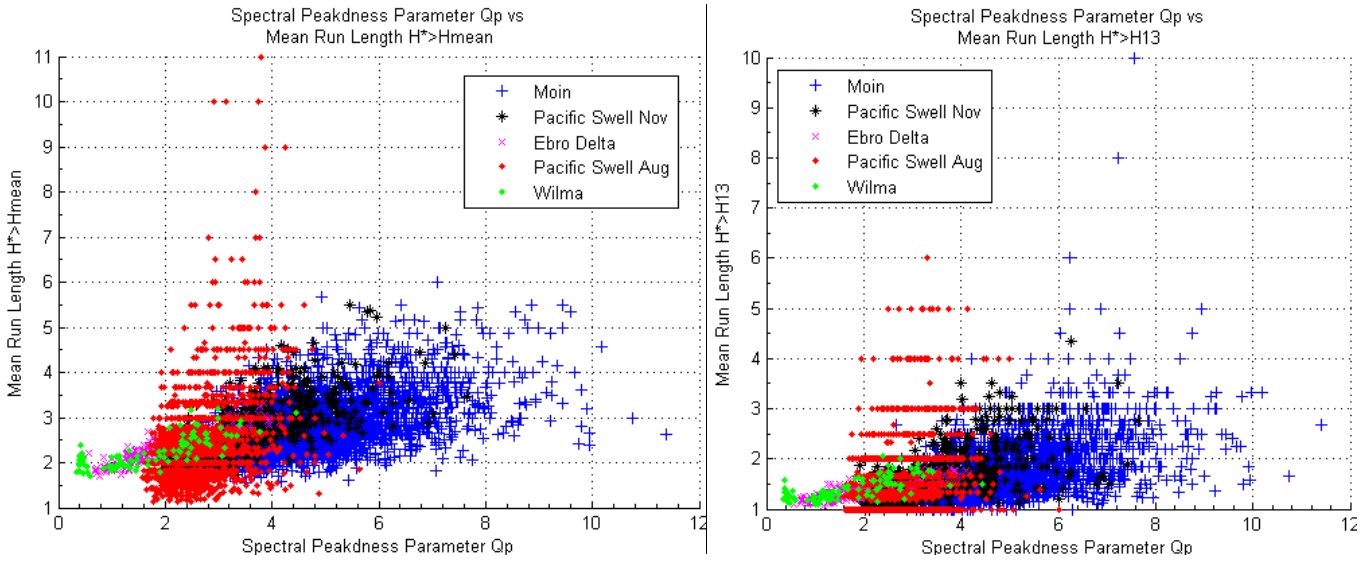

Figure 203: Relation between Qp and mean run length

4.3 Analysis Measured Long Wave Characteristics

The amount of wave energy with frequencies lower than the ones expected to be found within the gravity wave definition from Kinsmann (1965) was thoroughly investigated in the all wave measurements from each site. The presence of these infra gravity waves was well documented for each case. However the relative amount of low frequency energy relative to the total energy within the different locations was very different. Several reasons could explain such differences found. The relative depth, h/L, were L is the wave length and h the depth was very different in all cases, the relative wave height, H/h, was also very different, with breaking wave conditions in some cases. The distance from the measurement site to the coast was also very different, in the Ebro Delta wave measurements the beach was about 300 meters from the site, low frequency reflected waves and/or low frequency trapped waves could have been measured. Finally for Hurricane Wilma's wave measurements abrupt changes in atmospheric pressure, the interaction of the hurricane surge with the coast, and large setup produced by the very high winds all contributed in these long measured waves. The physics of the measured infra gravity waves is clearly very different for these sites and it would be wrong to compare the measured long wave energy between the different sites, in summary it would be like trying to compare oranges with apples, both are round but their different fruits. The long wave analysis will be carried separating the sites.

The measured long wave spectral heights, H_{molong}, and peak spectral period were compared with the measured total spectral wave height, H_{mo} and peak spectral period for each site. Then Longuet-Higgins set down equation for a group of waves in shallow water, (equation 51) was fitted with the measured H_{molong}, using a K factor for each site. It would also have been possible to use the Ursell number for the comparison, which in fact is resembled in the modified equation 51.

$$H_{Long} = K * \frac{3gH^2}{4\omega^2 d^2}$$

Eq. (51)

Equation 51 takes into account several wave parameters that were very different in each site. The water depth, d, which varied between 3.5 meters, at the Ebro Delta, and 20 meters in the Pacific. The wave angular frequency, w=2p/T, varied between 1.57 and 0.286 from wave periods between 4 and 22 seconds, and the H the significant wave height varied between 0.30 to 9 meters. Equation 51 is not valid after the wave breaks, or the long wave is freed.

4.3.1 Long wave conditions measured at Costa Rica

The measured wave conditions at the Pacific coast and the Atlantic of Costa Rica were done in similar conditions, both were done at a distance of several kilometers from the coast and both were carried at water similar water depths; reflected waves from the coast play a minor role and wave breaking did not occur. The relation between

the spectral significant wave height, H_{mo} and the long wave spectral wave height was investigated for the wave measurements from both sites. Figure 204 shows the scatter plot of these two variables for the 3 data sets available, a total of 5493 records were included. The segregation between the wind waves measured at Moin and the swell waves measured in Samara is clear, the swell waves contain longer wave energy, especially for the higher significant wave heights, while the highest long waves for Moin have 0.075 meters, for the swell waves the long waves were more than 0.20 meters high. This is more than 100% of low frequency energy. This difference is explained by Longuet Higgins formula, equation 51, where the long period wave energy is dependent on the square of the angular frequency. Furthermore during the wave measurements at Moin it was observed that the wave period was almost uniform and very narrow banded, these could explain the almost linear trend that the data shows in figure 204.

A second order polynomial regression fit between H_{mo} and H_{molong} was done to determine if equation 51 could be applicable on the data. Clearly with the current data set the wave period and the water depth were different at each site, nevertheless a correlation between these two values is observed in figure 204-2. The determination coefficient, r^2, is of 0.502, and a correlation coefficient of 0.709, that when considering that 5493 wave records are included in the regression, a clear correlation is obtained.

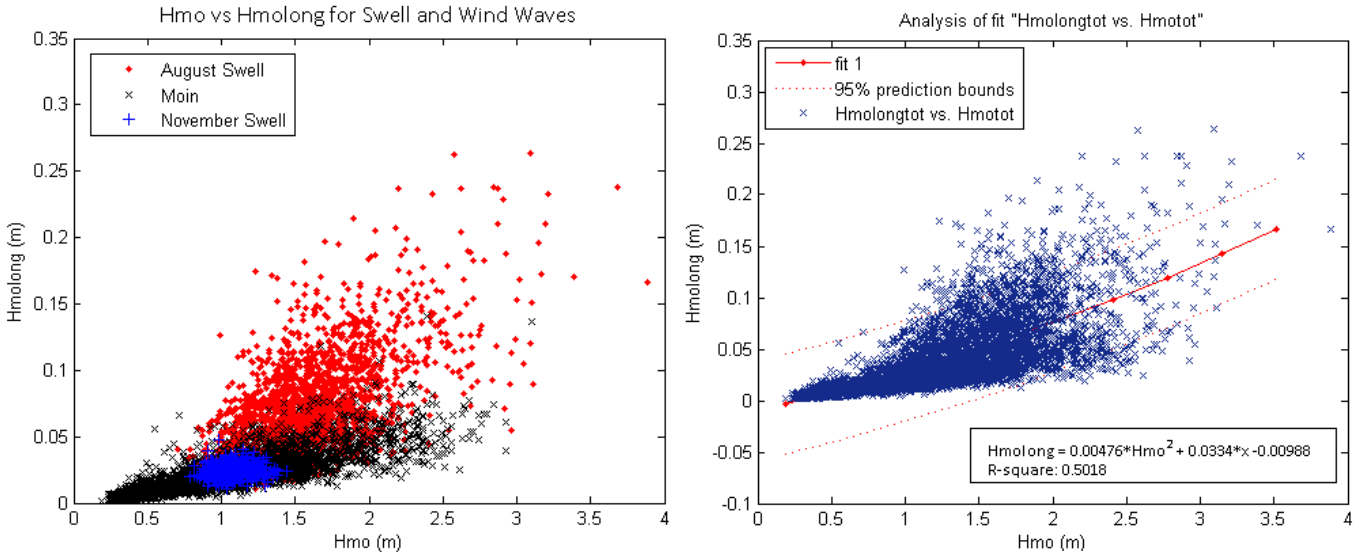

Figure 204: Relation Hmo and Hmolong for the wind and swell waves

The dependency of the measured long wave height, H_{molong}, on the measured peak spectral period was then investigated. Equation 51 shows a quadratic relation between the wave period and the long wave height. Figure 205-1 shows the long wave heights for the given peak spectral period for each site. The regression analysis is shown in figure 205-2. The determination coefficient is lower, 0.382, a correlation coefficient of 0.62. Given the differences between the data sets some correlation can be observed.

The data was fitted against equation 51 using a mean depth between the data sets of 18.5 meters. The K adjustment factor was obtained as the mean value of the calculated H_{long} divided by the measured H_{molong}.

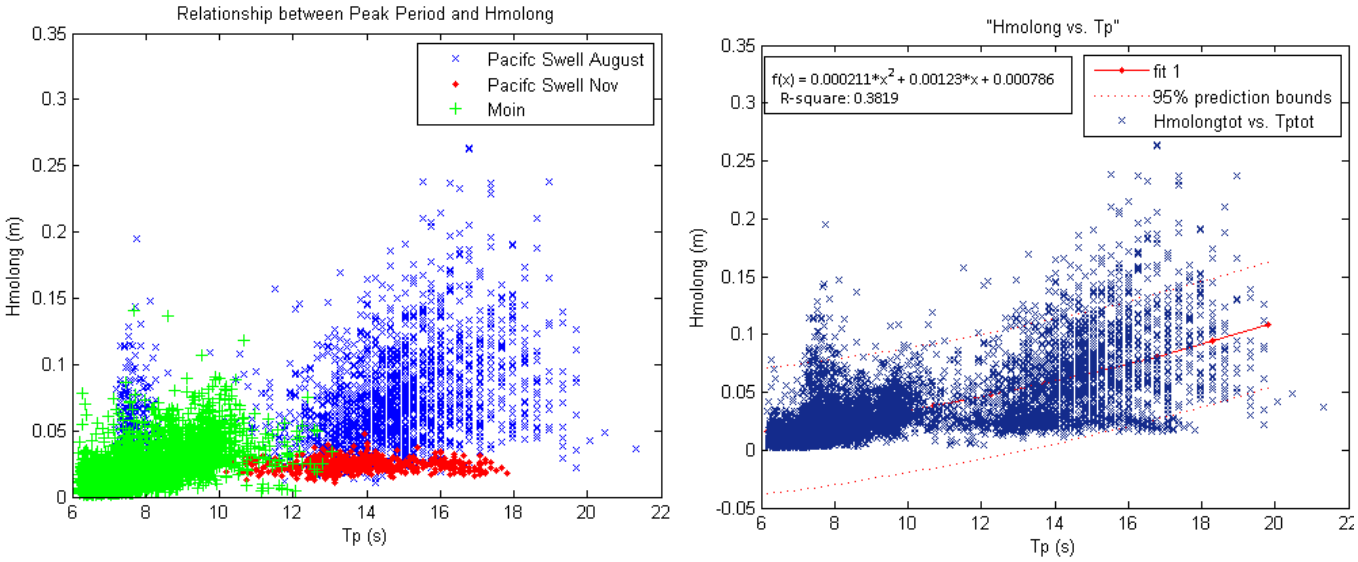

Figure 205: Relation Tp and Hmolong for the wind and swell waves

A K adjustment value of 0.136 was found. The validity of equation 51 with the K value of 0.136 was then evaluated by fitting the calculated value $K*H_{long}$ with the measured H_{molong}. Figure 206 shows the obtained fit. The determination coefficient was 0.575, a correlation coefficient of 0.76. The obtained slope is 1, which shows the validity of equation 51. Nevertheless given the difference in water depths equation 51 was then fitted for each site.

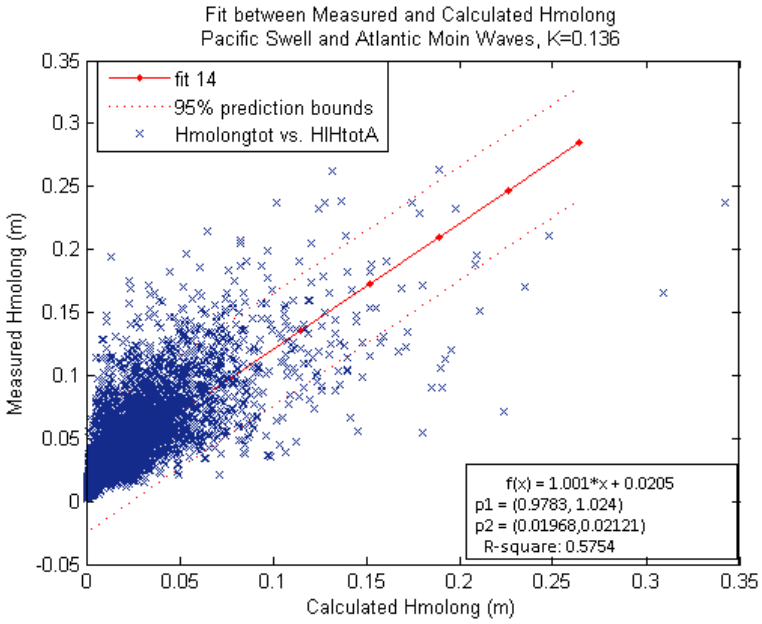

Figure 206: Relation measured and calculated Hmolong for the wind and swell waves

4.3.2 Long waves for the Pacific Coast of Costa Rica

The long wave energy measured at the Pacific coast of Costa Rica was investigated. The amount of long wave energy with respect to the measured spectral significant wave height was obtained for the two wave measurement campaign of August and November 2010. Figure 207 shows the regression analysis of 2568 wave records. The best regression fit was found for a second order polynomial expression, where the determination coefficient was of 0.491. In general significant wave heights above 3 meters would produce 0.20 meters of long waves.

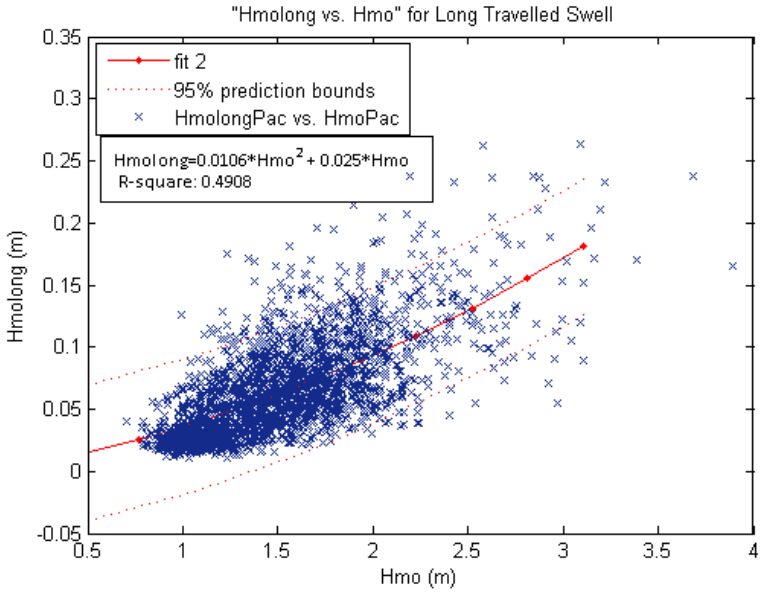

Figure 207: Relation Hmo and Hmolong for the swell waves

The correspondent K value of equation 51 for the data, given the peak spectral period, T_p and significant wave height H_{mo}, was evaluated for a mean water depth of 21 meters. (The tidal variation at the site was above 2 meters). A K adjustment factor of 0.14 was found. Figure 208 shows the fit between the calculated long wave height using K=0.41 given the measured H_{mo} and T_p of the 2568 wave records, with the measured long wave height. A determination coefficient of 0.43 was found, a correlation coefficient of 0.66.

The period of the long waves was also investigated; figure 208 shows a scatter plot of the measured spectral peak wave period and the correspondent long wave period. No clear correlation is visible from the scatter plot, and long wave periods from 75 to 800 seconds seem to appear through out the wave measurements without any correlation to the measured peak spectral periods. This is not surprising given the fact that if these long waves are associated with the wave groups their period is bound to the run length of the group and not the period of one given wave. Nevertheless no correlation between the mean run lengths, or correlation coefficient between to consecutive waves with the long wave peak period was observed.

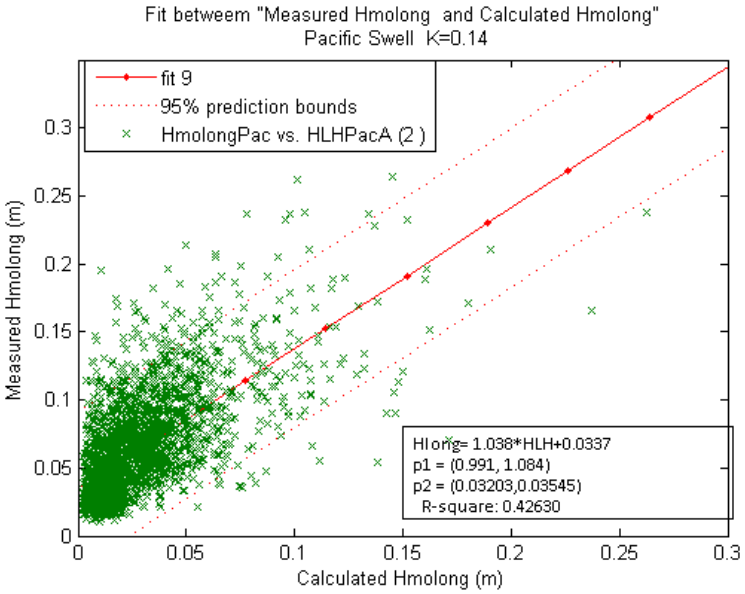

Figure 208: Fit between Measured and Calculated Long Wave Height for Pacific Swell

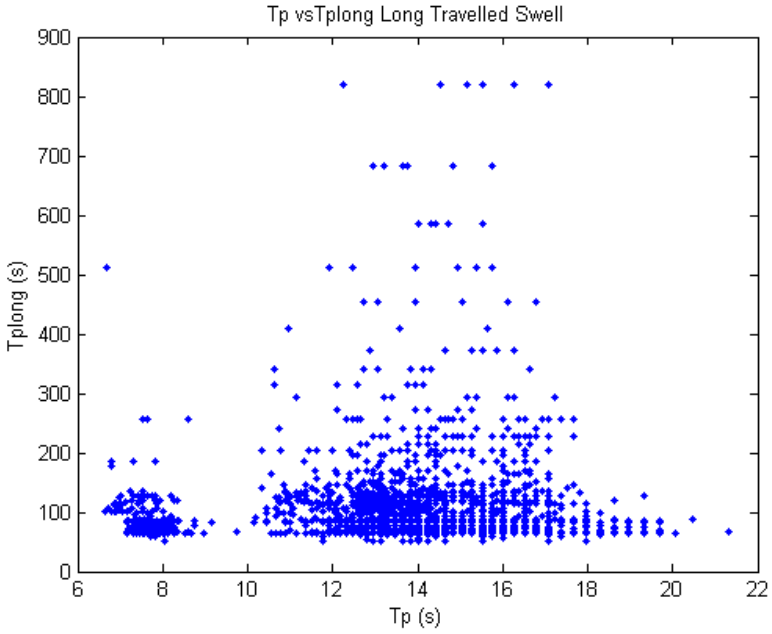

Figure 209: Relation Tp and Tplong for the swell waves

4.1.1 Long waves for the Atlantic coast of Costa Rica

The measured long wave heights at the Atlantic coast of Costa Rica were correlated with the measured significant wave height, Hmo. A linear relation was the best fit, with a determination coefficient of 0.64, figure 210. A adjustment K factor from equation 51of 0.184 was then obtained. The validity of equation 51 as a predictor of the long wave height was then investigated. The calculated long wave heights using equation 51 and the measured ones were then fitted to determine the validity. Figure 211 shows the regression analysis between them. A determination coefficient of 0.62 was obtained, which means a correlation coefficient of 0.79, with 2925 wave records. A good correlation was found. The different K adjustment values found between the swell waves from the Pacific and these waves means that equation 51 means only a 3% difference in the mean long wave height calculation.

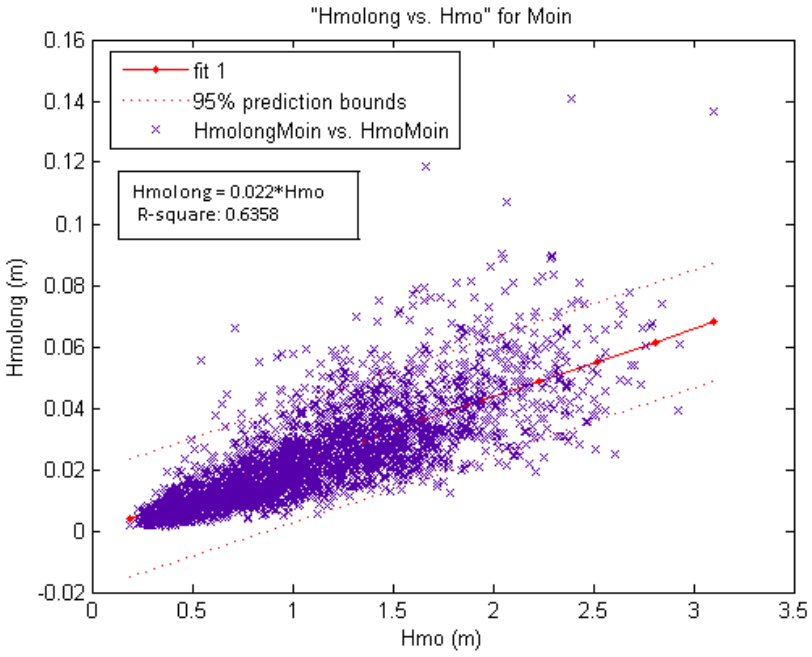

Figure 210: Relation Hmo and Hmolong for the wind waves at Moin

The long wave period was then investigated. Figure 212 shows that no correlation between T_p and T_{plong}. Furthermore several constant long wave periods are observed. The constant long wave periods could be caused by harmonics given the separations observed. These long waves are most probably not caused by bound long waves to groups or are caused by the non-linear nature of the bound long wave, composed of small set downs beneath high waves and small setups between the wave groups, where cosine or sine functions are not good to characterize these physical phenomenon and many spurious harmonic peak appear.

For the waves with long wave period lower than 50 seconds certain relation was observed with the measured mean run length for waves groups with heights larger than $H_{1/3,}$ shown in figure 212-2. This relation shows the three highest long wave spectral peaks measured since in most cases several frequency peaks were found in the long wave spectra.

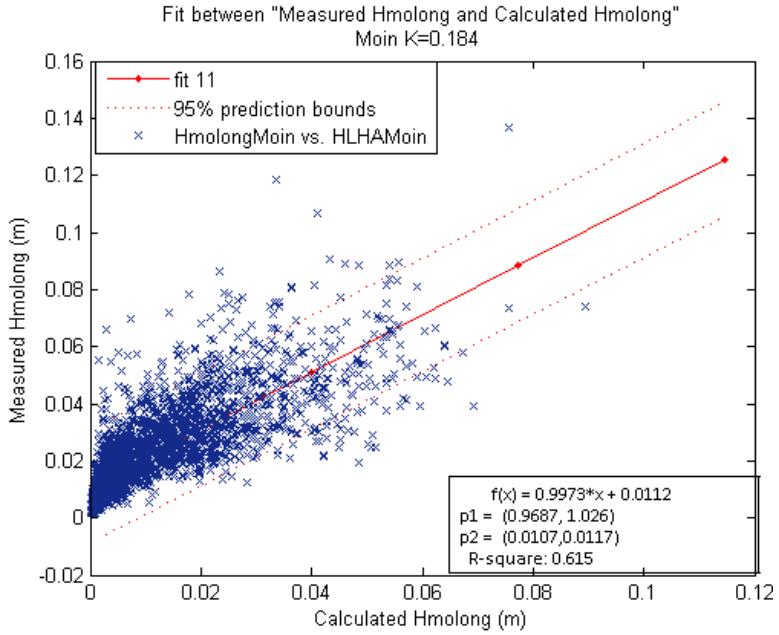

Figure 211: Fit between Measured and Calculated Long Wave Height for Moin

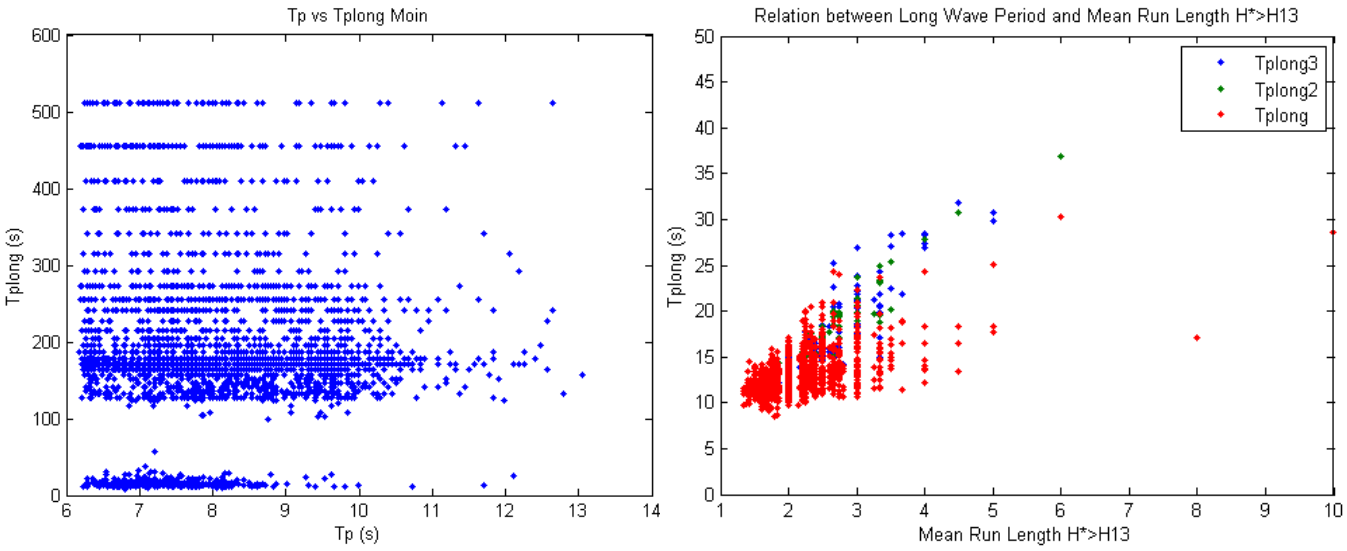

Figure 212: Relation Tp and Tplong for the wind waves at Moin

4.1.1 Long waves for at the Ebro Delta

When analyzing the long waves from Ebro Delta it was observed that a much larger relative long wave height to the significant wave height was measured. Theses larger energy content could be explained by the shallow water depth at which the wave measurements were carried out, 3.5 meters. In equation 51 the long wave height is proportional to $1/h^2$.

The relation between the measured long wave height and the significant wave height was obtained, figure 213. A clear quadratic relation was obtained, with a determination coefficient of 0.54, a determination coefficient of 0.73, with 194 wave records.

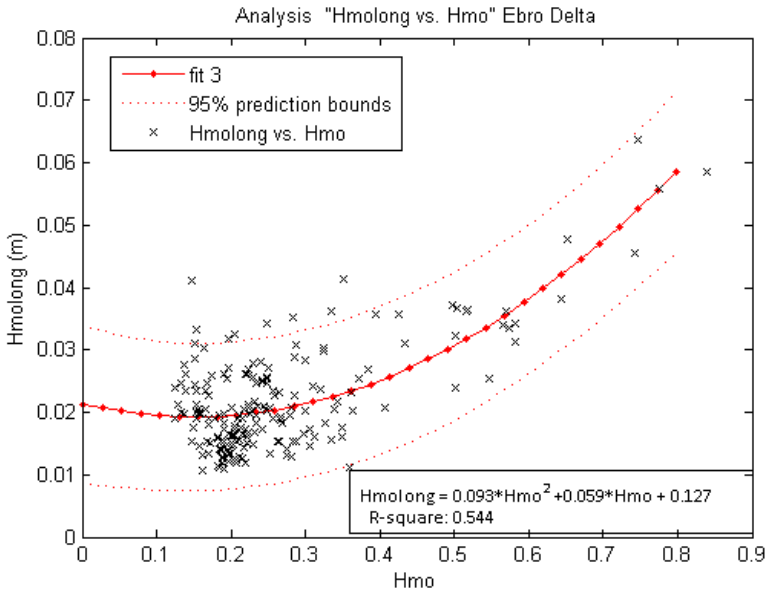

Figure 213: Relation Hmo and Hmolong for the near shore waves

The long wave height was calculated using equation 51 with the given H_{mo}, T_p and water depth of the site. The adjustment factor K from equation 51 was obtained between the calculated and measured long wave height. A K value of 0.18 was obtained. The validity of equation 51 and K adjustment factor was then obtained by fitting the measured and calculated long wave height, H_{molong}. Figure 214 shows the fitted values. A determination coefficient of 0.53, correlation coefficient of 0.73 was obtained.

These K adjustment factor is very similar to the one found for the wave measurements at Moin, and close the one found for the swell waves. Given the differences in wave heights, peak periods and water depths form the different sites the similarity in the K value is surprising, and these could mean that equation 51 is a very good predictor of the long wave height for almost sea state condition before breaking of the waves or the bound long wave is freed.

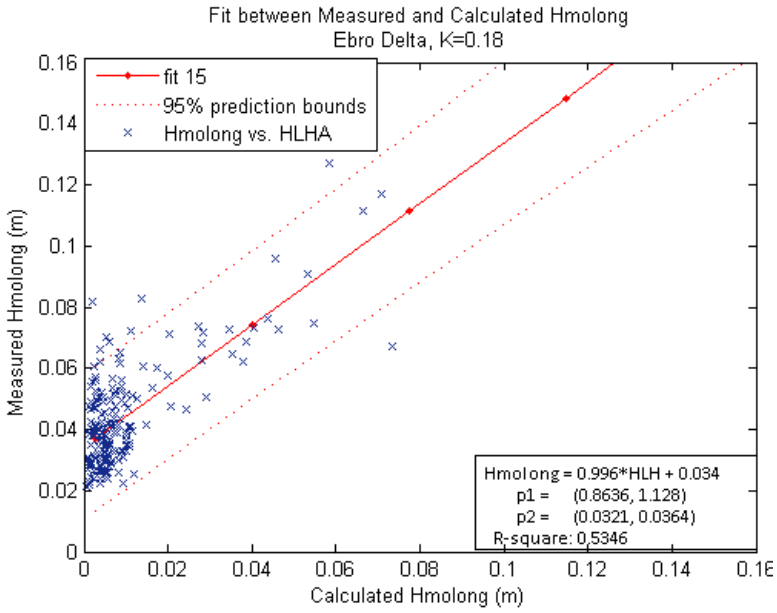

Figure 214: Fit between Measured and Calculated Long Wave Height for Ebro Delta

For the measured waves at Ebro Delta no relation between the long wave peak spectral period, T_{plong}, and the peak spectral T_p was found. As in the other sites constant T_{plong} values were obtained, particularly for the very long 16 minute periods. Such long waves are not associated with the wave groups of just several waves.

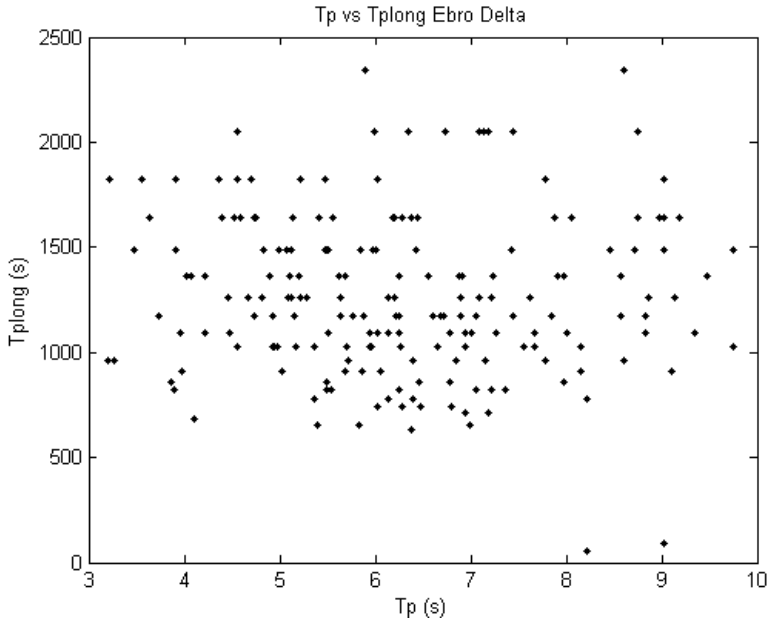

Figure 215: Relation Tp and Tplong for the Ebro Delta

4.1.1 Long waves for Hurricane Wilma

The measured long waves at Hurricane Wilma were surprisingly large, as was seen chapter 3.4.7. There was a jump of more energetic long waves during the period of time that the Hurricane affected the measuring site directly. These much larger long wave heights were associated to wave breaking, surge, and wind set up. The relation between the long wave height, H_{molong}, and the significant wave height for all the measured waves is shown in figure 216. Two different trends are visible, one for H_{mo} smaller than 6.5 meters, and H_{molong} higher than 1 meter, and the other for H_{mo} larger than 6.5 meters and H_{molong} larger than 1 meter. These differences could be associated with the wave breaking and the large wind set up and surge from the Hurricane.

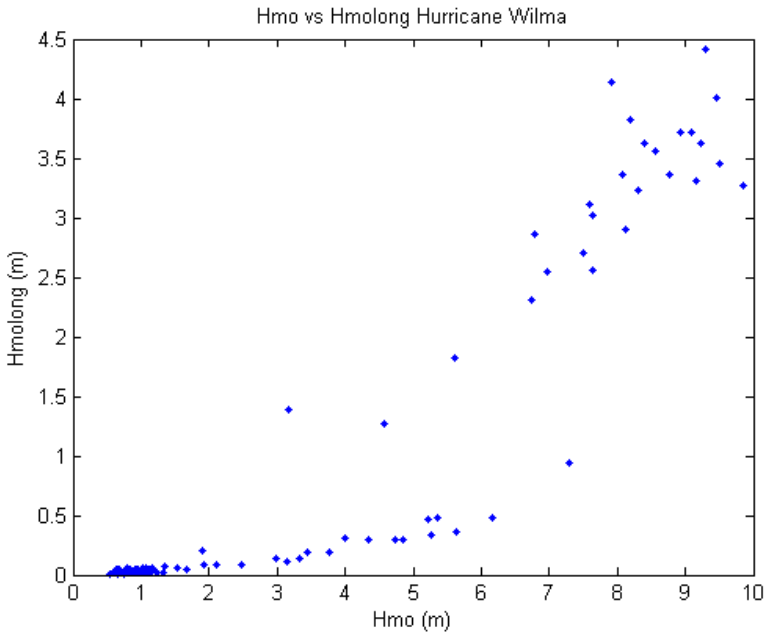

Figure 216: Relation Hmo and Hmolong for the waves for Hurricane Wilma

The wave records were then separated given the ranges of H_{mo} and H_{molong} explained above. The relation between the H_{mo} and H_{molong} for the "non breaking waves", is shown in figure 217. A clear quadratic trend is obtained with a determination coefficient of 0.93, correlation coefficient of 0.96 with 82 wave records. The relation for the breaking waves is shown in figure 218. In this case a linear trend was obtained, with slightly higher dispersion of the data points the determination coefficient was 0.76 with a correlation coefficient of 0.87 with 23 wave records.

The validity of equation 51 for the "wave breaking" conditions under the direct influence of the Hurricane is highly doubtful, furthermore the white noise spectrum observed during that period of time makes it impossible to evaluate; equation 51 was then evaluated only for the non breaking wave conditions, with H_{molong} smaller than 1 meter.

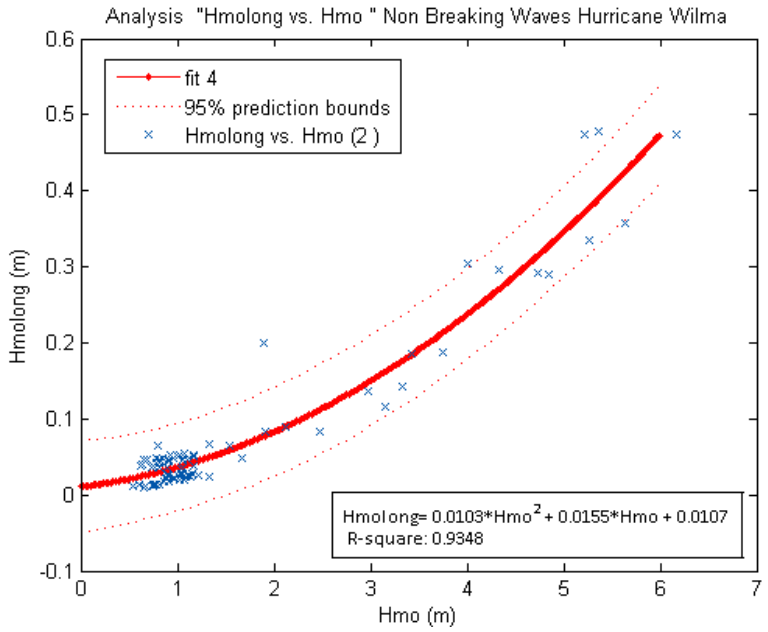

Figure 217: Relation Hmo and Hmolong for the non breaking waves for Hurricane Wilma

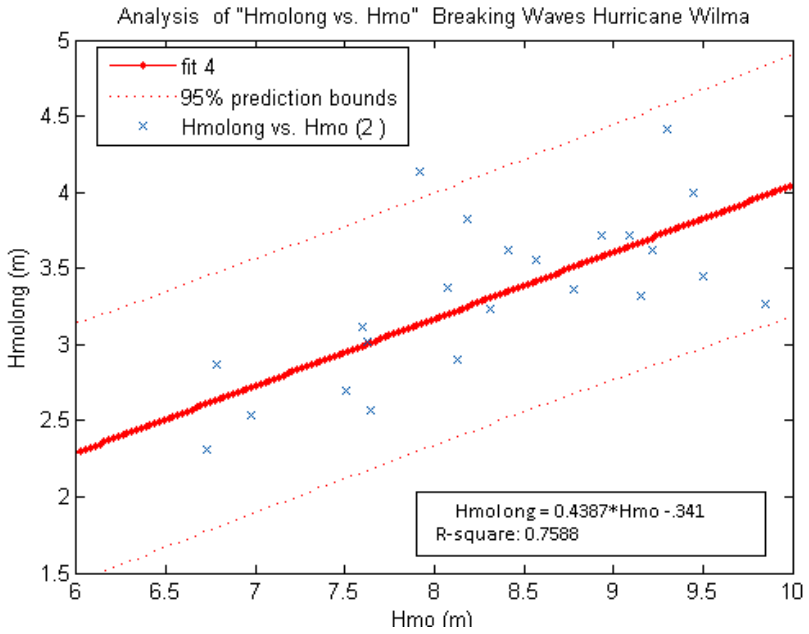

Figure 218: Relation Hmo and Hmolong for the breaking waves for Hurricane Wilma

A K adjustment value of 0.044 was obtained for equation 51. The validity of the fit is shown in figure 219, where a determination coefficient of 0.94 was found, correlation coefficient of 0.97 but with only 84 wave records. This K value is much smaller than the one found for the previous sites, where K was between 0.14 and 0.19.

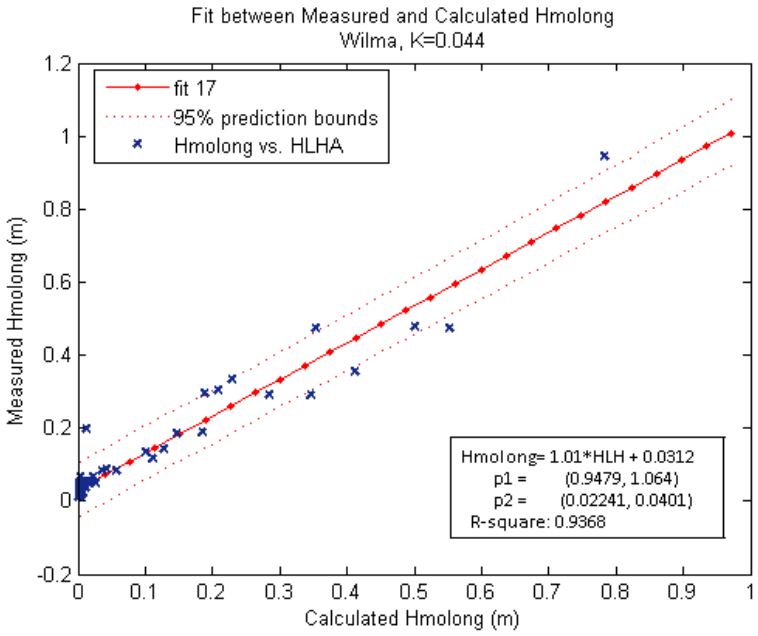

Figure 219: Fit between Measured and Calculated Long Wave Height for Hurricane Wilma

The relation between Tp and Tplong was also investigated. Again no relation was found and certain conspicuous constant long wave periods are observed in figure 220 at Tplong=350, 420, and 530 seconds.

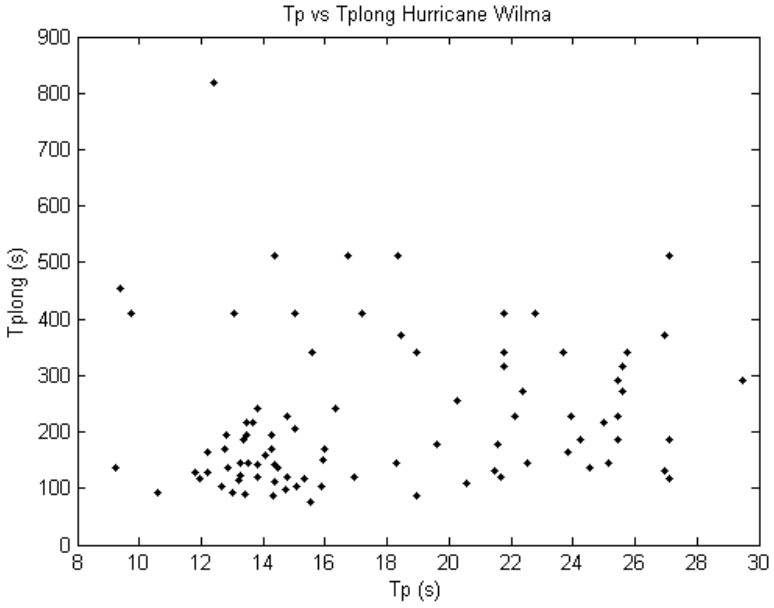

Figure 220: Relation Tp and Tplong for Hurricane Wilma

5.0 Conclusions and Recommendations

A new method to recover water surface elevation time series from submersible pressure sensors was proposed. This new method is based on the Hilbert Huang transform and the instantaneous frequency of a process. This new method was validated and calibrated using near full scale laboratory wave simulations from CIEM. The new proposed method provides a new way to calculate and apply frequency dependant transfer functions for non-stationary non-linear processes. The need to fit the processes to harmonic functions is eliminated with new proposed method. Further research on the application of the new proposed method to other processes, such as wind and wave load transfer functions is recommended.

The analyzed waves in the coastal zone fitted in all cases quite well the Rayleigh distribution. Deviation was found only for the waves that occurred during Hurricane Wilma, where wave breaking is expected to have occurred and a broad spectrum was found. These two conditions are outside the assumptions for which the Rayleigh distribution was found to describe ocean waves. Small deviations were observed for the long travelled swell waves, where the ratios between the characteristic wave heights were smaller than the ones predicted by the Rayleigh distribution. These a consequence of the regularity of the waves observed for the long travelled swell.

The individual wave height and period distributions for each site showed very different characteristics. The spreading of the marginal individual wave period distribution probability was correlated to the spectral characteristics, a narrow peaked spectra showed very little spreading of the individual wave period marginal distribution. The individual wave period distribution can be correlated with spectral characteristics, such as spectral peakdness or the peak enhancement parameter from the JONSWAP spectra.

The temporal variation of the energy spectra of the waves at different sites showed very clear differences. Storm events with a short duration for cases such as the observed from the wave measurements at Ebro Delta contrast significantly with the constant frequency decay energy between energetic events for the long travelled swell wave measurements from the Pacific Coast of Costa Rica. This constancy in the energetic fingerprint of long swells should be taken into account when calculating the potential energy that can be harnessed from the waves at different sites.

The ratio between the spectral and the zero down crossing significant wave height showed that the narrower the frequency distribution and more peaked spectra the closer the ratio is to 1, while the broader and closer the

spectra to a white noise spectra the ratio was lower than 0.80. This is associated with the content of energy in frequencies other than the zero down crossing frequency.

The energetic period, T_{m0-1}, was found to be unstable. For the measured swell waves T_{m0-1} completely missed the arrival of the first long swells and was lower than the spectral peak period. T_{m0-1} correlated with the zero down crossing significant period for the swell waves. However at the shallow wave measurements from Ebro Delta, where the amount of long "wave" energy was almost 20%, T_{m0-1} took values of up to 40 seconds while the peak spectral period was around 6 seconds. T_{m0-1} was stable for the wave measurements at Moin, where the peak period was 8 seconds and the water depth 17 meters. However again for the wave measurements during Hurricane Wilma T_{m0-1} received values of more than 100 seconds. This dramatic value changes doubts the use of T_{m0-1} for all wave conditions as the energetic wave period. Other spectral parameters should be used to account for the low frequency energy contributions. The energetic period, T_{m0-1}, *should not be used in breakwater or other coastal structure design formulas*, the peak spectral period, or the statistical significant period are much better options. If the low frequency energy wants to be included within the design formula, it is recommended to add a low frequency set up and or set down using the modified equation 51. If the effect of wave grouping is going to be included in research or design formulas the spectral grouping parameter Ka should be used.

The spectral peakdness, Qp, and the spectral grouping parameter Ka were found to be stable and to accurately depict the spectral temporal changes. The other spectral parameters evaluated did not follow the obvious spectral changes and their use is not recommended. Their dependency on the spectral resolution was clearly shown. A clear correlation between the spectral peakdness, Qp, and the spectral grouping parameter Ka was found regardless of the wave measurement site, water depth, or sea states.

The fit of the measured spectra to the JONSWAP spectra varied on each site. Long travelled swell waves showed a very good fit, with peak enhancement parameter, γ, between 3, when multiple swells are present, to 13 to very regular lower energy wave conditions. Occasions when double peaked spectra occurred showed a very bad fit, however these were also low energetic events. For this doubled peak spectra Ochi Hubble or other bimodal spectra should be investigated. For the wave measurements at Ebro Delta a reasonable fit for the most energetic wave conditions was observed, γ received values of 4 for these shallow water wave measurements. The most energetic measured waves at Moin also showed a reasonable fit with the JONSWAP spectrum, with γ values between 5 and 6.5. For the measured waves during Hurricane Wilma no correlation between the measured

spectra and JONSWAP spectra was found. Furthermore the observed white noise spectrum would be hard to fit to any other parametric representation known to the author. The peak enhancement parameter is highly dependent on the spectral resolution and the degrees of freedom of the real measured waves; care is advised to the coastal engineering community when using the JONSWAP spectra.

Wave groupiness, defined as the tendency of consecutive wave heights in a wave record, showed large differences between the different sites. No relation between a given spectral period and the groupiness of the waves was found. A relationship between the narrowness and peakdness of the spectra to the groupiness was observed.

A clear correlation between the correlation coefficient between two successive waves and the spectral groupiness parameter Ka was found for all the wave records from the different sites. Kimura's run length theory was also validated and good agreement in general was found between the measured and predicted values. The correlation coefficient between successive waves and the mean run length followed Kimura's theory. The spectral groupiness parameter Ka showed a good correlation with the mean run length, much better than the one obtained using the spectral peakdness parameter. The variance spectra based on the Fourier transform represents accurately the wave groupiness phenomena by means of the spectral groupiness parameter Ka.

The effect of the wave groupiness on the stability of coastal structures should be studied using the spectral wave groupiness parameter Ka. The spectral peakdness parameter Qp should not be used to study wave groupiness.

The low frequency energy content in the wave measurements was correlated to the spectral significant wave height, the peak spectral period and the water depth of each measurement through means of Longuet wave group set down modified equation 51. A surprisingly good fit was found between these equations using a K adjustment factor to the low frequency energy, known as bound long "wave". The K adjustment factor could be correlated to the spectral narrowness, or the spectral grouping parameter Ka, or wave directional spreading however longer wave records at different water depths are required. The fitted long wave height equation is valid for non-breaking waves in shallow or near shallow water conditions. This equation can be used to determine the long wave height just before the breaker zone to determine the low frequency energy content in the surf zone, to understand run up, overtopping processes and coastal processes. This fitted equation can also be used to determine the long wave height outside a harbor to study resonance and agitation problems within the harbor.

No relation was found between the peak spectral period and the measured long “wave” height peak period. Minor correlation was observed between the long “wave” peak period and the mean run length, however, conspicuous constant long “wave” peak periods were observed. These constant long “wave” periods at constant increments are a consequence of the nature of the bound long “wave”, where water set downs due to runs of high waves are followed by small water setups in lower waves. The randomness of the wave groups, the nonlinearity of the process, where they do not follow a harmonic shape makes it very hard to be interpreted by a Fourier series; hence the spurious harmonic frequencies appear. No improvement was found using the Hilbert Huang transform, nevertheless further research is recommended with longer wave records. Longer wave records should provide a stronger statistics to improve the fit of the modified equation 51 and to determine the associated periods of the low frequency set downs and set ups.

The Hilbert Huang spectrum showed new insight into the wave processes of the most energetic measured time series. It was possible to show that wave-wave interaction, between two swell waves around 12.5 and 25 seconds, was responsible for the highest measured wave of the long travelled swell. The instantaneous wave energy distribution between the different sites also showed clear differences between each site, the regularity and presence of the wave groups was clearly observed in the HHT spectra. The marginal HHT(w) spectra showed clear differences at all sites with respect to the FFT spectra, a higher lower frequency energy content was explained as a consequence of the energy contribution interpretation between both spectrums. Nevertheless double peaked FFT spectra where interpreted as single peaked spectra by the HHT spectra, this difference could not be explained, and could be a consequence of the harmonic interpretation of the FFT spectra.

References

LIU, PAUL C, “IS THE WIND WAVE FREQUENCY SPECTRUM OUTDATED”, OCEAN ENGINEERING 27 (2000) 577–588.

TITCHMARSH, E.C., 1948 “INTRODUCTION TO THE THEORY OF FOURIER INTEGRALS” OXFORD UNIVERSITY PRESS, OXFORD, UK.

MEDINA J.R., HUDSPETH R.T. “A REVIEW OF THE ANALYSES OF OCEAN WAVE GROUPS” COASTAL ENGINEERING, 14 (1990) 515-542

HALLER H.C., DALRYMPLE R.A. “LOOKING FOR WAVE GROUPS IN THE SURF ZONE”, COASTAL DYNAMICS ‘95

BOWERS, E.C. “WAVE GROUPING AND HARBOR DESIGN”, COASTAL ENGINEERING, JUNE 1988, 237-258

MELVILLE W.K. “WAVE MODULATION AND BREAKDOWN”, JOURNAL OF FLUID MECHANICS (1983), 128:489-506

COX, J.C. AND WESSON M.V., “MANIPULATING HARBOR GEOMETRIES TO DEFEAT LONG WAVE AGITATION PROBLEMS” ASCE PORTS 2007.

BURCHARTH, H.F., 1979. “THE EFFECT OF WAVE GROUPING ON ON-SHORE STRUCTURES”. COASTAL ENG.,2: 189--199.
BOWERS E. C. “HARBOR RESONANCE DUE TO SET-DOWN BENEATH WAVE GROUPS”, . FLUID MECH. (1977), VOL. 79, PART 1, PP. 71-92

VELTCHEVA A. B. “WAVE AND GROUP TRANSFORMATION BY A HILBERT SPECTRUM” COASTAL ENGINEERING JOURNAL, VOL. 44, NO. 4 (2002) 283-300

GODA Y. “ANALYSIS OF WAVE GROUPING AND SPECTRA OF LONG-TRAVELLED SWELL” 1983, PORT AND HARBOR RESEARCH INSTITUTE JAPAN.

NAESS A. “AN INTRODUCTION TO RANDOM VIBRATIONS”, CENTRE FOR SHIPS AND OCEAN STRUCTURES, NTNU.

GODA Y. “RANDOM SEAS AND DESIGN IN MARITIME STRUCTURES”, WORLD SCIENTIFIC PUBLISHING, 2000

SAND S.E. “WAVE GROUPING DESCRIBED BY BOUND LONG WAVES”. OCEAN ENGNG, VOL. 9, NO 6, PP.567-580, 1982.

G.H. HARDY, “A THEOREM CONCERNING FOURIER TRANSFORMS”. J. LONDON MATH. SOC . 8 (1933) 227–231

VERHAGEN, VANVLEDDER, ESLAMIARAB, “A PRACTICAL METHOD FOR DESIGN OF COASTAL STRUCTURES IN SHALLOW WATER” DELFT TECHNICAL UNIVERSITY, 2008.

GODA, YOSHIMI, “RANDOM SEAS AND DESIGN IN MARITIME STRUCTURES”, 2000.

PIERSON, WILLARD J., JR. AND MOSKOWITZ, LIONEL A. PROPOSED SPECTRAL FORM FOR FULLY DEVELOPED WIND SEAS BASED ON THE SIMILARITY THEORY OF S. A. KITAIGORODSKII, JOURNAL OF GEOPHYSICAL RESEARCH, VOL. 69, P.5181-5190, 1964

HASSELMANN, MEASUREMENTS OF WIND-WAVE GROWTH AND SWELL DECAY DURING THE JOINT NORTH SEA WAVE PROJECT (JONSWAP)., 1973.

BOSBOOM J., STIVE M.J.F, ”COASTAL DYNAMICS” LECTURE NOTES CT4305, DELFT TECHNICAL UNIVERSITY, 2010

HUANG, N. “THE EMPIRICAL MODE DECOMPOSITION AND THE HILBERT SPECTRUM FOR NONLINEAR AND NON-STATIONARY TIME SERIES ANALYSIS”. THE ROYAL SOCIETY LONDON, 1998.

SCHLURMANN T., DATIG M., “PERFORMANCE AND LIMITATIONS OF THE HILBERT-HUANG TRANSFORMATION (HHT) WITH AN APPLICATION TO IRREGULAR WATER WAVES”. OCEAN ENGINEERING NRO 31, 2004.

HWANG P., HUANG N. “A NOTE ON ANALYZING NONLINEAR NONSTATIONARY OCEAN WAVE DATA”, APPLIED OCEAN RESEARCH 25 (2003).

E.C. BOWERS. “HARBOR RESONANCE DUE TO SET DOWN BENEATH WAVE GROUPS”. HYDRAULICS RESEARCH STATION, WALLINGFORD, OXFORDSHIRE, 1977

BRODTKORB, P.A., JOHANNESSON, P., LINDGREN, G., RYCHLIK, I., RYDÃ©N, J. AND SJÃ¶, E. (2000). "WAFO - A MATLAB TOOLBOX FOR ANALYSIS OF RANDOM WAVES AND LOADS", PROC. 10TH INT. OFFSHORE AND POLAR ENG. CONF., SEATTLE, USA, VOL III, PP. 343-350.

IGOR RYCHLIK, MIKE LIN, GEORG LINDGREN, ” MARKOV BASED CORRELATIONS OF DAMAGE CYCLES IN GAUSSIAN AND NON-GAUSSIAN LOADS”. PROBABILISTIC ENGINEERING MECHANICS, VOL 10, PP 103-115, 1995.

F. E. SNODGRASS, G. W. GROVES,, K. F. HASSELMANN, G. R. MILLER, W. H. MUNK AND W. H. POWERS, “PROPAGATION OF OCEAN SWELL ACROSS THE PACIFIC”, PHILOSOPHICAL TRANSACTIONS OF THE ROYAL SOCIETY OF LONDON. SERIES A, MATHEMATICAL AND
PHYSICAL SCIENCES, VOL. 259, NO. 1103 (MAY 5, 1966), PP. 431-497

CHAKRABARTI S. AND COOLEY R. “THE STABILITY OF SOME CURRENTLY USED WAVE PARAMETERS – A DISCUSSION”, COASTAL ENGINEERING, 1(1977) 359-365

RYE, HENRIK, “THE STABILITY OF SOME CURRENTLY USED WAVE PARAMETERS”, COASTAL ENGINEERING, 1 (1977) 17-30

MOSSO C., PAU SIERRA J., RODRIGUEZ A., GRACIA V., BARNADAS J., “ESTUDIO EXPERIMETAL DE LA EVOLUCIÓN DEL ESPECTRO DEL OLEAJE EN UNA PLAYA”, INGENIERIA HIDRÁULICA EN MEXICO, VOL XXII, NUM1 PP.47-61, ENERO-MARZO DE 2007

SILVA R.C., MENDOZA E.B, ESCALANTE E.M, “OLEAJE INDUCIDO POR EL HURACÁN WILMA EN PUERTO MORELOS QUINTANA ROO, MÉXICO”, INGENIERIA HIDRÁULICA EN MÉXICO, VOL.XXIV, PP.93-109, ABRIL-JUNIO DE 2009

BRENT GALLAGHER, “GENERATION OF SURF BEAT BY NON-LINEAR WAVE INTERACTIONS”, J . FLUID MECK. (1971), WOE. 49, PART 1, PP. 1-20

M. S. LONGUET-HIGGINS “STATISTICAL PROPERTIES OF WAVE GROUPS IN A RANDOM SEA STATE”, PHILOSOPHICAL TRANSACTIONS OF THE ROYAL SOCIETY OF LONDON. SERIES A, MATHEMATICAL AND PHYSICAL SCIENCES, VOL. 312, NO. 1521, (OCT.12, 1984), PP. 219-250

WALTER MUNK, FRANK SNODGRASS, GEORGE CARRIER, “EDGE WAVES ON THE CONTINENTAL SHELF”SCIENCE, 27 JANUARY 1956, VOLUME 123, NUMBER 3187

CRAIG T. BISHOP AND MARK A. DONELAN, “MEASURING WAVES WITH PRESSURE TRANSDUCERS”, COASTAL ENGINEERING, 11 (1987) 309-328

HSIANG WANG, DONG-YOUNG LEE AND ALLEN GARCIA, “TIME SERIES SURFACE-WAVE RECOVERY FROM PRESSURE GAGE”, COASTAI ENGMEERING, 10 (1986) 379-393